# DESIGN AND EVALUATION OF MECHANISM-BASED SIRT2 INHIBITORS WITH ENHANCED ANTICANCER POTENCY

A Dissertation

Presented to the Faculty of the Graduate School

of Cornell University

In Partial Fulfillment of the Requirements for the Degree of

Doctor of Philosophy

by

Jun Young Hong

August 2021

# DESIGN AND EVALUATION OF MECHANISM-BASED SIRT2 INHIBITORS WITH ENHANCED ANTICANCER POTENCY

Jun Young Hong, Ph. D.

Cornell University 2021

SIRT2 regulates various biological pathways through lysine deacetylation and de-fatty acylation, thereby promoting tumor growth. Subsequently, many SIRT2 selective inhibitors have been developed to target cancers. Among them, a mechanism-based SIRT2 inhibitor named TM is a lead compound with a potent antiproliferative effect. TM-induced SIRT2 inhibition had degraded oncoprotein c-Myc and effectively reduced breast cancer tumor growth. Nevertheless, TM possesses several limitations. Due to its long thiomyristoyl hydrophobic chain, TM has poor aqueous solubility, which makes the collection of the X-ray crystal structure of TM and SIRT2 challenging. Also, TM with poor aqueous solubility portrays limited bioavailability in cellular and animal studies. Another limitation of TM is that it can only inhibit SIRT2 deacetylase, not de-fatty acylase. Such simultaneous inhibition of both SIRT2 enzymatic activities could potentially increase the antiproliferative effect.

In this thesis, several new SIRT2 selective inhibitors that have overcame these issues will be discussed. To improve the aqueous solubility, we have synthesized a glycoconjugated TM, named glucose-TM (Chapter Two). Even though glucose-TM had poor permeability, it had enabled us to collect X-ray co-crystal structure with SIRT2 and design additional inhibitors. To design a new SIRT2 modulator that inhibits both deacetylase and defatty-acylase, we have developed SIRT2 selective

Proteolysis Targeting Chimera (PROTAC) inhibitor named TM-P4-Thal to degrade SIRT2 in cells (Chapter Three). For the accurate comparison of a pan SIRT1-3 inhibitor and a SIRT2 selective inhibitor, we synthesized NH4-6 and NH4-13 that have only one atom difference, but completely different sirtuin inhibition profile (Chapter Four). From the previous chapters, we have learned that both solubility and permeability are important for drug designs. To gain both characteristics, we have designed a simpler SIRT2 inhibitor with a benzodiazapienedione core, named NH-C1-10 (Chapter Five). NH-C1-10 inhibited SIRT2 slightly weaker than TM. However, in cellular studies, NH-C1-10 with improved bioavailability had shown stronger cytotoxicity and SIRT2 inhibition than TM.

# BIOGRAPHICAL SKETCH

Jun Young (Nick) Hong was born in Hong Kong and grew up in Seoul, South Korea. He attended Seoul International School in Seoul, Korea. He obtained a bachelor's degree at Cornell University in Economics and Chemistry with Cum Laude honor. As an undergraduate student at Cornell University, he had received the American Chemistry Society Undergraduate Research Award. In 2015, he joined Chemistry and Chemical Biology Department as a graduate student and started his research on SIRT2 inhibitors with Professor Lin's support.

Dedication to my family – Dad, Mom, and Brother

# ACKNOWLEDGMENTS

First and foremost, I would like to thank Professor Lin for his support. I still remember the day I received his reply to my email asking for an undergraduate summer research position. This was the beginning of my entire research path. Without his guidance, I would have never thought about becoming a scientist. I am grateful to have Professor Lin as my mentor and hope to become a mentor like him.

I would also like to thank Professor Rick Cerione and Professor Frank Schroeder for their guidance as thesis committee. Also, I would like to acknowledge Professor Robert S. Weiss, Professor Ari Melnick, Professor Brian Weiser, and Professor Maureen Linder for the opportunity to collaborate on many exciting projects.

Many thanks to the people whom I have collaborated with – Irma Fernandez, Dr. Ian Price, Dr. Nicole Spiegelman, Ali Farooqi, Martin Ian Malgappo, and Yinong Liu. I have enjoyed the opportunity to get to work closely. I would like to give Irma special recognition for the mice experiments in SIRT2 and SIRT5 projects.

Luckily, I had many mentors throughout my Ph.D. program, who had helped me without any questions whenever I needed them. Dr. Ying-ling Chiang and Dr. Min Yang had taught me synthesis skills. Dr. Jing Hu and Dr. Xiaoyu Zhang had trained me biological experimental skills. Working with Dr. Meng Li, I had gained a wider scientific perspective. Also, I have learned a lot from discussing science with Dr. Shuai Zhang and Sonny Komaniecki from the lab.

I would like to thank Xuan for all her support in the lab. She had been amazing in organizing the lab supplies, keeping track of mice, and maintaining a healthy lab environment.

I had a great opportunity to work with many undergraduate students, who had assisted me in many projects. I would like to give special thanks to Jessica Bai for helping me with the cell culture and biological experiments in SIRT2 and SIRT5 inhibitors projects. Also, I would like to thank Stephen Ramirez and Yizhen Jin for synthesizing SIRT5 inhibitors.

I would like to thank all the Lin Lab members. Working with everyone was a great pleasure and I will never forget.

Lastly, I would like to thank my family and friends. Without their support and help, I would not have been able to finish my Ph.D. program.

Thank you, everyone.

TABLE OF CONTENTS

LIST OF FIGURES

LIST OF TABLES

LIST OF SCHEMES

# CHAPTER 1

## SIRTUIN MODULATORS IN CELLULAR AND ANIMAL MODELS OF HUMAN DISEASES.

This is a revised version of the submitted paper: Hong JY, Lin H. Sirtuin Modulators in Cellular and Animal Models of Human Diseases. *Frontiers in Physiology.*

### 1.1 Abstract

Sirtuins use $NAD^+$ to remove various acyl groups from protein lysine residues. Through working on different substrate proteins, they display many biological functions, including regulation of cell proliferation, genome stability, metabolism, and cell migration. There are seven sirtuins in humans, SIRT1-7, each with unique enzymatic activities, regulatory mechanisms, subcellular localizations, and substrate scopes. They have been indicated in many human diseases, including cancer, neurodegeneration, microbial infection, and autoimmune diseases. Consequently, interests in development of sirtuin modulators have increased in the past decade. In this brief review, we summarize sirtuin modulators with promising therapeutic effects in cellular and animal models of various human diseases. We further anticipate this review will be helpful for scrutinizing the significance of sirtuins in the studied diseases.

### 1.2 Introduction

Sirtuins, the class III histone deacetylase, use $NAD^+$ to remove various acyl modifications on lysine.[1-3] In humans, there are seven sirtuins (SIRT1-7), with

different acyl group specificities and subcellular localizations. Through deacylation, sirtuins regulate a wide range of biological functions, such as cell proliferation, metabolism, transcription, apoptosis, and cell signaling.[4-13] Consequently, sirtuins have been linked to various diseases, including cancer, neurological, and cardiovascular diseases.[6, 14-16] Many sirtuin activators and inhibitors have been designed and assessed in cellular and animal studies. In this review, we have summarized sirtuin modulators that showed promising therapeutic effects in cancer, neurological, and cardiovascular disease models.

The seven mammalian sirtuins localize to different cellular compartments. SIRT1, SIRT6, and SIRT7 mainly reside in the nucleus. SIRT2 is mainly in the cytoplasm and SIRT1 and SIRT6 are also found in the cytoplasm. SIRT3, SIRT4, and SIRT5 are primarily in the mitochondria.[1] Yet, under certain conditions, like cell division or stress, several sirtuins may change their cellular locations.[17-19]

All seven sirtuins possess a similar catalytic mechanism.[4, 13, 20] First, the acyl oxygen of the acyl lysine attacks C1 of the $NAD^+$ ribose, and releases nicotinamide (Figure 1.1). This forms a covalent C1'-O-alkylamidate intermediate. Then, the conserved histidine deprotonates the 3'-hydroxyl group of the $NAD^+$ ribose, which deprotonates the 2'-hydroxyl group. The deprotonated 2'-hydroxyl group attacks the nearby carbon of the C1'-O-alkylamidate intermediate. After forming a 1',2'-cyclic intermediate, the acyl group transfers to the 2'-hydroxyl group and releases the deacylated lysine product and 2'-O-acyl ADP-ribose.[4, 13, 20]

Even though SIRT1-7 operate through a similar catalytic mechanism, different sirtuin prefer different acyl substrates, because of differences in their substrate

pockets. SIRT1 and SIRT3 remove acetyl and long-chain fatty acyl groups from lysine *in vitro*, but so far known physiological substrates are all deacetylation substrates.[1, 21] SIRT2 removes acetyl, long-chain fatty acyl, 4-oxononanoyl, and benzoyl groups.[1, 21-23] SIRT4 removes lipoyl, biotinyl, methylglutaryl, hydroxymethylglutaryl, and 3-methylglutaconyl groups.[24-27] SIRT5 removes charged malonyl, succinyl, and glutaryl groups.[28] SIRT6 and SIRT7 remove acetyl and long-chain fatty acyl groups.[29, 30] Both acetyl and long-chain fatty acyl substrates were known for SIRT6, but for SIRT7, only physiological acetyl substrates are known.

Many modulators are strategically designed to target different sirtuins and generate beneficial effects in human disease models. Here we aim to summarize the various sirtuin modulators that have been developed. We focus on those that have demonstrated biological effects in cellular or animal models. Because one common concern about small molecules is whether their biological activity is through on-target effect or not, we will emphasize whether the sirtuin modulators' biological activity is confirmed by other means, such as knockdown, knockout, or overexpression of the sirtuin being targeted. Accordingly, we will spend more attention describe the sirtuin modulators for which the biological activity has been confirmed by other methods.

### 1.3 Overview of Sirtuin Modulators

Numerous activators and inhibitors of sirtuins have been synthesized. Before discussing the evaluation of the sirtuin modulators in the disease models, we will briefly provide an overview of the sirtuin modulators and their efficiency. The structures and other information of these modulators are summarized in Table 1.

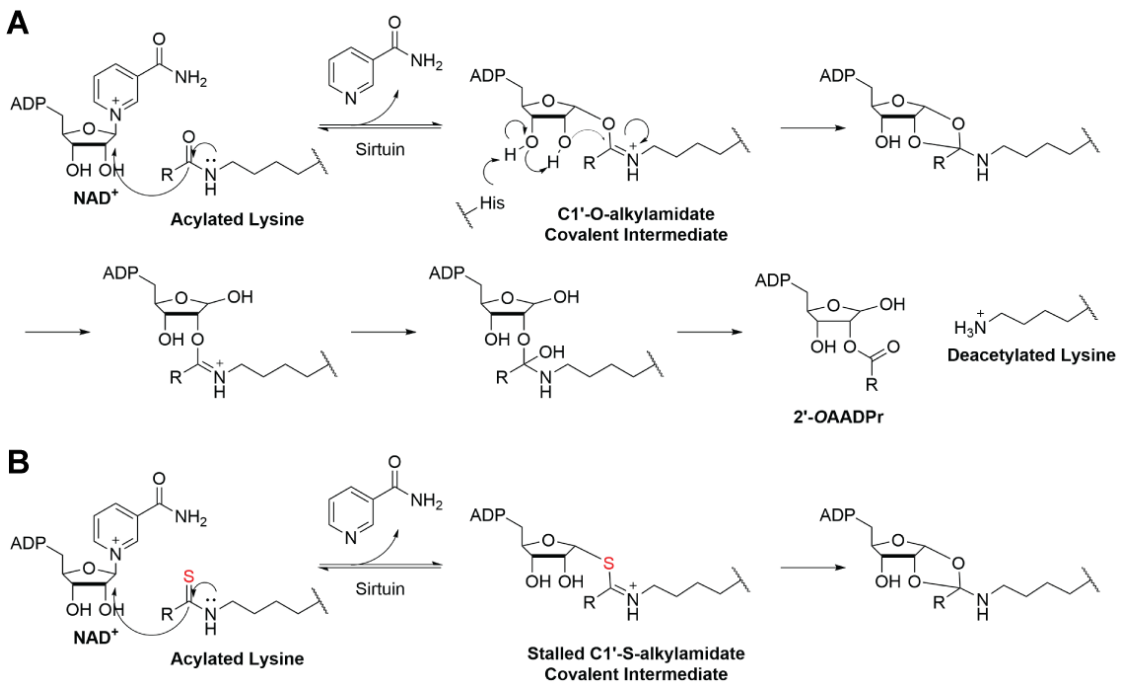


**Figure 1.1 Schematic summary of sirtuin mechanism.** (A) Schematic summary of sirtuin deacylation mechanism. (B) Schematic summary of mechanism-based inhibition of sirtuin

### 1.3.1 SIRT1 modulators

Because SIRT1 was initially connected to longevity, many small-molecule activators have been developed and tested for anti-aging purposes.[31-33] However, many follow-up studies questioned the activating mechanism, as the activation was only observed when using aminomethylcoumarin or fluorophore-tagged peptide substrate.[34, 35] The original authors have rebutted this by showing direct allosteric SIRT1 activation with biochemical assays and crystallography structures.[36, 37] Later, it was found that a SIRT1 activator could also inhibit SIRT3.[38] Thus, the effects of SIRT1 activators may not necessarily come from the activated SIRT1. Due to such complications, we have decided to leave out the discussion on SIRT1 activators in this review.

For SIRT1, EX-527 or selistat is the most used SIRT1 selective inhibitor in biological studies. EX-527 inhibited SIRT1 with an $IC_{50}$ of 38 nM with 200-fold selectivity over SIRT2 and SIRT3.[39] Only when using H3K56 fluorogenic substrate, 200 μM of EX-527 showed 56% SIRT6 inhibition.[40] Nevertheless, EX-527 still showed significantly stronger SIRT1 selectivity over SIRT6. In cells, EX-527 treatment significantly increased the acetylation of p53, a SIRT1 deacetylation substrate.[39] Additionally, several SIRT1 inhibitors were reported, but whether they selectively inhibit SIRT1 was not validated.[41, 42]

### 1.3.2 SIRT2 inhibitors

AGK2 was synthesized from a high-throughput screening and showed SIRT2 inhibition with an $IC_{50}$ of 8 μM. Also, AGK2 showed 5-fold selective SIRT2 inhibition over SIRT1.[43] In cells, Treatment of AGK2 had significantly increase acetylation levels of α-tubulin, a SIRT2 deacetylation substrate.[44, 45] A limitation of using AGK2 in biological studies is its poor solubility in water and ethanol. Furthermore, according to SelleckChem, its maximum solubility in DMSO is only about 23 mM at 50 °C.[44] Such poor solubility could make it difficult to accurately evaluate AGK2-induced SIRT2 inhibition in cells and animals.

AK-7 inhibited SIRT2 with an $IC_{50}$ of 15.5 μM and does not inhibit SIRT1 or SIRT3.[46] The main advantage of AK-7 is its brain permeability. After 2 hours of intraperitoneal injection to mice, about 2 μM of AK-7 was detected in the brain. As such, utilizing AK-7 in neurological diseases could be helpful.

SirReal2 binds and rearranges the hydrophobic pocket of SIRT2, where the long-chain fatty acyl group of a substrate occupies.[47] SirReal2 inhibited SIRT2 with an

$IC_{50}$ of 140 nM without any inhibition against other sirtuins. In cells, SirReal2 had increased acetylation levels of α-tubulin and BuBR1, acetylation targets of SIRT2. Furthermore, SirReal2 could not change the acetylation level of p53.[44, 47]

From a large library screening of 140,000 compounds, RK-91230156 was discovered to inhibit SIRT2 over SIRT1, SIRT3, HDAC1, and HDAC6. Moreover, RK-91230156 inhibits SIRT2 with an $IC_{50}$ of 0.18 μM. Treatment of RK-91230156 had significantly increased acetylation of eIF5a, another reported SIRT2 deacetylation target.[48]

NCO-90 and NCO-141 are nicotinamide-derived SIRT2 selective inhibitors with $IC_{50}$ values of 1 and 0.57 μM, respectively. In HCT-116 colorectal cells, NCO-90 had increased the acetylation level of α-tubulin, while kept the acetylation level of p53 constant.[49] By attaching NCO-90 to a thioacylated lysine, KPM-2 was synthesized. Unlike its parent compound, KPM-2 simultaneously inhibits SIRT1, SIRT2, and SIRT3 by occupying the substrate "selectivity" and $NAD^+$ pockets of sirtuins. Its measured SIRT1, SIRT2, and SIRT3 $IC_{50}$ were 1.56, 0.055, and 9.49 μM, respectively. In cells, KPM-2 had shown a dose-dependent increase of the acetylation of α-tubulin.[50] Compound 53 is an NCO-90-based diketopiperazine compound that inhibits SIRT2 by concurrently occupying the selectivity pocket, substrate-binding site, and $NAD^+$ binding site. Compound 53 inhibited SIRT2 at an $IC_{50}$ of 0.31 μM with 250 and 223-fold selectivity over SIRT1 and SIRT3, respectively. In MCF7 cells, Compound 53 had increased acetylation level of α-tubulin.[51]

Discovered from high-throughput screening of RIKEN NPDepo chemical library, NPD11033 selectively inhibited SIRT2 deacetylase activity with $IC_{50}$ of 0.46

μM, but it could not inhibit SIRT2 defatty-acylase activity.[52] This inhibitor creates a hydrophobic pocket near the substrate-binding pocket and forms a hydrogen bond to the active-side histidine. In addition, NPD11033 had increased acetylation level of eIF5A in PANC-1 pancreatic cells.[52]

Compound 6f and Compound 12a are Chroman-4-one and chromone-based SIRT2 inhibitors with $IC_{50}$ of 3.7 and 12.2 μM, respectively. Like other SIRT2 inhibitors, Compound 6f and 12a had increased the acetylation level of α-tubulin in cells.[53] 1,2,4-oxadizazole-based Compound 35 and 39 inhibited SIRT2 through an uncompetitive mechanism against α-tubulin peptide substrate and $NAD^+$. Their SIRT2 $IC_{50}$ were 10.4 and 1.5 μM, respectively. In NB4 and U937 cells, both Compound 35 and 39 increased acetyl α-tubulin.[54] A SIRT2 selective inhibitor, Compound 24a was discovered from a SAR study with N-(3-(phenoxymethyl)phenyl)acetamide derivatives.[55] It had bound to the hydrophobic pocket that accommodates the fatty acyl-lysine substrate to inhibit SIRT2 with an $IC_{50}$ of 0.815 μM. Furthermore, Compound 24a did not inhibit other sirtuins at 100 μM. In H441 non-small lung cancer cells, Compound 24a had increased the acetylation level of α-tubulin.[55]

As mentioned, sirtuins form a covalent O-acyl-ADP-ribose intermediate during its catalytical mechanism. Many thioacyl lysine peptides (or the corresponding thiourea peptides) form similar covalent intermediates, but the substitution of the oxygen atom by sulfur inhibits the attack of the 2'-hydroxyl group. Then, the following reaction step does not readily occur after the formation of the covalent S-acyl-ADP ribose intermediate. Therefore, the overall sirtuin activity gets inhibited by these pseudopeptide inhibitors.[20, 56, 57]

TM contains a thiomyristoyl lysine with an N-terminal carboxybenzoyl (Cbz) group and a C-terminal aniline.[56] Using its thiomyristoyl group, TM selectively inhibited SIRT2 by forming a stalled covalent intermediate, which was captured by mass spectrometry. In cells, treatment of TM increased acetylation of α-tubulin in a dose-dependent manner. Moreover, its SIRT2 $IC_{50}$ was 0.04 μM with 650-fold selectivity over SIRT1. TM could not inhibit SIRT3 even at 50 μM.[44] AF8, a derivative of TM with a thiourea moiety mimicking the thioacyl group, also formed a stalled covalent intermediate to selectively inhibit SIRT2 with an $IC_{50}$ of 0.061 μM and 180-fold selectivity over SIRT1. In HCT-116 colorectal cancer cells, AF8 had increased acetylation of α-tubulin in a dose-dependent manner but did not change the acetylation of p53.[58] Two other TM derivatives, NH4-6 and NH4-13 both have a trimethylamine moiety instead of the C-terminal aniline.[59] These two compounds have excellent aqueous solubility compared to TM. The difference between the two inhibitors is that NH4-6 has an amide linkage and NH4-13 has an ester linkage between the lysine and the trimethylamine moiety. This small difference led to a completely different inhibition profile. NH4-6 with the amide bond simultaneously inhibits SIRT1, 2, and 3 with $IC_{50}$ of 3, 0.032, and 2.3 μM, respectively. Meanwhile, NH4-13 with the ester bond selectively inhibits SIRT2 with an $IC_{50}$ of 0.087 μM. Furthermore, in cells, NH4-6 had increased acetylation levels of p53, α-tubulin, and IDH2, acetylation targets of SIRT1, SIRT2, and SIRT3, respectively. Meanwhile, NH4-13 could only increase the acetylation level of α-tubulin, not p53 and IDH2.[59]

Many reported SIRT2 inhibitors, including TM, efficiently inhibit SIRT2's deacetylase activity, but not its defatty-acylase activity. However, converting them to

proteolysis-targeting chimeras (PROTAC) could enable them to inhibit both activities. TM-P4-Thal is a PROTAC SIRT2 inhibitor with thalidomide on one end and TM on another end, connected by a polyethylene glycol (PEG) linker. The thalidomide recruits CRBN E3 ligase, while TM interacts with SIRT2. Such recruitment leads to polyubiquitination of SIRT2, thereby inducing proteolysis-mediated degradation. Degradation of SIRT2 could eradicate both SIRT2 activities in cells. As such, TM-P4-Thal had increased acetylation level of α-tubulin and fatty acylation level of K-Ras4a, a de-fatty acylation substrate of SIRT2.[60]

### 1.3.3 SIRT3 inhibitors

For SIRT3, there are not many established activators.[61, 62] Instead, there were a couple of inhibitors that were extensively studied. LC-0296 based on glutamic acid with heterocyclic rings inhibited SIRT3 with an $IC_{50}$ of 3.6 μM and a 10-fold selectivity over SIRT2.[63] Treatment of LC-0296 had specifically increased the global acetylation of mitochondrial extract and several SIRT3-specific deacetylation targets, including NDUFA9 and GDH.[63]

YC8-02 is another mechanism-based sirtuin inhibitor based on TM, with 3-aminophenol replacing the aniline, and triphenylphosphine group replacing the Cbz group of TM.[64] With the additional hydroxyl group of 3-aminophenol, YC8-02 simultaneously inhibits SIRT1, SIRT2, and SIRT3 with $IC_{50}$ of 2.8, 0.062, and 0.53 μM, respectively. Because SIRT3 is localized in mitochondria, the triphenylphosphine group, acting as a mitochondrial targeting moiety, helps to direct the inhibitor to the mitochondria and thus increase SIRT3 targeting in cells. After treating DLBLC cells, YC8-02 was detected by mass spectrometry in the purified mitochondria extract,

which confirms the mitochondrial targeting of YC8-02. In addition, increased global acetylation of mitochondria extract was observed upon treatment of YC8-02. Similar treatment with JH-T4, which also inhibits SIRT1, SIRT2, and SIRT3 *in vitro* but does not possess the triphenylphosphine group, did not alter the acetylation level of mitochondria extract.

### 1.3.4 SIRT5 inhibitors

Several SIRT5 inhibitors have been developed, but only a few of them were tested in cellular and mice models. A dipeptide SIRT5 selective inhibitor, DK1-04 contains a lysine with thiourea moiety mimicking the glutaryl group, N-terminal isoleucine, and C-terminal 3-aminophenol.[65] Like TM, DK1-04 inhibits SIRT5 by forming a covalent intermediate with $NAD^+$. DK1-04 selectively inhibited SIRT5 with an IC50 of 0.34 μM. Because the carboxylic acid of DK1-04 hinders the cell permeability, DK1-04e, a pro-drug with an ethyl ester group on the carboxylic acid, was synthesized for biological evaluations. In cells, DK1-04e had increased mitochondrial lysine succinylation, which validates its cellular SIRT5 inhibition.

### 1.3.5 SIRT6 modulators

Many SIRT6 activators have been recently developed and tested in cancer studies. Pyrrolo[1,2-α]quinoxaline-derived UBCS039 activated SIRT6 at $EC_{50}$ of 38 μM by binding to its fatty acyl pocket.[66] UBCS039 also mildly activated SIRT5 2-fold at 100 μM. *In Vitro*, incubation of purified SIRT6 and UBCS039 with full-length histones or complete HeLa nucleosomes significantly decreased in acetylation of H3K18. In H1299 non-small cell lung carcinoma cells, treatment of UBSC039 decreased acetylation of histone H3 K9 and K56, SIRT6 deacetylation targets.[67]

Utilizing the Allosite server, MDL-800 was discovered to activate SIRT6 by binding a pocket around Phe83 and Phe86 residues of SIRT6. MDL-800 activated SIRT6 with an $EC_{50}$ of 10.3 μM and 10-fold selectivity over SIRT2, SIRT5, and SIRT7. In BEL7405 hepatocellular carcinoma cells, MDL-800 decreased the acetylation level of H3K9 and H3K56, previously reported SIRT6 deacetylation substrates. [68]

In addition to the activators, several SIRT6 selective inhibitors have been reported. Quinazolinedione-based Compound 2, 3, and 8 inhibited SIRT6 at $IC_{50}$ of 60, 37, and 49 μM, respectively. Compound 2 mildly inhibited SIRT1 and SIRT2 with $IC_{50}$ of 238 and 159 μM, respectively. Also, Compound 3 mildly inhibited SIRT2 with an $IC_{50}$ of 85 μM. Compound 8 portrayed 5-fold SIRT6 selectivity over SIRT2. For SIRT1, Compound 3 and 8 had shown 11 and 133-fold SIRT6 selectivity. In BxPC-3 pancreatic cells, treatment of Compound 2, 3, and 8 had increased acetylation of H3K9.[69]

Salicylate-based, OSS-128167 had inhibited SIRT6 with an IC50 of 89 μM and 17 and 8-fold selectivity over SIRT1 and SIRT2, respectively. In BxPC-3 pancreatic cells, OSS-128167 had increased the acetylation level of H3K9 and glucose uptake, and decreased TNF-α secretion. These observations were also observed in SIRT6 deficient cells.[70] Later, Compound 5 and 11 were designed to have stronger potency than OSS-128167. These inhibitors had inhibited SIRT6 with $IC_{50}$ of 34 and 22 μM by binding the nicotinamide and substrate pocket. Furthermore, both inhibitors had shown 14-fold selective SIRT6 inhibition over SIRT1 and SIRT2. In BxPC-3 pancreatic cells, Compound 5 and 11 had increased the acetylation level of H3K9.[71] In

this same study, Compound 1 was also reported to inhibit SIRT6 with an $IC_{50}$ of 106 μM. Additionally, Compound 1 inhibited SIRT2 at an $IC_{50}$ of 114 μM. [71] Although Compound 1 inhibited both SIRT1 and SIRT6, Compound 1 had the most suitable physicochemical properties for the *in vivo* studies, as it had moderate oral absorption, aqueous solubility, and metabolic stability.[72]

### 1.3.6 Pan-sirtuin inhibitors

Because sirtuins share similar structures, many modulators simultaneously interact with multiple sirtuins and engender therapeutic benefits in cancers.

Identified in 2006, Cambinol moderately inhibits SIRT1 and 2 through competitive inhibition against histone H4 and noncompetitive inhibition against $NAD^+$. Cambinol inhibited SIRT1 and SIRT2 at $IC_{50}$ of 56 and 59 μM, respectively. In NCI H460 cells, treatment of Cambinol had significantly increased acetylation of p53 and α-tubulin.[73]

Through high-throughput screening and optimization, Sirtinol was identified to inhibit SIRT1 and SIRT2 with $IC_{50}$ of 131 and 58 μM, respectively.[74, 75] However, it failed to increase global acetylation levels of histone and α-tubulin in cells.[74] Salermide contains a reversed amide structure of sirtinol and shows mild SIRT1 and 2 inhibitions. Sirtinol had shown 80% inhibition of SIRT1 and SIRT2 at 100 and 25 μM, respectively. Only in some specific cell lines, Salermide treatment could increase the acetylation of α-tubulin and p53. Also, it could not increase global H4 acetylation levels, a previously reported SIRT2 substrate.[76] Thus, when using Sirtinol and Salermide, additional confirmation will be needed to verify whether the observed effects are due to the sirtuin inhibition.

From screening compounds for p53 activation, Tenovin-6 was discovered to simultaneously inhibit SIRT1 and 2 with $IC_{50}$ of 26 and 9 μM, respectively.[77, 78] In ARN8 melanoma cells, Tenovin-6 increased the acetylation level of p53 and α-tubulin. The increase of acetylation level of α-tubulin by Tenovin-6 was rescued with SIRT2 overexpression.[77] Despite its effective SIRT1 and SIRT2 inhibition, Tenovin-6 may target other proteins in cells. For instance, Tenovin-6 impaired cellular growth of canine hemangiosarcoma cells through a SIRT1-independent mechanism.[79] Tenovin-6's effect in DLBCL cells is also thought to be SIRT1/2/3 independent.[80] Another drawback of Tenovin-6 was its over-toxicity. In a direct comparative study with other SIRT2 inhibitors, even though Tenovin-6 showed the strongest antiproliferative effect, it also killed tested normal epithelial cell lines.[44] Thus, when using Tenovin-6 *in vitro* or *in vivo*, the experiments must be carefully designed, due to its off-target effect and potential over-toxicity issues.

BZD9L1, a highly fluorescent sirtuin inhibitor, inhibited SIRT1 and 2 with $IC_{50}$ of 42.9 and 9 μM, respectively. Based on the docking study with SIRT2, BZD9L1 had occupied where adenosine diphosphate ribose (ADPr) bound. In HCT-116 colorectal cells, BZD9L1 had increased acetylation of p53 after etoposide-induced DNA damage and α-tubulin. Because BZD9L1 possesses intrinsic fluorescence, the cellular distribution of BZD9L1 in HCT-116 and CCD18 colon fibroblasts could be detected using fluorescence microscopy.[81]

N-aryl-N'-3,4-dihydro-2,2-dimethyl-2H-1-benzopyran-4-yl)ureas-derived Compound 18 simultaneously inhibited SIRT1 and 2 with $IC_{50}$ of 6.2 and 4.2, respectively.[82] From the docking study, Compound 18 occupied the SIRT1 activity

pocket with hydrogen bond interactions with Ala262 and His363 and SIRT2 activity pocket with a hydrogen bond interaction with Val233. In U373 and Hs683 glioblastoma, treatment of Compound 18 had increased acetylation of histone H4 and α-tubulin. [82]

Compound 3g, an achiral indole analog of EX-527, showed potent inhibition against both SIRT1 and 2 with $IC_{50}$ of 4.9 and 1 (0.62-1.4) μM, respectively.[83]

MC2494 inhibited all SIRT1-6 with specific $IC_{50}$ of SIRT1 and SIRT2 as 38.5 and 58.6 μM. Upon thermal stress, MC2494 had protected degradation of SIRT1, SIRT2, and SIRT3. In cells, MC2494 had increased not only the global lysine acetylation but also acetylation levels of p53, tubulin, histone H3, and histone H4.[84]

JH-T4 is an analog of TM with a 3-aminophenol group replacing the aniline part of TM.[85] Interestingly, with just one additional hydroxyl group, JH-T4 inhibits SIRT1, 2, and 3. From the docking study with SIRT2, the hydroxyl group forms a hydrogen bond interaction with the protein backbone of the sirtuins, which could have contributed to its simultaneous inhibition. Moreover, JH-T4 inhibits both SIRT2 deacetylase and defatty-acylase, as increased acetylation of α-tubulin and fatty-acylation of K-Ras4a were observed upon treatment of JH-T4.[85]

### 1.4 Cancer

Because sirtuins are involved in a plethora of biological pathways, they could play both tumor suppressor and activator roles.[6, 86] In this section, we will briefly highlight the roles of sirtuins and the modulators in tumorigenesis.

### 1.4.1 SIRT1 inhibitors

SIRT1 could serve as a tumor suppressor as it deacetylates and inactivates various tumor-promoting transcriptional factors. For instance, SIRT1 deacetylates K310 of NF-κB and attenuates its transcriptional activity.[87] This promotes TNF-α induced apoptosis. Also, SIRT1 deacetylates and inactivates HIF-1α, which leads to repression of HIF-1α target genes. In mice, xenografted HT1080 tumors with SIRT1 overexpression formed smaller tumors than the xenografted wild-type HT1080 tumors.[88] Knockdown of SIRT1 in HMLER breast cancer cells had increased metastasis. In the same study, SIRT1 was reported to deacetylate Smad4 and subsequently keep β-catenin interact with E-adherin. This would suppress the epithelial-to-mesenchymal transition.[89]

In contrast, some studies reported SIRT1 as a tumor activator. SIRT1 deacetylates FOXO1 and inhibits FOXO1-induced apoptosis.[90] SIRT1 overexpression increases the expression of c-Myc, a key oncoprotein that increases the expression of many tumor proliferating genes. Furthermore, SIRT1 deacetylates C-Myc to promote its transcriptional activity.[91] SIRT1 deacetylates and represses p53, which exerts antiproliferative effects, including growth arrest, apoptosis, and cell senescence. Deacetylation of p53 also translocates p53 to mitochondria, which suppresses its transcriptional activity.[92] In MCF7 breast cancer cells, overexpression of SIRT1 had increased the proliferation, migration, and motility by increasing the POLD1 expression.[93] The dual role of SIRT1 is also depicted in HCT-116 colorectal cells. Heterozygous deletion of SIRT1 increased c-Myc expression, and thereby promoted tumor growth. Meanwhile, homozygous deletion of SIRT1 promoted apoptosis and

delayed cancer formation.[94] Thus, the role of SIRT1 in cancer may vary depending on the context.

There are only a few reports of EX-527 producing effective anticancer effects as a single agent (see summary in Table 2). In U87MG and LN-299 glioma cells, EX-527 decreased the cellular proliferation and anchorage-independent colony formation through p53 and acetylated-p53 upregulation, and caspase-dependent apoptosis activation.[95] In 5637 and T24 bladder cancer cells, SIRT1 overexpression promoted cell proliferation and GLUT1 expression. Hence, treatment of EX-527 in these cells had an opposite effect, which decreased the proliferation, glycolysis, and glucose uptake.[96]

In contrast, many reports indicate that EX-527 can enhance the sensitivity and show a synergistic effect with other treatments. For instance, by inhibiting the deacetylation of XRCC1, EX-527 increased sensitivity of H460-R cisplatin-resistant lung cancer cells to cisplatin. Overexpression of SIRT1 had rescued such effect, while the knockdown of SIRT1 also made cells vulnerable to cisplatin.[97] In addition, EX-527 impaired the proliferation of several cisplatin-resistant endometrial carcinoma cells, such as HEC151, HEC1B, and HHUA. In HHUA cells, Overexpression of SIRT1 had reversed effect by enhancing the resistant against cisplatin. In the HHUA tumor xenograft mice model, treatment of EX-527 significantly detained the tumor growth.[98] In PC-3 prostate cancer SIRT1 knockdown or EX-527 have increased the effect of vesicular stomatitis virus oncolysis treatment.[99] In chemoresistant stem-like cells from leukemia K562 cells, EX-527 or SIRT1 knockdown increased the effect of Hsp90 inhibitors like 17-AAG and AUY922. SIRT1 inhibition or depletion decreased

expression of heat shock proteins, and consequently increased the effects of Hsp90 inhibitors.[100] EX-527 and SIRT1 knockdown also induced a synergistic anticancer effect with MK-1775, a WEE1 inhibitor. In both cellular and xenograft mice models, treatment of EX-527 and MK-1775 suppressed the growth of A549 lung cancer cells. Meanwhile, a single treatment of EX-527 or MK-1775 did not affect the growth. Mechanistically, SIRT1 can deacetylate and inhibit NBS1 and Rad51 in homologous recombination repair. Thus, the combination of EX-527 and MK-1775 induced complete damage in the DNA replication process.[101] Lastly, in PANC-1 pancreatic cancer cells, EX-527 itself had decreased proliferation, and synergistically increased the antiproliferative effect of gemcitabine. However, in PANC-1 tumor xenograft mice, EX-527 promoted tumor growth and did not show any additive or synergistic effect with gemcitabine.[102]

### 1.4.2 SIRT2 inhibitors

Although SIRT2 was initially reported to be a tumor suppressor, as *Sirt2* knockout mice developed more tumors than wild-type mice as they age.[103] However, this effect is relatively weak as the mice only developed tumors when they reach about one year old. Also, this observation could depend on the strain, as another study did not observe this phenotype.[104] More evidence links SIRT2 as a tumor activator. SIRT2 deacetylates and stabilizes several oncoproteins. SIRT2 deacetylates and promotes KRAS activity, thereby inducing cell proliferation, colony formation, and tumor growth.[105] Also, SIRT2 deacetylates K116 of Slug, which subsequently stimulates the growth of basal-like breast cancer.[106] In addition, SIRT2-induced deacetylation of C-Myc promotes pancreatic cancer cell proliferation.[107] SIRT2 deacetylates and activates

LDH-A, which is responsible for lactate production in cancer cell growth.[108] In addition, SIRT2 interrupts FOXO1's interaction with ATG7 and inhibits apoptosis.[109] Through removal of a long-chain fatty acyl group on lysine, SIRT2 regulates K-Ras4a transformation activity and promotes cell migration via ARF6.[110, 111] With more reports highlighting SIRT2 as a tumor activator, numerous SIRT2 inhibitors have been developed and evaluated in cancer models (Table 3 and Table 4).

The earliest SIRT2 selective inhibitors, AGK2 was developed from high-throughput screening of a small-molecule library.[43] Consistent with the SIRT2 knockdown results, AGK-2 treatment inhibited the colony formation and induced apoptosis in GB2, GB4, GB11, and GB16 primary glioblastoma cells. In SIRT2 knockdown GB2 cells, AGK2 did not show any antiproliferative effect, which further confirms the SIRT2 selective inhibition of AGK2 in cells.[112] Due to the toxicity and impermeable blood-brain barrier characteristics of AGK2, another SIRT2 inhibitor, AK7 was tested in GB2 tumor xenograft mice models. After intraperitoneal injection of AK7, a significant impediment of tumor growth was observed. Mice with transplants of GB2 and GB16 SIRT2 knockout cells had survived longer and had shown less tumorigenicity than mice with transplants GB2 and GB16 SIRT2 wild-type cells. This had further confirmed that antitumor effect of AK-7 in this study is through SIRT2 purtubation.[112] In HCT-116 colorectal cancer cells with wild-type TP53 expression, AGK2 treatment decreased the effects of several chemotherapeutic drugs, including cisplatin, 5-fluorouracil, oxaliplatin, gefitinib, LY294002, and metformin. However, in SW620 colorectal cancer cells with mutant TP53 expression, AGK2 treatment enhanced the anticancer effects of these chemotherapeutic drugs.[113]

Through selective SIRT2 inhibition, SirReal2 decreased the migration and invasion of HGC-27 and MGC-803 gastric cancer cells. SirReal2 inhibited SIRT2 from deacetylating PEPCK1, which promoted degradation of PEPCK1 and decreased mitochondrial metabolism. As a result, the migration activity of gastric cells was impaired. HGC-27 and MGC-803 with SIRT2 knockdown showed less invasion activities, consistent with the inhibition results. Also, tumor xenograft of SIRT2 knockdown gastric cancer cells in mice formed less metastatic tumors and showed slower growth than that of SIRT2 wild type cells.[114] In a comparison study of SIRT2 inhibitors, SirReal2 showed antiproliferative effects in breast, colorectal, lung, lymphoma, and cervical cancer cells.[44]

In MCF7 breast cancer cells, the treatment of RK-9123016 increased the acetylated eIF5a level and hindered cell proliferation through degradation of c-Myc.[48]

NCO-90 and NCO-141 induced apoptosis and mitochondrial superoxide level in leukemic cells, such as HTLV-1-transformed T-cells.[115] In S1T, MT-2, Jurkat, and HL60 leukemia cells, NCO-90 and NCO-141 increased acetylation of histone H4, a previously reported SIRT2 substrate, but did not alter acetylation of p53. This confirmed that these compounds inhibited SIRT2, but not SIRT1, in cells. In addition, the treatment of NCO-90 and NCO-141 increased LC-II expression level and autophagosome, which could have induced autophagic cell death.[115] KPM-2, a pan SIRT1-3 inhibitor designed from NCO-90, impaired proliferation of MDA-MB-231 breast cancer cells. In the same study, Compound 9, an inhibitor with a similar structure as KPM-2 which shows 11-fold SIRT1 selective inhibition over SIRT2 did not show any antiproliferative effect. Also, Compound 6, a weaker SIRT2 selective

inhibitor with a similar structure as KPM-2 showed weaker cytotoxicity than KPM-2. Overall, both results confirmed that the cytotoxicity of KPM-2 is strongly correlated to its SIRT2 inhibition.[50]

In PANC-1 pancreatic cancer cells, NPD11033 not only decreased cell proliferation but also increased the acetylation level of eIF5a, a SIRT2 deacetylation substrate.[52] Knockdown of SIRT2 in PANC-1 cells also decreased cell proliferation. In addition, an inactive analog RK-0310020 did not show any antiproliferative effect in PANC-1 cells, which further supports that SIRT2 inhibition by NDP11033 induces its anticancer effect.[52]

Chroman-4-one and chromone-based SIRT2 inhibitors, Compound 6f and 12a impaired cellular proliferation of MCF7 breast cancer and A549 lung cancer cells. In addition, treatment of Compound 12a in these two cell lines led to cell cycle arrest in G1/G0 phase. Treatment of Compound 6f also showed similar results, but to less extent. In MCF7 cells, both Compound 6f and 12a had increased acetylation level of α-tubulin, a SIRT2 deacetylation target.[53]

Compound 35 induced apoptosis in NB4 and K562, and MDA-MB-231 breast cancer cells, and decreased cell proliferation of NB4, Karpas299, and MV4-11 leukemia cells.[54] Moreover, Compound 39 showed a broader anticancer effect in U937, HL-60, NB4, OCI-AML3, IMS-M2, OCI-AML2, MV4-11, Kasumi-1, and Karpass299 leukemia cells.[54]

In H441 non-small lung cancer cells, treatment of Compound 24a increased the acetylation level of α-tubulin, and decreased cell proliferation and migration.[55]

A mechanism-based SIRT2 inhibitor, TM showed broad anticancer effect in most of cancer cell lines from NCI-60 screening. These affected cancer cell types include leukemia, non-small lung cancer, colorectal, melanoma, ovarian, renal, prostate, breast, and central nervous system cancer cells. SIRT2 knockdown in MCF7, MDA-MB-468, and MDA-MB-231 breast cancer cells reduced the cell proliferation, confirming that SIRT2 inhibition or perturbation induces cytotoxicity. Interestingly, the control compound, M, which differs from TM just by one atom and could not inhibit SIRT2, does not have anticancer activity. These evidences further confirm that the anticancer activity is through SIRT2 inhibition. The anticancer effect of TM is at least partially through the promotion of c-Myc degradation and SIRT2 knockdown also had induced degradation of c-Myc in MCF7 cells. The treatment of TM did not impede the cellular proliferation of MCF-10A and HME1, normal breast epithelial cells. This suggests that TM treatment selectively impacts cancer cell proliferation. The intraperitoneal injection of TM significantly delayed breast cancer tumor growths in MDA-MB-231 xenograft and genetic MMTV-PyMT mice models without significant weight loss or other obvious toxicity.[56]

A derivative of TM, AF8 also showed a broad anticancer effect in breast, pancreatic, lung, and colorectal cancer cells. Also, AF8 inhibited the 3D anchorage-independent colony formation of HCT-116 colorectal cancer cells. Furthermore, treatment of AF8 had significantly reduced the tumor growth of HCT-116 tumor xenograft mice models in a dose-dependent manner.[58]

In breast, colorectal, cervical, lung, pancreatic, and glioblastoma cancer cells, low concentrations of NH4-6 and NH4-13 showed weaker cytotoxicity than TM, most

likely due to their poor permeability from the charged trimethylamine moiety. However, in these cancer cells, higher concentrations of both inhibitors showed stronger cytotoxicity than TM, due to their improved aqueous solubility overriding their poor permeability. Furthermore, NH4-6 hindered the cellular proliferation of these cancer cells slightly more potent than NH4-13. In HCT-116 colorectal tumor xenograft mice model, daily treatment of 50 mg/kg NH4-6 caused severe toxicity, while the same dosage of NH4-13 did not alter the overall health. Furthermore, 30 mg/kg every other day injection of NH4-6 and NH4-13 for two weeks delayed tumor growth similarly. Daily treatment of 50 mg/kg NH4-13 showed a stronger anticancer effect. Overall, NH4-6 and NH4-13 had similar anticancer but NH4-13 due to its SIRT2 selectivity, has much lower toxicity *in vivo*. Therefore, it could be advantageous to use SIRT2-selective inhibitors to treat cancers.[116]

Through selective degradation of SIRT2, TM-P4-Thal treatment increased the acetylation level of α-tubulin and fatty acylation level of K-Ras4a. Consequently, TM-P4-Thal showed a stronger antiproliferative effect in MCF7 and MDA-MB-231 breast cancer cells than TM at lower concentrations.[60]

### 1.4.3 SIRT3 inhibitors

SIRT3 regulates various mitochondrial functions, such as ATP generation, metabolism and reactive oxygen species stabilization.[6, 8, 117] For example, SIRT3 deacetylates and activates glutamate dehydrogenase, a mitochondrial enzyme that converts glutamate to α-ketoglutarate and controls the ATP/ADP ratio.[118, 119] In the beginning, many studies reported SIRT3 as a tumor suppressor. SIRT3 attenuates the stabilization of HIF1α and regulates metabolic reprogramming.[120, 121] In breast cancer

cell lines, SIRT3 is often less expressed, and the overexpression SIRT3 suppresses glycolysis and cell proliferation.[121] Patient clinical data also confirmed this trend, as most breast cancer patients had significantly lower SIRT3 expression levels.[122] Furthermore, SIRT3 knockout mice developed larger mammary gland tumors than the SIRT3 wild-type mice. In fact, SIRT3 WT mice did not develop any mammary tumors.[121]

In contrast, many studies reported SIRT3 as a tumor activator. In bladder cancer cells, SIRT3 deacetylates and inactivates p53, which subsequently promotes cellular proliferation.[123] Also, oral squamous cell carcinoma cells and tissues expressed higher SIRT3 levels.[124] Diffusive large B cell lymphomas (DLBCL) required SIRT3 for anaplerotic metabolism, growth, survival, and autophagy. Furthermore, SIRT3 knockdown in DLBCL cells and mice significantly impaired cell proliferation and tumor growth.[64] As such, the role of SIRT3 is likely context and cancer type dependent.

By increasing reactive oxygen species (ROS) levels, LC-0296 reduced cell proliferation and promoted apoptosis of UM-SCC-1 and UM-SCC-17B HNSCC cells (Table 5). Meanwhile, LC-0296 did not affect the cell proliferation of normal human oral keratinocytes. Even though these HNSCC cells are resistant to radiation and cisplatin, LC-0296 had enhanced effects of these treatments in HNSCC cells. In UM-SCC-17B cells, LC-2096 had increased acetylation levels of NDUFA9 and GDH, SIRT3 deacetylation substrates, and thereby enhanced ROS levels.[63]

Treatment of YC8-02 decreased cellular proliferation of OCL-LY1, HBL1, Pfeiffer, SU-DHL4, TMD3, Karpas 422, and OCL-LY7 lymphoma cells (Table 5). In

a Karpas 422 tumor xenograft model, YC8-02 had significantly impeded the tumor growths. Knockdown of SIRT3 in Karpas422, OCI-LY1, and HBL1 cells had impaired cellular proliferation, and xenografted tumors of Karpas422 with knockdown SIRT3 in mice had slower growth. These knockdown results had further confirmed the therapeutic benefits of YC8-02 and targeting SIRT3 in DLBCLs.[64]

### 1.4.4 SIRT5 inhibitors

Many reports showed that SIRT5 has pro-tumor role. The SIRT5 mRNA level is often amplified in tumors than in normal tissues.[125, 126] SIRT5 regulates several metabolic pathways important in cancer, such as glycolysis, TCA cycles, and urea cycles. For instance, SIRT5 demalonylates GAPDH to activate glycolysis.[17] Under oxidative stress, SIRT5 desuccinylates PKM2 to decrease the overall carbon flux in TCA cycles.[127] SIRT5 also activates LDHB, which induces autophagy and cell proliferation of HCT-116 colorectal cancer cells.[128] Also, overexpression of SIRT5 in hepatocellular carcinoma cells promotes cell proliferation.[129] In breast cancer cells, SIRT5 desuccinylates and stabilizes glutaminase, which regulates the overall glutaminolysis, a key metabolic hallmark of cancers. In MDA-MB-231 and MDA-MB-468 breast, and A-549 lung cancer cells, knockdown of SIRT5 decreases cell proliferation and anchorage-independent colony formations. Moreover, in mice xenograft studies, SIRT5-deficient MDA-MB-231 tumors were significantly smaller than wild-type tumors.[130] In HCT-116 colorectal cancer cells, SIRT5 removes succinyl groups from K393 and K395 of citrate synthase. The hypersuccinylation of citrate synthase decreases cell proliferation and migration, which supports the tumorigenic role of SIRT5.[131] Lastly, SIRT5 promotes the proliferation of cutaneous melanoma

genotypes, including uveal melanoma. In the A2058 melanoma tumor xenograft model, SIRT5 depletion significantly delayed the tumor growth.[132]

In MCF7 and MDA-MB-231 breast cancer cells, treatment of DK1-04e inhibited both cell proliferation and anchorage-independent colony formation (Table 5). Furthermore, DK1-04e had increased mitochondrial global succinylation in MCF7 cells. In both MMTV-PyMT and MDA-MB-231 tumor xenograft mice models, DK1-04e had significantly impaired the tumor growth without any bodyweight loss. The cytotoxicity of DK-104e was dependent on its SIRT5 inhibition. SIRT5 partial knockout in MDA-MB-231 cells have impaired anchorage-independent colony formation. Furthermore, *Sirt5* deletion PyMT mice had slower tumor growth and less metastasis. DK1-04e (O), an inactive derivative with an oxygen atom instead of the sulfur, showed weaker cytotoxicity than DK-104e. Overall, DK1-04e studies showed that SIRT5 inhibition can be an effective treatment in breast cancer cells.[65]

### 1.4.5 SIRT6 modulators

Through deacetylation and defatty-acylation, SIRT6 regulates numerous biological roles, including cell proliferation, DNA repair, and glucose metabolism.[7, 10] SIRT6 deacetylates histone H3K9, H3K18, and H3K56 to suppress the expression of several transcriptional factors, such as c-Jun, and NF-κB.[133-137] SIRT6 removes fatty acyl groups from TNF-α to promote its secretion.[138] In cancers, SIRT6 is also viewed as a both tumor activator and a tumor suppressor. As a tumor activator, SIRT6 promotes cell cycle and tumor proliferation while inhibiting apoptosis.[139, 140] In the esophagus, thyroid, and melanocytes, SIRT6 is expressed higher than in normal tissues.[140] SIRT6 attenuates migration and invasion of ovarian cancer cells.[141] As a

tumor suppressor, SIRT6 is down-regulated in colorectal, ovarian, breast, lung, pancreatic, and hepatocellular tumors.[142-144] Also, SIRT6 deficient MEF cells proliferate faster than control wild-type cells. In the same study, loss of SIRT6 induced faster tumor formations in mice. In colorectal cancer stem cells, SIRT6 impaired cellular proliferation and anchorage-independent colony formation.[145] Furthermore, through defatty-acylating, SIRT6 regulates R-Ras2 localization, and subsequently hinders cell proliferation.[146]

The SIRT6 modulators' effect in cancer cells is summarized in Table 6. UBCS039 induced autophagosome accumulation, thereby leading to apoptosis. UBCS060, an inactive analog of UBCS039, could not increase the autophagosome accumulation and autophagy-induced apoptosis.[66] A previous report suggested lack of SIRT6 had decreased oxygen consumption and ATP level in the heart.[147] In accordance with this, treatment of UBSC039 activated ROS production and increased ATP level in H1299 and HeLa cells.[67]

MDL-800 significantly suppressed proliferation of BEL7405 cells *in vitro* and in tumor xenograft mice studies.[68] Also, MDL-800 had arrested cell cycle in G0/G1 phase, as p21 and p27 expressions have increased, and CDK2, CDK4, cyclin D1, and cyclin D3 levels have decreased. To confirm whether the effect of MDL-800 depend on SIRT6 activation, SIRT6 knockout BEL6405 cells were treated with MDL-800. In these SIRT6 knockout cells, treatment of MDL-800 did not change any of the previously observed markers for the cell cycle arrest, which confirmed that the effect of MDL-800 is through SIRT6 activation.[68] In addition to the hepatocellular carcinoma cells, MDL-800 inhibited the proliferation of 12 non-small cell lung cancer

(NSCLC) cells from the NCI-60 screening. MDL-800 did not affect the proliferation of SIRT6-knockout HCC827 and PC9 NSCLC cells, which confirmed the on-target activation of SIRT6 by MDL-800. In the HCC827 tumor xenograft mice study, administration of MDL-800 had increased histone H3 acetylation and significantly decreased the tumor growth.[148]

In specific conditions, several SIRT6 inhibitors showed antiproliferative effects. As mentioned, Compound 2, 3, and 8 increased H3K9 acetylation in BxPC-3 pancreatic cancer cells.[69] Also, Compound 3 and 8 increased the glucose uptake in both BxPC-3 and L6 myoblasts. Among these three, only Compound 8 showed antiproliferative effect against BxPC-3 cells. Interestingly, Compound 2 and 3 showed synergistic effect with gemcitabine against proliferation of BxPC-3 cells.[69]

Compound 5 and 11 promoted glucose uptake and inhibited TNF-α production. Even though Compound 5 and 11 were not toxic, both SIRT6 inhibitors with gemcitabine had shown a stronger anticancer effect in BxPC-3 cell proliferation. In the pharmacokinetics study, as Compound 5 showed a relatively short half-life, additional modifications on this compound are needed to improve the bioavailability, which will allow more accurate assessment in animal studies.[71]

### 1.4.6 Pan-sirtuin inhibitors

In NCI-H460 lung cancer and HeLa cervical cancer cells, treatment of Cambinol increased acetylation levels of several sirtuin substrates, including p53, α-tubulin, FOXO3a, and Ku70.[73] Also, in RPMI8226 and U266 multiple myeloma cells treatment of Cambinol induced apoptosis, cell proliferation impairment, and cell cycle arrest by increasing acetyl p53, p21, cleaved PARP, and cleaved caspase3.[149] In

orthopedic tumor xenograft mice model with HepG2 hepatocarcinoma cells, Cambinol had significantly reduced tumor growth, which was consistent with the SIRT1 knockdown results of *in vivo* intrahepatic xenograft mouse model.[150] Also, it was reported that SIRT1 stabilizes N-Myc protein and promote neuroblastoma cell proliferation. Thus, the knockout SIRT1 BE(2)-C cells had lower N-Myc level than the wild-type cells. In accordance with this, Cambinol treatment in TH-MYCN transgenic mice had decreased neuroblastoma formation.[150, 151] In HepG2 and Huh7 hepatocarcinoma cells, compared to a single treatment of sorafenib, a combination of Cambinol and sorafenib showed an enhanced effect in reducing cell proliferation, migration, and invasion.[152]

In MCF7 breast and H1299 non-small lung cancer cells, treatment of Sirtinol led to senescence-like growth arrest and decreased activation of the RAS-MAPK pathway. Similar results were also observed with SIRT1 knockdown.[153] Furthermore, Sirtinol reduced cell proliferation of H1299 non-small lung, PC3 prostrate, DU145 prostate, HeLa cervical, S1T adult T-cell leukemia/lymphoma (ATL), and Jurkat ATL cancer cells.[154-156] In PC3, DU145, S1T and Jurkat cells, knockdown of SIRT1 also hindered cell proliferation.[155, 156] Combination treatment of sodium dichloroacetic acid (DCA) and Sirtinol led to synergistic anticancer effect in A549 and H129 NSCLC cells *in vitro*, and *in vivo* A549 tumor xenograft mice model.[157]

Through SIRT1 inhibition, Salermide induced apoptosis in MOL4 acute lymphoblastic leukemia, SW480 colorectal, KG-1a acute myelogenous leukemia, and Raji Burkitt's lymphoma cells. Based on the knockdown studies of SIRT1 and 2, Salermide-induced apoptosis is mainly through its SIRT1 inhibition.[76] Furthermore,

Salermide showed strong anti-proliferative effects in BE(2)-C neuroblastoma and MIA-PaCa-2 pancreatic cancer cells, consistent with the results from SIRT2 knockdown. Furthermore, SIRT2 knockdown and 50 μM of Salermide in these cell lines induced n-Myc and c-Myc degradation.[107]

In both cellular and tumor xenograft mice studies, treatment of Tenovin-6 showed strong antiproliferative effects against ARN8 melanoma cells. [77] In AGS, AGS-EBV, SNU-179, HGC-27, N87, SNU-1, and KATO-III gastric cancer cells, Tenovin-6 had decreased the cell proliferation. Moreover, Tenovin-6 hindered cell proliferation anchorage-independent colony formation of AGS, AGS-EBV, and HGC-27 through increasing acetyl p53 levels.[158] In A549 NSLCL cells, a combination of Tenovin-6 and metformin demonstrated a synergistic antiproliferative effect by HIC1-dependent SIRT1 level reduction.[159] By increasing the expression of p53 and ROS level, Tenovin-6 also attenuated migration and proliferation of 92.1, Mel-270, Omm-1, and Omm-2.3 uveal melanoma (UM) cells. Also, in 92.1, and Mel-270 cells, Tenovin-6 had a synergistic effect with Vinblastine, a chemotherapeutic agent for UM patients.[160]

BZD9L1 showed antiproliferative effects in HCT-116 colorectal, CCRF-CEM leukemia, and MDA-MB-468 breast cancer cells in a preliminary screening.[161] Furthermore, in HCT-116 and HT-29 colorectal cancer cells, BZD9L1 significantly decreased the cell migration and anchorage-independent colony formation.[161] Only in HCT-116 cells, BZD9L1 showed a synergistic anticancer effect with 5-Fluorouracil, a conventional chemotherapeutic agent. The combination of BZD9L1 and 5-Fluorouracil increased cell cycle, arrest, and apoptosis, while it decreased the spheroid

proliferation. In addition, the combination treatment of BZD9L1 and 5-Fluorouracil significantly impaired tumor growth of HCT-116 in tumor xenograft mice study.[162]

In U373 and Hs683 glioma cells, treatment of Compound 18 had increased acetylation levels of histone H4, histone H3K56, and α-tubulin, which confirmed cellular inhibition of SIRT1 and 2.[82] Consistent with the SIRT1 and 2 knockdown results, Compound 18 had impaired cell proliferation of U373 and Hs683 cells. Moreover, Compound 18 showed a broad anticancer effect, as its average $GI_{50}$ was about 3 μM in the NCI-60 screening. In the zebrafish xenotransplant model, Compound 18 treatment significantly reduced the growth of fluorescent-labeled HS683 and U373 tumors.[82]

Compound 3g exerted stronger cytotoxicity than EX-527 in several cancer cell lines, K562 leukemia, HCT-116 colorectal, HT-29 colorectal, H460 lung, A549 lung, and MCF7 breast cancer cells. Such increased potency of Compound 3g from EX-527 could come from the dual inhibition of SIRT1 and 2, but this was not confirmed in the study. Thus, future study proving cellular inhibition of SIRT1 and 2 by Compound 3g will be needed.[83]

A SIRT1-3 inhibitor, MC2494 decreased metabolic activity and proliferation of U937 leukemia cells.[163] Treatment of MC2494 decreased ATP production and expression levels of PGC1α and PGC1β, which are important for metabolism regulation. In addition, PGC1α is present in the cytoplasm under normal condition, but more perinuclear PGC1α was detected, after treatment of MC2494.[163]

JH-T4, a mechanism-based SIRT1-3 inhibitor, portrayed strong antiproliferative effects in a wide range of cancer cells, including MCF7 breast, MDA-

MB-231 breast, HCT-116 colorectal, and NCI-H23 lung cancer cells. However, JH-T4 also affected the proliferation of normal epithelial cells like HME1 and MCF-10A. Thus, usage of JH-T4 may cause an over-toxicity problem in animal studies.[85]

## 1.5 Neurological Diseases

### 1.5.1 SIRT1 inhibitors

**.** Both protective and detrimental effects of SIRT1 in neurological diseases have been reported. SIRT1 inhibits neurogenesis through inhibiting transcriptional factor Hes1 and Mash1.[164] SIRT1 maintains cognitive level and synaptic plasticity.[165] The brain of SIRT1 knockout mice looked normal but showed a significant decrease in dendritic extension, length, and complexity.[165] SIRT1 is also reported to promote neurite outgrowth through suppressing expression and phosphorylation of mTOR.[166] The parietal cortex of Alzheimer's disease patients showed lower expression of SIRT1, which may be connected to an increase of β-amyloid and tau.[167] Inhibiting NF-κB in β-amyloid plaques, SIRT1 hinders neuronal cell death.[168] Overexpression of SIRT1 decreases acetylation of FOXO3a, and consequently protects against huntingtin toxicity.[169] These reports highlights the beneficial effects of SIRT1 in the neurological system.

In contrast, other reports also point to the negative impacts of SIRT1 in neurological diseases. Knockdown of SIRT1 fostered neurogenesis of P19 embryonic carcinoma cells, Inhibiting SIRT1, EX-527 also promoted the differentiation of P19 cells into functional neurons with around 50% efficiency.[170] In single prolonged stress (SPS) mice mimicking post-traumatic stress disorder (PTSD), *Sirt1* deleted mice had less anxiety and freezing time, which indicated SIRT1 as a potential therapeutic target

for PTSD. Osmotic delivery of EX-527 to ventral CA1 of hippocampus had deactivated helix-loop-helix transcription factor 2 and subsequently hindered the expression of MAO-A. This further led to the stabilization of serotonin. In addition, the treatment of EX-527 ensured normal neuronal plasticity by decreasing dendritic spines and abnormal shapes.[171] Injection of EX-527 to the ventrolateral orbital cortex had ameliorated morphine addiction of rats. Morphine injected rats had elevated SIRT1 expression level, which got diminished with the administration of EX-527.[172] Lastly, in the rat model of middle cerebral artery occlusion, which simulates cerebral ischemia-reperfusion injury, EX-527 enhanced the survival rate and decreased cerebral infarction volume.[173]

In the subarachnoid hemorrhage rat model, Sirtinol treatment lowered SIRT1 expression, which further induced damage of the blood-brain barrier and neurological ability. In addition, Sirtinol aggravated brain edema and increased endothelial cell apoptosis.[174] Thus, for subarachnoid hemorrhage, a SIRT1 activator will be needed for an effective treatment.

### 1.5.2 SIRT2 inhibitors

Through deacetylation of α-tubulin and activation of the CREB signaling pathway, SIRT2 promotes neuronal differentiation of mesenchymal stem cells.[175] In oligodendroglia and myelin sheets, SIRT2 is often highly expressed.[176] Through increasing the expression level of myelin basic proteins and, SIRT2 boosts oligodendroglia differentiation.[177] Also, because of the acetylated FOXO3a level and decreased Bim expression, SIRT2 knockout mice showed resistance against 1-methyl-

4-phenyl-1,2,3,6-tetrahydropyridine (MPTP), which induces neurotoxicity like Parkinson's Disease.[178]

The SIRT2 inhibitor AGK2 showed a neuroprotective effect in Parkinson's Disease models. Releasing adenylate kinase to the media, AGK2 reduced α-Synuclein-mediated toxicity. α-Synuclein toxicity was decreased by SIRT2 knockdown in neuroglioma cells, which verified that the effect of AGK2 comes from its SIRT2 inhibition. Also, AGK2 treatment had increased viabilities of dopamine neurons in cellular and drosophila models.[43] In mice, AGK2 ameliorated lipopolysaccharides (LPS)-induced neuroinflammation, decreasing LPS-induced CD11b TNF-α, and IL-6 levels. AGK2 treatment in mice decreased TUNEL signals, which are indicators of brain apoptotic damage[179]. In the middle cerebral artery occlusion (MCAO) mice model simulating focal ischemic stroke, AGK2 administration lowered cleaved-caspase 3, Bim, and Bad, which consequently hindered apoptosis. [180] Lastly, in cultured hippocampal neurons, AGK2 protected cell deaths from exposure to $H_2O_2$. Also, in the same study, AGK2 had promoted VEGF and HO-1 mRNA levels, which stimulates neuroprotection against ischemic injury. This result was consistent from the experiments with SIRT2 knockout DT40 cells.[181]

In the MCAO mouse model, a SIRT2 selective inhibitor AK-7 had decreased the infarction volume and promoted neurological recovery. Moreover, AK-7 increased the activation of a MAP kinase, p38, *in vitro* and *in vivo*, which led to the neuroprotection from the ischemic injury. Knockdown of SIRT2 also activated p83 in Neuro-2a cells.[182] In the microglia from the sevoflurane-treated neonatal rat study, AK-7 decreased pro-inflammatory markers, while increasing anti-inflammatory

markers. Sevoflurane is used as an inhalational anesthetic, which could damage the developing brain.[183]

A nicotinamide-derived SIRT2 selective inhibitor, NCO-141 treatment had increased spatial learning and memory deficiency of 5-month-old senesce-accelerated mouse prone-8 (SAMP8) mice, which mimics Alzheimer's disease. For 8-month-old SAMP8 mice, NCO-141 treatment did not indicate any therapeutic results. Nevertheless, in both aged groups, NCO-141 had increased glutamate receptor subunits GluN2A, GluN2B, and GluA1, which are essential for synaptic plasticity. To confirm whether NCO-141 inhibited SIRT2 in hippocampus, ATP-binding cassette transporter Abca1 expression level was measured, as transcription of Abca1 is inhibited by SIRT2. As expected, NCO-141 treated SAMP8 mice had elevated level of Abca1.[184]

NCO-90-based SIRT2 inhibitor Compound 53 and pan SIRT1-3 inhibitor KPM-2 had significantly promoted neurite outgrowth of Neuro-2a cells.[50, 51]

### 1.5.3 SIRT6 inhibitors

SIRT6 regulates stem cell differentiation and neuroectoderm development through its deacetylation of histone H3. SIRT6 knockout mice showed higher expressions of Oct4, Sox2, and Nanog, which are important for stem cell pluripotency. Consequently, this led to higher expression of Tet enzymes, which produces 5-hydroxymethylcytosine. With increased 5-hydroxymethylcytosine, more embryonic stem cells have differentiated into neuroectoderm. When SIRT6 was present, expressions of Oct4, Sox2, and Nanog were repressed, and led to balanced differentiation of embryonic stem cells. [185] For immunity and inflammation, SIRT6

de-fatty acylates TNFα and promotes its secretion. This could potentially regulate inflammatory cytokine production and necrosis. [138] Mice with brains without SIRT6 showed behavioral abnormalities with DNA damage and increased phosphorylated Tau. Also, in patients with Alzheimer's disease, lower expression of SIRT6 was measured, which hints the neuroprotective role of SIRT6.[186] Lastly, SIRT6 promotes the differentiation of dendritic cells *in vitro* and *in vivo*.[187]

Compound 1 is a SIRT6 inhibitor that had shown therapeutic effect in autoimmune encephalomyelitis (EAE), an animal model of multiple sclerosis.[188] In a previous study, Compound 1 had increased glucose uptake and GLUT-1 expression, and decreased TNF-α in BxPC-3 pancreatic cancer cells. These observations indicate a potent cellular SIRT6 inhibition by Compound 1.[70] In C57bl/6 mice with MOG35-55 injection, which mimics EAE conditions, treatment of Compound 1 decreased the levels of TNFα and neurological impairments. Compound 1 also lowered IFNγ and IL12, which induce Th1 immune responses. Moreover, Compound 1 increased IL10, a cytokine with an anti-inflammatory effect, in the spinal cord. In dendritic cells, treatment of Compound 1 decreased cell migration.[188]

Since SIRT6 inhibitors may affect the development of neurological disorder, assessing SIRT6 activators in neurological disease models will be interesting, but so far there has been no report on this direction.

## 1.6 Cardiovascular Diseases

### 1.6.1 SIRT1/SIRT2 inhibitors

In addition to cancer and neurological disease, several sirtuins have been connected to cardiovascular diseases. Without SIRT1, mice possess congenital cardiac

abnormalities, and most could not survive beyond 2 weeks.[189] SIRT1 deacetylates and regulates sodium channel Nav1.5. Deficiency of SIRT1 decreased expression of Nav1.5 in the cardiomyocyte membrane and induced cardiac abnormalities.[190] Low to moderate overexpression of SIRT1 in transgenic mouse inhibited fibrosis and cardiac hypertrophy. However, high overexpression of SIRT1 aggravated hypertrophy.[191]

After Sirtinol treatment, neonatal rats showed a decrease in cardiomyocytes. In the same model, SIRT1 overexpression increased cardiomyocytes. Also, in the late phase of cardiac ischemia preconditioning in rats, treatment of Sirtinol significantly increased the infarct size, which made them more prone to the ischemia injury.[192] Splitomicin, a yeast sirtuin inhibitor, had promoted carotid artery thrombus formation in a photochemical injury mice study. In human endothelial cells, both SIRT1 siRNA and Splitomicin had increased and activated tissue factor protein which promotes coagulation and thrombus formation. As the SIRT1 inhibitor worsens cardiovascular diseases, a reliable SIRT1 activator may be needed for the therapeutic benefit.[193] The potential cardiovascular effect of SIRT1 inhibitors may also limit the use of them for treating other diseases.

### 1.6.2 SIRT6 inhibitors

SIRT6 suppresses IGF-Akt signaling, which promotes heart failure when activated. SIRT6 knockout mice promoted cardiac hypertrophy upon hypertrophic stimulus. [137] In a mouse model of transverse aortic constriction (TAC)-induced heart failure, SIRT6 maintained telomere integrity, thereby protecting the heart. Also, the knockout of SIRT6 promoted macrophage and atherosclerosis.[194]

Consistent with the role of SIRT6 to prevent cardiovascular diseases, a SIRT6 inhibitor, OSS-128267, intensified diabetic cardiomyopathy (DCM). In a separate study using BxPC-3 pancreatic cells, OSS-128267 increased glucose uptake and GLUT-1 expression, and decreased TNF-α, which suggests potent inhibition of SIRT6.[70] In the mice model of streptozotocin-induced diabetes and high glucose-treated cardiomyocytes, OSS-129167 promoted inflammation and oxidative stress, which led to diabetes-induced cardiomyocyte apoptosis.[195] In this DCM disease model, treatment of SIRT6 activators like MDL-800 or UBCS039 may be beneficial.

## 1.7 Concluding Remarks

In this review, we have summarized the effects of various sirtuin modulators in cancer, neurological, and cardiovascular diseases. We anticipate that this review can help the readers to choose a suitable sirtuin modulator in different disease models. Overall, although there may be a few contradicting reports, some general trends can be extracted from the majority of the literature. SIRT2 and SIRT5 inhibitors showed rather consistent and promising effect in treating cancers. SIRT2 inhibitors have also showed beneficial effects in neurological diseases. On the other hand, SIRT1 and SIRT6 inhibitors have aggravated cardiovascular diseases, which underlines the need for a reliable SIRT1 and SIRT6 activators. These generalized trends support that the development of sirtuin modulators with enhanced potency and selectivity will be essential to further validate the preclinical data and explore the potential for treating various human diseases.

**Table 1. Summary of the sirtuin modulators and its biological assessment in cellular and animal studies.**

| Compound | Structure | Modulation Profile | Cellular Studies | Animal Studies | References |
|---|---|---|---|---|---|
| **EX-527/ Selistat** | 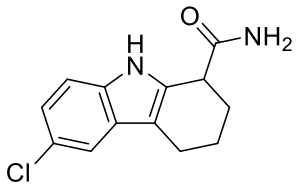 | Inhibits SIRT1 with 200-fold selectivity over SIRT2 | - **General:** increases several SIRT1 deacetylation targets, including p53, NBS, and Rad1<br>- **U87MG and LN0299 glioma:** decreased proliferation and colony formation through increasing p53 and ac-p53 levels, and caspase activation<br>- **5637 and T24 bladder:** decreased proliferation, glycolysis, and glucose uptake (Opposite results from SIRT1 overexpression)<br>- **H460-R cisplatin-resistant lung cancer:** increased sensitivity to cisplatin (Opposite results from SIRT1 overexpression; Confirmed by SIRT1 knockdown)<br>- **HEC151, HEC1B, and HHUA endometrial carcinoma**: decreased proliferation (Opposite results from SIRT1 overexpression)<br>- **PC-3 prostate:** increased the effect of vesicular stomatitis virus oncolysis (Confirmed by SIRT1 knockdown)<br>- **Chemo-resistant stem-like cells from leukemia K562 cells:** increased the anticancer effect of | - **HHUA endometrial carcinoma tumor xenograft mice:** decreased tumor growth<br>- **A549 lung tumor xenograft mice**: decreased tumor growth with MK-1775 combination<br>- **PANC-1 pancreatic tumor xenograft mice:** increased tumor growth and showed no synergistic effect with gemicitabine<br>- **Single prolonged stress mice mimicking post-**traumatic stress disorder: hindered expression of MAO-A, stabilized serotonin, and ensured normal neuronal plasticity (*Sirt1* deleted mice had less anxiety and freezing time)<br>- **Morphine addicted mice**: increased SIRT1 expression and alleviated morphine addiction | 39, 95-102, 170-173, 196, 197 |

| | | | | | |
|---|---|---|---|---|---|
| | | | 17-AAG and AUY922 (Confirmed by SIRT1 knockdown)<br>- **A549 lung**: showed synergistic antiproliferative effect with MK-1775 (through increasing ac-Rad51 and NBS1)<br>- **PANC-1 pancreatic:** decreased proliferation and increased the anticancer effect of gemcitabine (Confirmed by SIRT1 knockdown)<br>- **P19 embryonic carcinoma cell:** promoted differentiation into neuronal cells (Confirmed by SIRT1 knockdown) | - **Rat model of middle cerebral artery occlusion**: improved the survival rate, and decreased infarction volume. | |
| **AGK2** | 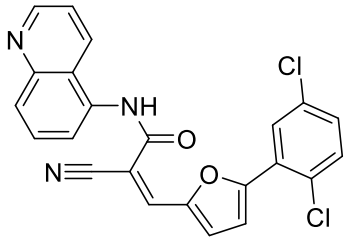 | Inhibits SIRT2 with 5-fold selectivity over SIRT1 | - **GB2, GB3, GB11, and GB16 glioblastoma:** decreased cell proliferation (did not show antiproliferative effect in SIRT2 knockdown GB2 cells) (SIRT2 knockdown GB2 and GB16 cells proliferated slower)<br>- **HCT-116 colorectal:** decreased effects of cisplatin, 5-FU, oxaliplatin, gefitinib, LY294002, and metformin<br>- **SW620 colorectal:** increased effects of cisplatin, 5-FU, oxaliplatin, gefitinib, LY294002, and metformin<br>- **Human neuroglioma cells (H4):** decreased α-Synuclein-mediated toxicity (Consistent with SIRT2 knockdown) | - **Drosophila model of Parkinson's Disease:** rescued the decrease of dorsomedial neurons<br>- **Lipopolysaccharides-induced brain injury mice:** lowered neuroinflammation and TUNEL signal<br>**Middle cerebral artery occlusion mice:** decreased apoptosis | 43, 112, 113, 179-181 |

| | | | | | |
|---|---|---|---|---|---|
| | | | - **Cultured hippocampal neurons:** protected cell deaths from $H_2O_2$ and stimulated neuroprotection (Consistent with SIRT2 knockout DT40 cells) | | |
| **AK7** | 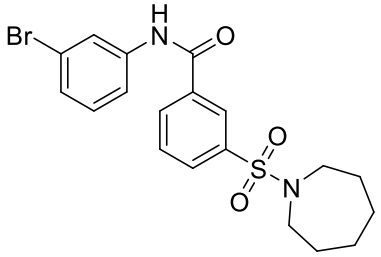 | Inhibits SIRT2 | | - **GB2 tumor xenograft mice:** decreased tumor growth (Mice with SIRT2 knockdown GB2 cells survived longer and had less tumorigenicity)<br>- **Middle cerebral artery occlusion mice:** decreased infarction volume and promoted neurological recovery through pP38 activation (SIRT2 knockdown neuro-2a cells activated pP38)<br>- **Sevoflurane-treated neonatal rat:** decreased pro-inflammatory marker and increased anti-inflammatory marker<br>- | 46, 112, 182,<br><br>183 |

| | | | | | |
|---|---|---|---|---|---|
| **SirReal2** | 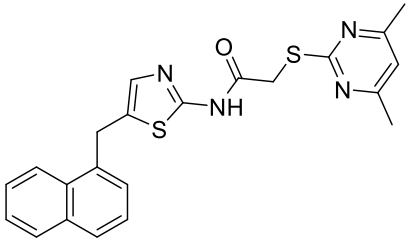 | Inhibits SIRT2 | - **HGC-27 and MGC-803 gastric:** decreased proliferation and migration (SIRT2 knockdown had less migration) (Mice with SIRT2 knockdown showed less metastatic tumors and tumor growth)<br>- **MCF7, MDA-MB-231, MDA-MB-468 breast, HCT-116, HT-29, SW948 colorectal, A549, H520 lung, K562 lymphoma, HeLa cervical:** decreased cell proliferation | | 44, 47, 114 |
| **RK-**<br><br>**91230156** | 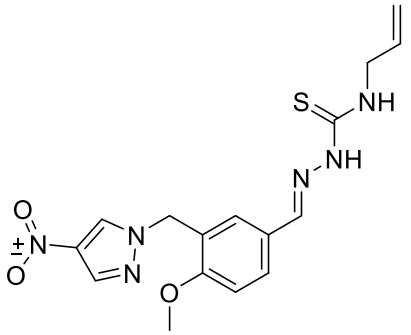 | Inhibits SIRT2 | - **MCF7 breast:** decreased cell proliferation through degradation of c-Myc and increased acetylated eIF5a | | 48 |

| | | | | | |
|---|---|---|---|---|---|
| **NCO-90/**<br><br>**141** | 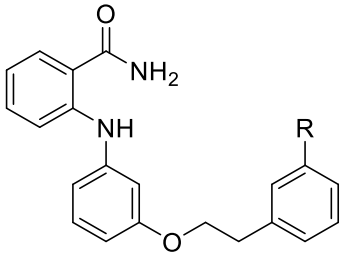 <br>R=H; NCO-90<br><br>R=F; NCO-141 | Inhibits SIRT2 | - **HTLV-1-trasnformed T-cells:** induced autophagic cell death and increased mitochondrial superoxide level<br>- **S1T, MT-2, Jurkat, and HL60 leukemia cells**: increased acetylation of histone H4, but did not alter acetylation of p53 | - **Senesce-accelerated mouse prone-8 mice:** increased spatial learning and memory deficiency of 5-month-old mice; did not have any effects on 8-month-old mice (proved SIRT2 inhibition in hippocampus by monitoring the elevated level of Abca1 | 49, 115, 184 |
| **KPM-2** | 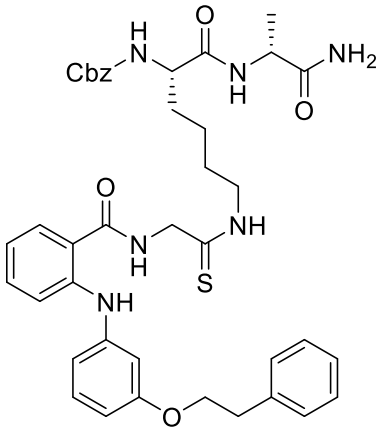 | Inhibits<br><br>SIRT1, SIRT2,<br><br>and SIRT3 | - **MDA-MB-231 breast:** decreased proliferation (usage of SIRT1 selective inhibitor with a similar structure as KPM-1 showed no effect; usage of less potent SIRT2 inhibitor with a similar structure showed weaker cytotoxicity)<br>- **Neuro-2a:** promoted neurite outgrowth | | 50 |
| **Compound**<br><br>**53** | 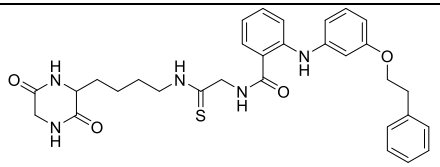 | Inhibits SIRT2 | - **Neuro-2a:** promoted neurite outgrowth<br>- **MCF7 breast:** decreased proliferation and increased acetyl α-tubuliin | | 51 |

| | | | | | |
|---|---|---|---|---|---|
| **NPD11033** | 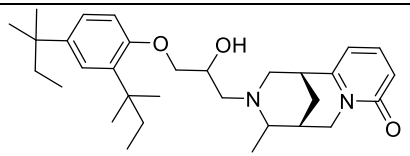 | Inhibits SIRT2 | - **PANC-1 pancreatic:** decreased proliferation and increased acetylated eIF5a (SIRT2 knockdown decreased proliferation) (inactive analog RK-0310020 did not have any affect) | | 52 |
| **Compound 6f** | 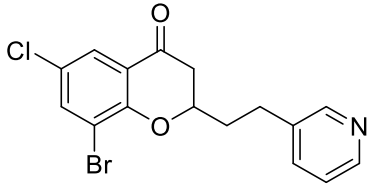 | Inhibits SIRT2 | - **MCF7 breast, and A549 lung:** decreased proliferation and arrested G1/G0 phase cell cycle arrest (increased acetyl α-tubulin in MCF7) | | 53 |
| **Compound 12a** | 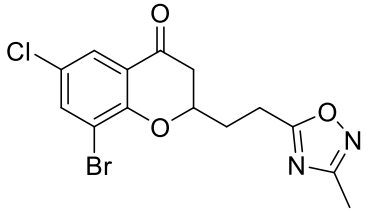 | Inhibits SIRT2 | **MCF7 breast, and A549 lung:** decreased proliferation and arrested G1/G0 phase cell cycle arrest (increased acetyl α-tubulin in MCF7) | | 53 |
| **Compound 35, and 39** | 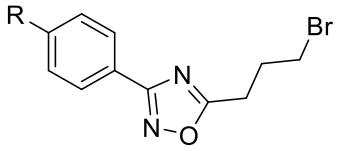 R=OMe; Compound 35 R=Br; Compound 39 | Inhibits SIRT2 | - **NB4, K562, Karpas299 leukemia, and MDA-MB-231 breast:** decreased proliferation (Compound 35) - **NB4, U937, HL-60, OCI-AML3, IMS-M2, OCl-AML2, MV4-11, Kasumi-1, and Karpas299 leukemia cells:** decreased proliferation (Compound 39) | | 54 |

| | | | | | |
|---|---|---|---|---|---|
| | | | - **NB4 and U937 leukemia cells:** increased acetyl α-tubulin (Compound 35 and 39)<br>- | | |
| **Compound 24a** | 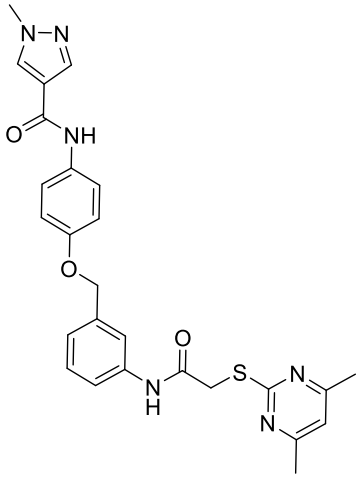 | Inhibits SIRT2 | - **H441 non-small lung:** decreased proliferation and migration, and increased acetylated α-tubulin | | 55 |
| **TM** | 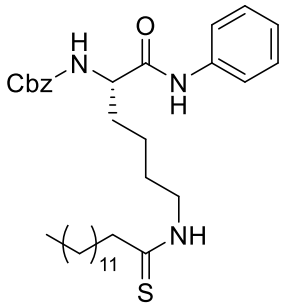 | Inhibits SIRT2 with 650-fold selectivity over SIRT1 | - **MCF7 breast:** increased acetyl α-tubulin, decreased proliferation and promoted c-Myc degradation (SIRT2 knockdown decreased proliferation and degraded c-Myc)<br>- **MDA-MB-231 and MDA-MB-468: decreased proliferation** (SIRT2 knockdown decreased proliferation)<br>- **NCI-60 screen:** decreased proliferation with $GI_{50}$ less than 10 μM<br>- **MCF-10A and HME1** normal breast epithelial: did not alter proliferation | - **MDA-MB-231 tumor xenograft mice and MMTV-PyMT genetic mice:** decreased tumor growths without any toxicity. | 44, 56 |

| | | | | | |
|---|---|---|---|---|---|
| **AF8** | 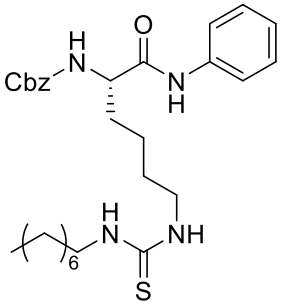 | Inhibits SIRT2 with 180-fold selectivity over SIRT1 | - **HCT-116 colorectal:** increased acetyl α-tubulin, and decreased proliferation and colony formation<br>- **MCF7, MDA-MB-468, MDA-MB-231 breast, BxPC-3 pancreatic, NCI-H23, A549 lung, and SW948 colorectal**: decreased proliferation | - **HCT-116 colorectal tumor xenograft mice:** decreased tumor growth without any toxicity | 58 |
| **NH4-6/**<br><br>**NH4-13** | 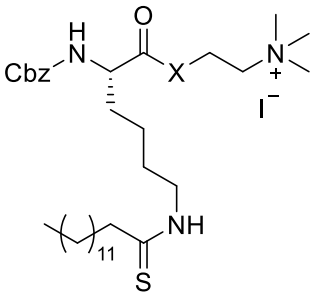 <br>X=NH; NH4-6<br>X=O; NH4-13 | Inhibits SIRT1, SIRT2, and SIRT3 (NH4-6)<br><br>Inhibits SIRT2 with 600-fold selectivity over SIRT1 (NH4-13) | - **MCF7, MDA-MB-231 breast, HCT-116, SW948 colorectal, HeLa cervical, A549, NCI-H23 lung, MIA-PaCa-2 pancreatic, and U87 glioblastoma:** decreased cell proliferation | - **HCT-116 colorectal tumor xenograft mice:** decreased tumor growth with severe toxicity at high dosage (NH4-6); decreased tumor growth without severe toxicity (NH4-13) | 60 |

| | | | | | |
|---|---|---|---|---|---|
| **TM-P4-Thal** | 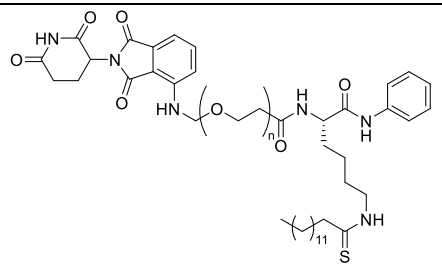 <br>n=4; TM-P4-Thal | Inhibits SIRT2 with 500-fold selectivity over SIRT1 | - **MCF7, MDA-MB-231, MDA-MB-468 breast, and BT-549 lung:** degraded SIRT2 selectively<br>- **MCF7 and MDA-MB-231 breast:** decreased proliferation at low concentrations. | | 60 |
| **LC-0296** | 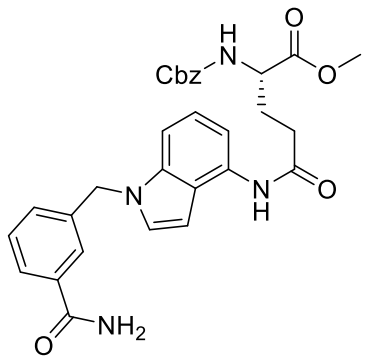 | Inhibits SIRT3 with 10-fold selectivity over SIRT2 | - **UM-SCC-1 and UM-SCC-17B head and neck squamous cell carcinoma (HNSCC):** decreased proliferation and enhanced effects of radiation and cisplatin<br>- **UM-SCC-17B (HNSCC):** Increased acetylation levels of NDUFA9 and GDH, and ROS levels | | 63 |
| **YC8-02** | 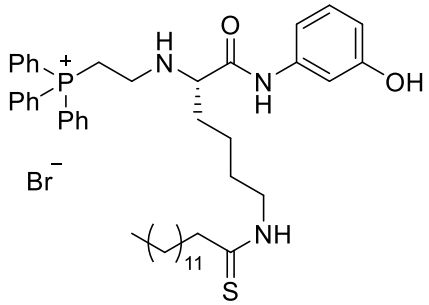 | Inhibits SIRT1, SIRT2, and SIRT3 | - **OCI-LY1 and Karpas422 lymphoma:** decreased cell proliferation, increased mitochondrial global acetylation, and decreased TCA cycle metabolites (SIRT3 knockdown had consistent results)<br>- **HBL1, Pfeiffer, SU-DHL4, TMD3, and OCL-LY7 lymphoma:** decreased cell proliferation | - **Karpas422 lymphoma tumor xenograft mice:** decreased tumor growth without toxicity (Karpas422 with SIRT3 knockdown also had slower tumor growth) | 64 |

| | | | | | |
|---|---|---|---|---|---|
| **DK1-04/**<br><br>**DK1-04e** | 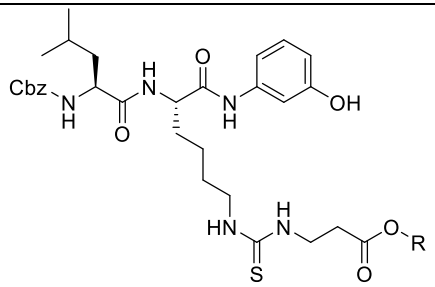 <br>R=H; DK1-04<br><br>R=$CH_2CH_3$; DK1-04e | Inhibits SIRT5<br><br>selectively<br><br>(DK1-04) | - **MCF7 and MDA-MB-231 breast:** (DK1-04e) decreased cell proliferation and colony formation, and increased mitochondrial global succinylation; its inactive derivative (DK1-04e(O) showed weaker cytotoxicity<br>- MDA-MB-231: partial SIRT5 knockout decreased colony formation | - **MDA-MB-231 breast tumor xenograft mice and MMTV-PyMT genetic mice:** decreased tumor growth without toxicity (*Sirt5* deficient PYMT mice impaired tumor growth) | 65 |
| **UBCS039** | 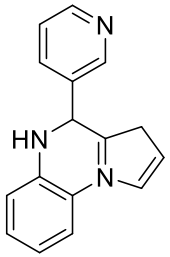 | Activates<br><br>SIRT6 | - **H1299 non-small cell lung carcinoma:** decreased acetyl H3K9 and H3K56, and induced apoptosis (inactive analog UBSC060 did not have any affect)<br>- **H1299 and HeLa:** activated ROS production and increased ATP level (consistent with a previous report on SIRT5 deficiency reducing oxygen consumption and ATP level) | | 66, 67 |

| | | | | | |
|---|---|---|---|---|---|
| **MDL-800** | 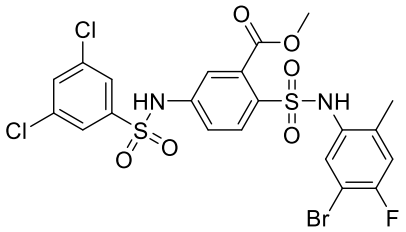 | Activates<br><br>SIRT6 | - **Bel7405 hepatocellular carcinoma: decreased acetyl H3K9 and H3K56,** decreased cell proliferation, and arrested cell cycle (MDL-800 treated SIRT6 knockout did not induce any changes in cell cycle arrest markers)<br>- **NCI-60:** decreased cell proliferation of the 12 non-small lung carcinoma lines<br>- **SIRT6 KO HCC527 and PC9 non-small lung carcinoma:** did not affect growth | - **Bel7405 hepatocellular tumor xenograft mice and HCC827 non-small lung carcinoma:** increased histone H3 acetylation and decreased tumor growth | 68, 148 |
| **Compound**<br><br>**2, 3, and 8** | 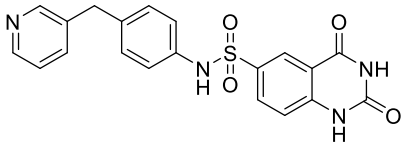 <br>Compound 2<br> 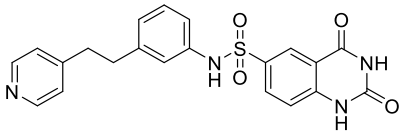 <br>Compound 3 | Inhibits SIRT6 | - **BxPC-3 pancreatic:** increased H3K9 acetylation, increased glucose uptake (Compound 3 and 8), decreased proliferation (only Compound 8), and increased antiproliferative affect with gemcitabine (Compound 2 and 3) | | 69 |

| | | | | | |
|---|---|---|---|---|---|
| | 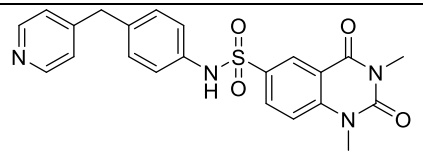 <br>Compound 8 | | | | |
| **OSS-**<br><br>**128167** | 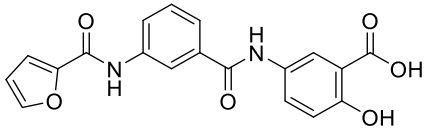 | Inhibits SIRT6 | - **BxPC-3 pancreatic:** increased glucose uptake and GLUT-1 expression, and decreased TNF-α<br>- | - **Mice model of streptozotocin-induced diabetes and high glucose-treated cardiomyocytes:** promoted inflammation, oxidative stress, and diabetes-induced cardiomyocyte apoptosis | 69, 195 |
| **Compound**<br><br>**5 and 11** | 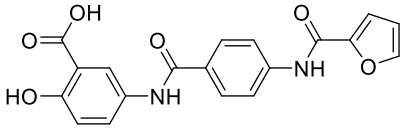 <br>Compound 5<br><br> 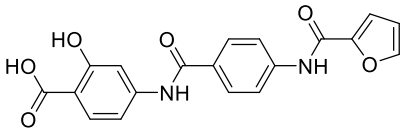 <br>Compound 11 | Inhibits SIRT6<br><br>with mild<br><br>inhibition of<br><br>SIRT2 | - **BxPC-3 pancreatic:** increased H3K9 acetylation, increased glucose uptake, decreased TNF-α, and decreased proliferation with gemcitabine | | 71 |

| | | | | | |
|---|---|---|---|---|---|
| **Compound 1** | 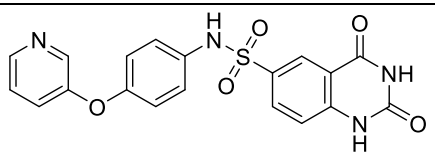 | Inhibits SIRT2 and SIRT6 | - **Dendritic cells:** decreased migration<br>- **BxPC-3 pancreatic:** increased glucose uptake and GLUT-1 expression and decreased TNF-α | - **C57bl/6 mice with MOG35-55 injection:** decreased TNFα and neurological impairment, lowered IFNγ and IL12, increased IL10 | 71, 72, 188 |
| **Cambinol** | 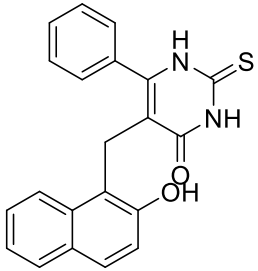 | Inhibits SIRT1 and SIRT2 | - **NCI-H460 lung and HeLa cervical:** increased acetylation levels of p53, α-tubulin, FOXO3a, and Ku70<br>- **RPMI8226 and U266 multiple myeloma:** induced apoptosis, cell proliferation impairment, and apoptosis<br>- **HepG2 and Huh7 hepatocarcinoma:** decreased cell proliferation, migration, and invasion with sorafenib | - **Orthopedic tumor xenograft mice with HepG2:** decreased tumor growth (consistent with SIRT1 knockdown results of intrahepatic xenograft mice study)<br>- **TH-MYCN transgenic mice:** decreased neuroblastoma formation through N-Myc degradation (SIRT1 knockdown BE(2)-C cells had N-Myc degradation) | 73, 149-152 |
| **Sirtinol** | 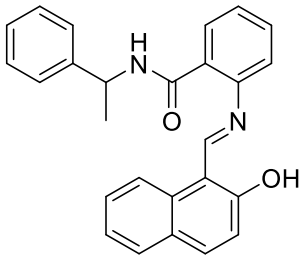 | Inhibits SIRT1 and SIRT2 | - **MCF7 breast and H1299 non-small lung:** decreased senescence-like growth and activation of the RAS-MAPK pathway (Similar results with SIRT1 knockdown)<br>- **H1299 non-small lung and HeLa cervical:** decreased cell proliferation<br>- **PC3 prostrate, DU145 prostate, S1T adult T-cell leukemia/lymphoma (ATL), and Jurkat ATL:** decreased cell | - **A549 non-small lung tumor xenograft mice:** decreased tumor growth with sodium dichloroacetic acid<br>- **Subarachnoid hemorrhage rat:** lowered SIRT1 expression, damaged the blood-brain barrier and neurological activity, aggravated brain | 74, 75, 153-157, 174, 192 |

| | | | | | |
|---|---|---|---|---|---|
| | | | proliferation (SIRT1 knockdown decreased proliferation)<br>- **A549 and H1299 non-small lung:** decreased cell proliferation with sodium dichloroacetic acid | edema, and increased endothelial cell apoptosis<br>- **Neonatal rat:** decreased cardiacmyocytes<br>- **Cardiac ischemia preconditioned rats:** decreased the infarct size | |
| **Salermide** | 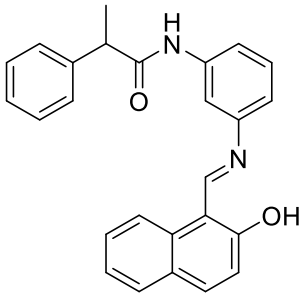 | Inhibits SIRT1 and SIRT2 | - **MOL4 acute lymphomastic leukemia, SW480 colorectal, KG1a acute myelogenous leukemia, and Raji Burkitt's lymphoma:** induced apoptosis through SIRT1 inhibition (confirmed with SIRT1 knockdown)<br>- **BE(2)-C neuroblastoma and MIA-PaCa-2 pancreatic:** decreased cell proliferation through c-Myc and n-Myc degradation (confirmed with SIRT2 knockdown) | | 76, 107 |
| **Tenovin-6** | 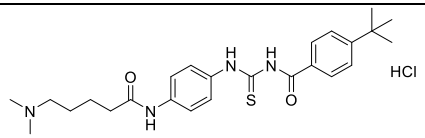 | Inhibits SIRT1 and SIRT2, but also target other unknown proteins. | - **ARN8 melanoma:** decreased cell proliferation<br>- **AGS, AGS-EBV, and HGC-27 gastric:** decreased cell proliferation and colony formation through increasing acetyl p53 levels<br>- **SNU-179, N87, and SNU-1, KATO-III gastric:** decreased cell proliferation | | 44, 77-79, 158-160 |

| | | | | | |
|---|---|---|---|---|---|
| | | | - **HME-1 and MCF-10A normal breast:** decreased cell proliferation<br>- **A549 non-small lung:** decreased proliferation with metformin by HIC1-dependent SIRT1 level reduction<br>- **92.1, Mel-270, Omm-1, Om-2.3 uveal melanoma:** decreased migration and proliferation; displayed synergistic effect with Vinblastine<br>- **Canine hemangiosarcoma:** decreased proliferation with SIRT1-independent mechanism<br>- **OCI-Ly1 DLBCL:** decreased cell proliferation and induced apoptosis through SIRT1/2/3-independent mechanism | | |
| **BZD9L1** | 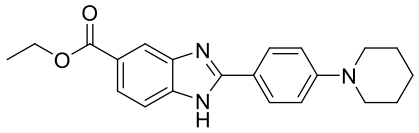 | Inhibits SIRT1<br><br>and SIRT2 | - **HCT-116 colorectal, CCRF-CEM leukemia, and MDA-MB-468 breast:** decreased cell proliferation<br>- **HCT-116 and HT-29** colorectal: decrsaed cell migration and colony formation<br>- **HCT-116 colorectal:** increased cell cycle, arrest, and apopotosis, and decreased the spheroid formation with 5-Fluorouracil | - **HCT-116 colorectal tumor xenograft mice:** decreased tumor growth with 5-Fluorouracil | 81, 161, 162 |

| | | | | | |
|---|---|---|---|---|---|
| **Compound 18** | 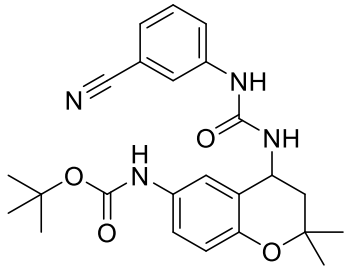 | Inhibits SIRT1 and SIRT2 | - **HS683 and U373 glioma:** decreased proliferation (consistent with SIRT1/2 knockdown) and increased acetylation of H4, H3K56 and α-tubulin<br>- **NCI-60 screen:** decreased proliferation with an average $GI_{50}$ of 3 μM | - **HS683 an dU373 glioma zebrafish xenotransplant model:** decreased tumor growth | 82 |
| **Compound 3g** | 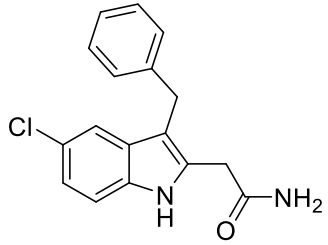 | Inhibits SIRT1 and SIRT2 | - **K562 leukemia, HCT-116, HT-29 colorectal, H460, A549 lung, and MCF7 breast:** decreased proliferation (need additional data to show cellular inhibition of SIRT1 and 2) | | 83 |
| **MC2494** | 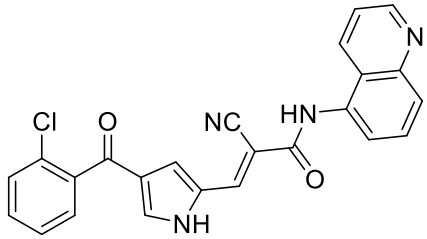 | Inhibits SIRT1, SIRT2, and SIRT3 | - **U937 lymphoma:** decreased metabolic activity and proliferation; lowered decreased ATP production and expression level of PGC1α and PGC1β | | 84, 163 |

| | | | | | |
|---|---|---|---|---|---|
| **JH-T4** | 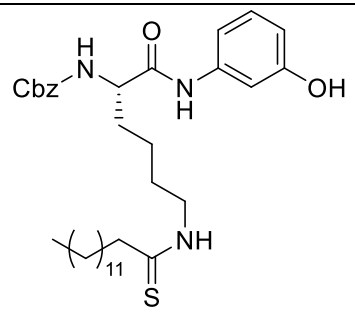 | Inhibits<br><br>SIRT1, SIRT2,<br><br>and SIRT3 | - **MCF7, MDA-MB-231 breast, HCT-116 colorectal, NCI-H23 lung, HME1 and MCF-10A normal epithelial cells:** decreased cell proliferation | | 85 |
| **35.**<br><br>**Splitomicin** | 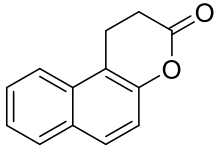 | Inhibits yeast<br><br>sirtuins | - **Human endothelial cells:** increased and activated tissue factor expression (confirmed with SIRT1 knockdown) | - **Photochemical injury mice:** promoted carotid artery thrombus formation | 193 |

**Table 2. Cell lines affected by SIRT1 Inhibitors.**

| | | SIRT1 Inhibitor | | |
|---|---|---|---|---|
| Type | Line | EX-527 | | |
| Glioma | U87MG | ↓ proliferation | | |
| | LN0299 | ↓ proliferation | | |
| Bladder | 5637 | ↓ proliferation | | |
| | T24 | ↓ proliferation | | |
| Lung | H-460-R- cisplatin resistant | ↑ senstivity to cisplatin | | |
| | A549 | ↑senstivity with MK-1775 | | |
| | A549 (xenograft) | ↓ tumor growth with MK-1775 | | |
| Endometrial Carcinoma | HEC151 | ↓ proliferation | | |
| | HEC1B | ↓ proliferation | | |
| | HHUA | ↓ proliferation | | |
| | HHUA (xenograft) | ↓ tumor growth | | |
| Prostate | PC-3 | ↑ senstivity to vesicular stomatitis virus oncolysis | | |
| Pancreatic | PANC-1 | ↓ proliferation ↑senstivitiy to gemcitabine | | |
| | PANC-1 (xenograft) | ↑ tumor growth | | |
| Colorectal | HCT-116 | | | |
| Leukemia | S1T | | | |
| | MT-2 | | | |
| | Jurkat | | | |
| | HL60 | | | |
| Lymphoma | Chemo-resistant K562 | ↑ sensitivity to 17-AAG and AUY922 | | |
| | Daudi Lymphoma | | | |

**Table 3. Cell lines affected by SIRT2 Inhibitors (#1 set).**

| | | SIRT2 Inhibitor | | | | | | |
|---|---|---|---|---|---|---|---|---|
| Type | Line | AGK2 | AK7 | SirReal2 | RK-91230156 | NCO-90/141 | NPD11033 | Compound 6f/12a |
| Glioma | GB2 | ↓ proliferation | | | | | | |
| | GB2 (xenograft) | | ↓ tumor growth | | | | | |
| | GB3 | ↓ proliferation | | | | | | |
| | GB11 | ↓ proliferation | | | | | | |
| | GB16 | ↓ proliferation | | | | | | |
| Lung | A549 | | | ↓ proliferation | | | | ↓ proliferation |
| | H520 | | | ↓ proliferation | | | | |
| Pancreatic | PANC-1 | | | | | | ↓ proliferation | |
| Colorectal | HCT-116 | ↓ effect of chemotherapeutic agents | | ↓ proliferation | | | | |
| | SW620 | ↑ effect of chemotherapeutic agents | | | | | | |
| | SW948 | | | ↓ proliferation | | | | |
| Leukemia | S1T | | | | | ↑ acetylation of H4 | | |
| | MT-2 | | | | | ↑ acetylation of H4 | | |
| | Jurkat | | | | | ↑ acetylation of H4 | | |
| | HL60 | | | | | ↑ acetylation of H4 | | |
| Lymphoma | Chemo-resistant K562 | | | ↓ proliferation | | | | |
| | K562 | | | ↓ proliferation | | | | |
| Gastric | HGC-27 | | | ↓ proliferation | | | | |
| | MGC-803 | | | ↓ proliferation | | | | |
| Breast | MCF7 | | | ↓ proliferation | ↓ proliferation | | | ↓ proliferation |
| | MDA-MB-231 | | | ↓ proliferation | | | | |
| | MDA-MB-468 | | | ↓ proliferation | | | | |
| Cervical | HeLa | | | ↓ proliferation | | | | |

**Table 4. Cell lines affected by SIRT2 Inhibitors (#2 set).**

| | | SIRT2 Inhibitor | | | | | | | |
|---|---|---|---|---|---|---|---|---|---|
| Type | Line | Compound 35 | Compound 39 | Compound 24a | Compound 53 | TM | AF8 | NH4-13 | TM-P4-Thal |
| NCI-60 | NCI-60 | | | | | ↓ proliferation | | | |
| Glioma | U87MG | | | | | | | ↓ proliferation | |
| | GB2 | | | | | | | | |
| | GB2 (xenograft) | | | | | | | | |
| | GB3 | | | | | | | | |
| | GB11 | | | | | | | | |
| | GB16 | | | | | | | | |
| Lung | A549 | | | | | | ↓ proliferation | ↓ proliferation | |
| | NCI-H23 | | | | | | | ↓ proliferation | |
| Non-small Lung | H441 | | | ↓ proliferation | | | | | |
| Pancreatic | BxPC-3 | | | | | | ↓ proliferation | | |
| | Mia-PaCa-2 | | | | | | | ↓ proliferation | |
| Colorectal | HCT-116 | | | | | | ↓ proliferation | ↓ proliferation | |
| | HCT-116 (xenograft) | | | | | | ↓ tumor growth | ↓ tumor growth | |
| | SW948 | | | | | | ↓ proliferation | ↓ proliferation | |
| Leukemia | HL60 | | ↓ proliferation | | | | | | |
| | NB4 | ↓ proliferation | ↓ proliferation | | | | | | |
| Lymphoma | Chemo-resistant K562 | | | | | | | | |
| | K562 | ↓ proliferation | | | | | | | |
| | Karpas299 | ↓ proliferation | ↓ proliferation | | | | | | |
| | U937 | | ↓ proliferation | | | | | | |
| | OCI-AML3 | | | | | | | | |
| | IMS-M2 | | ↓ proliferation | | | | | | |
| | OCI-AML3 | | ↓ proliferation | | | | | | |
| | MV4-11 | | ↓ proliferation | | | | | | |
| | Kasumi1 | | ↓ proliferation | | | | | | |
| Breast | MCF7 | | | | ↓ proliferation | ↓ proliferation | ↓ proliferation | ↓ proliferation | ↓ proliferation |
| | MDA-MB-231 | ↓ proliferation | | | | ↓ proliferation | ↓ proliferation | ↓ proliferation | ↓ proliferation |
| | MDA-MB-231 (xenograft) | | | | | ↓ tumor growth | | | |
| | MDA-MB-468 | | | | | ↓ proliferation | ↓ proliferation | | |
| Cervical | HeLa | | | | | | | ↓ proliferation | |
| Normal Epithelial | MCF-10A | | | | | No effect | | | |
| | HME1 | | | | | No effect | | | |

**Table 5. Cell lines affected by SIRT3/SIRT5 inhibitors.**

| | | SIRT3 Inhibitor | | SIRT5 Inhibitor |
|---|---|---|---|---|
| Type | Line | LC-0296 | YC8-02 | DK1-04e |
| Lymphoma | OCL-LY-1 | | ↓ proliferation | |
| | Karpas422 | | ↓ proliferation | |
| | Karpas422 (xenograft) | | ↓ tumor growth | |
| | HBL1 | | ↓ proliferation | |
| | Pfeiffer | | ↓ proliferation | |
| | SU-DHL4 | | ↓ proliferation | |
| | TMD3 | | ↓ proliferation | |
| | OCL-LY7 | | ↓ proliferation | |
| Breast | MCF7 | | | ↓ proliferation |
| | MDA-MB-231 | | | ↓ proliferation |
| | MDA-MB-231 (xenograft) | | | ↓ tumor growth |
| HNSCC | UM-SCC-1 | ↓ proliferation | | |
| | UM-SCC-17B | ↓ proliferation | | |

**Table 6. Cell lines affected by SIRT6 modulators.**

| | | SIRT6 Activator | | SIRT6 Inhibitor | | | | |
|---|---|---|---|---|---|---|---|---|
| Type | Line | UBCS039 | MDL-800 | Compound 2 | Compound 3 | Compound 8 | Compound 5 | Compound 11 |
| NCI-60 | NCI-60 | | ↓ proliferation | | | | | |
| Non-small Lung | H1299 | ↓ proliferation | | | | | | |
| Hepatocellular carcinoma | Bel7405 | | ↓ proliferation | | | | | |
| Pancreatic | BxPC-3 | | | ↑ senstivity | ↑ senstivity | ↓ proliferation | ↑ senstivity | ↑ senstivity |
| | | | | to gemcitabine | to gemcitabine | | to gemcitabine | to gemcitabine |

## 1.8 References


1. Feldman, J. L., Dittenhafer-Reed, K. E., and Denu, J. M. (2012) Sirtuin Catalysis and Regulation, *J. Biol. Chem. 287*, 42419-42427.

2. Sauve, A. A., Celic, I., Avalos, J., Deng, H., Boeke, J. D., and Schramm, V. L. (2001) Chemistry of gene silencing: the mechanism of NAD+-dependent deacetylation reactions, *Biochemistry 40*, 15456-15463.

3. Sauve, A. A., Wolberger, C., Schramm, V. L., and Boeke, J. D. (2006) The biochemistry of sirtuins, *Annu. Rev. Biochem. 75*, 435-465.

4. Avalos, J. L., Bever, K. M., and Wolberger, C. (2005) Mechanism of sirtuin inhibition by nicotinamide: altering the NAD(+) cosubstrate specificity of a Sir2 enzyme, *Mol. Cell 17*, 855-868.

5. Bheda, P., Jing, H., Wolberger, C., and Lin, H. (2016) The Substrate Specificity of Sirtuins, *Annu. Rev. Biochem. 85*, 405-429.

6. Hu, J., Jing, H., and Lin, H. (2014) Sirtuin inhibitors as anticancer agents, *Future Med. Chem. 6*, 945-966.

7. Jing, H., and Lin, H. (2015) Sirtuins in Epigenetic Regulation, *Chem. Rev. 115*, 2350-2375.

8. Morris, B. J. (2013) Seven sirtuins for seven deadly diseases of aging, *Free Radical Biol. Med. 56*, 133-171.

9. Machado de Oliveira, R., Sarkander, J., Kazantsev, A. G., and Outeiro, T. F. (2012) SIRT2 as a Therapeutic Target for Age-Related Disorders, *Front. Pharmacol. 3*.

10. Kosciuk, T., Wang, M., Hong, J. Y., and Lin, H. (2019) Updates on the epigenetic roles of sirtuins, *Curr. Opin. Chem. Biol. 51*, 18-29.

11. Blank, M. F., Chen, S., Poetz, F., Schnolzer, M., Voit, R., and Grummt, I. (2017) SIRT7-dependent deacetylation of CDK9 activates RNA polymerase II transcription, *Nucleic Acids Res. 45*, 2675-2686.

12. Cha, Y., Han, M. J., Cha, H. J., Zoldan, J., Burkart, A., Jung, J. H., Jang, Y., Kim, C. H., Jeong, H. C., Kim, B. G., Langer, R., Kahn, C. R., Guarente, L., and Kim, K. S. (2017) Metabolic control of primed human pluripotent stem cell fate and function by the miR-200c-SIRT2 axis, *Nat. Cell Biol. 19*, 445-456.

13. Wang, M., and Lin, H. (2021) Understanding the Function of Mammalian Sirtuins and Protein Lysine Acylation, *Annu. Rev. Biochem.*

14. Fujita, Y., and Yamashita, T. (2018) Sirtuins in Neuroendocrine Regulation and

Neurological Diseases, *Front. Neurosci. 12*, 778.

15. Haigis, M. C., and Sinclair, D. A. (2010) Mammalian sirtuins: biological insights and disease relevance, *Annu. Rev. Pathol. 5*, 253-295.

16. Borradaile, N. M., and Pickering, J. G. (2009) NAD(+), sirtuins, and cardiovascular disease, *Curr. Pharm. Des. 15*, 110-117.

17. Nishida, Y., Rardin, M. J., Carrico, C., He, W., Sahu, A. K., Gut, P., Najjar, R., Fitch, M., Hellerstein, M., Gibson, B. W., and Verdin, E. (2015) SIRT5 Regulates both Cytosolic and Mitochondrial Protein Malonylation with Glycolysis as a Major Target, *Mol. Cell 59*, 321-332.

18. North, B. J., and Verdin, E. (2007) Interphase Nucleo-Cytoplasmic Shuttling and Localization of SIRT2 during Mitosis, *PLoS One 2*, e784.

19. Tanno, M., Sakamoto, J., Miura, T., Shimamoto, K., and Horio, Y. (2007) Nucleocytoplasmic shuttling of the NAD+-dependent histone deacetylase SIRT1, *J. Biol. Chem. 282*, 6823-6832.

20. Feldman, J. L., Dittenhafer-Reed, K. E., Kudo, N., Thelen, J. N., Ito, A., Yoshida, M., and Denu, J. M. (2015) Kinetic and Structural Basis for Acyl-Group Selectivity and NAD <sup>+</sup> Dependence in Sirtuin-Catalyzed Deacylation, *Biochemistry 54*, 3037-3050.

21. Teng, Y.-B., Jing, H., Aramsangtienchai, P., He, B., Khan, S., Hu, J., Lin, H., and Hao, Q. (2015) Efficient Demyristoylase Activity of SIRT2 Revealed by Kinetic and Structural Studies, *Sci. Rep. 5*, 8529.

22. Jin, J., He, B., Zhang, X., Lin, H., and Wang, Y. (2016) SIRT2 Reverses 4-Oxononanoyl Lysine Modification on Histones, *J. Am. Chem. Soc. 138*, 12304-12307.

23. Huang, H., Zhang, D., Wang, Y., Perez-Neut, M., Han, Z., Zheng, Y. G., Hao, Q., and Zhao, Y. (2018) Lysine benzoylation is a histone mark regulated by SIRT2, *Nat. Commun. 9*, 3374.

24. Pannek, M., Simic, Z., Fuszard, M., Meleshin, M., Rotili, D., Mai, A., Schutkowski, M., and Steegborn, C. (2017) Crystal structures of the mitochondrial deacylase Sirtuin 4 reveal isoform-specific acyl recognition and regulation features, *Nat. Commun. 8*, 1513.

25. Mathias, R. A., Greco, T. M., Oberstein, A., Budayeva, H. G., Chakrabarti, R., Rowland, E. A., Kang, Y., Shenk, T., and Cristea, I. M. (2014) Sirtuin 4 is a lipoamidase regulating pyruvate dehydrogenase complex activity, *Cell 159*, 1615-1625.

26. Anderson, K. A., Huynh, F. K., Fisher-Wellman, K., Stuart, J. D., Peterson, B. S., Douros, J. D., Wagner, G. R., Thompson, J. W., Madsen, A. S., Green, M. F., Sivley, R. M., Ilkayeva, O. R., Stevens, R. D., Backos, D. S., Capra, J. A., Olsen, C. A., Campbell, J. E., Muoio, D. M., Grimsrud, P. A., and Hirschey, M. D. (2017) SIRT4 Is a Lysine Deacylase that Controls Leucine Metabolism and Insulin Secretion, *Cell Metab. 25*, 838-855 e815.

27. Kumar, S., and Lombard, D. B. (2017) For Certain, SIRT4 Activities!, *Trends in Biochemical Sciences 42*, 499-501.

28. Du, J., Zhou, Y., Su, X., Yu, J., Khan, S., Jiang, H., Kim, J., Woo, J., Kim, J. H., Choi, B. H., He, B., Chen, W., Zhang, S., Cerione, R. A., Auwerx, J., Hao, Q., and Lin, H. (2011) Sirt5 is an NAD-dependent protein lysine demalonylase and desuccinylase, *Science 334*, 806-809.

29. Zhang, X., Khan, S., Jiang, H., Antonyak, M. A., Chen, X., Spiegelman, N. A., Shrimp, J. H., Cerione, R. A., and Lin, H. (2016) Identifying the functional contribution of the defatty-acylase activity of SIRT6, *Nat. Chem. Biol. 12*, 614-620.

30. Tong, Z., Wang, M., Wang, Y., Kim, D. D., Grenier, J. K., Cao, J., Sadhukhan, S., Hao, Q., and Lin, H. (2017) SIRT7 Is an RNA-Activated Protein Lysine Deacylase, *ACS Chem. Biol. 12*, 300-310.

31. Borra, M. T., Smith, B. C., and Denu, J. M. (2005) Mechanism of human SIRT1 activation by resveratrol, *J. Biol. Chem. 280*, 17187-17195.

32. Howitz, K. T., Bitterman, K. J., Cohen, H. Y., Lamming, D. W., Lavu, S., Wood, J. G., Zipkin, R. E., Chung, P., Kisielewski, A., Zhang, L. L., Scherer, B., and Sinclair, D. A. (2003) Small molecule activators of sirtuins extend Saccharomyces cerevisiae lifespan, *Nature 425*, 191-196.

33. Milne, J. C., Lambert, P. D., Schenk, S., Carney, D. P., Smith, J. J., Gagne, D. J., Jin, L., Boss, O., Perni, R. B., Vu, C. B., Bemis, J. E., Xie, R., Disch, J. S., Ng, P. Y., Nunes, J. J., Lynch, A. V., Yang, H., Galonek, H., Israelian, K., Choy, W., Iffland, A., Lavu, S., Medvedik, O., Sinclair, D. A., Olefsky, J. M., Jirousek, M. R., Elliott, P. J., and Westphal, C. H. (2007) Small molecule activators of SIRT1 as therapeutics for the treatment of type 2 diabetes, *Nature 450*, 712-716.

34. Pacholec, M., Bleasdale, J. E., Chrunyk, B., Cunningham, D., Flynn, D., Garofalo, R. S., Griffith, D., Griffor, M., Loulakis, P., Pabst, B., Qiu, X., Stockman, B., Thanabal, V., Varghese, A., Ward, J., Withka, J., and Ahn, K. (2010) SRT1720, SRT2183, SRT1460, and resveratrol are not direct activators of SIRT1, *J. Biol. Chem. 285*, 8340-8351.

35. Beher, D., Wu, J., Cumine, S., Kim, K. W., Lu, S. C., Atangan, L., and Wang, M. (2009) Resveratrol is not a direct activator of SIRT1 enzyme activity, *Chem.*

*Biol. Drug Des. 74*, 619-624.

36. Dai, H., Kustigian, L., Carney, D., Case, A., Considine, T., Hubbard, B. P., Perni, R. B., Riera, T. V., Szczepankiewicz, B., Vlasuk, G. P., and Stein, R. L. (2010) SIRT1 activation by small molecules: kinetic and biophysical evidence for direct interaction of enzyme and activator, *J. Biol. Chem. 285*, 32695-32703.

37. Hubbard, B. P., Gomes, A. P., Dai, H., Li, J., Case, A. W., Considine, T., Riera, T. V., Lee, J. E., E, S. Y., Lamming, D. W., Pentelute, B. L., Schuman, E. R., Stevens, L. A., Ling, A. J., Armour, S. M., Michan, S., Zhao, H., Jiang, Y., Sweitzer, S. M., Blum, C. A., Disch, J. S., Ng, P. Y., Howitz, K. T., Rolo, A. P., Hamuro, Y., Moss, J., Perni, R. B., Ellis, J. L., Vlasuk, G. P., and Sinclair, D. A. (2013) Evidence for a common mechanism of SIRT1 regulation by allosteric activators, *Science 339*, 1216-1219.

38. Nguyen, G. T., Schaefer, S., Gertz, M., Weyand, M., and Steegborn, C. (2013) Structures of human sirtuin 3 complexes with ADP-ribose and with carba-NAD+ and SRT1720: binding details and inhibition mechanism, *Acta Crystallogr. Sect. D. Biol. Crystallogr. 69*, 1423-1432.

39. Solomon, J. M., Pasupuleti, R., Xu, L., McDonagh, T., Curtis, R., DiStefano, P. S., and Huber, L. J. (2006) Inhibition of SIRT1 catalytic activity increases p53 acetylation but does not alter cell survival following DNA damage, *Mol. Cell. Biol. 26*, 28-38.

40. Kokkonen, P., Rahnasto-Rilla, M., Mellini, P., Jarho, E., Lahtela-Kakkonen, M., and Kokkola, T. (2014) Studying SIRT6 regulation using H3K56 based substrate and small molecules, *Eur. J. Pharm. Sci. 63*, 71-76.

41. Ghosh, A., Sengupta, A., Seerapu, G. P. K., Nakhi, A., Shivaji Ramarao, E. V. V., Bung, N., Bulusu, G., Pal, M., and Haldar, D. (2017) A novel SIRT1 inhibitor, 4bb induces apoptosis in HCT116 human colon carcinoma cells partially by activating p53, *Biochem. Biophys. Res. Commun. 488*, 562-569.

42. Kozako, T., Suzuki, T., Yoshimitsu, M., Uchida, Y., Kuroki, A., Aikawa, A., Honda, S., Arima, N., and Soeda, S. (2015) Novel small-molecule SIRT1 inhibitors induce cell death in adult T-cell leukaemia cells, *Sci. Rep. 5*, 11345.

43. Outeiro, T. F., Kontopoulos, E., Altmann, S. M., Kufareva, I., Strathearn, K. E., Amore, A. M., Volk, C. B., Maxwell, M. M., Rochet, J.-C., McLean, P. J., Young, A. B., Abagyan, R., Feany, M. B., Hyman, B. T., and Kazantsev, A. G. (2007) Sirtuin 2 inhibitors rescue alpha-synuclein-mediated toxicity in models of Parkinson's disease, *Science 317*, 516-519.

44. Spiegelman, N. A., Price, I. R., Jing, H., Wang, M., Yang, M., Cao, J., Hong, J. Y., Zhang, X., Aramsangtienchai, P., Sadhukhan, S., and Lin, H. (2018) Direct Comparison of SIRT2 Inhibitors: Potency, Specificity, Activity-Dependent

Inhibition, and On-Target Anticancer Activities, *ChemMedChem 13*, 1890-1894.

45. Mangas-Sanjuan, V., Olah, J., Gonzalez-Alvarez, I., Lehotzky, A., Tokesi, N., Bermejo, M., and Ovadi, J. (2015) Tubulin acetylation promoting potency and absorption efficacy of deacetylase inhibitors, *Br. J. Pharmacol. 172*, 829-840.

46. Taylor, D. M., Balabadra, U., Xiang, Z., Woodman, B., Meade, S., Amore, A., Maxwell, M. M., Reeves, S., Bates, G. P., Luthi-Carter, R., Lowden, P. A., and Kazantsev, A. G. (2011) A brain-permeable small molecule reduces neuronal cholesterol by inhibiting activity of sirtuin 2 deacetylase, *ACS Chem. Biol. 6*, 540-546.

47. Rumpf, T., Schiedel, M., Karaman, B., Roessler, C., North, B. J., Lehotzky, A., Olah, J., Ladwein, K. I., Schmidtkunz, K., Gajer, M., Pannek, M., Steegborn, C., Sinclair, D. A., Gerhardt, S., Ovadi, J., Schutkowski, M., Sippl, W., Einsle, O., and Jung, M. (2015) Selective Sirt2 inhibition by ligand-induced rearrangement of the active site, *Nat. Commun. 6*, 6263.

48. Shah, A. A., Ito, A., Nakata, A., and Yoshida, M. (2016) Identification of a Selective SIRT2 Inhibitor and Its Anti-breast Cancer Activity, *Biological and Pharmaceutical Bulletin 39*, 1739-1742.

49. Suzuki, T., Khan, M. N., Sawada, H., Imai, E., Itoh, Y., Yamatsuta, K., Tokuda, N., Takeuchi, J., Seko, T., Nakagawa, H., and Miyata, N. (2012) Design, synthesis, and biological activity of a novel series of human sirtuin-2-selective inhibitors, *J. Med. Chem. 55*, 5760-5773.

50. Mellini, P., Itoh, Y., Tsumoto, H., Li, Y., Suzuki, M., Tokuda, N., Kakizawa, T., Miura, Y., Takeuchi, J., Lahtela-Kakkonen, M., and Suzuki, T. (2017) Potent mechanism-based sirtuin-2-selective inhibition by an in situ-generated occupant of the substrate-binding site, "selectivity pocket" and NAD(+)-binding site, *Chem. Sci. 8*, 6400-6408.

51. Mellini, P., Itoh, Y., Elboray, E. E., Tsumoto, H., Li, Y., Suzuki, M., Takahashi, Y., Tojo, T., Kurohara, T., Miyake, Y., Miura, Y., Kitao, Y., Kotoku, M., Iida, T., and Suzuki, T. (2019) Identification of Diketopiperazine-Containing 2-Anilinobenzamides as Potent Sirtuin 2 (SIRT2)-Selective Inhibitors Targeting the "Selectivity Pocket", Substrate-Binding Site, and NAD(+)-Binding Site, *J. Med. Chem. 62*, 5844-5862.

52. Kudo, N., Ito, A., Arata, M., Nakata, A., and Yoshida, M. (2018) Identification of a novel small molecule that inhibits deacetylase but not defatty-acylase reaction catalysed by SIRT2, *Philos. Trans. R. Soc. Lond., B, Biol. Sci. 373*.

53. Seifert, T., Malo, M., Kokkola, T., Engen, K., Friden-Saxin, M., Wallen, E. A., Lahtela-Kakkonen, M., Jarho, E. M., and Luthman, K. (2014) Chroman-4-one-

and chromone-based sirtuin 2 inhibitors with antiproliferative properties in cancer cells, *J. Med. Chem. 57*, 9870-9888.

54. Moniot, S., Forgione, M., Lucidi, A., Hailu, G. S., Nebbioso, A., Carafa, V., Baratta, F., Altucci, L., Giacche, N., Passeri, D., Pellicciari, R., Mai, A., Steegborn, C., and Rotili, D. (2017) Development of 1,2,4-Oxadiazoles as Potent and Selective Inhibitors of the Human Deacetylase Sirtuin 2: Structure-Activity Relationship, X-ray Crystal Structure, and Anticancer Activity, *J. Med. Chem. 60*, 2344-2360.

55. Yang, L. L., Wang, H. L., Zhong, L., Yuan, C., Liu, S. Y., Yu, Z. J., Liu, S., Yan, Y. H., Wu, C., Wang, Y., Wang, Z., Yu, Y., Chen, Q., and Li, G. B. (2018) X-ray crystal structure guided discovery of new selective, substrate-mimicking sirtuin 2 inhibitors that exhibit activities against non-small cell lung cancer cells, *Eur. J. Med. Chem. 155*, 806-823.

56. Jing, H., Hu, J., He, B., Negron Abril, Y. L., Stupinski, J., Weiser, K., Carbonaro, M., Chiang, Y. L., Southard, T., Giannakakou, P., Weiss, R. S., and Lin, H. (2016) A SIRT2-Selective Inhibitor Promotes c-Myc Oncoprotein Degradation and Exhibits Broad Anticancer Activity, *Cancer Cell 29*, 767-768.

57. Smith, B. C., and Denu, J. M. (2007) Mechanism-Based Inhibition of Sir2 Deacetylases by Thioacetyl-Lysine Peptide, *Biochemistry 46*, 14478-14486.

58. Farooqi, A. S., Hong, J. Y., Cao, J., Lu, X., Price, I. R., Zhao, Q., Kosciuk, T., Yang, M., Bai, J. J., and Lin, H. (2019) Novel Lysine-Based Thioureas as Mechanism-Based Inhibitors of Sirtuin 2 (SIRT2) with Anticancer Activity in a Colorectal Cancer Murine Model, *J. Med. Chem. 62*, 4131-4141.

59. Hong, J. Y., Fernandez, I., Anmangandla, A., Lu, X., Bai, J. J., and Lin, H. (2021) Pharmacological Advantage of SIRT2-Selective versus pan-SIRT1-3 Inhibitors, *ACS Chem. Biol. 16*, 1266-1275.

60. Hong, J. Y., Jing, H., Price, I. R., Cao, J., Bai, J. J., and Lin, H. (2020) Simultaneous Inhibition of SIRT2 Deacetylase and Defatty-Acylase Activities via a PROTAC Strategy, *ACS Med. Chem. Lett. 11*, 2305-2311.

61. Wang, J., Nisar, M., Huang, C., Pan, X., Lin, D., Zheng, G., Jin, H., Chen, D., Tian, N., Huang, Q., Duan, Y., Yan, Y., Wang, K., Wu, C., Hu, J., Zhang, X., and Wang, X. (2018) Small molecule natural compound agonist of SIRT3 as a therapeutic target for the treatment of intervertebral disc degeneration, *Exp. Mol. Med. 50*, 1-14.

62. Lu, J., Zhang, H., Chen, X., Zou, Y., Li, J., Wang, L., Wu, M., Zang, J., Yu, Y., Zhuang, W., Xia, Q., and Wang, J. (2017) A small molecule activator of SIRT3 promotes deacetylation and activation of manganese superoxide dismutase, *Free Radical Biol. Med. 112*, 287-297.

63. Alhazzazi, T. Y., Kamarajan, P., Xu, Y., Ai, T., Chen, L., Verdin, E., and Kapila, Y. L. (2016) A Novel Sirtuin-3 Inhibitor, LC-0296, Inhibits Cell Survival and Proliferation, and Promotes Apoptosis of Head and Neck Cancer Cells, *Anticancer Res. 36*, 49-60.

64. Li, M., Chiang, Y. L., Lyssiotis, C. A., Teater, M. R., Hong, J. Y., Shen, H., Wang, L., Hu, J., Jing, H., Chen, Z., Jain, N., Duy, C., Mistry, S. J., Cerchietti, L., Cross, J. R., Cantley, L. C., Green, M. R., Lin, H., and Melnick, A. M. (2019) Non-oncogene Addiction to SIRT3 Plays a Critical Role in Lymphomagenesis, *Cancer Cell 35*, 916-931 e919.

65. Abril, Y. L. N., Fernandez, I. R., Hong, J. Y., Chiang, Y. L., Kutateladze, D. A., Zhao, Q., Yang, M., Hu, J., Sadhukhan, S., Li, B., He, B., Remick, B., Bai, J. J., Mullmann, J., Wang, F., Maymi, V., Dhawan, R., Auwerx, J., Southard, T., Cerione, R. A., Lin, H., and Weiss, R. S. (2021) Pharmacological and genetic perturbation establish SIRT5 as a promising target in breast cancer, *Oncogene 40*, 1644-1658.

66. You, W., Rotili, D., Li, T. M., Kambach, C., Meleshin, M., Schutkowski, M., Chua, K. F., Mai, A., and Steegborn, C. (2017) Structural Basis of Sirtuin 6 Activation by Synthetic Small Molecules, *Angew. Chem. Int. Ed. Engl. 56*, 1007-1011.

67. Iachettini, S., Trisciuoglio, D., Rotili, D., Lucidi, A., Salvati, E., Zizza, P., Di Leo, L., Del Bufalo, D., Ciriolo, M. R., Leonetti, C., Steegborn, C., Mai, A., Rizzo, A., and Biroccio, A. (2018) Pharmacological activation of SIRT6 triggers lethal autophagy in human cancer cells, *Cell Death Dis. 9*, 996.

68. Huang, Z., Zhao, J., Deng, W., Chen, Y., Shang, J., Song, K., Zhang, L., Wang, C., Lu, S., Yang, X., He, B., Min, J., Hu, H., Tan, M., Xu, J., Zhang, Q., Zhong, J., Sun, X., Mao, Z., Lin, H., Xiao, M., Chin, Y. E., Jiang, H., Xu, Y., Chen, G., and Zhang, J. (2018) Identification of a cellularly active SIRT6 allosteric activator, *Nat. Chem. Biol. 14*, 1118-1126.

69. Sociali, G., Galeno, L., Parenti, M. D., Grozio, A., Bauer, I., Passalacqua, M., Boero, S., Donadini, A., Millo, E., Bellotti, M., Sturla, L., Damonte, P., Puddu, A., Ferroni, C., Varchi, G., Franceschi, C., Ballestrero, A., Poggi, A., Bruzzone, S., Nencioni, A., and Del Rio, A. (2015) Quinazolinedione SIRT6 inhibitors sensitize cancer cells to chemotherapeutics, *Eur. J. Med. Chem. 102*, 530-539.

70. Parenti, M. D., Grozio, A., Bauer, I., Galeno, L., Damonte, P., Millo, E., Sociali, G., Franceschi, C., Ballestrero, A., Bruzzone, S., Del Rio, A., and Nencioni, A. (2014) Discovery of novel and selective SIRT6 inhibitors, *J. Med. Chem. 57*, 4796-4804.

71. Damonte, P., Sociali, G., Parenti, M. D., Soncini, D., Bauer, I., Boero, S., Grozio, A., Holtey, M. V., Piacente, F., Becherini, P., Sanguineti, R., Salis, A., Damonte,

G., Cea, M., Murone, M., Poggi, A., Nencioni, A., Del Rio, A., and Bruzzone, S. (2017) SIRT6 inhibitors with salicylate-like structure show immunosuppressive and chemosensitizing effects, *Bioorg. Med. Chem. 25*, 5849-5858.

72. Sociali, G., Magnone, M., Ravera, S., Damonte, P., Vigliarolo, T., Von Holtey, M., Vellone, V. G., Millo, E., Caffa, I., Cea, M., Parenti, M. D., Del Rio, A., Murone, M., Mostoslavsky, R., Grozio, A., Nencioni, A., and Bruzzone, S. (2017) Pharmacological Sirt6 inhibition improves glucose tolerance in a type 2 diabetes mouse model, *FASEB J. 31*, 3138-3149.

73. Heltweg, B., Gatbonton, T., Schuler, A. D., Posakony, J., Li, H., Goehle, S., Kollipara, R., Depinho, R. A., Gu, Y., Simon, J. A., and Bedalov, A. (2006) Antitumor activity of a small-molecule inhibitor of human silent information regulator 2 enzymes, *Cancer Res. 66*, 4368-4377.

74. Grozinger, C. M., Chao, E. D., Blackwell, H. E., Moazed, D., and Schreiber, S. L. (2001) Identification of a class of small molecule inhibitors of the sirtuin family of NAD-dependent deacetylases by phenotypic screening, *J. Biol. Chem. 276*, 38837-38843.

75. Mai, A., Massa, S., Lavu, S., Pezzi, R., Simeoni, S., Ragno, R., Mariotti, F. R., Chiani, F., Camilloni, G., and Sinclair, D. A. (2005) Design, synthesis, and biological evaluation of sirtinol analogues as class III histone/protein deacetylase (Sirtuin) inhibitors, *J. Med. Chem. 48*, 7789-7795.

76. Lara, E., Mai, A., Calvanese, V., Altucci, L., Lopez-Nieva, P., Martinez-Chantar, M. L., Varela-Rey, M., Rotili, D., Nebbioso, A., Ropero, S., Montoya, G., Oyarzabal, J., Velasco, S., Serrano, M., Witt, M., Villar-Garea, A., Imhof, A., Mato, J. M., Esteller, M., and Fraga, M. F. (2009) Salermide, a Sirtuin inhibitor with a strong cancer-specific proapoptotic effect, *Oncogene 28*, 781-791.

77. Lain, S., Hollick, J. J., Campbell, J., Staples, O. D., Higgins, M., Aoubala, M., McCarthy, A., Appleyard, V., Murray, K. E., Baker, L., Thompson, A., Mathers, J., Holland, S. J., Stark, M. J., Pass, G., Woods, J., Lane, D. P., and Westwood, N. J. (2008) Discovery, in vivo activity, and mechanism of action of a small-molecule p53 activator, *Cancer Cell 13*, 454-463.

78. McCarthy, A. R., Pirrie, L., Hollick, J. J., Ronseaux, S., Campbell, J., Higgins, M., Staples, O. D., Tran, F., Slawin, A. M., Lain, S., and Westwood, N. J. (2012) Synthesis and biological characterisation of sirtuin inhibitors based on the tenovins, *Bioorg. Med. Chem. 20*, 1779-1793.

79. Igase, M., Fujiki, N., Shibutani, S., Sakai, H., Noguchi, S., Nemoto, Y., and Mizuno, T. (2020) Tenovin-6 induces the SIRT-independent cell growth suppression and blocks autophagy flux in canine hemangiosarcoma cell lines, *Exp. Cell Res. 388*,

111810.

80. Yuan, H., He, M., Cheng, F., Bai, R., da Silva, S. R., Aguiar, R. C., and Gao, S. J. (2017) Tenovin-6 inhibits proliferation and survival of diffuse large B-cell lymphoma cells by blocking autophagy, *Oncotarget 8*, 14912-14924.

81. Yoon, Y. K., Ali, M. A., Wei, A. C., Choon, T. S., Shirazi, A. N., and Parang, K. (2015) Discovery of a potent and highly fluorescent sirtuin inhibitor, *MedChemComm 6*, 1857-1863.

82. Schnekenburger, M., Goffin, E., Lee, J. Y., Jang, J. Y., Mazumder, A., Ji, S., Rogister, B., Bouider, N., Lefranc, F., Miklos, W., Mathieu, V., de Tullio, P., Kim, K. W., Dicato, M., Berger, W., Han, B. W., Kiss, R., Pirotte, B., and Diederich, M. (2017) Discovery and Characterization of R/S-N-3-Cyanophenyl-N'-(6-tert-butoxycarbonylamino-3,4-dihydro-2,2-dimethyl-2H-1- benzopyran-4-yl)urea, a New Histone Deacetylase Class III Inhibitor Exerting Antiproliferative Activity against Cancer Cell Lines, *J. Med. Chem. 60*, 4714-4733.

83. Laaroussi, H., Ding, Y., Teng, Y., Deschamps, P., Vidal, M., Yu, P., and Broussy, S. (2020) Synthesis of indole inhibitors of silent information regulator 1 (SIRT1), and their evaluation as cytotoxic agents, *Eur. J. Med. Chem. 202*, 112561.

84. Carafa, V., Nebbioso, A., Cuomo, F., Rotili, D., Cobellis, G., Bontempo, P., Baldi, A., Spugnini, E. P., Citro, G., Chambery, A., Russo, R., Ruvo, M., Ciana, P., Maravigna, L., Shaik, J., Radaelli, E., De Antonellis, P., Tarantino, D., Pirolli, A., Ragno, R., Zollo, M., Stunnenberg, H. G., Mai, A., and Altucci, L. (2018) RIP1-HAT1-SIRT Complex Identification and Targeting in Treatment and Prevention of Cancer, *Clinical Cancer Research 24*, 2886-2900.

85. Spiegelman, N. A., Hong, J. Y., Hu, J., Jing, H., Wang, M., Price, I. R., Cao, J., Yang, M., Zhang, X., and Lin, H. (2019) A Small-Molecule SIRT2 Inhibitor That Promotes K-Ras4a Lysine Fatty-Acylation, *ChemMedChem 14*, 744-748.

86. Bosch-Presegue, L., and Vaquero, A. (2011) The dual role of sirtuins in cancer, *Genes Cancer 2*, 648-662.

87. Yeung, F., Hoberg, J. E., Ramsey, C. S., Keller, M. D., Jones, D. R., Frye, R. A., and Mayo, M. W. (2004) Modulation of NF-kappaB-dependent transcription and cell survival by the SIRT1 deacetylase, *EMBO J. 23*, 2369-2380.

88. Lim, J. H., Lee, Y. M., Chun, Y. S., Chen, J., Kim, J. E., and Park, J. W. (2010) Sirtuin 1 modulates cellular responses to hypoxia by deacetylating hypoxia-inducible factor 1alpha, *Mol. Cell 38*, 864-878.

89. Simic, P., Williams, E. O., Bell, E. L., Gong, J. J., Bonkowski, M., and Guarente,

L. (2013) SIRT1 suppresses the epithelial-to-mesenchymal transition in cancer metastasis and organ fibrosis, *Cell Rep. 3*, 1175-1186.

90. Yang, Y., Hou, H., Haller, E. M., Nicosia, S. V., and Bai, W. (2005) Suppression of FOXO1 activity by FHL2 through SIRT1-mediated deacetylation, *EMBO J. 24*, 1021-1032.

91. Menssen, A., Hydbring, P., Kapelle, K., Vervoorts, J., Diebold, J., Luscher, B., Larsson, L. G., and Hermeking, H. (2012) The c-MYC oncoprotein, the NAMPT enzyme, the SIRT1-inhibitor DBC1, and the SIRT1 deacetylase form a positive feedback loop, *Proc. Natl. Acad. Sci. USA 109*, E187-196.

92. Yi, J., and Luo, J. (2010) SIRT1 and p53, effect on cancer, senescence and beyond, *Biochim. Biophys. Acta 1804*, 1684-1689.

93. Xu, Y., Qin, Q., Chen, R., Wei, C., and Mo, Q. (2018) SIRT1 promotes proliferation, migration, and invasion of breast cancer cell line MCF-7 by upregulating DNA polymerase delta1 (POLD1), *Biochem. Biophys. Res. Commun. 502*, 351-357.

94. Ren, N. S. X., Ji, M., Tokar, E. J., Busch, E. L., Xu, X., Lewis, D., Li, X., Jin, A., Zhang, Y., Wu, W. K. K., Huang, W., Li, L., Fargo, D. C., Keku, T. O., Sandler, R. S., and Li, X. (2017) Haploinsufficiency of SIRT1 Enhances Glutamine Metabolism and Promotes Cancer Development, *Curr. Biol. 27*, 483-494.

95. Wang, T., Li, X., and Sun, S. L. (2020) EX527, a Sirt-1 inhibitor, induces apoptosis in glioma via activating the p53 signaling pathway, *Anticancer Drugs 31*, 19-26.

96. Chen, J., Cao, L., Li, Z., and Li, Y. (2019) SIRT1 promotes GLUT1 expression and bladder cancer progression via regulation of glucose uptake, *Hum. Cell 32*, 193-201.

97. Yousafzai, N. A., Zhou, Q., Xu, W., Shi, Q., Xu, J., Feng, L., Chen, H., Shin, V. Y., Jin, H., and Wang, X. (2019) SIRT1 deacetylated and stabilized XRCC1 to promote chemoresistance in lung cancer, *Cell Death Dis. 10*, 363.

98. Asaka, R., Miyamoto, T., Yamada, Y., Ando, H., Mvunta, D. H., Kobara, H., and Shiozawa, T. (2015) Sirtuin 1 promotes the growth and cisplatin resistance of endometrial carcinoma cells: a novel therapeutic target, *Lab. Invest. 95*, 1363-1373.

99. Muscolini, M., Castiello, L., Palermo, E., Zevini, A., Ferrari, M., Olagnier, D., and Hiscott, J. (2019) SIRT1 Modulates the Sensitivity of Prostate Cancer Cells to Vesicular Stomatitis Virus Oncolysis, *J. Virol. 93*.

100. Kim, H. B., Lee, S. H., Um, J. H., Kim, M. J., Hyun, S. K., Gong, E. J., Oh, W. K., Kang, C. D., and Kim, S. H. (2015) Sensitization of chemo-resistant human chronic myeloid leukemia stem-like cells to Hsp90 inhibitor by SIRT1

inhibition, *Int. J. Biol. Sci. 11*, 923-934.

101. Chen, G., Zhang, B., Xu, H., Sun, Y., Shi, Y., Luo, Y., Jia, H., and Wang, F. (2017) Suppression of Sirt1 sensitizes lung cancer cells to WEE1 inhibitor MK-1775-induced DNA damage and apoptosis, *Oncogene 36*, 6863-6872.

102. Oon, C. E., Strell, C., Yeong, K. Y., Ostman, A., and Prakash, J. (2015) SIRT1 inhibition in pancreatic cancer models: contrasting effects in vitro and in vivo, *Eur. J. Pharmacol. 757*, 59-67.

103. Kim, H. S., Vassilopoulos, A., Wang, R. H., Lahusen, T., Xiao, Z., Xu, X., Li, C., Veenstra, T. D., Li, B., Yu, H., Ji, J., Wang, X. W., Park, S. H., Cha, Y. I., Gius, D., and Deng, C. X. (2011) SIRT2 maintains genome integrity and suppresses tumorigenesis through regulating APC/C activity, *Cancer Cell 20*, 487-499.

104. Serrano, L., Martinez-Redondo, P., Marazuela-Duque, A., Vazquez, B. N., Dooley, S. J., Voigt, P., Beck, D. B., Kane-Goldsmith, N., Tong, Q., Rabanal, R. M., Fondevila, D., Munoz, P., Kruger, M., Tischfield, J. A., and Vaquero, A. (2013) The tumor suppressor SirT2 regulates cell cycle progression and genome stability by modulating the mitotic deposition of H4K20 methylation, *Genes Dev. 27*, 639-653.

105. Yang, M. H., Laurent, G., Bause, A. S., Spang, R., German, N., Haigis, M. C., and Haigis, K. M. (2013) HDAC6 and SIRT2 regulate the acetylation state and oncogenic activity of mutant K-RAS, *Mol. Cancer Res. 11*, 1072-1077.

106. Zhou, W., Ni, T. K., Wronski, A., Glass, B., Skibinski, A., Beck, A., and Kuperwasser, C. (2016) The SIRT2 Deacetylase Stabilizes Slug to Control Malignancy of Basal-like Breast Cancer, *Cell Rep. 17*, 1302-1317.

107. Liu, P. Y., Xu, N., Malyukova, A., Scarlett, C. J., Sun, Y. T., Zhang, X. D., Ling, D., Su, S. P., Nelson, C., Chang, D. K., Koach, J., Tee, A. E., Haber, M., Norris, M. D., Toon, C., Rooman, I., Xue, C., Cheung, B. B., Kumar, S., Marshall, G. M., Biankin, A. V., and Liu, T. (2013) The histone deacetylase SIRT2 stabilizes Myc oncoproteins, *Cell Death Differ. 20*, 503-514.

108. Zhao, D., Zou, S. W., Liu, Y., Zhou, X., Mo, Y., Wang, P., Xu, Y. H., Dong, B., Xiong, Y., Lei, Q. Y., and Guan, K. L. (2013) Lysine-5 acetylation negatively regulates lactate dehydrogenase A and is decreased in pancreatic cancer, *Cancer Cell 23*, 464-476.

109. Zhao, Y., Yang, J., Liao, W., Liu, X., Zhang, H., Wang, S., Wang, D., Feng, J., Yu, L., and Zhu, W. G. (2010) Cytosolic FoxO1 is essential for the induction of autophagy and tumour suppressor activity, *Nat. Cell Biol. 12*, 665-675.

110. Jing, H., Zhang, X., Wisner, S. A., Chen, X., Spiegelman, N. A., Linder, M. E., and Lin, H. (2017) SIRT2 and lysine fatty acylation regulate the transforming

activity of K-Ras4a, *eLife 6*, e32436.

111. Kosciuk, T., Price, I. R., Zhang, X., Zhu, C., Johnson, K. N., Zhang, S., Halaby, S. L., Komaniecki, G. P., Yang, M., DeHart, C. J., Thomas, P. M., Kelleher, N. L., Fromme, J. C., and Lin, H. (2020) NMT1 and NMT2 are lysine myristoyltransferases regulating the ARF6 GTPase cycle, *Nat. Commun. 11*, 1067.

112. Funato, K., Hayashi, T., Echizen, K., Negishi, L., Shimizu, N., Koyama-Nasu, R., Nasu-Nishimura, Y., Morishita, Y., Tabar, V., Todo, T., Ino, Y., Mukasa, A., Saito, N., and Akiyama, T. (2018) SIRT2-mediated inactivation of p73 is required for glioblastoma tumorigenicity, *EMBO Reports 19*.

113. Yang, H., Chen, Y., Jiang, Y., Wang, D., Yan, J., and Zhou, Z. (2020) TP53 mutation influences the efficacy of treatment of colorectal cancer cell lines with a combination of sirtuin inhibitors and chemotherapeutic agents, *Exp. Ther. Med. 20*, 1415-1422.

114. Li, Y., Zhang, M., Dorfman, R. G., Pan, Y., Tang, D., Xu, L., Zhao, Z., Zhou, Q., Zhou, L., Wang, Y., Yin, Y., Shen, S., Kong, B., Friess, H., Zhao, S., Wang, L., and Zou, X. (2018) SIRT2 Promotes the Migration and Invasion of Gastric Cancer through RAS/ERK/JNK/MMP-9 Pathway by Increasing PEPCK1-Related Metabolism, *Neoplasia 20*, 745-756.

115. Kozako, T., Mellini, P., Ohsugi, T., Aikawa, A., Uchida, Y. I., Honda, S. I., and Suzuki, T. (2018) Novel small molecule SIRT2 inhibitors induce cell death in leukemic cell lines, *BMC Cancer 18*, 791.

116. Hong, J. Y., Fernandez, I., Anmangandla, A., Lu, X., Bai, J. J., and Lin, H. (2021) Pharmacological Advantage of SIRT2-Selective versus pan-SIRT1-3 Inhibitors, *ACS Chem. Biol.*

117. Carafa, V., Rotili, D., Forgione, M., Cuomo, F., Serretiello, E., Hailu, G. S., Jarho, E., Lahtela-Kakkonen, M., Mai, A., and Altucci, L. (2016) Sirtuin functions and modulation: from chemistry to the clinic, *Clin. Epigenet. 8*, 61.

118. Plaitakis, A., Kalef-Ezra, E., Kotzamani, D., Zaganas, I., and Spanaki, C. (2017) The Glutamate Dehydrogenase Pathway and Its Roles in Cell and Tissue Biology in Health and Disease, *Biology (Basel) 6*.

119. Torrens-Mas, M., Oliver, J., Roca, P., and Sastre-Serra, J. (2017) SIRT3: Oncogene and Tumor Suppressor in Cancer, *Cancers (Basel) 9*.

120. Bell, E. L., Emerling, B. M., Ricoult, S. J., and Guarente, L. (2011) SirT3 suppresses hypoxia inducible factor 1alpha and tumor growth by inhibiting mitochondrial ROS production, *Oncogene 30*, 2986-2996.

121. Finley, L. W., Carracedo, A., Lee, J., Souza, A., Egia, A., Zhang, J., Teruya-Feldstein, J., Moreira, P. I., Cardoso, S. M., Clish, C. B., Pandolfi, P. P., and Haigis, M. C. (2011) SIRT3 opposes reprogramming of cancer cell metabolism through HIF1alpha destabilization, *Cancer Cell 19*, 416-428.

122. Alhazzazi, T. Y., Kamarajan, P., Verdin, E., and Kapila, Y. L. (2011) SIRT3 and cancer: tumor promoter or suppressor?, *Biochim. Biophys. Acta 1816*, 80-88.

123. Li, S., Banck, M., Mujtaba, S., Zhou, M. M., Sugrue, M. M., and Walsh, M. J. (2010) p53-induced growth arrest is regulated by the mitochondrial SirT3 deacetylase, *PLoS One 5*, e10486.

124. Alhazzazi, T. Y., Kamarajan, P., Joo, N., Huang, J. Y., Verdin, E., D'Silva, N. J., and Kapila, Y. L. (2011) Sirtuin-3 (SIRT3), a novel potential therapeutic target for oral cancer, *Cancer 117*, 1670-1678.

125. Igci, M., Kalender, M. E., Borazan, E., Bozgeyik, I., Bayraktar, R., Bozgeyik, E., Camci, C., and Arslan, A. (2016) High-throughput screening of Sirtuin family of genes in breast cancer, *Gene 586*, 123-128.

126. Bringman-Rodenbarger, L. R., Guo, A. H., Lyssiotis, C. A., and Lombard, D. B. (2018) Emerging Roles for SIRT5 in Metabolism and Cancer, *Antioxid. Redox Signal. 28*, 677-690.

127. Xiangyun, Y., Xiaomin, N., Linping, G., Yunhua, X., Ziming, L., Yongfeng, Y., Zhiwei, C., and Shun, L. (2017) Desuccinylation of pyruvate kinase M2 by SIRT5 contributes to antioxidant response and tumor growth, *Oncotarget 8*, 6984-6993.

128. Shi, L., Yan, H., An, S., Shen, M., Jia, W., Zhang, R., Zhao, L., Huang, G., and Liu, J. (2019) SIRT5-mediated deacetylation of LDHB promotes autophagy and tumorigenesis in colorectal cancer, *Mol. Oncol. 13*, 358-375.

129. Zhang, R., Wang, C., Tian, Y., Yao, Y., Mao, J., Wang, H., Li, Z., Xu, Y., Ye, M., and Wang, L. (2019) SIRT5 Promotes Hepatocellular Carcinoma Progression by Regulating Mitochondrial Apoptosis, *J. Cancer 10*, 3871-3882.

130. Greene, K. S., Lukey, M. J., Wang, X., Blank, B., Druso, J. E., Lin, M. J., Stalnecker, C. A., Zhang, C., Negron Abril, Y., Erickson, J. W., Wilson, K. F., Lin, H., Weiss, R. S., and Cerione, R. A. (2019) SIRT5 stabilizes mitochondrial glutaminase and supports breast cancer tumorigenesis, *Proc. Natl. Acad. Sci. U. S. A.*

131. Ren, M., Yang, X., Bie, J., Wang, Z., Liu, M., Li, Y., Shao, G., and Luo, J. (2020) Citrate synthase desuccinylation by SIRT5 promotes colon cancer cell proliferation and migration, *Biol. Chem.*

132. Giblin, W., Bringman-Rodenbarger, L., Guo, A. H., Kumar, S., Monovich, A. C., Mostafa, A. M., Skinner, M. E., Azar, M., Mady, A. S., Chung, C. H., Kadambi, N., Melong, K. A., Lee, H. J., Zhang, L., Sajjakulnukit, P., Trefely, S., Varner, E. L., Iyer, S., Wang, M., Wilmott, J. S., Soyer, H. P., Sturm, R. A., Pritchard, A. L., Andea, A. A., Scolyer, R. A., Stark, M. S., Scott, D. A., Fullen, D. R., Bosenberg, M. W., Chandrasekaran, S., Nikolovska-Coleska, Z., Verhaegen, M. E., Snyder, N. W., Rivera, M. N., Osterman, A., Lyssiotis, C. A., and Lombard, D. B. (2021) The deacylase SIRT5 supports melanoma viability by influencing chromatin dynamics, *J. Clin. Invest.*

133. Michishita, E., McCord, R. A., Berber, E., Kioi, M., Padilla-Nash, H., Damian, M., Cheung, P., Kusumoto, R., Kawahara, T. L., Barrett, J. C., Chang, H. Y., Bohr, V. A., Ried, T., Gozani, O., and Chua, K. F. (2008) SIRT6 is a histone H3 lysine 9 deacetylase that modulates telomeric chromatin, *Nature 452*, 492-496.

134. Kawahara, T. L., Michishita, E., Adler, A. S., Damian, M., Berber, E., Lin, M., McCord, R. A., Ongaigui, K. C., Boxer, L. D., Chang, H. Y., and Chua, K. F. (2009) SIRT6 links histone H3 lysine 9 deacetylation to NF-kappaB-dependent gene expression and organismal life span, *Cell 136*, 62-74.

135. Tasselli, L., Xi, Y., Zheng, W., Tennen, R. I., Odrowaz, Z., Simeoni, F., Li, W., and Chua, K. F. (2016) SIRT6 deacetylates H3K18ac at pericentric chromatin to prevent mitotic errors and cellular senescence, *Nat. Struct. Mol. Biol. 23*, 434-440.

136. Michishita, E., McCord, R. A., Boxer, L. D., Barber, M. F., Hong, T., Gozani, O., and Chua, K. F. (2009) Cell cycle-dependent deacetylation of telomeric histone H3 lysine K56 by human SIRT6, *Cell Cycle 8*, 2664-2666.

137. Sundaresan, N. R., Vasudevan, P., Zhong, L., Kim, G., Samant, S., Parekh, V., Pillai, V. B., Ravindra, P. V., Gupta, M., Jeevanandam, V., Cunningham, J. M., Deng, C. X., Lombard, D. B., Mostoslavsky, R., and Gupta, M. P. (2012) The sirtuin SIRT6 blocks IGF-Akt signaling and development of cardiac hypertrophy by targeting c-Jun, *Nat. Med. 18*, 1643-1650.

138. Jiang, H., Khan, S., Wang, Y., Charron, G., He, B., Sebastian, C., Du, J., Kim, R., Ge, E., Mostoslavsky, R., Hang, H. C., Hao, Q., and Lin, H. (2013) SIRT6 regulates TNF-alpha secretion through hydrolysis of long-chain fatty acyl lysine, *Nature 496*, 110-113.

139. Garcia-Peterson, L. M., Ndiaye, M. A., Singh, C. K., Chhabra, G., Huang, W., and Ahmad, N. (2017) SIRT6 histone deacetylase functions as a potential oncogene in human melanoma, *Genes Cancer 8*, 701-712.

140. Huang, N., Liu, Z., Zhu, J., Cui, Z., Li, Y., Yu, Y., Sun, F., Pan, Q., and Yang, Q. (2017) Sirtuin 6 plays an oncogenic role and induces cell autophagy in

esophageal cancer cells, *Tumor Biol. 39*, 1010428317708532.

141. Bae, J. S., Noh, S. J., Kim, K. M., Park, S. H., Hussein, U. K., Park, H. S., Park, B. H., Ha, S. H., Lee, H., Chung, M. J., Moon, W. S., Cho, D. H., and Jang, K. Y. (2018) SIRT6 Is Involved in the Progression of Ovarian Carcinomas via beta-Catenin-Mediated Epithelial to Mesenchymal Transition, *Front. Oncol. 8*, 538.

142. Zhang, G., Liu, Z., Qin, S., and Li, K. (2015) Decreased expression of SIRT6 promotes tumor cell growth correlates closely with poor prognosis of ovarian cancer, *Eur. J. Gynaecol. Oncol. 36*, 629-632.

143. Kugel, S., Sebastian, C., Fitamant, J., Ross, K. N., Saha, S. K., Jain, E., Gladden, A., Arora, K. S., Kato, Y., Rivera, M. N., Ramaswamy, S., Sadreyev, R. I., Goren, A., Deshpande, V., Bardeesy, N., and Mostoslavsky, R. (2016) SIRT6 Suppresses Pancreatic Cancer through Control of Lin28b, *Cell 165*, 1401-1415.

144. Marquardt, J. U., Fischer, K., Baus, K., Kashyap, A., Ma, S., Krupp, M., Linke, M., Teufel, A., Zechner, U., Strand, D., Thorgeirsson, S. S., Galle, P. R., and Strand, S. (2013) Sirtuin-6-dependent genetic and epigenetic alterations are associated with poor clinical outcome in hepatocellular carcinoma patients, *Hepatology 58*, 1054-1064.

145. Sebastian, C., Zwaans, B. M., Silberman, D. M., Gymrek, M., Goren, A., Zhong, L., Ram, O., Truelove, J., Guimaraes, A. R., Toiber, D., Cosentino, C., Greenson, J. K., MacDonald, A. I., McGlynn, L., Maxwell, F., Edwards, J., Giacosa, S., Guccione, E., Weissleder, R., Bernstein, B. E., Regev, A., Shiels, P. G., Lombard, D. B., and Mostoslavsky, R. (2012) The histone deacetylase SIRT6 is a tumor suppressor that controls cancer metabolism, *Cell 151*, 1185-1199.

146. Zhang, X., Spiegelman, N. A., Nelson, O. D., Jing, H., and Lin, H. (2017) SIRT6 regulates Ras-related protein R-Ras2 by lysine defatty-acylation, *eLife 6*, e25158.

147. Khan, D., Sarikhani, M., Dasgupta, S., Maniyadath, B., Pandit, A. S., Mishra, S., Ahamed, F., Dubey, A., Fathma, N., Atreya, H. S., Kolthur-Seetharam, U., and Sundaresan, N. R. (2018) SIRT6 deacetylase transcriptionally regulates glucose metabolism in heart, *J. Cell. Physiol. 233*, 5478-5489.

148. Shang, J. L., Ning, S. B., Chen, Y. Y., Chen, T. X., and Zhang, J. (2021) MDL-800, an allosteric activator of SIRT6, suppresses proliferation and enhances EGFR-TKIs therapy in non-small cell lung cancer, *Acta Pharmacol. Sin. 42*, 120-131.

149. Lu, B., Zhang, D., Wang, X., Lin, D., Chen, Y., and Xu, X. (2021) Targeting SIRT1 to inhibit the proliferation of multiple myeloma cells, *Oncol. Lett. 21*, 306.

150. Portmann, S., Fahrner, R., Lechleiter, A., Keogh, A., Overney, S., Laemmle, A., Mikami, K., Montani, M., Tschan, M. P., Candinas, D., and Stroka, D. (2013) Antitumor effect of SIRT1 inhibition in human HCC tumor models in vitro and in vivo, *Mol. Cancer Ther. 12*, 499-508.

151. Marshall, G. M., Liu, P. Y., Gherardi, S., Scarlett, C. J., Bedalov, A., Xu, N., Iraci, N., Valli, E., Ling, D., Thomas, W., van Bekkum, M., Sekyere, E., Jankowski, K., Trahair, T., Mackenzie, K. L., Haber, M., Norris, M. D., Biankin, A. V., Perini, G., and Liu, T. (2011) SIRT1 promotes N-Myc oncogenesis through a positive feedback loop involving the effects of MKP3 and ERK on N-Myc protein stability, *PLoS Genet. 7*, e1002135.

152. Ceballos, M. P., Angel, A., Delprato, C. B., Livore, V. I., Ferretti, A. C., Lucci, A., Comanzo, C. G., Alvarez, M. L., Quiroga, A. D., Mottino, A. D., and Carrillo, M. C. (2021) Sirtuin 1 and 2 inhibitors enhance the inhibitory effect of sorafenib in hepatocellular carcinoma cells, *Eur. J. Pharmacol. 892*, 173736.

153. Ota, H., Tokunaga, E., Chang, K., Hikasa, M., Iijima, K., Eto, M., Kozaki, K., Akishita, M., Ouchi, Y., and Kaneki, M. (2006) Sirt1 inhibitor, Sirtinol, induces senescence-like growth arrest with attenuated Ras-MAPK signaling in human cancer cells, *Oncogene 25*, 176-185.

154. Fong, Y., Lin, Y. C., Wu, C. Y., Wang, H. M., Lin, L. L., Chou, H. L., Teng, Y. N., Yuan, S. S., and Chiu, C. C. (2014) The antiproliferative and apoptotic effects of sirtinol, a sirtuin inhibitor on human lung cancer cells by modulating Akt/beta-catenin-Foxo3a axis, *ScientificWorldJournal 2014*, 937051.

155. Kojima, K., Ohhashi, R., Fujita, Y., Hamada, N., Akao, Y., Nozawa, Y., Deguchi, T., and Ito, M. (2008) A role for SIRT1 in cell growth and chemoresistance in prostate cancer PC3 and DU145 cells, *Biochem. Biophys. Res. Commun. 373*, 423-428.

156. Kozako, T., Aikawa, A., Shoji, T., Fujimoto, T., Yoshimitsu, M., Shirasawa, S., Tanaka, H., Honda, S., Shimeno, H., Arima, N., and Soeda, S. (2012) High expression of the longevity gene product SIRT1 and apoptosis induction by sirtinol in adult T-cell leukemia cells, *Int. J. Cancer 131*, 2044-2055.

157. Ma, W., Zhao, X., Wang, K., Liu, J., and Huang, G. (2018) Dichloroacetic acid (DCA) synergizes with the SIRT2 inhibitor Sirtinol and AGK2 to enhance anti-tumor efficacy in non-small cell lung cancer, *Cancer Biol. Ther. 19*, 835-846.

158. Ke, X., Qin, Q., Deng, T., Liao, Y., and Gao, S. J. (2020) Heterogeneous Responses of Gastric Cancer Cell Lines to Tenovin-6 and Synergistic Effect with Chloroquine, *Cancers (Basel) 12*.

159. Lee, B. B., Kim, Y., Kim, D., Cho, E. Y., Han, J., Kim, H. K., Shim, Y. M., and Kim, D. H. (2019) Metformin and tenovin-6 synergistically induces apoptosis

through LKB1-independent SIRT1 down-regulation in non-small cell lung cancer cells, *Journal of Cellular and Molecular Medicine 23*, 2872-2889.

160. Dai, W., Zhou, J., Jin, B., and Pan, J. (2016) Class III-specific HDAC inhibitor Tenovin-6 induces apoptosis, suppresses migration and eliminates cancer stem cells in uveal melanoma, *Sci. Rep. 6*, 22622.

161. Tan, Y. J., Lee, Y. T., Yeong, K. Y., Petersen, S. H., Kono, K., Tan, S. C., and Oon, C. E. (2018) Anticancer activities of a benzimidazole compound through sirtuin inhibition in colorectal cancer, *Future Med. Chem. 10*, 2039-2057.

162. Tan, Y. J., Lee, Y. T., Petersen, S. H., Kaur, G., Kono, K., Tan, S. C., Majid, A., and Oon, C. E. (2019) BZD9L1 sirtuin inhibitor as a potential adjuvant for sensitization of colorectal cancer cells to 5-fluorouracil, *Ther. Adv. Med. Oncol. 11*, 1758835919878977.

163. Carafa, V., Russo, R., Della Torre, L., Cuomo, F., Dell'Aversana, C., Sarno, F., Sgueglia, G., Di Donato, M., Rotili, D., Mai, A., Nebbioso, A., Cobellis, G., Chambery, A., and Altucci, L. (2020) The Pan-Sirtuin Inhibitor MC2494 Regulates Mitochondrial Function in a Leukemia Cell Line, *Front. Oncol. 10*, 820.

164. Prozorovski, T., Schulze-Topphoff, U., Glumm, R., Baumgart, J., Schroter, F., Ninnemann, O., Siegert, E., Bendix, I., Brustle, O., Nitsch, R., Zipp, F., and Aktas, O. (2008) Sirt1 contributes critically to the redox-dependent fate of neural progenitors, *Nat. Cell Biol. 10*, 385-394.

165. Michan, S., Li, Y., Chou, M. M., Parrella, E., Ge, H., Long, J. M., Allard, J. S., Lewis, K., Miller, M., Xu, W., Mervis, R. F., Chen, J., Guerin, K. I., Smith, L. E., McBurney, M. W., Sinclair, D. A., Baudry, M., de Cabo, R., and Longo, V. D. (2010) SIRT1 is essential for normal cognitive function and synaptic plasticity, *J. Neurosci. 30*, 9695-9707.

166. Guo, W., Qian, L., Zhang, J., Zhang, W., Morrison, A., Hayes, P., Wilson, S., Chen, T., and Zhao, J. (2011) Sirt1 overexpression in neurons promotes neurite outgrowth and cell survival through inhibition of the mTOR signaling, *J. Neurosci. Res. 89*, 1723-1736.

167. Julien, C., Tremblay, C., Emond, V., Lebbadi, M., Salem, N., Jr., Bennett, D. A., and Calon, F. (2009) Sirtuin 1 reduction parallels the accumulation of tau in Alzheimer disease, *J. Neuropathol. Exp. Neurol. 68*, 48-58.

168. Chen, J., Zhou, Y., Mueller-Steiner, S., Chen, L. F., Kwon, H., Yi, S., Mucke, L., and Gan, L. (2005) SIRT1 protects against microglia-dependent amyloid-beta toxicity through inhibiting NF-kappaB signaling, *J. Biol. Chem. 280*, 40364-40374.

169. Jeong, H., Cohen, D. E., Cui, L., Supinski, A., Savas, J. N., Mazzulli, J. R., Yates, J. R., 3rd, Bordone, L., Guarente, L., and Krainc, D. (2011) Sirt1 mediates neuroprotection from mutant huntingtin by activation of the TORC1 and CREB transcriptional pathway, *Nat. Med. 18*, 159-165.

170. Kim, B. S., Lee, C. H., Chang, G. E., Cheong, E., and Shin, I. (2016) A potent and selective small molecule inhibitor of sirtuin 1 promotes differentiation of pluripotent P19 cells into functional neurons, *Sci. Rep. 6*, 34324.

171. Li, W., Guo, B., Tao, K., Li, F., Liu, Z., Yao, H., Feng, D., and Liu, X. (2019) Inhibition of SIRT1 in hippocampal CA1 ameliorates PTSD-like behaviors in mice by protections of neuronal plasticity and serotonin homeostasis via NHLH2/MAO-A pathway, *Biochem. Biophys. Res. Commun. 518*, 344-350.

172. Wei, L., Liu, B., Yao, Z., Yuan, T., Wang, C., Zhang, R., Wang, Q., and Zhao, B. (2021) Sirtuin 1 inhibitor EX527 suppresses morphine-induced behavioral sensitization, *Neurosci. Lett. 744*, 135599.

173. Nikseresht, S., Khodagholi, F., and Ahmadiani, A. (2019) Protective effects of ex-527 on cerebral ischemia-reperfusion injury through necroptosis signaling pathway attenuation, *J. Cell. Physiol. 234*, 1816-1826.

174. Zhou, X. M., Zhang, X., Zhang, X. S., Zhuang, Z., Li, W., Sun, Q., Li, T., Wang, C. X., Zhu, L., Shi, J. X., and Zhou, M. L. (2014) SIRT1 inhibition by sirtinol aggravates brain edema after experimental subarachnoid hemorrhage, *J. Neurosci. Res. 92*, 714-722.

175. Jeong, S. G., and Cho, G. W. (2017) The tubulin deacetylase sirtuin-2 regulates neuronal differentiation through the ERK/CREB signaling pathway, *Biochem. Biophys. Res. Commun. 482*, 182-187.

176. Li, W., Zhang, B., Tang, J., Cao, Q., Wu, Y., Wu, C., Guo, J., Ling, E. A., and Liang, F. (2007) Sirtuin 2, a mammalian homolog of yeast silent information regulator-2 longevity regulator, is an oligodendroglial protein that decelerates cell differentiation through deacetylating alpha-tubulin, *J. Neurosci. 27*, 2606-2616.

177. Ji, S., Doucette, J. R., and Nazarali, A. J. (2011) Sirt2 is a novel in vivo downstream target of Nkx2.2 and enhances oligodendroglial cell differentiation, *J. Mol. Cell. Biol. 3*, 351-359.

178. Liu, L., Arun, A., Ellis, L., Peritore, C., and Donmez, G. (2014) SIRT2 enhances 1-methyl-4-phenyl-1,2,3,6-tetrahydropyridine (MPTP)-induced nigrostriatal damage via apoptotic pathway, *Front. Aging Neurosci. 6*, 184.

179. Wang, B., Zhang, Y., Cao, W., Wei, X., Chen, J., and Ying, W. (2016) SIRT2 Plays Significant Roles in Lipopolysaccharides-Induced Neuroinflammation

and Brain Injury in Mice, *Neurochem. Res. 41*, 2490-2500.

180. She, D. T., Wong, L. J., Baik, S. H., and Arumugam, T. V. (2018) SIRT2 Inhibition Confers Neuroprotection by Downregulation of FOXO3a and MAPK Signaling Pathways in Ischemic Stroke, *Mol. Neurobiol. 55*, 9188-9203.

181. Kaitsuka, T., Matsushita, M., and Matsushita, N. (2020) SIRT2 inhibition activates hypoxia-inducible factor 1alpha signaling and mediates neuronal survival, *Biochem. Biophys. Res. Commun. 529*, 957-962.

182. Wu, D., Lu, W., Wei, Z., Xu, M., and Liu, X. (2018) Neuroprotective Effect of Sirt2-specific Inhibitor AK-7 Against Acute Cerebral Ischemia is P38 Activation-dependent in Mice, *Neuroscience 374*, 61-69.

183. Wu, Z., Zhang, Y., Zhang, Y., and Zhao, P. (2020) Sirtuin 2 Inhibition Attenuates Sevoflurane-Induced Learning and Memory Deficits in Developing Rats via Modulating Microglial Activation, *Cellular and Molecular Neurobiology 40*, 437-446.

184. Diaz-Perdigon, T., Belloch, F. B., Ricobaraza, A., Elboray, E. E., Suzuki, T., Tordera, R. M., and Puerta, E. (2020) Early sirtuin 2 inhibition prevents age-related cognitive decline in a senescence-accelerated mouse model, *Neuropsychopharmacology 45*, 347-357.

185. Etchegaray, J. P., Chavez, L., Huang, Y., Ross, K. N., Choi, J., Martinez-Pastor, B., Walsh, R. M., Sommer, C. A., Lienhard, M., Gladden, A., Kugel, S., Silberman, D. M., Ramaswamy, S., Mostoslavsky, G., Hochedlinger, K., Goren, A., Rao, A., and Mostoslavsky, R. (2015) The histone deacetylase SIRT6 controls embryonic stem cell fate via TET-mediated production of 5-hydroxymethylcytosine, *Nat. Cell Biol. 17*, 545-557.

186. Kaluski, S., Portillo, M., Besnard, A., Stein, D., Einav, M., Zhong, L., Ueberham, U., Arendt, T., Mostoslavsky, R., Sahay, A., and Toiber, D. (2017) Neuroprotective Functions for the Histone Deacetylase SIRT6, *Cell Rep. 18*, 3052-3062.

187. Lasiglie, D., Boero, S., Bauer, I., Morando, S., Damonte, P., Cea, M., Monacelli, F., Odetti, P., Ballestrero, A., Uccelli, A., Mostoslavsky, R., Poggi, A., and Nencioni, A. (2016) Sirt6 regulates dendritic cell differentiation, maturation, and function, *Aging (Albany N. Y.) 8*, 34-49.

188. Ferrara, G., Benzi, A., Sturla, L., Marubbi, D., Frumento, D., Spinelli, S., Abbotto, E., Ivaldi, F., von Holtey, M., Murone, M., Nencioni, A., Uccelli, A., and Bruzzone, S. (2020) Sirt6 inhibition delays the onset of experimental autoimmune encephalomyelitis by reducing dendritic cell migration, *J. Neuroinflammation 17*, 228.

189. Cheng, H. L., Mostoslavsky, R., Saito, S., Manis, J. P., Gu, Y., Patel, P., Bronson, R., Appella, E., Alt, F. W., and Chua, K. F. (2003) Developmental defects and p53 hyperacetylation in Sir2 homolog (SIRT1)-deficient mice, *Proc. Natl. Acad. Sci. U. S. A. 100*, 10794-10799.

190. Vikram, A., Lewarchik, C. M., Yoon, J. Y., Naqvi, A., Kumar, S., Morgan, G. M., Jacobs, J. S., Li, Q., Kim, Y. R., Kassan, M., Liu, J., Gabani, M., Kumar, A., Mehdi, H., Zhu, X., Guan, X., Kutschke, W., Zhang, X., Boudreau, R. L., Dai, S., Matasic, D. S., Jung, S. B., Margulies, K. B., Kumar, V., Bachschmid, M. M., London, B., and Irani, K. (2017) Sirtuin 1 regulates cardiac electrical activity by deacetylating the cardiac sodium channel, *Nat. Med. 23*, 361-367.

191. Alcendor, R. R., Gao, S., Zhai, P., Zablocki, D., Holle, E., Yu, X., Tian, B., Wagner, T., Vatner, S. F., and Sadoshima, J. (2007) Sirt1 regulates aging and resistance to oxidative stress in the heart, *Circulation Research 100*, 1512-1521.

192. Safari, F., Shekarforoosh, S., Hashemi, T., Namvar Aghdash, S., Fekri, A., and Safari, F. (2017) Sirtinol abrogates late phase of cardiac ischemia preconditioning in rats, *J. Physiol. Sci. 67*, 515-522.

193. Breitenstein, A., Stein, S., Holy, E. W., Camici, G. G., Lohmann, C., Akhmedov, A., Spescha, R., Elliott, P. J., Westphal, C. H., Matter, C. M., Luscher, T. F., and Tanner, F. C. (2011) Sirt1 inhibition promotes in vivo arterial thrombosis and tissue factor expression in stimulated cells, *Cardiovasc. Res. 89*, 464-472.

194. Li, Y., Meng, X., Wang, W., Liu, F., Hao, Z., Yang, Y., Zhao, J., Yin, W., Xu, L., Zhao, R., and Hu, J. (2017) Cardioprotective Effects of SIRT6 in a Mouse Model of Transverse Aortic Constriction-Induced Heart Failure, *Front. Physiol. 8*, 394.

195. Huang, Y., Zhang, J., Xu, D., Peng, Y., Jin, Y., and Zhang, L. (2021) SIRT6 specific inhibitor OSS128167 exacerbates diabetic cardiomyopathy by aggravating inflammation and oxidative stress, *Mol. Med. Report. 23*.

196. Napper, A. D., Hixon, J., McDonagh, T., Keavey, K., Pons, J. F., Barker, J., Yau, W. T., Amouzegh, P., Flegg, A., Hamelin, E., Thomas, R. J., Kates, M., Jones, S., Navia, M. A., Saunders, J. O., DiStefano, P. S., and Curtis, R. (2005) Discovery of indoles as potent and selective inhibitors of the deacetylase SIRT1, *J. Med. Chem. 48*, 8045-8054.

197. Gertz, M., Fischer, F., Nguyen, G. T., Lakshminarasimhan, M., Schutkowski, M., Weyand, M., and Steegborn, C. (2013) Ex-527 inhibits Sirtuins by exploiting their unique NAD+-dependent deacetylation mechanism, *Proc. Natl. Acad. Sci. U. S. A. 110*, E2772-2781.

# CHAPTER 2

## A GLYCOCONJUGATED SIRT2 INHIBITOR WITH AQUEOUS SOLUBILITY ALLOWS STRUCTURE-BASED DESIGN OF SIRT2 INHIBITORS

This is a revised version of the published paper: Hong JY, Price IR, Bai JJ, Lin H. A Glycoconjugated SIRT2 Inhibitor with Aqueous Solubility Allows Structure-Based Design of SIRT2 Inhibitors. *ACS Chem Biol.* 2019 Aug 16;14(8):1802-1810.

J.Y.H. and I.R.P. contributed equally to this work. J.Y.H., I.R.P. and H.L. conceived the concept. J.Y.H. designed, synthesized and the small molecules. J.Y.H. further tested these small molecules in solubility tests, enzymatic assays, 2D cellular proliferation assays, cell permeability assays, and 3D soft agar assays. I.R.P. purified the enzymes. I.R.P. solved and analyzed the crystal structures of SIRT2 with Glucose-TM. J.J.B. helped test the compounds in 3D soft agar assays. J.Y.H., I.R.P. and H.L. wrote the manuscript. All the authors have given approval to the final version of the manuscript.

### 2.1 Abstract

Small molecule inhibitors for SIRT2, a member of the sirtuin family of nicotinamide adenine dinucleotide-dependent protein lysine deacylases, have shown promise in treating cancer and neurodegenerative diseases. Developing SIRT2-selective inhibitors with better pharmacological properties is key to further realize the therapeutic potential of targeting SIRT2. One of the best SIRT2-selective inhibitors reported is a thiomyristoyl lysine compound called TM, which showed promising anticancer activity in mouse models without much toxicity to normal cells. The main limitations of TM, how-ever, are the low aqueous solubility and lack of X-ray crystal structures to aid future drug design. Here, we designed and synthesized a glucose-conjugated TM (glucose-TM) analog with superior aqueous solubility. Although glucose-TM is not cell permeable, the excellent aqueous solubility allowed us to

obtain a crystal structure of SIRT2 in complex with it. The structure enabled us to design several new TM analogs, one of which, NH4-6, showed superior water solubility and better anticancer activity in cell culture. The results of these studies provided important insights that will further fuel the future development of improved SIRT2 inhibitors as promising therapeutics for treating cancer and neurodegeneration.

## 2.2 Introduction

Sirtuins are class III histone deacetylases that use nicotinamide adenine dinucleotide ($NAD^+$) as a co-substrate. Initially thought to remove only acetyl groups, sirtuins have been shown to have additional enzymatic activities. For instance, SIRT2 removes fatty acyl groups on lysine with catalytic efficiency similar to its deacetylase, and SIRT5 possesses demalonyl, desuccinyl, and deglutaryl activities.[1-5] Among all the seven sirtuins, SIRT2 is the only sirtuin that is mainly localized in the cytosol.[6] SIRT2 has been reported to deacetylate various substrate proteins, including transcription factors, metabolic enzymes and signaling proteins. For instance, SIRT2 regulates cellular iron levels through de-acetylation of transcription factor, NRF2.[7] Through removing acetyl group from K116 of Slug, SIRT2 prevents its degradation and consequently promotes growth of basal-like breast cancer.[8] Besides these transcription factors, SIRT2 promotes tumor growth through deacetylating and activating metabolic enzymes, like pyruvate kinase M2 (PKM2) and lactate dehydrogenase A (LDH-A).[9,10] Furthermore, SIRT2 inhibitors have been reported to have beneficial effects in neurodegenerative diseases, such as Alzheimer's and Parkinson's disease.[11,12] Lastly, SIRT2 stabilizes oncoprotein c-Myc and further regulates transformation of tumor cells by removing fatty acyl groups on K-Ras4a.[13-15]

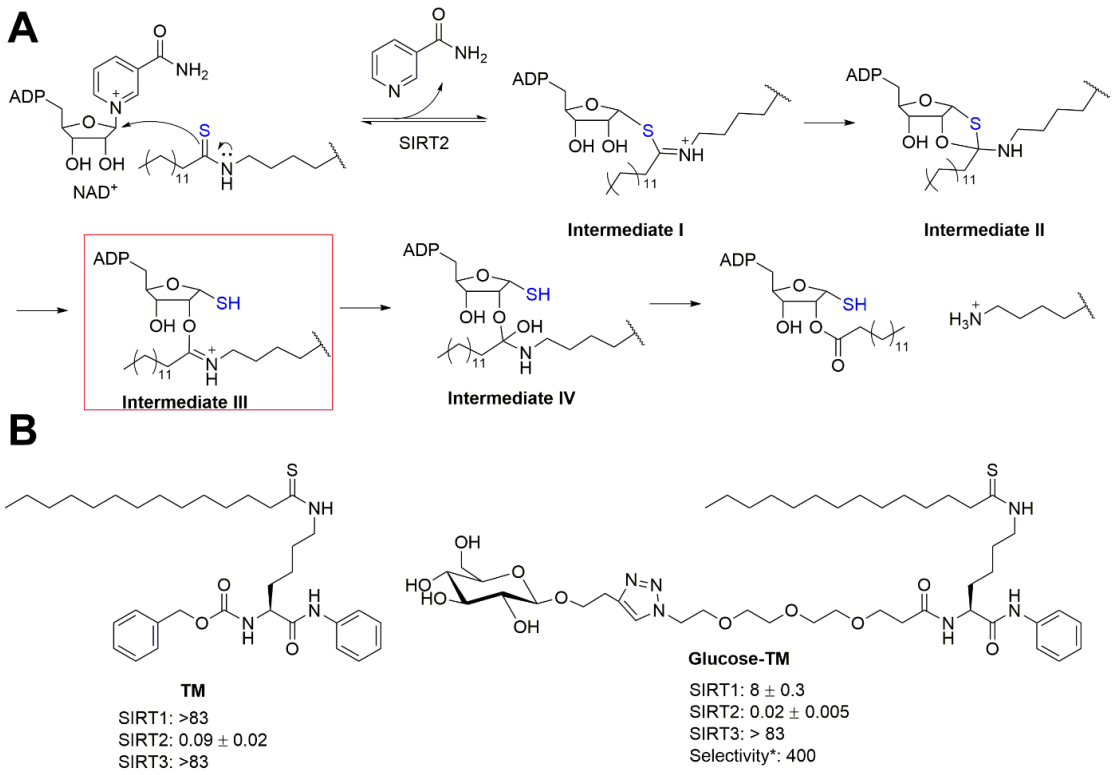


**Figure 2.1 Glucose-TM is a SIRT2 selective inhibitor *in vitro***. (A) Schematic showing how SIRT2 mechanism-based inhibitors work. (B) Structures and measured $IC_{50}$ values (μM) of TM and Glucose-TM.

Because SIRT2 regulates numerous biological functions and promotes tumors, interests in inhibitor development have increased significantly.

Several SIRT2-selective inhibitors have been reported from various groups, including Diketopiperazine-Containing 2-Anilinobenzamides (Compound 53), NCO-90/140, KPM-1/2, AGK2, Tenovin-6 and SirReal2.[12,16-21] Previously, we also reported a mechanism-based SIRT2-selective inhibitor, TM.[14] The compound contains a thiomyristoyl group, which forms a covalent 1'-S-alkylimidate intermediate to detain the activity of SIRT2 (Figure 2.1). TM is cytotoxic in various cancer cell lines,

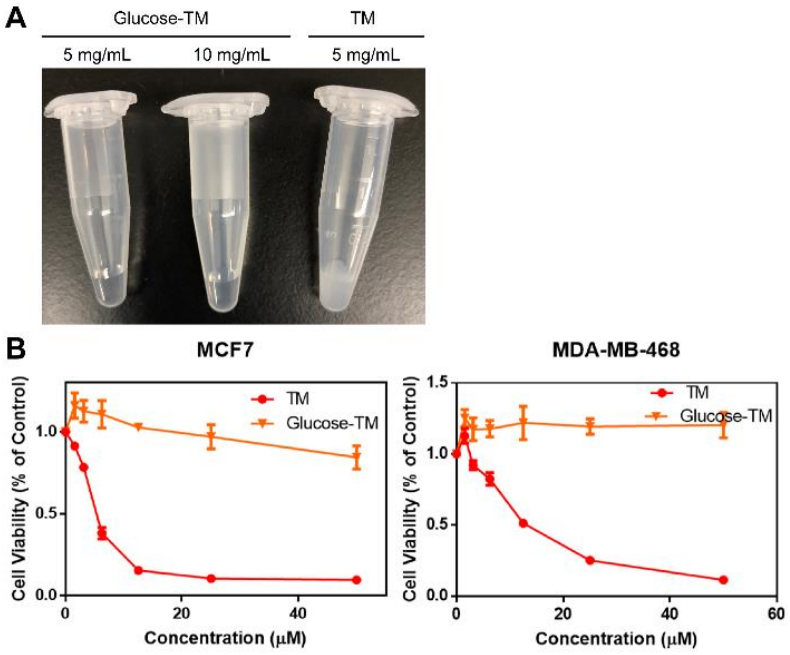


**Figure 2.2 Glucose-TM showed increased solubility in PBS but decreased cancer cell cytotoxicity.** (A) Solubility tests of Glucose-TM and TM at indicated concentrations in PBS (B) Cell viability of MCF7 and MDA-MB-468 cells after treatment of TM and Glucose-TM for 72 hours.

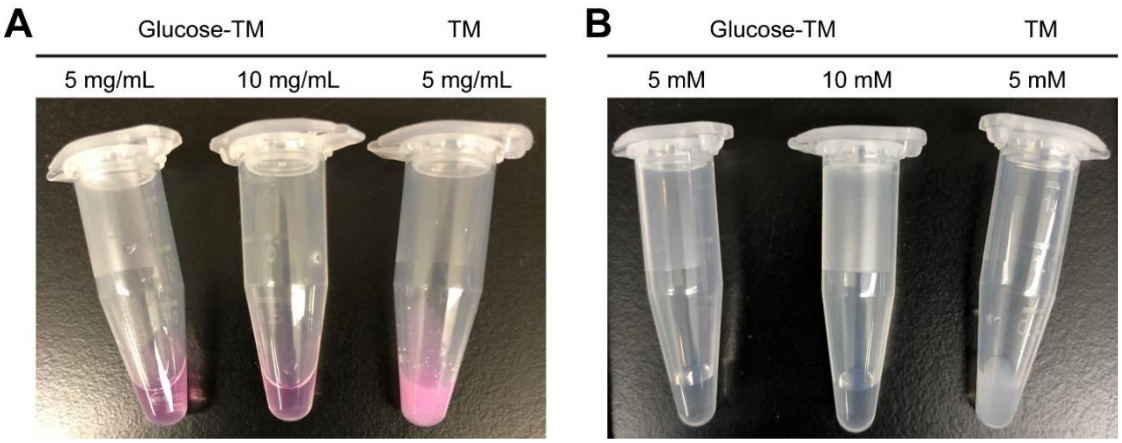


**Figure 2.3 Glucose-TM showed increased solubility in DMEM and PBS.** (A) Solubility tests of Glucose-TM and TM at indicated concentrations in DMEM medium. (B) Solubility tests of Glucose-TM and TM at indicated concentrations in PBS.

including breast, pancreatic, colon, lung and many more, with relatively little toxicity in normal mammary epithelial cells. In addition, the compound inhibited tumor growth in a xenograft model and a genetic model of breast cancers in mice.[14]

Although TM shows promising anticancer activity in mouse models, it has poor aqueous solubility due to its long hydrophobic thiomyristoyl group. The poor aqueous solubility is a practical problem and causes inconveniences in many studies. For example, when attempting to crystalize SIRT2 with TM for the purpose of structure-based inhibitor design, TM often precipitate out by itself. In addition, drugs with poor aqueous solubility often cause delivery problems, which can impede cellular and *in vivo* experiments. Thus, improving TM's aqueous solubility became of interest to us.

The strategy of glycoconjugation has been widely used to improve the cancer cells selectivity (cancer cells often heavily rely on glycolysis, a phenomenon termed the Warburg effect) and aqueous solubility of parental drugs.[22,23] For instance, glycoconjugates of docetaxel, which has poor aqueous solubility, were synthesized to improve its poor water solubility and to target cancer cells selectively. As a result, the conjugated compounds exerted 3- to 18- fold improvements in inhibitory activity compared to the aglycones.[24] Therefore, we decided to synthesize a glycoconjugated SIRT2 selective inhibitor named Glucose-TM to target cancer cells selectively and improve solubility. Glucose-TM maintains the SIRT2 inhibition potency and selectivity while at the same time has dramatically improved aqueous solubility. Contrary to our expectation, Glucose-TM has decreased cell permeability compared to TM, which leads to decreased cellular activity. However, because of the significantly improved aqueous solubility, we were able to co-crystallize Glucose-TM with SIRT2.

The structure shows that the N- and C-terminal ends of the thiomyristoyl lysine structure do not significantly contribute to binding of Glucose-TM. This structure insight allowed us to design various modifications on the N- and C-terminals of thiomyristoyl lysine, leading to compounds that maintained SIRT2-selective inhibition but with improved solubility.

## 2.3 Results and Discussion

### 2.3.1 Glucose-TM design and synthesis.

TM contains a thiomyristoyl lysine moiety with a carboxybenzyl protecting group (Cbz) on the N-terminal, and a phenylamide on the C-terminal.[14] TM analogues with shorter fatty acids lost SIRT2 selectivity and inhibited SIRT1 and SIRT3. Thus, the thiomyristoyl group of TM is important for selective SIRT2 inhibition. Adding a hydroxyl group on the para-position of C-terminal aniline also led to loss of SIRT2 selectivity.[25,26] Because of these observations, we decided to modify the N-terminal of TM to increase its water solubility.

We decided to conjugate glucose to TM using an azido-PEG linker, which is known to increase solubility (Figure 2.1).[27] Click chemistry was utilized to link the azido-PEGylated TM and alkyne tagged glucose. The 1β position of glucose was chosen to attach the alkyne functional group (Scheme 2.1). Using DataWarrior Software, the simulated cLogP value of Glucose-TM was approximately 4.05, while that of TM was approximately 8.81. This simulation suggests that glucose-TM should have significantly im-proved aqueous solubility.

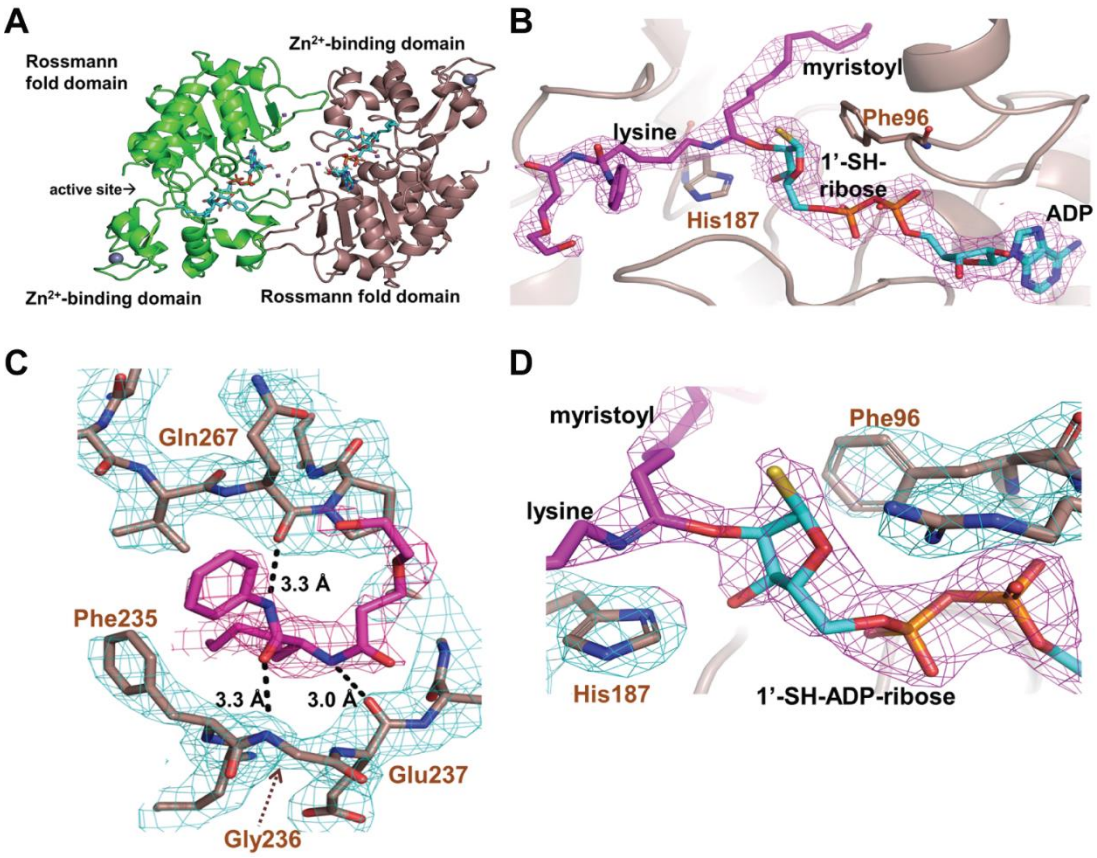


**Figure 2.4 Crystal structure of SIRT2 in complex with Glucose-TM (PDB 6NR0).** (A) Overall structure. Two copies of SIRT2(56-356) are found in the asymmetric unit. The Glucose-TM binds at the active site cleft between the Rossmann and $Zn^{2+}$-binding domains in each SIRT2 molecule. (B) Glucose-TM at the active site. The $2F_O$-$F_C$ map at 1.0 σ shows continuous electron density for the head group, lysine, myristoyl, and 1'-SH-ADP-ribose. (C) The modeled head group of the Glucose-TM hydrogen bonds at the peptide binding site. $2F_O$-$F_C$ map is shown at 1.0 σ. (D) Close-up of the captured Intermediate III with 3'-O-myristoyl lysine linkage. The $2F_O$-$F_C$ map is shown at 1.5 σ. The N-ribose stacks below Phe96 and the 2'-OH hydrogen bonds with His187.

### 2.3.2 Glucose-TM demonstrated increased solubility in PBS.

We tested whether there is an improvement in aqueous solubility by adding TM or Glucose-TM to Phosphate Buffered Saline (PBS). The compound was first dissolved at 50 mM in DMSO. Then, the DMSO stock was further diluted to 5 mg/ml (5.5 mM for Glucose-TM and 8.6 mM for TM) or 10 mg/ml (11 mM for Glucose-TM) in PBS. As expected, when TM was diluted to 5 mg/ml in PBS, white precipitation formed instantly. In comparison, Glucose-TM at 5 mg/ml and 10 mg/ml in PBS did not form any precipitation – instead, the mixtures remained transparent (Figure 2.2). Furthermore, both TM and Glucose-TM were added to Dulbecco's Modified Eagle Media (DMEM) at 5 mg/mL and 10 mg/mL. Like the previous results, TM precipitated out, while Glucose-TM remained dissolved in DMEM (Figure 2.3). These experiments proved that the glycoconjugation strategy for TM did enhance the aqueous solubility significantly.

### 2.3.3 Glucose-TM maintained SIRT2 selective inhibition *in vitro* but has poor cellular activity.

After confirming the solubility improvement, Glucose-TM was assayed against the deacetylase activities of SIRT1, 2 and 3 using previously established methods.[14,28] Both Glucose-TM and TM impeded SIRT2 deacetylase activity, with $IC_{50}$ values of 0.019 and 0.093 μM, respectively. In addition, both compounds did not inhibit any SIRT3 activity at 83 μM. Glucose-TM exerted mild inhibition on SIRT1 with $IC_{50}$ of 7.5 μM, while TM did not inhibit SIRT1 at 83 μM. Nevertheless, the fold of SIRT2 selectivity over SIRT1 was about 400 for Glucose-TM, suggesting that Glucose-TM still inhibits SIRT2 selectively over other sirtuins.

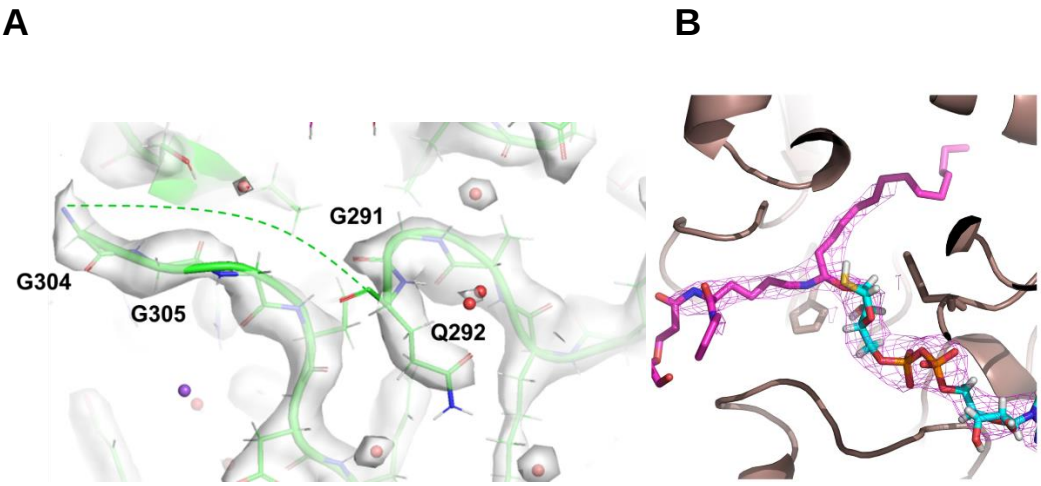


Figure 2.5 **Detailed images of the crystal structure of SIRT2 in complex with Glucose-TM (PDB 6NR0). (**A) $2F_O$-$F_C$ map (white surface, 1.5 sigma level) showing that residues 293-303 of chain A are unstructured and have no observed electron density. Chain B (not shown) is similar. (B) SIRT2(56-356)-$NAD^+$-Glucose-TM co-crystal structure from an isomorphous crystal in the presence of 160 mM sodium acetate (pH 5.0). The 2Fo-FC map at level 1.5 sigma (purple) shows continuous electron density for lysine.

**Additional text associated with Figure 2.5.** The region around residues 293-305 is flexible (dotted line in A) and has been seen in other SIRT2 structures as lacking electron density (such as in PDB 4R8M, SIRT2 with BHJH-TM1).[33] As we saw a similar situation, we asked whether the peptide binding site of SIRT2 could be occupied by this region from a neighboring molecule, rather than by the Glucose-TM. This was also observed in the structure of SIRT2 with ADP-ribose (PDB 3ZGV),[38] in which the peptide backbone around Leu297 binds at the substrate peptide binding site. In our structure, the flexible region can be found with very weak or no electron density in a solvent channel with potential access to the peptide binding site. However, there is no electron density connecting the two regions (Figure 2.5A). Conversely, in structures in which the region around Leu297 of a neighboring molecule is bound at the peptide binding site, there is clear density for the entire region.[3] The strongest support for our model is the clear electron density for the myristoyl chain in the stalled intermediate at the binding site cleft of SIRT2, as the myristoyl could only come from Glucose-TM (see Figure 2.4B). In the higher-resolution (2.45 Å) structure, when the map is viewed at 1.5 sigma level, there is a gap in the electron density at carbons 4-5 of the lysine in the Glucose-TM at the active site of chain A. At lower sigma level (1.1), it is continuous. This suggests flexibility there, or that a fraction of the crystals have formed the reaction product, the diffusible free lysine compound. Interestingly, when concentration of sodium acetate pH 5.0 in the crystal solution was doubled to 160 mM, this gap in density was not seen, even at 2.0 sigma level (Figure 2.5B).

**Table 7. Data collection and refinement statistics.** Statistics for the highest-resolution shell are shown in parentheses. Calculated using Phenix suite.[39]

| **Data collection:** | |
|---|---|
| Wavelength (Å) | 0.9765 |
| Resolution range | 63.69 - 2.45 (2.54 - 2.45) |
| Space group | I 1 2 1 |
| Unit cell | a/b/c: 82.31 Å/ 76.84 Å / 114.46 Å<br>α/β/γ: 90°/ 95.87°/ 90° |
| Total reflections | 50504 (4921) |
| Unique reflections | 25380 (2474) |
| Multiplicity | 2.0 (2.0) |
| Completeness (%) | 91.83 (82.50) |
| Mean I/sigma(I) | 13.33 (2.06) |
| Wilson B-factor ($Å^2$) | 41.82 |
| R-merge | 0.0359 (0.3884) |
| R-meas | 0.0507 (0.549) |
| R-pim | 0.0359 (0.388) |
| CC1/2 | 0.999 (0.722) |
| CC* | 1 (0.916) |
| **Refinement:** | |
| Reflections used in refinement | 24105 (2126) |
| Reflections used for R-free | 1889 (162) |
| R-work | 0.2169 (0.298) |
| R-free | 0.2531 (0.356) |
| CC(work) | 0.929 (0.804) |
| CC(free) | 0.930 (0.626) |
| Number of non-hydrogen atoms | 4966 |
| macromolecules | 4651 |
| ligands | 181 |
| solvent | 134 |
| Protein residues | 580 |
| RMS(bonds) | 0.013 |
| RMS(angles) | 1.55 |
| Ramachandran favored (%) | 95.98 |
| Ramachandran allowed (%) | 4.02 |

| | |
|---|---|
| Ramachandran outliers (%) | 0.00 |
| Rotamer outliers (%) | 0.20 |
| Clashscore | 12.66 |
| Average B-factor (Å$^2$) | 47.62 |
| macromolecules | 47.40 |
| ligands | 55.34 |
| solvent | 44.72 |

With its SIRT2 selective inhibition *in vitro*, we tested Glucose-TM in cellular proliferation assays, hoping to see an improvement in cytotoxicity. However, Glucose-TM did not exert any impediment in cellular proliferation, much worse than TM (Figure 2.2B). Using DataWarrior Software, the simulated topological polar surface area of Glucose-TM was about 260. Compounds with topological polar surface area higher than 140 often portray poor cellular permeability.[29,30] Also, glucose transporters might not recognize the glycoconjugated compound as a substrate[31], rendering the active transport process inefficient. These factors may lead to very poor cellular permeability/availability of Glucose-TM. not recognize the glycoconjugated compound as a substrate[31], rendering the active transport process inefficient. These factors may lead to very poor cellular permeability/availability of Glucose-TM.

We next attempted to test whether the poor cellular cytotoxicity of Glucose-TM arises from its poor cellular permeability/availability. Traditional Caco-2 permeability assay or PAMPA transwell assay do not work for such compounds because the hydrophobicity of the thiomyristoyl groups make these compounds readily bind to the plastic surfaces, membranes of the transwell plates, and cellullar membranes. Thus, to better reflect the over-all cellular permeability/availability of such compounds, we treated MCF7 cells with the compounds for 6 hours, and then

collected the cells, extracted the compound, detected and quantified using LC-MS. Only approximately 0.085 μg/million cells of Glucose-TM was detected in the treated cells. Meanwhile, approximately 0.30 μg/million cells of TM was detected, which was about 3.5 fold great-er than that of Glucose-TM. The decreased cellular permeability/availability plus the decreased SIRT2 inhibition potency of Glucose-TM could explain why the compound did not exert much cytotoxicity.

### 2.3.4 Crystal structure of SIRT2(56-356) with Glucose-TM and $NAD^+$.

To guide further development of TM-based inhibitors, we decided to obtain the crystal structure of SIRT2 in complex with Glucose-TM. Our previous attempts to crystalize SIRT2 in complex with TM all failed due to the poor aqueous solubility of TM. Co-crystals of SIRT2(56-356), $NAD^+$, and glucose-TM were obtained, and the structure was solved and refined to 2.45-Å resolution. The overall structure is similar to previously-determined structures of SIRT2.[33] In the structure, the $NAD^+$ and Glucose-TM have reacted to form a covalent intermediate at the reaction site cleft (Figure 3A). The electron density at the active site indicates a 3-way junction between the lysine, the myristoyl, and the N-ribose of the ADP-ribose, supporting the mechanism-based nature of this class of thiomyristoyl SIRT2 inhibitors (Figure 2.4 and 2.5).

The thiomyristoyl lysine moiety of Glucose-TM binds at a cleft between residues 235-237 and 267-268 (Figure 2.4C). There is strong electron density from the C1 of the phenyl ring to the carbonyl adjacent to the PEG linker. The direction of the peptide backbone was determined by the rounded density for the phenyl ring, the longer continuous density toward the PEG linker, the shape of the backbone, and by

comparison to the backbone in previously-reported peptide-bound SIRT2 structures.33 Directly analogous to the binding of peptide at this site, Glucose-TM forms hydrogen bonds to the main chain of SIRT2, with the lysine carbonyl binding to the backbone nitrogen of Gly236 (3.3 Å O-N distance), the lysine nitrogen binding to the carbonyl of Glu237 (3.0 Å), and the phenyl amide nitrogen binding to the backbone carbonyl of Gln267 (3.3 Å).

Beyond the hydrogen bonding, we also observed that the phenyl ring of Glucose-TM is within ~4 Å of the phenyl ring of Phe235 (6 Å center-to-center distance). This is near the limit for potential "pi-pi" or hydrophobic interactions. Though some interaction may be possible, the electron density for the aniline ring does not suggest a strong stable conformation of the ring, at least at this resolution. Additionally, there is little electron density beyond the beginning of the PEG linker. Hence, the rest of the PEG linker and glucose were not modeled, and they likely do not contribute to the binding affinity.

This information suggests that it is really the thiomyristoyl lysine moiety of the TM-based inhibitors that makes the binding contributions to SIRT2, leaving the periphery of the inhibitor structure open for modifications to improve other pharmacological properties of the inhibitors, such as solubility.

Interestingly, the 2Fo-Fc electron density map around the N-ribose (Figure 2.4D) suggests formation of a 2'-O myristoyl inhibitor linkage (Intermediate III, see Figure 2.1A), rather than the 1'-SH-thioalkylimidate linkage (Intermediate I) as originally predicted for this mechanism-based inhibitor.[14] This observation of a 2'-O linkage was also made for a peptide-based thiomyristoyl SIRT2 inhibitor.[33] Though it

is possible that a small portion of asymmetric units contain a 1'-S linkage, several features of the structure support the 2'-O linkage as the dominant species in the crystal. First, the concave shape of the electron density around the ribose can be seen at this resolution, with the 1', 2', and 3' groups pointing up and left in Figure 2.4D. Second, the 3′-OH is documented in several other sirtuin structures to form a hydrogen bond with His187. If we model Intermediate I in the structure, the electron density in this structure indicates that the ribose would have to be flipped, due to the clear position of the myristoyl linkage.[34] In this case, the hydrogen bond with His187 would be lost and the concave shape of the electron density would not fit the ribose as well. Indeed, in the SIRT3 structure with intermediate I, the ribose is flipped[34]. After modeling and refining the structure both ways, intermediate III better fits our data and the recent structure with BHJH-TM1.[33]

The observation of intermediate III raises the question of why this is the structure seen rather than intermediate I. It was previously hypothesized that intermediate I would be the stalled intermediate likely because the S-alkylamidate is more stable than an O-alkylamidate, which would form with regular substrate. However, the structure actually captured an O-alkylamidate intermediate III. Perhaps a sulfhydryl at the 1' position interferes sterically with nucleophilic attack of water to form inter-mediate IV. Or, perhaps a hydroxyl at position 1' is important in abstracting a proton from the attacking water to form intermediate IV, while a sulfydryl is not as efficient. It could also be that the crystallization condition required for co-crystallization favors the later intermediate III rather than Intermediate I.

### 2.3.5 Development of new SIRT2 inhibitors based on the structure of SIRT2 in complex with Glucose-TM.

As seen from the crystal structure of Glucose-TM in complex with SIRT2, neither end of the thiomyristoyl lysine structure contributes much to the binding to SIRT2. Thus, we decided to modify the N-terminal and C-terminal groups of TM to further test this. An additional goal is to obtain SIRT2 inhibitors that are similar to TM in potency, selectivity, and cellular activity, but with improved solubility and perhaps even metabolic stability for future animal and clinical studies. Using TM as a reference structure, we removed the Cbz protecting group (NH3), replaced Cbz with a β-alanine (NH3-6), removed the C-terminal aniline (NH4-3), removed Cbz and replaced the phenyl amide with a methyl ester (NH4-4) introduced a trimethylamine group on the C-terminal to improve aqueous solubility (NH4-6), and lastly, added methyl ester group on the C-terminal (NH4-8) (Figure 2.6A).

Interestingly, all six compounds inhibited SIRT2 deacetylase at $IC_{50}$ values lower than 0.5 μM (Figure 2.6A). Compounds without the C-terminal phenyl amide, NH4-3, NH4-6 and NH4-8 inhibit SIRT2 at much lower $IC_{50}$ at 0.012, 0.032 and 0.018 μM, respectively. These values are slightly better than that for TM, suggesting that the C-terminal aniline does not contribute to the inhibition and can be replaced. This is consistent with the structure of SIRT2 in complex with Glucose-TM. In contrast, compared to TM, compounds without the Cbz group at the N-terminal (NH3, NH3-6, NH4-4) all showed slightly worse $IC_{50}$ values for SIRT2 (~0.4 μM). This suggests that the Cbz group contributes a little to the inhibition efficiency. Because the structure of

Glucose-TM did not have the Cbz group, the crystal structure of SIRT2 with Glucose-TM could not reveal the interaction between Cbz and SIRT2.

We next examined the specificity of the new SIRT2 inhibitors. All the new compounds, except NH4-6, did not inhibit SIRT3 even at 83 μM (Figure 2.6A). For SIRT1, at 83 μM, three compounds did not inhibit SIRT1 activity (Figure 2.6A). NH3-6, NH4-3 and NH4-6 had $IC_{50}$ for SIRT1 of 12, 4.4 and 3 μM, respectively. Nevertheless, even these three compounds still showed strong selectivity towards SIRT2 (NH3-6, NH4-3 and NH4-6 showed 30-, 366-, and 94-fold SIRT2 selectivity over SIRT1, respectively). Furthermore, NH3, NH3-6 and NH4-8 did not exert any inhibition against SIRT6 demyristoylase, while NH4-3, NH4-4 and NH4-6 demonstrated very weak inhibitory behaviors against SIRT6 with $IC_{50}$ of ~50 μM. Considering all the $IC_{50}$ values, these five TM analogues all displayed SIRT2-selective inhibition, supporting that the thiomyristoyl lysine is essential, but the N- and C-terminal are unimportant or less important.

We have chosen two compounds, NH4-6 and NH4-8, to evaluate their effects on the viability of MCF7 and MBA-MB-231 breast cancer cells. NH4-8 was designed to act as “semi” pro-drug. It can inhibit SIRT2 by itself but can also transform to NH4-3 by non-specific esterases in the cells. After the transformation, NH4-3 with carboxylic acid moiety, which often shows poor cellular permeability, can be trapped inside of the cell. NH4-6 contains charged trimethylamine group, which increases aqueous solubility significantly (simulated cLogP of 3.86). Through improved aqueous solubility, more compounds will remain dissolved at higher concentrations, which could increase cellular cytotoxicity.

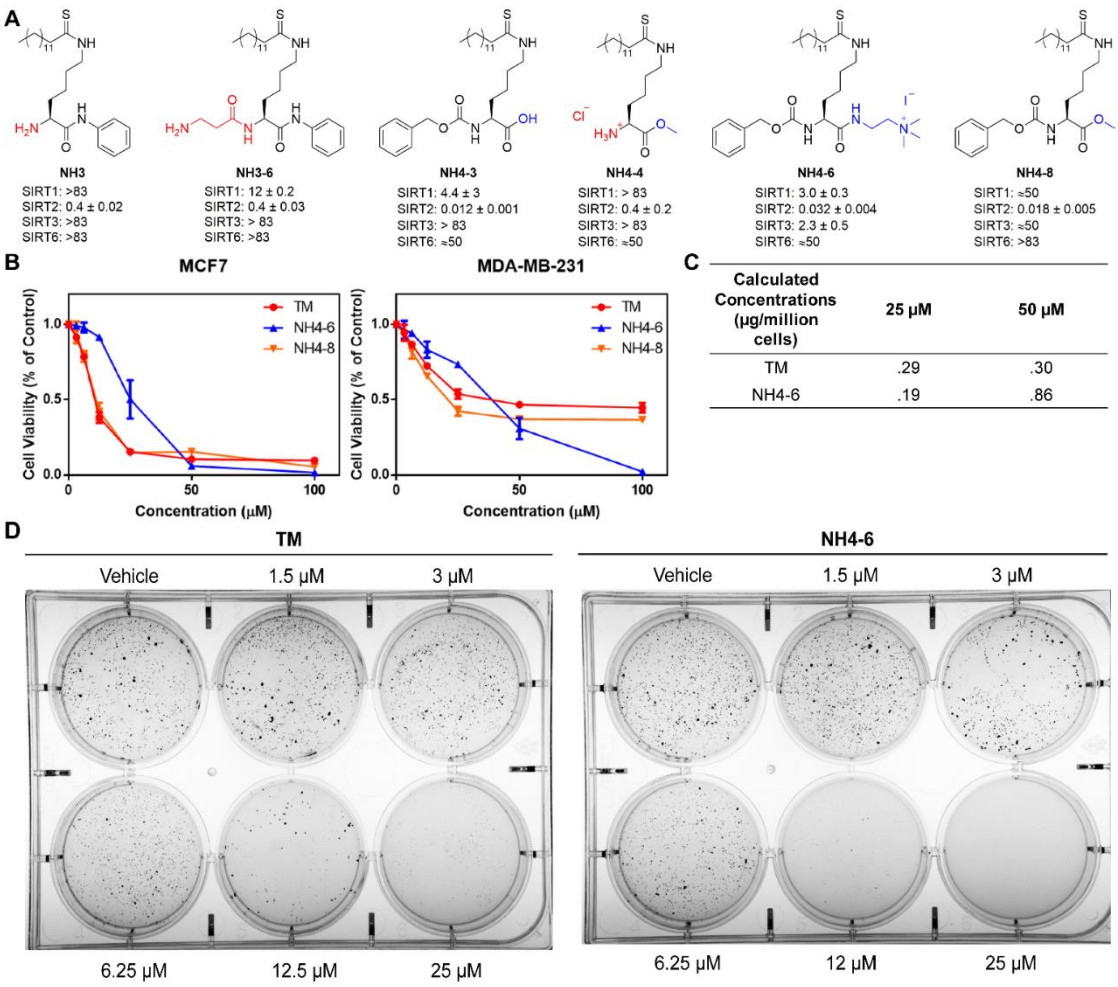


**Figure 2.6 New TM analogs synthesized based on the structural information and their properties**. (A) Synthesized TM analogs and their $IC_{50}$ (μM) values for SIRT1-3. (B) Cell viability of MCF7 and MDA-MB-231 cells after treatment of TM, NH4-6 and NH4-8 for 72 hours. (C) Calculated concentrations (μg/million cells) of TM and NH4-6 detected from MCF7 cell permeability assay. MCF7 cells were treated with 25 and 50 μM of indicated inhibitors for 6 hours. (D) Soft agar colony formation assays of MCF7 cells treated with inhibitors at indicated concentrations for 10 days.

In both MCF7 and MDA-MB-231 cells in 2D cell proliferation assays, treatment of NH4-8 showed a similar trend to that of TM (Figure 2.6B). NH4-6 interestingly showed a slightly worse effect than that of TM at lower concentrations in both MCF7 and MDA-MB-231 cells. This is most likely because the charged trimethylamine group of NH4-6 increases the overall polar surface area, which impairs the cellular permeability (Figure 2.6B). However, at higher concentrations, NH4-6 showed stronger cytotoxicity than TM in both MCF7 and MDA-MB-231 cells. This is likely because NH4-6 is more soluble and could reach higher concentrations and thus show stronger cytotoxicity than TM, which has very poor aqueous solubility and will precipitate out at higher concentrations.

To test this hypothesis, we treated MCF7 cells with TM and NH4-6 at 25 and 50 μM, and then detected the amount of inhibitors in cells (Figure 2.6C). The levels of TM detect-ed in the cells were about 0.29 and 0.30 μg/million cells after 6 hours of 25 and 50 μM treatment, respectively. Interestingly, the concentrations of TM in the cells did not change significantly between the two tested concentrations. This shows why there was no significant difference in cellular proliferation between 25 and 50 μM of TM in both MCF7 and MDA-MB-231 cells. The concentrations of NH4-6 inside the cells were about 0.19 and 0.86 μg/million cells after treatment with 25 and 50 μM, respectively. Thus, at 25 μM, the concentration of NH4-6 in the cells was slightly lower than TM, while at 50 μM treatment, the concentration of NH4-6 in the cells was about 2.8 times higher than that of TM. This explains why NH4-6 had weaker cytotoxicity than TM at 25 μM but stronger cytotoxicity at 50 μM than TM. Simply put, at higher concentrations, more NH4-6 was dissolved in the media and had entered

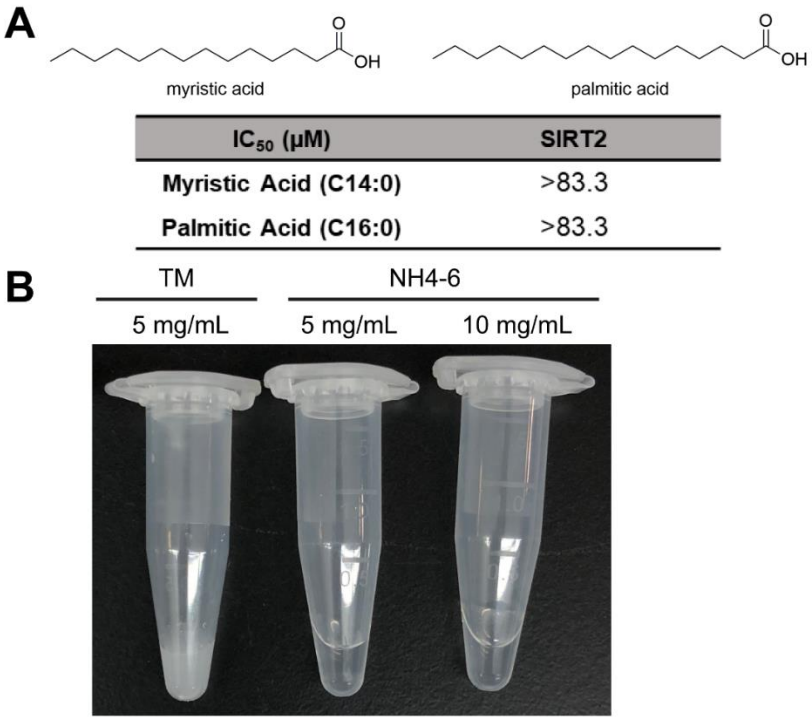


**Figure 2.7. Myristic acid and palmitic acid do not inhibit SIRT2.** (A) Structures and measured SIRT2 $IC_{50}$ (μM) of myristic acid and palmitic acid are shown. (B) Solubility tests of TM and NH4-6 at indicated concentrations in PBS.

the cell membrane, which led to increased cytotoxicity, while TM was already saturated at 25 μM and thus higher amount of TM did not result in higher cytotoxicity.

Next, we examined the effect of TM and NH4-6 against anchorage-independent growth, a cancer cell-specific phenotype, through soft agar colony formation assay (Figure 2.6D).[35] We specifically chose NH4-6 to test, be-cause it not only showed improved solubility but also improved cytotoxicity in the cellular proliferation assays at higher concentration. MCF7 cells were suspended in soft agar mixture with various concentrations of inhibitors for 10 days to observe the colony

formation. At 12 μM treatment, TM-treated cells formed many colonies, while cells treated with NH4-6 did not have any colonies at all. This suggests that NH4-6 has stronger effects than TM against anchorage-independent growth of cancer cells. We believe the increased solubility of NH4-6 is again re-sponsible for the increased efficacy.

To further confirm the permeability trend and on-target effect of TM, NH4-6 and NH4-8, we evaluated acetylation of α-tubulin as SIRT2's target in cells, confirmed by previous reports.[36] We treated MCF7 cells with either DMSO, TM, NH4-6, or NH4-8 at indicated concentrations for 6 hours, and monitored acetylated α-tubulin by immuno-fluorescence. As expected, acetylation levels of α-tubulin were increased upon treatment of TM at all concentrations. Similar trend was observed for NH4-8. Treatment with 25 μM of NH4-6 did not increase the acetylation levels of α-tubulin, but 50 and 100 μM treatment of NH4-6 increased the levels, comparable to that of TM treated samples. This result is consistent with the permeability/cellular availability assay results described above.

Next, we examined whether TM, NH4-6 and NH4-8 inhibit SIRT1 in cells by looking at acetylated p53 (lysine 382), previously reported SIRT1 substrate.37 Consistent with previously reported results, treatment of EX527 significantly increased the acetylation level of p53, com-pared to that of DMSO control.34,38 At all the tested concentrations, TM and NH4-8 did not increase acetylation levels of p53. This was consistent with *in vitro* SIRT1 $IC_{50}$ values of TM (>83 μM) and NH4-8 (~50 μM).

Because the $IC_{50}$ value of NH4-6 for SIRT1 is 3.0 μM, we expected NH4-6 to increase the acetylation levels of p53. However, 10, 25 and 50 μM of NH4-6 did not increase acetylation levels of p53, but 100 μM of NH4-6 did. Thus, at lower concentrations, NH4-6 could not inhibit SIRT1 most likely because of its low permeability/cellular availability, but its improved solubility allows more NH4-6 to accumulate in cells to inhibit SIRT1 at 100 μM. It is possible that simultaneous inhibition of SIRT1, 2 and 3 may have contributed to improved cytotoxicity of NH4-6 at higher concentrations.

## 2.4 Conclusion

In conclusion, we showed that the glycoconjugation strategy on TM lead to a SIRT2 inhibitor Glucose-TM with enhanced aqueous solubility. Although it has poor cell permeability, the high-water solubility allowed us to obtain a co-crystal structure with SIRT2. Crystallography data suggested that the C-terminal phenyl amide and N-terminal Cbz groups are not required for the interaction between the inhibitor and SIRT2. Several TM analogues with various modifications on both N and C-terminals further confirmed and refined this hypothesis. This finding has led to SIRT2 inhibitors with improved properties and will facilitate the introduction of even further modifications to the thiomyristoyl lysine core to obtain SIRT2-selective inhibitors with improved chemical and biological characteristics. Such inhibitors will find important applications given the interesting biological functions of SIRT2 and the potential of SIRT2 inhibitors in treating cancer and neurological diseases.

## 2.5 References


1. Feldman, J. L., Dittenhafer-Reed, K. E., Kudo, N., Thelen, J. N., Ito, A., Yoshida, M., and Denu, J. M. (2015) Kinetic and Structural Basis for Acyl-Group Selectivity and NAD <sup>+</sup> Dependence in Sirtuin-Catalyzed Deacylation, *Biochemistry 54*, 3037-3050.

2. Teng, Y.-B., Jing, H., Aramsangtienchai, P., He, B., Khan, S., Hu, J., Lin, H., and Hao, Q. (2015) Efficient Demyristoylase Activity of SIRT2 Revealed by Kinetic and Structural Studies, *Sci. Rep. 5*, 8529.

3. Cui, Y., Li, X., Lin, J., Hao, Q., and Li, X. D. (2017) Histone Ketoamide Adduction by 4-Oxo-2-nonenal Is a Reversible Posttranslational Modification Regulated by Sirt2, *ACS Chem. Biol. 12*, 47-51.

4. Du, J., Zhou, Y., Su, X., Yu, J. J., Khan, S., Jiang, H., Kim, J., Woo, J., Kim, J. H., Choi, B. H., He, B., Chen, W., Zhang, S., Cerione, R. A., Auwerx, J., Hao, Q., and Lin, H. (2011) Sirt5 Is a NAD-Dependent Protein Lysine Demalonylase and Desuccinylase, *Science 334*, 806-809.

5. Pannek, M., Simic, Z., Fuszard, M., Meleshin, M., Rotili, D., Mai, A., Schutkowski, M., and Steegborn, C. (2017) Crystal structures of the mitochondrial deacylase Sirtuin 4 reveal isoform-specific acyl recognition and regulation features, *Nat Commun 8*, 1513.

6. North, B. J., and Verdin, E. (2007) Interphase nucleo-cytoplasmic shuttling and localization of SIRT2 during mitosis, *PLoS One 2*, e784.

7. Yang, X., Park, S. H., Chang, H. C., Shapiro, J. S., Vassilopoulos, A., Sawicki, K. T., Chen, C., Shang, M., Burridge, P. W., Epting, C. L., Wilsbacher, L. D., Jenkitkasemwong, S., Knutson, M., Gius, D., and Ardehali, H. (2017) Sirtuin 2 regulates cellular iron homeostasis via deacetylation of transcription factor NRF2, *J. Clin. Invest. 127*, 1505-1516.

8. Zhou, W., Ni, T. K., Wronski, A., Glass, B., Skibinski, A., Beck, A., and Kuperwasser, C. (2016) The SIRT2 Deacetylase Stabilizes Slug to Control Malignancy of Basal-like Breast Cancer, *Cell Rep 17*, 1302-1317.

9. Park, S. H., Ozden, O., Liu, G., Song, H. Y., Zhu, Y., Yan, Y., Zou, X., Kang, H. J., Jiang, H., Principe, D. R., Cha, Y. I., Roh, M., Vassilopoulos, A., and Gius, D. (2016) SIRT2-Mediated Deacetylation and Tetramerization of Pyruvate Kinase Directs Glycolysis and Tumor Growth, *Cancer Res 76*, 3802-3812.

10. Zhao, D., Zou, S. W., Liu, Y., Zhou, X., Mo, Y., Wang, P., Xu, Y. H., Dong, B., Xiong, Y., Lei, Q. Y., and Guan, K. L. (2013) Lysine-5 acetylation negatively regulates lactate dehydrogenase A and is decreased in pancreatic cancer, *Cancer Cell 23*, 464-476.

11. Herskovits, A. Z., and Guarente, L. (2013) Sirtuin deacetylases in neurodegenerative diseases of aging, *Cell Res. 23*, 746-758.

12. Outeiro, T. F., Kontopoulos, E., Altmann, S. M., Kufareva, I., Strathearn, K. E., Amore, A. M., Volk, C. B., Maxwell, M. M., Rochet, J.-C., McLean, P. J., Young, A. B., Abagyan, R., Feany, M. B., Hyman, B. T., and Kazantsev, A. G. (2007) Sirtuin 2 inhibitors rescue alpha-synuclein-mediated toxicity in models of Parkinson's disease, *Science (New York, N.Y.) 317*, 516-519.

13. Liu, P. Y., Xu, N., Malyukova, A., Scarlett, C. J., Sun, Y. T., Zhang, X. D., Ling, D., Su, S. P., Nelson, C., Chang, D. K., Koach, J., Tee, A. E., Haber, M., Norris, M. D., Toon, C., Rooman, I., Xue, C., Cheung, B. B., Kumar, S., Marshall, G. M., Biankin, A. V., and Liu, T. (2013) The histone deacetylase SIRT2 stabilizes Myc oncoproteins, *Cell Death Differ 20*, 503-514.

14. Jing, H., Hu, J., He, B., Negrón Abril, Y. L., Stupinski, J., Weiser, K., Carbonaro, M., Chiang, Y.-L., Southard, T., Giannakakou, P., Weiss, R. S., and Lin, H. (2016) A SIRT2-Selective Inhibitor Promotes c-Myc Oncoprotein Degradation and Exhibits Broad Anticancer Activity, *Cancer Cell 29*, 297-310.

15. Jing, H., Zhang, X., Wisner, S. A., Chen, X., Spiegelman, N. A., Linder, M. E., and Lin, H. (2017) SIRT2 and lysine fatty acylation regulate the transforming activity of K-Ras4a, *eLife Sciences 6*.

16. Kozako, T., Mellini, P., Ohsugi, T., Aikawa, A., Uchida, Y. I., Honda, S. I., and Suzuki, T. (2018) Novel small molecule SIRT2 inhibitors induce cell death in leukemic cell lines, *BMC Cancer 18*, 791.

17. Suzuki, T., Khan, M. N., Sawada, H., Imai, E., Itoh, Y., Yamatsuta, K., Tokuda, N., Takeuchi, J., Seko, T., Nakagawa, H., and Miyata, N. (2012) Design, synthesis, and biological activity of a novel series of human sirtuin-2-selective inhibitors, *J Med Chem 55*, 5760-5773.

18. Mellini, P., Itoh, Y., Tsumoto, H., Li, Y., Suzuki, M., Tokuda, N., Kakizawa, T., Miura, Y., Takeuchi, J., Lahtela-Kakkonen, M., and Suzuki, T. (2017) Potent mechanism-based sirtuin-2-selective inhibition by an in situ-generated occupant of the substrate-binding site, "selectivity pocket" and NAD(+)-binding site, *Chem Sci 8*, 6400-6408.

19. Rumpf, T., Schiedel, M., Karaman, B., Roessler, C., North, B. J., Lehotzky, A., Olah, J., Ladwein, K. I., Schmidtkunz, K., Gajer, M., Pannek, M., Steegborn, C., Sinclair, D. A., Gerhardt, S., Ovadi, J., Schutkowski, M., Sippl, W., Einsle, O., and Jung, M. (2015) Selective Sirt2 inhibition by ligand-induced rearrangement of the active site, *Nat Commun 6*, 6263.

20. Lain, S., Hollick, J. J., Campbell, J., Staples, O. D., Higgins, M., Aoubala, M., McCarthy, A., Appleyard, V., Murray, K. E., Baker, L., Thompson, A., Mathers,

J., Holland, S. J., Stark, M. J., Pass, G., Woods, J., Lane, D. P., and Westwood, N. J. (2008) Discovery, in vivo activity, and mechanism of action of a small-molecule p53 activator, *Cancer Cell 13*, 454-463.

21. Mellini, P., Itoh, Y., Elboray, E. E., Tsumoto, H., Li, Y., Suzuki, M., Takahashi, Y., Tojo, T., Kurohara, T., Miyake, Y., Miura, Y., Kitao, Y., Kotoku, M., Iida, T., and Suzuki, T. (2019) Identification of Diketopiperazine-Containing 2-Anilinobenzamides as Potent Sirtuin 2 (SIRT2)-Selective Inhibitors Targeting the "Selectivity Pocket", Substrate-Binding Site, and NAD(+)-Binding Site, *J Med Chem 62*, 5844-5862.

22. Pohl, J., Bertram, B., Hilgard, P., Nowrousian, M. R., Stüben, J., and Wießler, M. (1995) D-19575—a sugar-linked isophosphoramide mustard derivative exploiting transmembrane glucose transport, *Cancer Chemother. Pharmacol. 35*, 364-370.

23. Stüben, J., Port, R., Bertram, B., Bollow, U., Hull, W. E., Schaper, M., Pohl, J., and Wiessler, M. (1996) Pharmacokinetics and whole-body distribution of the new chemotherapeutic agent β- D -glucosylisophosphoramide mustard and its effects on the incorporation of [methyl- 3 H]-thymidine in various tissues of the rat, *Cancer Chemother. Pharmacol. 38*, 355-365.

24. Mikuni, K., Nakanishi, K., Hara, K., Hara, K., Iwatani, W., Amano, T., Nakamura, K., Tsuchiya, Y., Okumoto, H., and Mandai, T. (2008) In vivo antitumor activity of novel water-soluble taxoids, *Biol. Pharm. Bull. 31*, 1155-1158.

25. Spiegelman, N. A., Hong, J. Y., Hu, J., Jing, H., Wang, M., Price, I. R., Cao, J., Yang, M., Zhang, X., and Lin, H. (2019) A Small-Molecule SIRT2 Inhibitor That Promotes K-Ras4a Lysine Fatty-Acylation, *ChemMedChem 14*, 744-748.

26. Farooqi, A. S., Hong, J. Y., Cao, J., Lu, X., Price, I. R., Zhao, Q., Kosciuk, T., Yang, M., Bai, J. J., and Lin, H. (2019) Novel Lysine-Based Thioureas as Mechanism-Based Inhibitors of Sirtuin 2 (SIRT2) with Anticancer Activity in a Colorectal Cancer Murine Model, *J Med Chem 62*, 4131-4141.

27. Milla, P., Dosio, F., and Cattel, L. (2012) PEGylation of Proteins and Liposomes: a Powerful and Flexible Strategy to Improve the Drug Delivery, *Curr. Drug Metab. 13*, 105-119.

28. Spiegelman, N. A., Price, I. R., Jing, H., Wang, M., Yang, M., Cao, J., Hong, J. Y., Zhang, X., Aramsangtienchai, P., Sadhukhan, S., and Lin, H. (2018) Direct Comparison of SIRT2 Inhibitors: Potency, Specificity, Activity-Dependent Inhibition, and On-Target Anticancer Activities, *ChemMedChem 13*, 1890-1894.

29. Shultz, M. D. (2018) Two Decades under the Influence of the Rule of Five and the

Changing Properties of Approved Oral Drugs, *J Med Chem*.

30. Pajouhesh, H., and Lenz, G. R. (2005) Medicinal chemical properties of successful central nervous system drugs, *NeuroRx 2*, 541-553.

31. Patra, M., Awuah, S. G., and Lippard, S. J. (2016) Chemical Approach to Positional Isomers of Glucose−Platinum Conjugates Reveals Specific Cancer Targeting through Glucose-Transporter-Mediated Uptake in Vitro and in Vivo, *J. Am. Chem. Soc. 138*, 12541-12551.

32. Wang, Y., Fung, Y. M. E., Zhang, W., He, B., Chung, M. W. H., Jin, J., Hu, J., Lin, H., and Hao, Q. (2017) Deacylation Mechanism by SIRT2 Revealed in the 1'-SH-2'-O-Myristoyl Intermediate Structure, *Cell Chem Biol 24*, 339-345.

33. Gertz, M., Fischer, F., Nguyen, G. T., Lakshminarasimhan, M., Schutkowski, M., Weyand, M., and Steegborn, C. (2013) Ex-527 inhibits Sirtuins by exploiting their unique NAD+-dependent deacetylation mechanism, *Proc Natl Acad Sci U S A 110*, E2772-2781.

34. Mori, S., Chang, J. T., Andrechek, E. R., Matsumura, N., Baba, T., Yao, G., Kim, J. W., Gatza, M., Murphy, S., and Nevins, J. R. (2009) Anchorage-independent cell growth signature identifies tumors with metastatic potential, *Oncogene 28*, 2796-2805.

35. North, B. J., Marshall, B. L., Borra, M. T., Denu, J. M., and Verdin, E. (2003) The human Sir2 ortholog, SIRT2, is an NAD+-dependent tubulin deacetylase, *Mol Cell 11*, 437-444.

36. Vaziri, H., Dessain, S. K., Ng Eaton, E., Imai, S. I., Frye, R. A., Pandita, T. K., Guarente, L., and Weinberg, R. A. (2001) hSIR2(SIRT1) functions as an NAD-dependent p53 deacetylase, *Cell 107*, 149-159.

37. Solomon, J. M., Pasupuleti, R., Xu, L., McDonagh, T., Curtis, R., DiStefano, P. S., and Huber, L. J. (2006) Inhibition of SIRT1 catalytic activity increases p53 acetylation but does not alter cell survival following DNA damage, *Mol Cell Biol 26*, 28-38.

38. Moniot, S., Schutkowski, M., and Steegborn, C. (2013) Crystal structure analysis of human Sirt2 and its ADP-ribose complex, *J. Struct. Biol.* 182, 136-143.

39. Adams, P. D., Afonine, P. V., Bunkoczi, G., Chen, V. B., Davis, I. W., Echols, N., Headd, J. J., Hung, L. W., Kapral, G. J., Grosse-Kunstleve, R. W., McCoy, A. J., Moriarty, N. W., Oeffner, R., Read, R. J., Richardson, D. C., Richardson, J. S., Terwilliger, T. C., and Zwart, P. H. (2010) PHENIX: a comprehensive Python-based system for macromolecular structure solution, *Acta Crystallogr. D Biol. Crystallogr.* 66, 213-221.

## 2.6 Methods

### General experimental methods

All reagents and solvents were analytical grade and purchased from commercial vendors. All reactions took place under inert nitrogen gas. $^{1}H$ and $^{13}C$ NMR were obtained on Bruker 500 spectrometers. The molecular weights of the compounds were obtained on a Shimadzu HPLC LC20-AD and Thermo Scientific LCQ Fleet Mass Spectrometer at positive ion mode. The column used in the LC-MS system was Kinetex 5u EVO C18 100 Å Column (30 x 2.1 mm, 5 μm), and solvents used were water with 0.1 % HPLC-grade acetic acid and acetonitrile with 0.1 % HPLC-grade acetic acid. The LC-MS monitored the compound using both 215 and 260 nm absorption. The silica used for column purification was SiliaFlash Irregular Silica Gel, P60, 40 - 63 μm, 60 Å. The analytical HPLC used to monitor the enzymatic reactions of sirtuins was Shimadzu HPLC LC20-AD with Kinetex 5 μm EVO C18 100 Å column (100 mm × 4.60 mm, 5 μm), at 215 and 280 nm. Solvents used for the analytical HPLC was water with 0.1 % HPLC-grade trifluoroacetic acid and acetonitrile with 0.1 % HPLC-grade trifluoroacetic acid. The compounds were eluted at 0.5 mL/min for the enzymatic reactions.

### Solubility tests in phosphate buffered saline (PBS) and Dulbecco's Modified Eagle Media (DMEM)

TM, Glucose-TM and NH4-6 were initially prepared at 50 mM in DMSO solutions. Then, the compounds were diluted into listed concentrations in either PBS or DMEM media. The mixtures were vortexed thoroughly. The mixtures were imaged using commercial digital cameras.

**Cloning, expression and purification of SIRT1 and SIRT3**

Human SIRT1 and SIRT3 were cloned, expressed and purified as previously reported[1, 2].

**Enzymatic assays of SIRT1, 2 and 3 deacetylase, and SIRT6 demyristoylase activity**

Measuring *in vitro* $IC_{50}$ values against SIRT1, 2 and 3 deacetylase and SIRT6 demyristoylase activity was performed by following previously reported procedures[1-3]. Various concentrations of inhibitors or DMSO were pre-incubated with either SIRT1, 2,3 or 6 (0.05 μM SIRT1, 0.2 μM SIRT2, 0.1 μM SIRT3 and 1 μM SIRT6) and 1 mM $NAD^+$ in 20 mM Tris-HCl buffer (pH 8.0) and 1 mM DTT for 15 minutes at 37 °C. Then, 10 μM final concentrations of acetyl-H3K9 (SIRT1-3 assay) or 50 μM of myristoyl-H3K9 (SIRT6 assay) was added to the reaction mixture. After incubating at 37 °C for either 3 minutes (SIRT1), 5 minutes (SIRT2), 15 minutes (SIRT3) or 20 minutes (SIRT6), the reaction was quenched with acidic aqueous solution (0.2 M HCl and 6 M acetic acid in water). The reaction times were chosen specifically to ensure the 15 – 18% of acetylated peptides to be converted to free-lysine products for DMSO control samples. After vortexing and centrifuging at 17,000g for 8 minutes to remove the precipitated enzyme, the supernatant was loaded to HPLC with Kinetex EVO C18 column (100 × 4.60 mm, 5 μM, 100 Å) for analysis.

**SIRT2 cloning, purification, crystallization, and structure determination**

For the crystalization construct, the human SIRT2 cDNA coding for residues 56-356 was cloned into the pET28a-SUMO (ppSUMO) vector encoding an N-terminal His-SUMO tag using the BamHI and XhoI sites, inserting a stop codon directly after

residue 356. The sequenced plasmid was transformed to BL-21 (DE3) chemically competent *E. coli*. 6-8 L of 1.5x LB broth with 50 μg/mL Kanamycin was inoculated with 100 mL of an overnight starter grown at 30° C in LB. The cultures were grown at 33° C to an optical density at 600 nm of 0.5-0.7, 0.1 mM IPTG was added, the temperature was reduced to 18° C, and the protein was expressed for 18-20 h. Cells were harvested by centrifugation at 5000 *g*. Cell pellets were frozen at -80° C or immediately used for purification. Pellets were resuspended in a final volume of 100 mL using 40 mM Tris pH 7.5, 400 mM NaCl, 10 mM imidazole, 5% glycerol, 1 mM PMSF, 0.5 mg/mL lysozyme, and 5 uL Pierce universal nuclease. After 20 min incubation, cells were sonicated on ice for a total of 5 min on a Fisherbrand sonic dismembrator at level 7, using a cycle of 2 s on/2 s off with stirring every 2 min. The lysate was cleared by centrifugation at 30,000 *g* for 45 min, and the soluble His-SUMO tagged SIRT2 was purified from the supernatant over 6 mL of Co-NTA resin, washed with 45 mL of 50 mM Tris pH 7.5, 400 mM NaCl, 5% glycerol, 1 mM ATP, 4 mM $MgOAc_2$, 10 mM imidazole, and eluted with 20 mL of 40 mM Tris pH 7.5, 200 mM NaCl, 5% glycerol, 200 mM imidazole pH 8. The eluted fraction was treated with ULP1 SUMO protease on ice overnight, concentrated, and purified on a Superdex 75 gel filtration column in a buffer of 20 mM Tris pH 7.5 and 160 mM NaCl using an ÄKTA pure FPLC system. The 34.0-kDa SIRT2(56-356) peak fractions were combined, concentrated, run over 2 mL Co-NTA resin to remove any contaminating His-tagged ULP1, and concentrated to 20 mg/mL in a buffer of 20 mM Tris pH 7.5, 160 mM NaCl. Concentrations were determined by the Bradford assay.

For crystal screens, 2.5 mM $NAD^+$ and then 2.5 mM Glyco-TM were added to a solution of 20 mg/mL SIRT2(56-356) in 20 mM Tris/HCl pH 7.5, 160 mM NaCl (final SIRT2 concentration was 15 mg/mL, 0.44 mM). The solution was incubated at RT for 15 min before dispensing to crystal trays. An initial crystal hit was obtained from the Wizard Classic crystal screen in 2 M $(NH_4)_2SO_4$, 100 mM Na acetate/HCl pH 4.6. A drop with no $NAD^+$ produced no crystals. The crystal condition was optimized to 2 M $(NH_4)_2SO_4$, 80 mM Na acetate/HCl pH 5.0. Crystals grew in 3-4 days and after 8 days, were flash-frozen in liquid $N_2$ in well solution plus 20% glycerol. SIRT2(34-356), cloned and purified similarly to the SIRT2(56-356) construct, did not produce crystals with Glyco-TM bound.

An initial solution was obtained from data collected at APS beamline 24-ID-C. The reported dataset was collected on September 10, 2018 on ALS beamline 5.0.2. Diffraction data was processed in the I2 space group using iMosflm[4] and Aimless[5] in the CCP4 suite[6]. The structure was determined by molecular replacement using PHASER[7] in the Phenix suite [8] using PDB structure 4X3O to prepare the search model [9]. Structure building was done in Coot [10]. Refinement was done using Phenix suite, including phenix.refine [11], MolProbity [12], with both manually-defined and ReadySet-generated ligand restraints. Figures were prepared in PyMOL version 2.0, Schrödinger LLC.

**Cell culture and transfection**

Dulbecco's Modified Eagle Medium (DMEM) with 10% Fetal Bovine Serum (Invitrogen) was used to culture MCF7, MDA-MB-231, and MDA-MB-468 cells. All cells were cultured at the $CO_2$ incubator set to 37 °C with 5% $CO_2$.

**Cellular viability assay**

To each well of 96-well plates, 2000 or 3000 cells in 100 µL of media were seeded. After 18 hours, inhibitors dissolved in 100 µL of media were added to each well in various concentrations, making the final concentration to range from 1.56 µM to 100 µM. After 72 hours, CellTiter Blue (Promega) was added and the viability was measured according to the manufacturer's protocol.

**Cell Permeability Assay**

When the MCF7 cells in 10 cm plate reached 80% confluency, the cells were treated with the indicated concentrations of Glucose-TM, TM or NH4-6. After 6 hours of incubation at 37°C with 5% $CO_2$, the cells were washed with cold PBS three times, and were collected by 4°C centrifuge. Then, 110 µL of ice-cold methanol was added to the tube with cells to extract small molecule. The tube with cells were vortexed and centrifuged at 15,000 x *g* for 10 minutes. After transferring the supernatant to a clean tube, 100 µL of the supernatant was loaded to Shimadzu HPLC LC20-AD and Thermo Scientific LCQ Fleet Mass Spectrometer LC-MS system with Kinetex 5u EVO C18 100 Å Column (30 x 2.1 mm, 5 µm) for analysis. The UV peak of each sample from detector A (215 nm) was integrated to calculate the concentration of the compound. The standard curves of Glucose-TM, TM and NH4-6 at concentrations ranging from 2 µM to 200 µM were prepared accordingly. Using the standard curve as reference, the estimated concentrations of Glucose-TM, TM and NH4-6 that had entered the cell were calculated.

**Soft Agar Colony Formation Assay**

To each well of 6-well plates, 2 mL mixture of 0.3% low melting point agar (.4 mL), DMEM (1.6 mL) and appropriate amount of inhibitor for indicated final concentration (2 µL) was added to form the solid base layer. The plate was left in room temperature for 15 minutes to let the agar to solidify. Then, 1 mL mixture of 0.3% low melting point agar (0.1 mL), DMEM (0.9 mL), appropriate amount of inhibitor for indicated final concentration (2 µL) and 4000 cells (100 µL) was added to each well to form the growth layer. After every 4 days, additional 1 mL mixture of 0.3% low melting point agar (0.1 mL), DMEM and appropriate amount of inhibitor for indicated final concentration (2 µL) was added. After 10 days of incubation at 37 °C with 5% $CO_2$, 200 µL of nitro blue tetrazolium chloride in autoclaved water at 2 mg/mL concentration was added to each well for staining. After overnight incubation at 37 °C with 5% $CO_2$, the images of the plates were taken using ChemiDoc MP Imaging System.

**Antibodies**

The anti-acetyl-α-tubulin (6-11B-1) (MABT868), anti-Ac-p53 (K382) (CST 2525S) and anti-β-Actin (C4) conjugated to horseradish peroxidase (SC 47778) were used for immunofluorescence and immunoblots. The anti-rabbit IgG-horseradish peroxidase (#7074) was used as secondary antibody for Ac-p53 antibody. The Cy3-conjugated goat α-mouse (Thermo A10521) was used as secondary antibody for immunofluorescence of acetyl- α-tubulin.

**Immunofluorescence of Ac-α-tubulin**

200,000 MCF7 cells were seeded to 35 mm-glass bottom dishes (MatTek). After 18 hours, the cells were treated with DMSO, TM, NH4-6 or NH4-8 at indicated

concentrations for 6 hours. Then, the cells were washed with PBS three times and fixed with methanol. The cells were treated with 0.5% Triton-X in PBS for 10 minutes. Again, the cells were washed with PBS three times and blocked by 1% BSA in TBST buffer for 1 hour. Then, the cells were incubated with Ac-α-tubulin antibody (1:100) for 16 hours at 4 °C. After washing the cells with TBST three times, Cy3 conjugated antibody (1:1000) dissolved in 1% BSA in TBST buffer was added to the cells. Then, the cells were incubated in the dark for 1 hour at room temperature. After washing the cells with TBST three times, the cells were mounted and stained by DAPI fluoromount. The cells were imaged by Cytation 5 Cell Imaging Multi-mode Reader (Biotek).

**Immunoblotting Ac-p53**

MCF7 cells were co-treated with 400 nM of Trichostatin A and indicated concentrations of EX527, TM, NH4-6 and NH4-8 for 6 hours. Then, the cells were collected and lysed by 4% SDS-lysis buffer with protease inhibitor cocktail (Sigma) and universal cell nuclease (Thermo). The acetylation levels of p53 were detected by western blot using anti-Ac-p53 (K382) (CST 2525S). β-Actin was used as loading control.

**Synthesis of Ac-H3K9 peptide**

The sequence of Ac-H3K9 peptide used in this paper was KQTAR-(Ac-K)-STGGWW. It was synthesized using a FOCUS peptide synthesizer, following the steps from the previously reported paper[1].

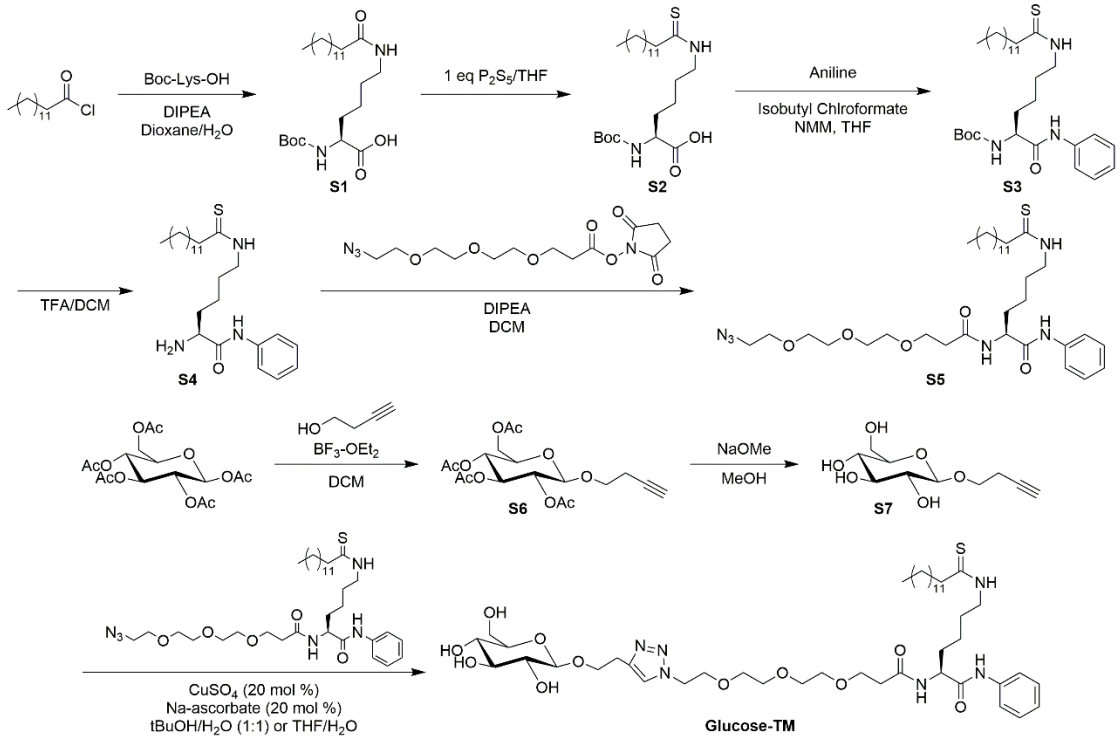


**Scheme 2.1 Synthesis of Glucose-TM.**

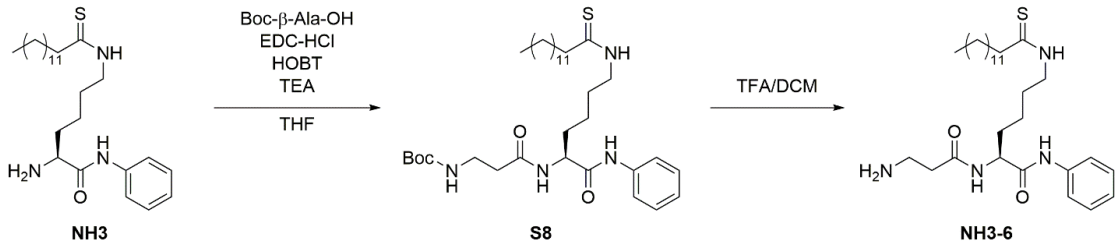


**Scheme 2.2 Synthesis of NH3-6.**

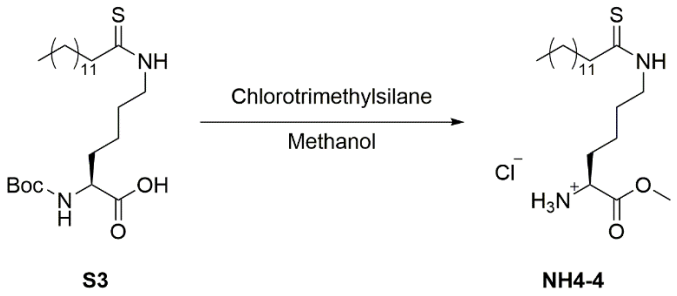


**Scheme 2.3 Synthesis of NH4-4.**

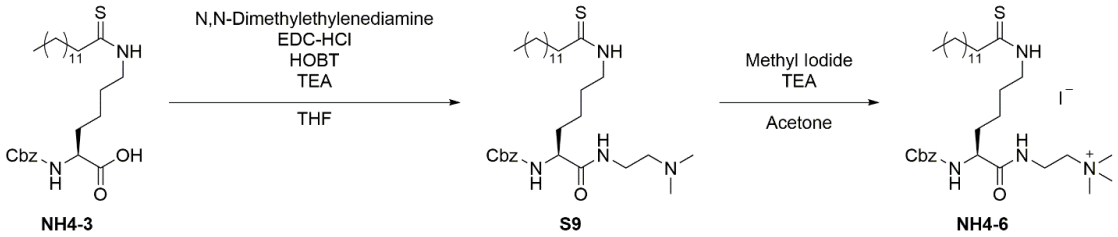


**Scheme 2.4 Synthesis of NH4-6.**

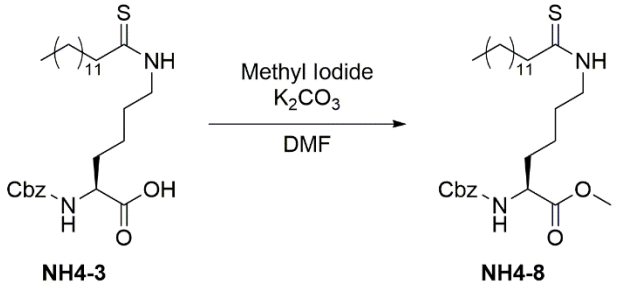


**Scheme 2.5 Synthesis of NH4-8.**

**Synthesis of Compounds Glucose-TM, NH3, NH3-6, NH4-3, NH4-4, NH4-6 and NH4-8**

***N*$^2$-(*tert*-butoxycarbonyl)-*N*$^6$-tetradecanoyl-*L*-lysine (S1).**

To *Boc*-*L*-Lysine (5g, 20.3 mmol) dissolved in water (60 mL) and dioxane (60 mL), $NaHCO_3$ (5.11 g, 60.9 mmol) was added. The reaction mixture was stirred for 2 hours until *Boc*-*L*-Lysine dissolved. After 2 hours, myristoyl chloride (6.05 mL, 22.3

mmol) was added to the mixture. The reaction mixture was stirred overnight at room temperature. dicholoromethane (DCM, 180 mL) was added to the mixture, which then was washed with 1N HCl (100 mL, 2 times), brine (120 mL, 2 times) and dried over $Na_2SO_4$. The collected DCM layer was evaporated using a rotary evaporator. Then, the crude residue was purified by column chromatography using DCM and methanol (DCM: methanol = 95:5 to 9:1) to afford the final compound S1 (5.28 g, 55%). $^1$H NMR (500 MHz, $CD_3OD$) δ 4.06 (dd, J = 9.2, 4.7 Hz, 1H), 3.17 (t, J = 6.9 Hz, 2H), 2.16 (t, J = 7.5 Hz, 2H), 1.88 – 1.75 (m, 1H), 1.71 – 1.49 (m, 5H), 1.44 (s, 11H), 1.31 – 1.21 (m, 20H), 0.90 (t, J = 6.9 Hz, 3H). $^{13}$C NMR (126 MHz, $CD_3OD$) δ 174.89, 174.83, 156.76, 79.03, 53.42, 38.63, 35.77, 31.68, 31.06, 29.40, 29.36, 29.32, 29.23, 29.07, 29.03, 28.91, 28.58, 27.34, 25.69, 22.91, 22.33, 13.03. LCMS (ESI) calcd. for $[M+H\text{-}Boc]^+$ ($C_{20}H_{41}N_2O_3^+$) 357.30, obsd. 357.90

**$N^2$-(*tert*-butoxycarbonyl)-$N^6$-tetradecanethioyl-*L*-lysine (S2).**

To $P_2S_5$ (0.509 g, 2.29 mmol) in THF (40 mL), $NaHCO_3$ (0.120 g, 1.43 mmol) was added slowly while stirring at room temperature (RT) for 1 hour at RT. Then, the reaction mixture was cooled down to 0 °C using an ice bath and S1 (1.31 g, 2.86 mmol) was added slowly. After 1 h, the ice bath was removed, and the reaction mixture was stirred overnight at RT. THF was removed using a rotary evaporator. The reaction mixture was dissolved in DCM (70 mL), and washed with 15% citric acid (40 mL, 2 times), water (40 mL, 1 time) and brine (40 mL, 2 times). The collected DCM layer was dried over $Na_2SO_4$ and was then concentrated by rotary evaporator. The crude residue was purified by column chromatography using hexane and ethyl acetate (hexane: ethyl acetate 1:2), affording the final compound S2 (.676 g, 50%). $^1$H NMR

(500 MHz, $CD_3OD$) δ 4.08 (dd, J = 9.1, 4.7 Hz, 1H), 3.19 (t, J = 6.9 Hz, 2H), 2.18 (t, J = 7.5 Hz, 2H), 1.92 – 1.77 (m, 1H), 1.73 – 1.50 (m, 5H), 1.46 (s, 11H), 1.31 – 1.21 (m, 20H), 0.92 (t, J = 6.9 Hz, 3H). $^{13}C$ NMR (126 MHz, $CD_3OD$) δ 205.06, 174.78, 156.77, 79.08, 53.35, 45.66, 45.16, 31.68, 31.11, 29.41, 29.40, 29.35, 29.31, 29.22, 29.08, 29.06, 28.53, 27.34, 26.87, 23.03, 22.34, 13.04. LCMS (ESI) calcd. for $[M+H]^+$ ($C_{25}H_{49}N_2O_4S^+$) 473.33, obsd. 473.06.

***tert*-butyl (*S*)-(1-oxo-1-(phenylamino)-6-tetradecanethioamidohexan-2-yl)carbamate (S3).**

To S2 (0.608 g, 1.29 mmol) dissolved in THF (15 mL), DIPEA (0.673 mL, 3.86 mmol) and isobutyl chloroformate (0.217 mL, 1.67 mmol) were added. The reaction mixture was stirred for 1 hour at RT. Then, aniline (0.176 mL, 1.93 mmol) was added to the reaction mixture. After stirring overnight at RT, THF was removed using a rotary evaporator. The reaction mixture was re-dissolved in ethyl acetate (50 mL), and washed by 1N HCl (30 mL, 1 time), water (30 mL, 1 time) and brine (30 mL, 2 times). The collected ethyl acetate layer was dried over $Na_2SO_4$ and concentrated using a rotary evaporator. The concentrated crude residue was purified by column purification using DCM and methanol (DCM: methanol = 95:5) to afford the final product S3 (0.352 g, 49%). $^1H$ NMR (500 MHz, $CD_3OD$) δ 7.57 (d, J = 7.9 Hz, 2H), 7.31 (t, J = 7.8 Hz, 2H), 7.11 (t, J = 7.4 Hz, 1H), 4.19 (dd, J = 8.7, 5.4 Hz, 1H), 3.62 (t, J = 7.2 Hz, 2H), 2.69 – 2.49 (m, 2H), 1.85 (m, J = 19.0, 7.5, 6.6 Hz, 1H), 1.72 (m, J = 8.8, 2.7 Hz, 5H), 1.47 (s, 11H), 1.31 – 1.21 (m, 20H), 0.95 – 0.88 (t, J = 6.9 Hz, 3H). $^{13}C$ NMR (126 MHz, $CD_3OD$) δ 205.04, 172.10, 156.52, 138.09, 128.42, 124.00, 120.06, 79.29, 55.21, 45.72, 45.15, 31.92, 31.71, 29.45, 29.44, 29.39, 29.35,

29.26, 29.11, 29.08, 28.59, 27.39, 27.04, 23.04, 22.37, 13.13. LCMS (ESI) calcd. for $[M+H]^+$ ($C_{31}H_{54}N_3O_3S^+$) 548.38, obsd. 548.14.

**(*S*)-2-amino-*N*-phenyl-6-tetradecanethioamidohexanamide (NH3) (S4)**

To S3 (1.24 g, 2.26 mmol) dissolved in DCM (12 mL), trifluoroacetic acid (8 mL) was added slowly while stirring at room temperature. After 2 hours of stirring, additional DCM (75 mL) was added to dilute the reaction mixture. Then, the reaction mixture was washed with 1M NaOH (50 mL, 2 time) and brine (60 mL, 1 time) and dried over $Na_2SO_4$. After removing the collected DCM layer by rotary evaporator, the crude residue was purified by column purification using DCM and methanol (DCM: methanol = 96:4 → 9:1) to afford the final product 2 (.608 g, 60%). $^1$H NMR (500 MHz, $CD_3OD$) δ 7.67 – 7.49 (m, 2H), 7.38 – 7.24 (m, 2H), 7.15 – 7.09 (m, 1H), 3.70 – 3.56 (m, 2H), 3.48 (t, J = 6.5 Hz, 1H), 2.60 – 2.54 (m, 2H), 1.82 (ddt, J = 12.7, 10.2, 6.2 Hz, 1H), 1.77 – 1.64 (m, 5H), 1.48 (dddd, J = 23.4, 11.2, 8.6, 5.4 Hz, 2H), 1.31 – 1.21 (m, 20H), 0.92 (t, J = 6.9 Hz, 3H). $^{13}$C NMR (126 MHz, $CD_3OD$) δ 205.05, 174.40, 138.06, 128.44, 123.97, 119.92, 55.14, 45.67, 45.16, 34.60, 31.68, 29.42, 29.40, 29.36, 29.31, 29.22, 29.08, 29.03, 28.54, 27.20, 22.76, 22.34, 13.05. LCMS (ESI) calcd. for $[M+H]^+$ ($C_{26}H_{46}N_3OS^+$) 448.33, obsd. 448.13.

**(*S*)-2-(3-(2-(2-(2-azidoethoxy)ethoxy)ethoxy)propanamido)-*N*-phenyl-6-tetradecanethioamidohexanamide (S5)**

To 2 (.0939g, .210 mmol) dissolved in THF (2.1 mL), DIPEA (.110 mL, .629 mmol) was added slowly. After 15 minutes, azido-PEG3-NHS ester (.0722 g, .210 mmol) was added to the reaction mixture, while stirring at room temperature. After overnight stirring, THF was removed by rotary evaporator. Then, the reaction mixture

was dissolved in ethyl acetate (30 mL), followed by washings with water (20 mL, 2 times) and brine (20 mL, 2 times). The collected ethyl acetate layer was dried over $Na_2SO_4$ and removed by rotary evaporator. The crude residue was further purified by column purification using DCM and methanol (DCM: methanol = 98:2 → 95:5) to afford the final product S4 (.0718 g, 51%). 1H NMR (500 MHz, $CD_3OD$) δ 7.60 – 7.54 (m, 2H), 7.33 (t, J = 7.9 Hz, 2H), 4.50 (dd, J = 8.7, 5.5 Hz, 1H), 3.79 (td, J = 6.1, 1.4 Hz, 2H), 3.68 – 3.60 (m, 12H), 3.37 (t, J = 5.0 Hz, 2H), 2.62 – 2.53 (m, 4H), 1.93 (ddt, J = 13.5, 10.1, 5.9 Hz, 1H), 1.80 (ddt, J = 13.8, 8.8, 4.7 Hz, 1H), 1.72 (q, J = 7.4 Hz, 5H), 1.50 (dtt, J = 20.6, 14.2, 7.3 Hz, 2H), 1.31 – 1.21 (m, 20H), 0.92 (t, J = 6.8 Hz, 3H). $^{13}C$ NMR (126 MHz, $CD_3OD$) δ 205.08, 172.75, 171.13, 138.05, 128.41, 124.05, 120.15, 70.22, 70.14, 70.11, 69.98, 69.70, 66.91, 53.92, 50.36, 45.69, 45.15, 36.08, 31.68, 31.58, 29.43, 29.40, 29.36, 29.32, 29.23, 29.08, 29.05, 28.56, 27.02, 22.95, 22.34, 13.05. LCMS (ESI) calcd. for $[M+H]^+$ ($C_{35}H_{61}N_6O_5S^+$) 677.43, obsd. 677.12.

**(2*R*,3*R*,4*S*,5*R*,6*R*)-2-(acetoxymethyl)-6-(but-3-yn-1-yloxy)tetrahydro-2*H*-pyran-3,4,5-triyl triacetate (S6)**

To D-glucose pentaacetate (1.13 g, 2.90 mmol) dissolved in DCM (45 mL), 3-butyn-1-ol (.440 mL, 5.80 mmol) was added, while stirring. Then, boron trifluoride diethyl etherate (1.07 mL, 8.70 mmol) was added slowly to the reaction mixture, which then stirred overnight at room temperature. After overnight stirring, the reaction mixture was diluted with DCM (80 mL), and washed with saturated $NaHCO_3$ (50 mL, 2 times) and brine (50 mL, 2 times). The collected DCM layer was dried over $Na_2SO_4$ and concentrated by rotary evaporator. The crude residue was purified by column

chromatography using hexane and ethyl acetate (hexane: ethyl acetate = 4:1 → 3:1 → 2:1) to afford the final compound S5 (.650 g, 56%). $^{1}$H NMR (500 MHz, $CDCl_3$) δ 5.21 (td, J = 9.5, 1.4 Hz, 1H), 5.09 (t, J = 9.7 Hz, 1H), 5.03 – 4.94 (m, 1H), 4.57 (d, J = 7.9 Hz, 1H), 4.26 (dd, J = 12.3, 4.8 Hz, 1H), 4.14 (dd, J = 12.2, 2.4 Hz, 1H), 3.94 (dt, J = 9.8, 6.6 Hz, 1H), 3.78 – 3.60 (m, 2H), 2.47 (td, J = 7.0, 2.6 Hz, 2H), 2.11 – 1.99 (m, 12H), 1.96 (t, J = 2.7 Hz, 1H). $^{13}$C NMR (126 MHz, $CDCl_3$) δ 170.69, 170.30, 169.40, 169.36, 100.85, 80.57, 72.74, 71.87, 71.12, 69.52, 68.37, 67.94, 61.91, 20.76, 20.71, 20.64, 20.61, 19.86.

**(2*R*,3*R*,4*S*,5*S*,6*R*)-2-(but-3-yn-1-yloxy)-6-(hydroxymethyl)tetrahydro-2*H*--3,4,5-triol (S7)**

To S6 (.116 g, .288 mmol) dissolved in methanol (1.4 mL), sodium methoxide (1.3 µL, .00577 mmol) was added. The reaction mixture was stirred for 6 hours. Activated Dowex 50WX4-200 ion exchange resin was added to adjust the pH of the reaction mixture to 7. The resin was filtered off and the reaction mixture was concentrated by using rotary evaporator to afford the final compound S6 (.0598 g, 89%). $^{1}$H NMR (500 MHz, $CD_3OD$) δ 4.31 (d, J = 7.8 Hz, 1H), 3.97 (dt, J = 9.7, 7.3 Hz, 1H), 3.88 (dd, J = 11.9, 1.7 Hz, 1H), 3.75 – 3.64 (m, 2H), 3.36 (s, 2H), 3.29 (d, J = 5.4 Hz, 1H), 3.18 (dd, J = 9.1, 7.8 Hz, 1H), 2.52 (td, J = 7.3, 2.7 Hz, 2H), 2.28 (t, J = 2.7 Hz, 1H). $^{13}$C NMR (126 MHz, $CD_3OD$) δ 102.99, 80.34, 76.61, 76.58, 73.60, 70.17, 69.21, 67.60, 61.31, 19.18, 19.15.

**(*S*)-*N*-phenyl-6-tetradecanethioamido-2-(3-(2-(2-(2-(4-(2-(((2*S*,3*S*,4*R*,5*R*,6*S*)-3,4,5-trihydroxy-6-(hydroxymethyl)tetrahydro-2*H*-pyran-2-yl)oxy)ethyl)-1*H*-1,2,3-triazol-1-yl)ethoxy)ethoxy)ethoxy)propanamido)hexanamide (Glucose-TM)**

To 2 (.0581 g, .250 mmol) and S6 (.169 g, .250 mmol) dissolved in water (1 mL) and methanol (1 mL), $NaHCO_3$ (.0631 g.750 mmol), $CuSO_4$-$5H_2O$ (3.13 mg, .0125 mmol) and sodium ascorbate (9.92 mg, .0500 mmol) were added in order. The reaction mixture was stirred overnight in room temperature. After the stir, ethyl acetate (15 mL) was added to the reaction mixture, which was then washed by water (10 mL, 2 times) and brine (10 mL, 1 time). The collected ethyl acetate layer was dried over $Na_2SO_4$ and concentrated using rotary evaporator. The crude residue was purified by column purification using DCM and methanol (DCM: methanol = 9:1) to afford the final compound 1 (.0409g, 18%). $^1$H NMR (500 MHz, $CD_3OD$) δ 7.92 (s, 1H), 7.57 (dd, J = 8.5, 1.2 Hz, 2H), 7.32 (t, J = 8.5, 7.4 Hz, 2H), 7.12 (t, 1H), 4.55 – 4.48 (m, 3H), 4.33 (d, J = 7.8 Hz, 1H), 4.16 (dt, J = 9.8, 6.5 Hz, 1H), 3.92 – 3.74 (m, 6H), 3.71 – 3.66 (m, 1H), 3.64 – 3.56 (m, 11H), 3.41 – 3.35 (m, 1H), 3.31 – 3.28 (m, 2H), 3.22 (dd, J = 9.1, 7.8 Hz, 1H), 3.03 (t, J = 6.5 Hz, 2H), 2.66 – 2.42 (m, 4H), 1.92 (ddt, J = 13.6, 10.0, 6.0 Hz, 1H), 1.85 – 1.64 (m, 5H), 1.49 (dddd, J = 23.7, 16.4, 12.0, 6.8 Hz, 2H), 1.31 – 1.21 (m, 20H), 0.92 (t, J = 6.9 Hz, 3H). $^{13}$C NMR (126 MHz, $CD_3OD$) δ 205.06, 172.70, 171.16, 144.66, 138.06, 128.43, 124.06, 123.61, 120.13, 103.02, 76.65, 76.60, 73.69, 70.23, 70.09, 70.05, 70.03, 69.99, 68.97, 68.13, 66.88, 61.37, 53.93, 49.92, 45.69, 45.16, 36.06, 31.68, 31.61, 29.43, 29.41, 29.36, 29.33, 29.23, 29.08, 29.06, 28.57, 27.02, 25.83, 22.96, 22.34, 13.06. LCMS (ESI) calcd. for $[M+H]^+$ ($C_{45}H_{77}N_6O_{11}S^+$) 909.53, obsd. 909.22.

**_tert_-butyl (_S_)-(3-oxo-3-((1-oxo-1-(phenylamino)-6-tetradecanethioamidohexan-2-yl)amino)propyl)carbamate (S8)**

To 2 (.162 g, .296 mmol) dissolved in THF (3 mL), *boc*-β-alanine-OH (.0615 g, .325 mmol), EDC-HCl (.0623 g, .325 mmol), TEA (.124 mL, .887 mmol) and HOBT (.0499 g, .325 mmol) were added, while stirring. The reaction mixture was stirred for overnight at room temperature. THF was evaporated using rotary evaporator. Then, the reaction mixture was dissolved in ethyl acetate (15 mL) and washed by water (10 mL, 2 times) and brine (10 mL, 2 times). The collected ethyl acetate layer was dried over $Na_2SO_4$ and concentrated by rotary evaporator. The crude residue S7 was taken to next step without further purification (.0473 g, 26%). LCMS (ESI) calcd. for $[M+H]^+$ ($C_{34}H_{59}N_4O_4S^+$) 619.42, obsd. 619.06.

**(*S*)-2-(3-aminopropanamido)-*N*-phenyl-6-tetradecanethioamidohexanamide (NH3-6)**

To S7 (.0452 g, .0730 mmol) dissolved in DCM (.440 mL), trifluoroacetic acid (.292 mL) was added slowly, while stirring. The reaction mixture was stirred for 2 hours. Additional DCM (7 mL) was added to mixture, which was washed by 1M NaOH (4 mL, 2 times) and brine (4mL, 2 times). The collected DCM layer was dried over $Na_2SO_4$ and concentrated by rotary evaporator. The residue crude was purified using column purification with DCM and methanol (DCM: methanol = 85:15) to afford the final product 3 (.0331 g, 87%). $^1$H NMR (500 MHz, $CD_3OD$) δ 7.56 (d, J = 7.6 Hz, 2H), 7.31 (t, J = 7.9 Hz, 2H), 7.10 (t, J = 7.4 Hz, 1H), 4.45 (dd, J = 8.7, 5.6 Hz, 1H), 3.61 (td, J = 7.1, 2.9 Hz, 2H), 3.07 (t, J = 6.5 Hz, 1H), 2.69 – 2.37 (m, 4H), 1.96 – 1.76 (m, 2H), 1.70 (q, J = 7.2 Hz, 5H), 1.50 (dddd, J = 31.0, 16.8, 13.7, 6.4 Hz, 2H), 1.31 – 1.21 (m, 20H), 0.90 (t, J = 6.8 Hz, 3H). $^{13}$C NMR (126 MHz, $CD_3OD$) δ 205.11, 172.08, 171.44, 138.09, 128.41, 124.04, 120.04, 54.16, 45.69, 45.06, 36.58,

34.25, 31.68, 31.47, 29.42, 29.40, 29.36, 29.32, 29.23, 29.08, 29.05, 28.55, 27.05, 23.02, 22.34, 13.05. LCMS (ESI) calcd. for $[M+H]^+$ ($C_{29}H_{51}N_4O_2S^+$) 519.37, obsd. 519.25.

**$N^2$-((benzyloxy)carbonyl)-$N^6$-tetradecanethioyl-*L*-lysine (NH4-3)**

Synthesis of Compound 4 was followed by the procedure as previously reported. $^1$H NMR (500 MHz, $CD_3OD$) δ 7.48 – 7.13 (m, 5H), 5.12 (d, J = 2.7 Hz, 2H), 4.18 (dd, J = 9.2, 4.7 Hz, 1H), 3.60 (t, J = 7.1 Hz, 2H), 2.60 (t, J = 7.5 Hz, 2H), 1.88 (ddd, J = 12.9, 9.6, 5.5 Hz, 1H), 1.71 (ddq, J = 29.4, 14.0, 7.7, 6.9 Hz, 5H), 1.55 – 1.41 (m, 2H), 1.31 – 1.21 (m, 20H), 0.92 (t, J = 6.8 Hz, 3H). $^{13}$C NMR (126 MHz, $CD_3OD$) δ 205.08, 174.47, 157.31, 136.83, 128.05, 127.56, 127.34, 66.20, 53.78, 45.66, 45.15, 33.36, 31.68, 31.04, 29.40, 29.35, 29.31, 29.22, 29.08, 29.05, 28.52, 26.82, 23.00, 22.33, 13.04. LCMS (ESI) calcd. for $[M+H]^+$ ($C_{28}H_{47}N_2O_4S^+$) 507.32, obsd. 507.22.

**(*S*)-1-methoxy-1-oxo-6-tetradecanethioamidohexan-2-aminium (NH4-4)**

To S2 (.142 g, .300 mmol) dissolved in methanol (5 mL), chlorotrimethylsilane (76.0 µL, .600 mmol) was added slowly, while stirring. The reaction mixture was stirred overnight at room temperature and concentrated by rotary evaporator. The crude residue was purified by column purification using DCM and methanol (DCM: methanol = 95:5) to afford the final product 6 (.0837 g, 66%). $^1$H NMR (500 MHz, $CD_3OD$) δ 3.75 (s, 3H), 3.60 (t, J = 7.2 Hz, 2H), 3.55 (t, J = 6.5 Hz, 1H), 2.59 (t, J = 7.5 Hz, 2H), 1.82 – 1.65 (m, 6H), 1.43 (dqd, J = 15.2, 7.8, 7.4, 5.1 Hz, 2H), 1.31 – 1.21 (m, 20H), 0.95 – 0.88 (m, 3H). $^{13}$C NMR (126 MHz, $CD_3OD$) δ 205.11, 174.70, 53.36, 51.22, 45.66, 45.05, 33.15, 31.68, 29.42, 29.40, 29.36, 29.31,

29.22, 29.08, 29.07, 28.52, 27.01, 22.48, 22.33, 13.03. $[M\text{-}Cl]^+$ ($C_{21}H_{44}N_2O_2S^+$) 387.30, obsd. 387.25.

**benzyl (*S*)-(1-((2-(dimethylamino)ethyl)amino)-1-oxo-6-tetradecanethioamidohexan-2-yl)carbamate (S9)**

To 4 (.460 g, .908 mmol) dissolved in THF (9 mL), N,N-Dimethylethylenediamine (.109 mL, .999 mmol), EDC-HCl (.209 g, 1.09 mmol), HOBT (.167 g, 1.09 mmol) and TEA (.379 mL, 2.72 mmol) were added, while stirring. The reaction mixture was stirred for overnight at room temperature. THF was removed using rotary evaporator. The reaction mixture was dissolved in ethyl acetate (30 mL) and washed by water (20 mL, 2 times) and brine (20 mL, 2 times). The collected ethyl acetate layer was dried over $Na_2SO_4$ and concentrated by rotary evaporator. The crude residue was purified using column purification with DCM and methanol (DCM: methanol = 9:1) to afford the final product S8 (.306 g, 58%). $^1$H NMR (500 MHz, $CD_3OD$) δ 7.39 – 7.30 (m, 5H), 5.18 – 5.08 (m, 2H), 4.00 (dd, J = 8.8, 5.5 Hz, 1H), 3.69 – 3.54 (m, 3H), 3.52 – 3.38 (m, 1H), 3.17 (s, 2H), 2.83 (s, 6H), 2.61 – 2.55 (m, 2H), 1.88 – 1.59 (m, 6H), 1.58 – 1.37 (m, 2H), 1.34 – 1.28 (m, 20H), 0.91 (t, J = 6.9 Hz, 3H). $^{13}$C NMR (126 MHz, $CD_3OD$) δ 205.08, 173.80, 157.18, 136.76, 128.10, 127.65, 127.40, 66.35, 57.59, 55.18, 45.68, 45.09, 43.71, 36.08, 31.68, 31.36, 29.42, 29.40, 29.36, 29.31, 29.22, 29.08, 29.06, 28.55, 26.93, 22.95, 22.34, 13.04. (ESI) calcd. for $[M+H]^+$ ($C_{32}H_{57}N_4O_3S^+$) 577.41, obsd. 577.54.

**(*S*)-2-(2-(((benzyloxy)carbonyl)amino)-6-tetradecanethioamidohexanamido)-*N,N,N*-trimethylethan-1-aminium iodide (NH4-6)**

To S8 (.360 g, .624 mmol) dissolved in acetone (6.2 mL), methyl iodide (77.8 µL, 1.25 mmol) and TEA (.174 mL, 1.25 mmol) were added at 0 °C. The reaction mixture was initially stirred at 0 °C and slowly raised to room temperature overnight. Acetone was removed by rotary evaporator. Then, the mixture was dissolved in DCM (20 mL) and washed with water (10 mL, 1 time) and brine (10 mL, 1 time). The collected DCM layer was dried over $Na_2SO_4$ and concentrated by rotary evaporator. The crude residue was purified using column purification with DCM and methanol (DCM: methanol = 85:15) to afford the final product 6 (.125 g, 28%). $^1$H NMR (500 MHz, $CD_3OD$) δ 7.45 – 7.28 (m, 5H), 5.17 – 5.05 (m, 2H), 4.03 (dd, J = 9.1, 5.2 Hz, 1H), 3.61 (t, J = 7.2 Hz, 4H), 3.48 (t, J = 6.4 Hz, 2H), 3.18 (s, 9H), 2.60 (t, J = 7.6 Hz, 2H), 1.93 – 1.59 (m, 6H), 1.57 – 1.38 (m, 2H), 1.36 – 1.28 (m, 20H), 0.92 (t, J = 6.9 Hz, 3H). $^{13}$C NMR (126 MHz, $CD_3OD$) δ 205.11, 174.36, 157.19, 136.76, 128.11, 127.68, 127.41, 66.33, 64.51, 55.38, 52.71, 52.68, 52.64, 45.69, 44.97, 33.47, 31.68, 30.95, 29.43, 29.40, 29.36, 29.32, 29.23, 29.08, 29.07, 28.55, 26.93, 22.99, 22.33, 13.04. (ESI) calcd. for [$M^+$-I] ($C_{33}H_{60}N_4O_3S^+$) 591.43, obsd. 591.44.

**methyl *N*$^2$-((benzyloxy)carbonyl)-N6-tetradecanethioyl-*L*-lysinate (NH4-8)**

To 4 (.207 g, .408 mmol) dissolved in THF (5 mL), $K_2CO_3$ (.620 g, .448 mmol) were added at room temperature. After stirring for 2 hours, methyl iodide (30.4 µL, .489 mmol) was added to the mixture at 0 °C. The reaction mixture was then stirred overnight at room temperature. THF was removed by rotary evaporator. Then, the reaction mixture was dissolved with ethyl acetate (18 mL) and washed by water (10 mL, 2 times) and brine (10 mL, 2 times). The collected ethyl acetate layer was dried over $Na_2SO_4$ and concentrated by rotary evaporator. The crude residue was

purified using column purification with DCM and methanol (DCM: methanol = 95:5) to afford the final product 7 (.164 g, 77%). $^{1}$H NMR (500 MHz, $CD_3OD$) δ 7.45 – 7.25 (m, 5H), 5.10 (s, 2H), 4.19 (dd, J = 9.3, 4.9 Hz, 1H), 3.72 (s, 3H), 3.58 (t, J = 7.1 Hz, 2H), 2.62 – 2.53 (m, 2H), 1.76 – 1.65 (m, 5H), 1.51 – 1.37 (m, 2H), 1.34 – 1.28 (m, 20H), 0.91 (t, J = 6.9 Hz, 3H). $^{13}$C NMR (126 MHz, $CD_3OD$) δ 205.11, 173.20, 157.28, 136.79, 128.06, 127.59, 127.34, 66.24, 53.94, 51.26, 45.66, 45.05, 32.45, 31.68, 30.89, 29.40, 29.35, 29.31, 29.22, 29.08, 29.05, 28.51, 26.79, 22.93, 22.33, 13.04. (ESI) calcd. for $[M+H]^+$ ($C_{29}H_{49}N_2O_4S^+$) 521.33, obsd. 521.32

### 2.6.1 References for methods


1. Jing, H., Hu, J., He, B., Negrón Abril, Y. L., Stupinski, J., Weiser, K., Carbonaro, M., Chiang, Y.-L., Southard, T., Giannakakou, P., Weiss, R. S., and Lin, H. (2016) A SIRT2-Selective Inhibitor Promotes c-Myc Oncoprotein Degradation and Exhibits Broad Anticancer Activity, Cancer Cell 29, 297-310.

2. Spiegelman, N. A., Price, I. R., Jing, H., Wang, M., Yang, M., Cao, J., Hong, J. Y., Zhang, X., Aramsangtienchai, P., Sadhukhan, S., and Lin, H. (2018) Direct Comparison of SIRT2 Inhibitors: Potency, Specificity, Activity-Dependent Inhibition, and On-Target Anticancer Activities, ChemMedChem 13, 1890-1894.

3. Hong, J. Y., Zhang, X., and Lin, H. (2018) HPLC-Based Enzyme Assays for Sirtuins, Methods Mol Biol 1813, 225-234.

4. Battye, T. G., Kontogiannis, L., Johnson, O., Powell, H. R., and Leslie, A. G. (2011) iMOSFLM: a new graphical interface for diffraction-image processing with MOSFLM, Acta Crystallogr. D Biol. Crystallogr. 67, 271-281.

5. Evans, P. R., and Murshudov, G. N. (2013) How good are my data and what is the resolution?, Acta Crystallogr. D Biol. Crystallogr. 69, 1204-1214.

6. Winn, M. D., Ballard, C. C., Cowtan, K. D., Dodson, E. J., Emsley, P., Evans, P. R., Keegan, R. M., Krissinel, E. B., Leslie, A. G., McCoy, A., McNicholas, S. J., Murshudov, G. N., Pannu, N. S., Potterton, E. A., Powell, H. R., Read, R. J., Vagin, A., and Wilson, K. S. (2011) Overview of the CCP4 suite and current developments, Acta Crystallogr. D Biol. Crystallogr. 67, 235-242.

7. McCoy, A. J., Grosse-Kunstleve, R. W., Adams, P. D., Winn, M. D., Storoni, L. C., and Read, R. J. (2007) Phaser crystallographic software, J. Appl. Crystallogr. 40, 658-674.

8. Adams, P. D., Afonine, P. V., Bunkoczi, G., Chen, V. B., Davis, I. W., Echols, N., Headd, J. J., Hung, L. W., Kapral, G. J., Grosse-Kunstleve, R. W., McCoy, A. J., Moriarty, N. W., Oeffner, R., Read, R. J., Richardson, D. C., Richardson, J. S., Terwilliger, T. C., and Zwart, P. H. (2010) PHENIX: a comprehensive Python-based system for macromolecular structure solution, Acta Crystallogr. D Biol. Crystallogr. 66, 213-221.

9. Wang, Y., Fung, Y. M. E., Zhang, W., He, B., Chung, M. W. H., Jin, J., Hu, J., Lin, H., and Hao, Q. (2017) Deacylation Mechanism by SIRT2 Revealed in the 1'-SH-2'-O-Myristoyl Intermediate Structure, Cell Chem Biol 24, 339-345.

10. Emsley, P., Lohkamp, B., Scott, W. G., and Cowtan, K. (2010) Features and development of Coot, Acta Crystallogr. D Biol. Crystallogr. 66, 486-501.

11. Afonine, P. V., Poon, B. K., Read, R. J., Sobolev, O. V., Terwilliger, T. C., Urzhumtsev, A., and Adams, P. D. (2018) Real-space refinement in PHENIX for cryo-EM and crystallography, Acta Crystallogr D Struct Biol 74, 531-544.

12. Chen, V. B., Arendall, W. B., 3rd, Headd, J. J., Keedy, D. A., Immormino, R. M., Kapral, G. J., Murray, L. W., Richardson, J. S., and Richardson, D. C. (2010) MolProbity: all-atom structure validation for macromolecular crystallography, Acta Crystallogr. D Biol. Crystallogr. 66, 12-21.

# CHAPTER 3

## SIMULTANEOUS INHIBITION OF SIRT2 DEACETYLASE AND DEFATTY-ACYLASE ACTIVITIES VIA A PROTAC STRATEGY

This is a revised version of the published paper: Hong JY, Jing H, Price IR, Cao J, Bai JJ, Lin H. Simultaneous Inhibition of SIRT2 Deacetylase and Defatty-Acylase Activities via a PROTAC Strategy. *ACS Med Chem Lett* . 2020 Sep 21;11(11):2305-2311.

J.Y.H., and H.L. wrote the manuscript. All the authors have given approval to the final version of the manuscript.

### 3.1 Abstract

As a member of the sirtuin family of enzymes, SIRT2 promotes tumor growth and regulates various biological pathways through lysine deacetylation and defatty-acylation. In the past few years, many SIRT2 small molecule inhibitors had been developed, but none had demonstrated simultaneous inhibition of both SIRT2 activities in cells. To further scrutinize the physiological importance and significance of SIRT2 deacetylase and defatty-acylase activities, a small molecule that can selectively inhibit both activities of SIRT2 in living cells are needed. Here, we have applied Proteolysis Targeting Chimera (PROTAC) strategy and synthesized a new SIRT2 inhibitor (TM-P4-Thal) to degrade SIRT2 selectively, which led to simultaneous inhibition of its deacetylase and defatty-acylase in living cells. Additionally, this compound exemplifies the advantage of PROTAC strategy that allows complete eradication of an enzyme and its activity in biological settings.

## 3.2 Introduction

The mammalian sirtuin family of enzymes remove various acyl groups from protein lysine residues, using nicotinamide adenine dinucleotide ($NAD^+$) as a cosubstrate.[1-4] They are involved in many biological processes, including metabolism, DNA damage repair, and cell growth.[5-9] Among the seven sirtuins, SIRT2 is the only one that is primarily localized in the cytosol and can remove both acetyl and other acyl groups from protein lysine residues.[10-12] SIRT2 was initially reported to deacetylate protein substrates, including hypoxia-inducible factor 1 - α (HIF1α) and α-tubulin.[13, 14] Through deacetylation of various substrates, SIRT2 promotes tumorigenesis. For example, SIRT2 deacetylates Slug to increase its stability, and promotes breast cancer progression.[15] By deacetylating lactate dehydrogenase A (LDH-A), which is often overexpressed in cancer cells and responsible for lactate production, SIRT2 promotes pancreatic cancer growth.[16] In many cancer cell lines, the inhibition of SIRT2 leads to degradation of C-Myc, impeding cancer cell growth in vitro and tumor growth in mice.[17] Besides the deacetylation activity of SIRT2, SIRT2 can also efficiently remove long chain fatty acyl groups from lysine.[10, 18] SIRT2 can defatty-acylate K-Ras4a and promote K-Ras-mediated transformation.[19] Recently, SIRT2 is also reported to defatty-acylate RalB, another small GTPase in the Ras subfamily.[20] Through both deacetylation and defatty-acylation, SIRT2 plays significant roles in cancer growth and metabolism, which made SIRT2 an attractive target for cancer treatment.

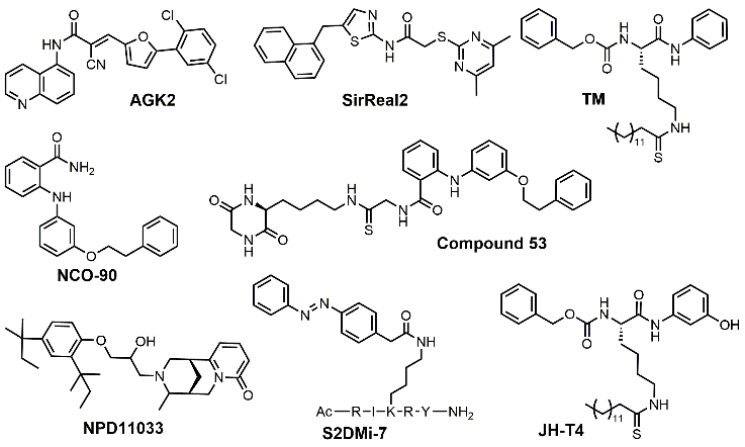


**Figure 3.1 Examples of previously reported SIRT2 inhibitors**

In recent years, many SIRT2 inhibitors have been developed and shown to impede cancer growth. From a high throughput screen effort, AGK2 was developed to be a SIRT2 selective inhibitor that binds to the "C-pocket" of SIRT2.[21] Later, another SIRT2 selective inhibitor, SirReal2 was synthesized, which decreases migration and invasion of gastric cancer cells.[22, 23] NCO-90/140 slowed down cellular growth of several leukemia cells through simultaneous induction of apoptosis and autophagy.[24] Compound 53, based on NCO-90, had demonstrated enhanced antiproliferative effect in breast cancer cells and promoted neurite outgrowth.[25] NPD11033 effectively delayed the cell proliferation of pancreatic cancer cells.[26] TM, a mechanism-based SIRT2 selective inhibitor, portrayed broad anti-cancer effects by promoting the degradation of c-Myc (Figure 3.1).[17]

Interestingly, recent studies that directly compared these inhibitors in various assays revealed that AGK2, SirReal2, and TM inhibit SIRT2 deacetylation activity, but not the defatty-acylation activity.[27] In contrast, a peptide-based SIRT2 inhibitor,

S2DMi-7, could efficiently inhibit the defatty-acylase activities of SIRT1, SIRT2, and SIRT3.[28] Nevertheless, being a peptide, S2DMi-7 may have limited utility for cellular and *in vivo* studies. We recently reported that JH-T4 and NH-TM, which can hinder both activities of SIRT2 (Figure 3.1).[29] However, these two compounds also inhibit SIRT1 and SIRT3, making it difficult to study SIRT2's specific roles in cells.

Given the two different physiological catalytic activities of SIRT2, one interesting question is whether small molecules that can inhibit both activities of SIRT2 would produce different biological effects. To address this question, new inhibitors that can inhibit both the deacetylase and defatty-acylase activities of SIRT2 in live cells, but are specific for SIRT2 are needed.

Proteolysis Targeting Chimera (PROTAC) uses a hetero-dimeric compound consisting of a ligand interacting with the protein-of-interest and another ligand recruiting E3 ligase to degrade the protein of interest.[30-32] This strategy gained attention for its ability to enhance the effects of small molecule inhibitors. Traditionally, most inhibitors bind to an enzyme to inhibit its activity. PROTAC compounds, instead, can not only catalytically remove the target proteins but also

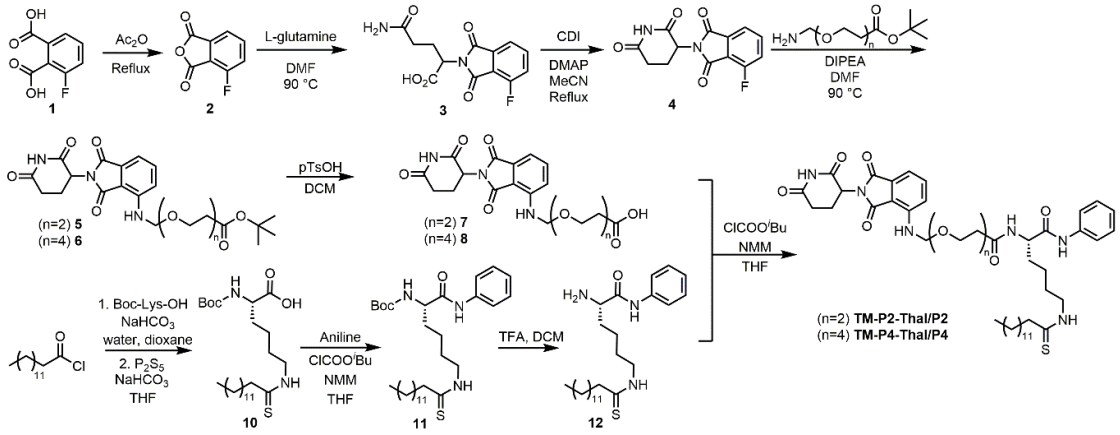


**Scheme 3.1 Synthesis of TM-P2-Thal and TM-P4-Thal.**

eliminate non-enzymatic functions of SIRT2 through degradation..[30, 31] Here we set out to test another possibility that could make the PROTAC strategy more effective: when an inhibitor of SIRT2 could only inhibit one catalytic activity of SIRT2, we could enable it to inhibit all the catalytic activities of SIRT2 using the PROTAC strategy. As such, applying PROTAC strategy to specifically degrade SIRT2 would inhibit both catalytic activities of SIRT2, deacetylation and defatty-acylation that currently existing small molecule inhibitors could not achieve. PROTAC utilizing SirReal2 as the ligand was synthesized, but was not tested to show the advantage of the PROTAC strategy.[33] Here we introduce two new PROTAC compounds, TM-P2-Thal and TM-P4-Thal, which can degrade SIRT2 efficiently in various cancer cells. Through SIRT2 degradation, we demonstrate that these compounds inhibit both activities of SIRT2 in living cells and achieve enhanced antiproliferative effect in cancer cells.

## 3.3 Results and Discussion

### 3.3.1 PROTAC Design and Synthesis.

TM is a thiomyristoyl lysine-based SIRT2 selective inhibitor. Its thiomyristoyl lysine is important for SIRT2 inhibition, as this portion forms a stalled covalent intermediate with $NAD^+$ to inhibit the activity of SIRT2.[17] The C- and N-termini of the thiomyristoyl lysine serves as the potential modification sites to attach the linker and thalidomide, the ligand that recruit the E3 ubiquitin ligase cereblon (CRBN). According to the previously reported co-crystal structures of SIRT2 in complex with two inhibitors, BHJH-TM1 and Glucose-TM (PDB: 4R8M, 6NR0), the thiomyristoyl lysine points inward towards the enzyme pocket, while both the N- and C-terminal

amino acids of the lysine are located outside of the pocket.[18, 34] The introduction of a hydroxyl group to the C-terminal phenyl group of TM, resulting in a new inhibitor, JH-T4, disrupted the selectivity of TM for SIRT2, as JH-T4 inhibits SIRT1, SIRT2 and SIRT3.[29] From this finding, we hypothesized that altering the C-terminal phenyl ring for thalidomide attachment could potentially ruin SIRT2 selectivity. Thus, we decided to attach thalidomide to the N-terminus of TM (Scheme 3.1).

TM contains the carboxybenzoyl group (Cbz) on the N-terminal site of the lysine backbone. We replaced this Cbz group with thalidomide via a 2- or 4-repeating units of the polyethylene glycol (PEG) linker (Scheme 3.1). The PEG linker was chosen because of its aqueous solubility.[35] In addition, being flexible on its own, the PEG linker could allow the thalidomide-CRBN complex to reach SIRT2's ubiquitination site easier. PEG linkers with two different lengths were used because the linker may affect the ubiquitination/degradation efficiency. If the linker is too short, SIRT2 and CRBN could clash with each other and not be able to form the PROTAC complex. However, if the linker is too long, CRBN and SIRT2 could be too wide apart and decrease ubiquitination.

The synthesis of TM-P2-Thal or TM-P4-Thal required a total of 10 steps (Scheme 3.1). PEG linkers with two different lengths were attached to the thalidomide. *tert-Butyloxycarbonyl (Boc)-L*-lysine was used to synthesize the TM analog with a free N-terminal. Then, at the last step, thalidomide with the PEG linkers was coupled to the TM analog with a free N-terminus using isobutyl chloroformate to produce TM-P2-Thal and TM-P4-Thal as the final products (Scheme 3.1).

**Table 8. *In Vitro* Enzymatic $IC_{50}$ values of TM-P2-Thal and TM-P4-Thal.**

| $IC_{50}$ (μM) | TM-P2-Thal | TM-P4-Thal | TM |
|---|---|---|---|
| **SIRT1** | 37 ± 3.5 | 41 ± 5.1 | >83 |
| **SIRT2 Deacetylase** (with pre-incubation) | 0.069 ± 0.032 | 0.078 ± 0.018 | 0.093 ± 0.012 |
| **SIRT2 Deacetylase** (without pre-incubation) | 0.12 ± 0.020 | 0.093 ± 0.025 | 0.15 ± 0.036 |
| **SIRT2 Defatty-acylase** (with pre-incubation) | 0.17 ± 0.044 | 0.11 ± 0.063 | 0.37 ± 0.031 |
| **SIRT2 Defatty-acylase** (without pre-incubation) | >83 | >83 | >83 |
| **SIRT3** | >83 | >83 | >83 |
| **SIRT5** | >83 | >83 | >83 |
| **SIRT6** | >83 | >83 | >83 |

### 3.3.2 TM-P2-Thal and TM-P4-Thal maintain SIRT2 selectivity.

*In Vitro* enzymatic $IC_{50}$ values of TM-P2-Thal and TM-P4-Thal on the sirtuin family members, SIRT1, SIRT2, SIRT3, SIRT5 and SIRT6, were measured to see if the selectivity toward SIRT2 had been preserved. Each compound at different concentrations was added to the sirtuin enzymatic reaction mixture to measure its inhibitory activities.[17, 27] Because the tested compounds inhibit sirtuin activities through forming a stable stalled covalent intermediate with $NAD^+$, we have pre-incubated these compounds with $NAD^+$ and the corresponding sirtuin enzyme, prior to the addition of the substrate peptide. With pre-incubation time, the $IC_{50}$ of TM-P2-Thal and TM-P4-Thal for SIRT2 deacetylase were 0.069 and 0.078 μM, respectively.

Meanwhile, the $IC_{50}$ of TM-P2-Thal and TM-P4-Thal for SIRT1 deacetylase were 37 and 41 μM, respectively. The selectivity for SIRT2 over SIRT1 ($IC_{50}$ SIRT1/$IC_{50}$ SIRT2) was about 500 times for both TM-P2-Thal and TM-P4-Thal. In addition, both compounds did not show inhibitory activity on SIRT3, SIRT5, or SIRT6 (Table 8). In addition, Compound 8, thalidomide with PEG4 linker, could not inhibit any of the sirtuin activities (Table 9). Overall, even with the modifications on the N-terminus, both TM-P2-Thal and TM-P4-Thal retained SIRT2 selectivity.

We have further tested TM, TM-P2-Thal and TM-P4-Thal against SIRT2 deacetylase and defatty-acylase with and without the pre-incubation time. Regardless of the pre-incubation time, these three compounds could inhibit SIRT2 deacetylase efficiently. However, for SIRT2 defatty-acylase without the pre-incubation, they could not inhibit even at 83 μM. With the pre-incubation, the $IC_{50}$ for TM, TM-P2-Thal and TM-P4-Thal were 0.37, 0.17 and 0.11 μM, respectively. This $IC_{50}$ difference between with and without the pre-incubation may explain why TM could not inhibit SIRT2 defatty-acylase in cells from previous studies.[29]

**Table 9. *In Vitro* Enzymatic $IC_{50}$ values of Compound 8.**

| **$IC_{50}$ (μM)** | **Compound 8** |
|---|---|
| **SIRT1 Deacetylase** | > 83 |
| **SIRT2 Deacetylase** | > 83 |
| **SIRT2 Defatty-acylase** | > 83 |
| **SIRT3** | > 83 |

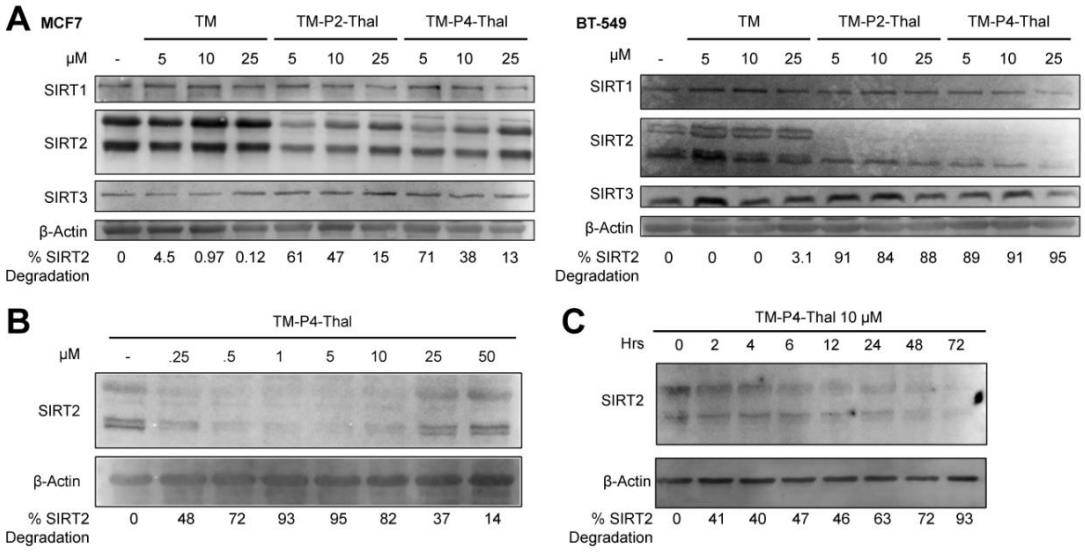


**Figure 3.2 TM-P2-Thal and TM-P4-Thal degrade SIRT2 selectively in cells.** (A) Immunoblots for SIRT1, SIRT2 and SIRT3 after treating with indicated concentrations of inhibitors for 48 hours in MCF7 and BT-549 cells. (B) Immunoblot for SIRT2 after MCF7 cells were treated with indicated concentrations of TM-P4-Thal for 48 hours. (C) Immunoblot for SIRT2 after MCF7 cells were treated with 10 μM of TM-P4-Thal for the indicated incubation times.

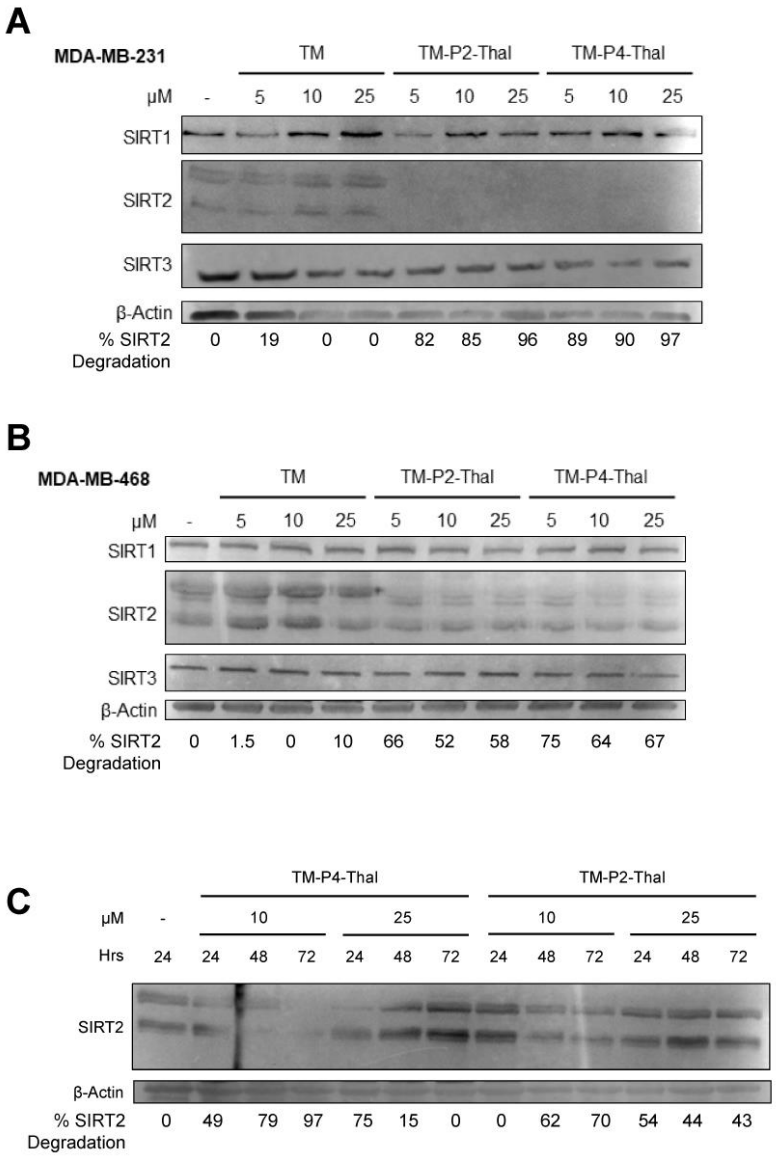


**Figure 3.3 Additional data on SIRT2 degradation by TM-P2-Thal and TM-P4-Thal.** (A) Immunoblots for SIRT1, SIRT2, and SIRT3 after treatment with indicated concentrations of inhibitors for 48 hours in MDA-MB-231 cells. (B) Immunoblots for SIRT1, SIRT2, and SIRT3 after treatment with indicated concentrations of inhibitors for 48 hours in MDA-MB-468 cells. (C) Immunoblot for SIRT2 after treatment with indicated concentrations of TM-P4-Thal or TM-P2-Thal at indicated time points.

### 3.3.3 TM-P2-Thal and TM-P4-Thal degrade SIRT2 selectively in cells.

We next set out to check the effects of TM, TM-P2-Thal, and TM-P4-Thal on SIRT2 protein levels in two breast cancer cell lines, MCF7 and BT549. After 48 hours of treatment at various concentrations, TM-P2-Thal and TM-P4-Thal degraded SIRT2 selectively without changing the levels of SIRT1 and SIRT3 (Figure 3.2A). As expected, TM did not decrease the level of SIRT2 in the two cell lines. In MCF7 cells, 5 μM of the PROTAC compounds degraded SIRT2 more effectively than 25 μM, which is likely due to the mechanism of the PROTAC strategy. When excess amounts of PROTAC compounds are introduced to the cells, CRBN and SIRT2 are each bound by a PROTAC compound instead of forming a trimeric complex of CRBN-PROTAC-SIRT2. Similarly, SIRT2 selective degradations were observed in MDA-MB-231 and MDA-MB-468 cell lines (Figure 3.3A and B) in the presence of TM-P2-Thal and TM-P4-Thal.

In MCF7 cells, we then further tested SIRT2-selective degradation with lower than 5 μM of TM-P4-Thal for 48 hours. Even at 0.5 μM, SIRT2 level was significantly decreased compared to that of a vehicle treated sample. Furthermore, the decreased levels of SIRT2 at both 0.5 and 10 μM were similar, suggesting the high efficiency of TM-P4-Thal (Figure 3.2B). Again, at 50 μM of TM-P4-Thal, SIRT2 level did not change much. This is due to the hook effect. High concentrations of PROTAC primarily form binary complex with either E3 ligase or protein target, and thereby preventing the ternary complex formation that is for the efficient degradation.[36]

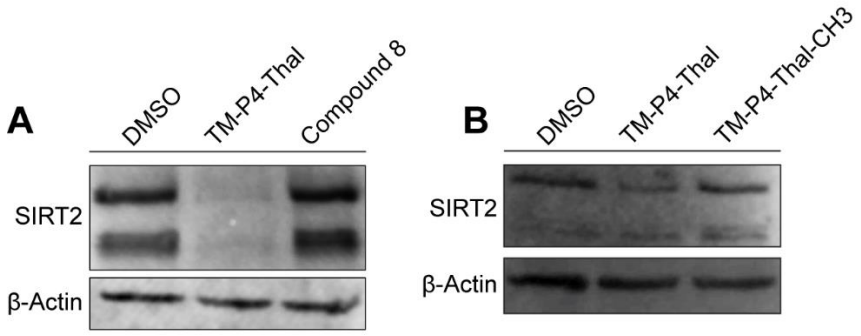


**Figure 3.4 Compound 8 and TM-P4-Thal-CH3 could not degrade SIRT2.** (A) Immunoblots of SIRT2 after treatment of 5 μM TM-P4-Thal and Compound 8 for 16 hours in MCF7 cells. (B) Immunoblots of SIRT2 after treatment of 5 μM TM-P4-Thal and TM-P4-Thal-CH3 for 12 hours in MCF7 cells.

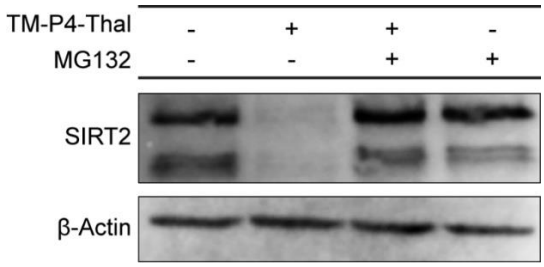


**Figure 3.5 MG132 rescues SIRT2 degradation by TM-P4-Thal.** Immunoblots of SIRT2 after treatment of 5 μM MG132 for 2 hours, followed with co-treatment of 5 μM MG132 and 5 μM TM-P4-Thal for additional 16 hours in MCF7 cells.

Next, we examined the time course of TM-P4-Thal-induced SIRT2 degradation in MCF7 cells. As the incubation time increased, 10 μM of TM-P4-Thal lowered SIRT2 even further. Thus, SIRT2 was degraded by TM-P4-Thal in a time-dependent manner (Figure 3.2C). However, the results with 25 μM of TM-P4-Thal was different. With 24-hour treatment, SIRT2 level decreased sharply, but as the treatment time increased, SIRT2 level recovered (Figure 3.3C). Such recovery likely is

due to the combined effects of new SIRT2 protein synthesis and the PROTAC compound being degraded with longer treatment time. We also treated cells with 10 and 25 μM of TM-P2-Thal in different time points. Similar result was observed, but the overall efficiency in the degradation of SIRT2 was lower compared to that with TM-P4-Thal (Figure 3.3C). Thus, we mainly used TM-P4-Thal for the rest of the study. Furthermore, we have treated MCF7 cells with Compound 8, thalidomide with PEG4 linker, and detected SIRT2 level through immunoblotting. As expected, without the TM moiety, Compound 8 could not degrade SIRT2 (Figure 3.4A). Also, we have synthesized TM-P4-Thal-CH3 with a methyl group on the thalidomide, which disrupts the overall binding to CRBN. This would further hinder PROTAC degradation.[37] Like Compound 8, TM-P4-Thal-CH3 could not degrade SIRT2 in cells, as well (Figure 3.4B).

To validate that SIRT2 degradation occurs through CRBN and ubiquitin-proteasome system (UPS), we have tried to rescue the degradation through co-treatment of proteasome inhibitor, MG132. MCF7 cells were pre-treated with MG132 (5 μM) for 2 hours, followed by co-treatment of TM-P4-Thal (5 μM) and MG132 (5 μM) for additional 16 hours. While the treatment with TM-P4-Thal decreased SIRT2 level, the co-treatment with TM-P4-Thal and MG132, a proteasome inhibitor, did not decrease SIRT2 level, suggesting that TM-P4-Thal promotes proteasome-dependent degradation of SIRT2. (Figure 3.5).

To further validate SIRT2 degradation by TM-P4-Thal, we have performed Tandem Mass Tag (TMT) global proteomic with HEK 293T cells treated with 5 μM of TM-P4-Thal for 16 hours. Consistent with the immunoblots, the SIRT2 abundance

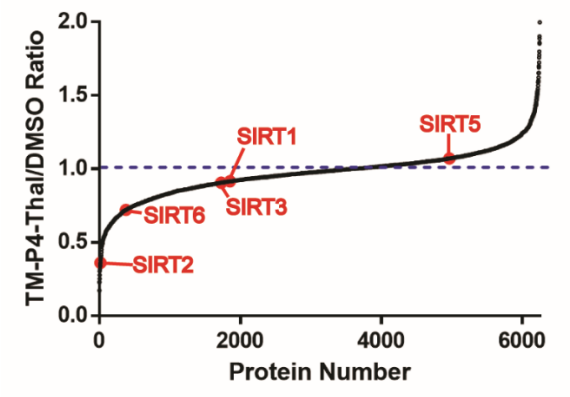


**Figure 3.6 Tandem Mass Tag (TMT) labeling with TM-P4-Thal**. Tandem Mass Tag (TMT) Labeling (TM-P4-Thal/DMSO) Abundance Ratio Values of Proteins after treatment of 5 μM treatment of TM-P4-Thal for 16 hours in HEK 293T cells.

**Table 10. Important identified proteins and corresponding abundance ratio (TM-P4-Thal/DMSO) from Tandem Mass Tag (TMT) global proteomics.**

| Protein | Abundance Ratio (TM-P4-Thal/DMSO) |
|---|---|
| **SIRT1** | 0.92 |
| **SIRT2** | 0.36 |
| **SIRT3** | 0.91 |
| **SIRT5** | 1.1 |
| **SIRT6** | 0.72 |

ratio between TM-P4-Thal and DMSO treated cells was about 0.36, suggesting substantial degradation of SIRT2. Meanwhile, abundance ratios of other sirtuins, including SIRT1, 3, 5 and 6, did not alter significantly after TM-P4-Thal treatment.

Overall, the TMT global proteomic result further confirms selective SIRT2 degradation by TM-P4-Thal (Figure 3.6, Table 10).

### 3.3.4 TM-P4-Thal efficiently inhibits both SIRT2 deacetylation and defatty-acylation in cells.

To assess the inhibition of SIRT2 deacetylation by TM-P4-Thal in cells, acetylation of α-tubulin, a previously reported SIRT2 deacetylation target, was examined by immunofluorescence after treating MCF7 cells with 5 and 10 μM of TM-P4-Thal for 12 hours.[14] If SIRT2 deacetylation is inhibited, the level of acetylation would be increased by the treatments. TM-P4-Thal or TM at 5 and 10 μM concentrations significantly increased the acetylation of α-tubulin (Figure 3.7A). Furthermore, quantification of the fluorescence signals indicated that at 5 μM, TM-P4-Thal increased approximately 2.9-fold while TM increased about 2.6-fold compared to the vehicle control (Figure 3.7B), suggesting both compounds inhibit SIRT2 deacetylase at similar efficiency.

Through robust cellular and biochemical experiments, SIRT2 was discovered to efficiently remove long chain fatty acyl groups from K182, 184, and 185 of K-Ras4a. As such, SIRT2 knockdown consequently increased K-Ras4a lysine fatty acylation.[19] Furthermore, we also found that TM could not inhibit SIRT2's activity on K-Ras4a lysine fatty acylation.[29] Because TM-P4-Thal degrades SIRT2, we expected that TM-P4-Thal could effectively inhibit not only the deacetylase but also the defatty-acylase activity of SIRT2.

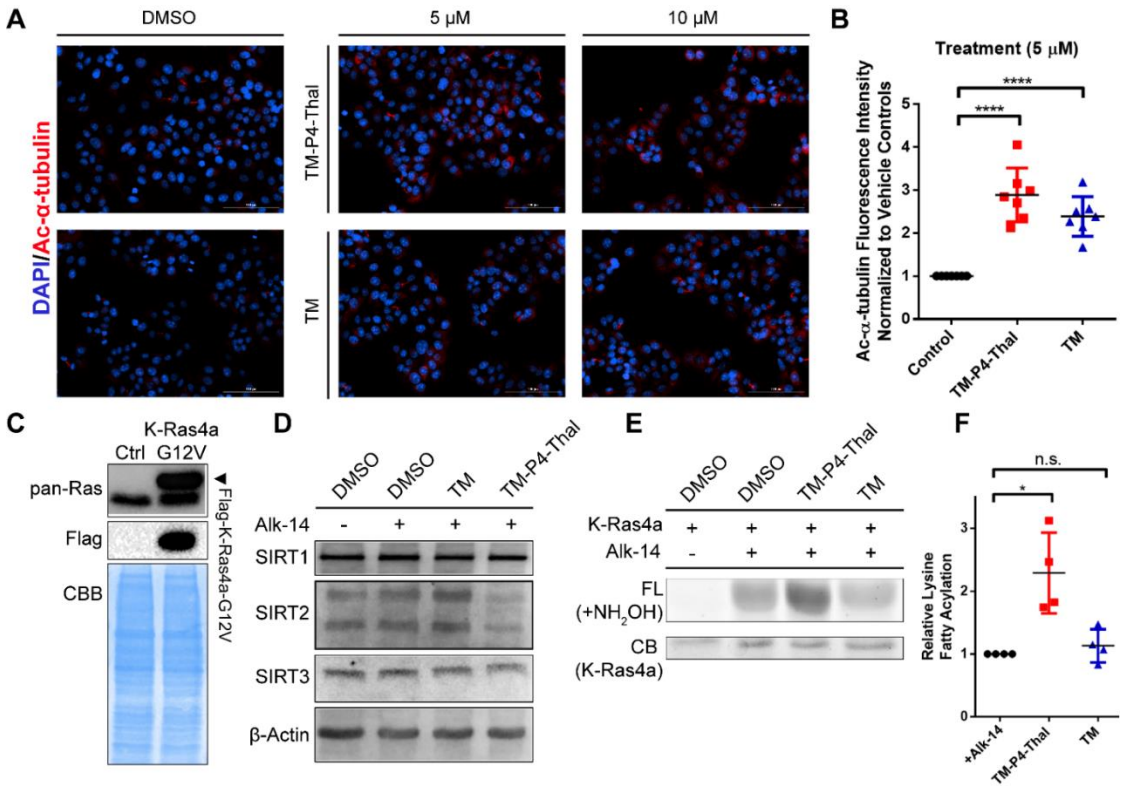


**Figure 3.7 TM-P4-Thal inhibits both SIRT2 deacetylase and defatty-acylase activities in cells.** (A) Immunofluorescence images of acetyl α-tubulin (K40) in MCF7 cells treated with DMSO (control), TM-P4-Thal (5, 10 μM) and TM (5, 10 μM) for 12 hours. (B) Normalized Ac-α-tubulin fluorescence intensity level of 5 μM TM-P4-Thal and TM for 12 hours, using ImageJ software for quantification. (C) Immunoblot with pan-Ras antibody to show the stable overexpression of Flag-tagged K-Ras4a-G12V in HEK 293T cells. (D) Immunoblots for SIRT1, SIRT2, and SIRT3 after treating HEK 293T cells with 1 μM of TM-P4-Thal or 10 μM of TM in the presence of 50 μM of Alk-14 for 24 hours. (E) Alk14 labeling and in-gel fluorescence to detect lysine fatty acylation of K-Ras4a in HEK 293T cells. Cells were treated with 1 μM of TM-P4-Thal or 10 μM of TM in the presence of 50 μM of Alk-14. (F) Quantified relative lysine fatty acylation level of K-Ras4a from Figure 3E, using ImageJ for quantification.

To test this, we generated HEK 293T stably expressing Flag-tagged K-Ras4a-G12V (Figure 3.7C). In these cells, 1 μM of TM-P4-Thal treatment for 48 hours decreased SIRT2 level. Meanwhile, both SIRT1 and SIRT3 levels remained unchanged upon treatment (Figure 3.7D). Next, to visualize K-Ras4a fatty acylation levels, the cells were treated with 1 μM of TM-P4-Thal or 10 μM of TM for 42 hours and then incubated with Alkyne-14 (Alk-14) for additional 6 hours to label fatty acylated proteins. After immunoprecipitating the Flag-tagged K-Ras4a-G12V, attaching a fluorescent dye through click chemistry and treating with $NH_2OH$ to remove cysteine fatty acylation, we detected the lysine fatty acylation level by in-gel fluorescence (Figure 3.7E, F). TM-P4-Thal increased fluorescence significantly compared to the DMSO control, suggesting efficient inhibition of SIRT2 defatty-acylation by TM-P4-Thal. In contrast, TM did not significantly increase the fluorescence level of K-Ras4a (Figure 3.7E, F). This suggests that while TM could not inhibit SIRT2 defatty-acylation, its PROTAC-version induced degradation of SIRT2 efficiently and inhibited the defatty-acylation activity in live cells.

### 3.3.5 TM-P4-Thal shows improved cytotoxicity in breast cancer cells at lower concentrations.

After demonstrating that TM-P4-Thal can inhibit both activities of SIRT2, we evaluated its effect on the cellular proliferation of MCF7 and MDA-MB-231 (Figure 4). In both breast cancer cell lines, we had previously observed selective SIRT2 degradation after treatment of TM-P4-Thal. In MCF7 cells, after 72 hours incubation, TM-P4-Thal showed much stronger cytotoxicity than TM at lower concentrations. However, towards higher concentrations, the difference between TM and TM-P4-Thal

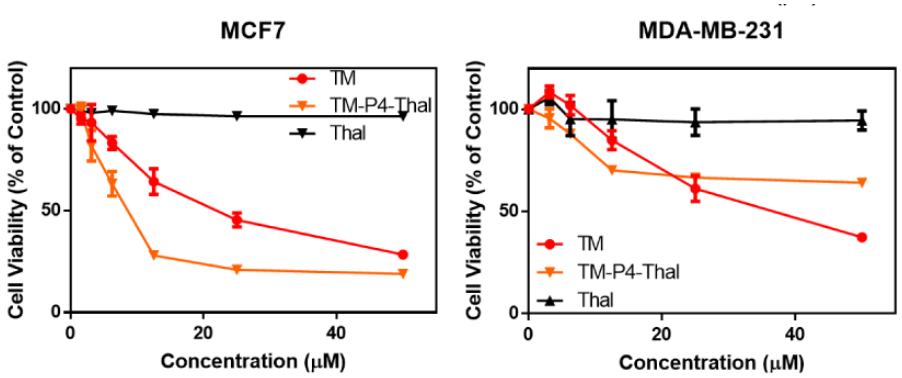


**Figure 3.8 TM-P4-Thal shows improved cellular cytotoxicity in breast cancer cell lines at lower concentrations.** Cell viability of MCF7 and MDA-MB-231 cells after treatment of TM, TM-P4-Thal, and thalidomide for 72 hours.

became smaller. Similar trend was observed in MDA-MB-231. However, at higher concentrations, cytotoxicity of TM exceeded that of TM-P4-Thal (Figure 3.8). This is likely because of inefficient SIRT2 degradation at high concentrations of TM-P4-Thal due to the hook effect.[36]

There may be some discrepancy between the SIRT2 level and the cytotoxicity. For instance, 1 μM of TM-P4-Thal induced SIRT2 degradation but did not exert significant cytotoxicity in the cellular proliferation assay. Depending on the degraded target, even though there is a significant decrease in the protein level, the biological impact may not be affected much. SIRT2 may need to be completely degraded for longer period to see a stronger impact. Also, there could be an undiscovered reparative biological mechanism for the deceased protein level, as well. Further biological studies are needed to study for this difference.

To test the cellular permeabilities, after treatment of TM-P4-Thal and TM (50 μM) for 6 hours, MCF7 cells were washed with cold PBS three times, and the small

**Table 11. Calculated concentrations (μg/million cells) of TM and TM-P4-Thal detected from MCF7 cell permeability assay.** MCF7 cells were treated with 50 μM of indicated inhibitors for 6 hours.

| | Calculated Concentrations (μg/million cells) |
|---|---|
| **TM** | .24 |
| **TM-P4-Thal** | .032 |

molecules were extracted using methanol. The extracted samples were injected into liquid chromatography-mass spectrometer to detect the final concentration of the compounds inside the cells. Because these compounds with poor aqueous solubility are not suitable for traditional PAMPA assays, we have tried to measure the cellular permeability in this way. Overall, TM-P4-Thal showed less efficient cell permeability, which could explain the lower cytotoxicity of TM-P4-Thal than that of TM at high concentrations (Table 11). Thalidomide did not affect cellular proliferation, suggesting that the cytotoxicity of TM-P4-Thal did not originate from the thalidomide moiety (Figure 3.8).

The stronger cytotoxicity of TM-P4-Thal may come from the inhibition of SIRT2 defatty-acylase activity. As shown earlier, at the same concentrations (5 and 10 μM), TM and TM-P4-Thal inhibited SIRT2 deacetylase similarly (Figure 3.7A, B), while only TM-P4-Thal could inhibit SIRT2 defatty-acylase. As such, the inhibition of SIRT2 defatty-acylase activity may have led to the stronger cytotoxicity of TM-P4-Thal, suggesting that inhibiting the defatty-acylation activity of SIRT2 could enhance the anticancer activity of SIRT2 inhibitors.

## 3.4 Conclusion

Here, we introduced two new PROTAC compounds, TM-P2-Thal and TM-P4-Thal, which can degrade SIRT2 efficiently and selectively in living cells. In addition, degradation of SIRT2 by TM-P4-Thal allowed inhibition of both the deacetylation and defatty-acylation activities of SIRT2. As a comparison, previously reported traditional SIRT2 inhibitors could not inhibit the defatty-acylation activity of SIRT2.[27] As such, this case portrays the advantage of PROTAC strategy over traditional inhibition strategy. Furthermore, degradation of SIRT2 led to stronger cytotoxicity, suggesting the importance of defatty-acylation activity of SIRT2 in cancer cells. Since not much has currently been revealed about SIRT2's defatty-acylation activity, TM-P4-Thal, together with TM, can be utilized as useful chemical tools to further scrutinize and understand the biological significance of SIRT2's defatty-acylation activity.

## 3.5 References


1. Feldman, J. L., Dittenhafer-Reed, K. E., and Denu, J. M. (2012) Sirtuin Catalysis and Regulation, *J. Biol. Chem. 287*, 42419-42427.

2. Sauve, A. A., Celic, I., Avalos, J., Deng, H., Boeke, J. D., and Schramm, V. L. (2001) Chemistry of gene silencing: the mechanism of NAD+-dependent deacetylation reactions, *Biochemistry 40*, 15456-15463.

3. Sauve, A. A., Wolberger, C., Schramm, V. L., and Boeke, J. D. (2006) The biochemistry of sirtuins, *Annu. Rev. Biochem. 75*, 435-465.

4. Imai, S.-i., Armstrong, C. M., Kaeberlein, M., and Guarente, L. (2000) Transcriptional silencing and longevity protein Sir2 is an NAD-dependent histone deacetylase, *Nature 403*, 795-800.

5. Hu, J., Jing, H., and Lin, H. (2014) Sirtuin inhibitors as anticancer agents, *Future Med. Chem. 6*, 945-966.

6. Tao, R., Xiong, X., DePinho, R. A., Deng, C. X., and Dong, X. C. (2013) FoxO3

transcription factor and Sirt6 deacetylase regulate low density lipoprotein (LDL)-cholesterol homeostasis via control of the proprotein convertase subtilisin/kexin type 9 (Pcsk9) gene expression, *J Biol Chem 288*, 29252-29259.

7. Du, C., Lin, X., Xu, W., Zheng, F., Cai, J., Yang, J., Cui, Q., Tang, C., Cai, J., Xu, G., and Geng, B. (2019) Sulfhydrated Sirtuin-1 Increasing Its Deacetylation Activity Is an Essential Epigenetics Mechanism of Anti-Atherogenesis by Hydrogen Sulfide, *Antioxid Redox Signal 30*, 184-197.

8. Jing, H., and Lin, H. (2015) Sirtuins in Epigenetic Regulation, *Chem. Rev. 115*, 2350-2375.

9. Kosciuk, T., Wang, M., Hong, J. Y., and Lin, H. (2019) Updates on the epigenetic roles of sirtuins, *Curr. Opin. Chem. Biol. 51*, 18-29.

10. Wang, Y., Fung, Y. M. E., Zhang, W., He, B., Chung, M. W. H., Jin, J., Hu, J., Lin, H., and Hao, Q. (2017) Deacylation Mechanism by SIRT2 Revealed in the 1'-SH-2'-O-Myristoyl Intermediate Structure, *Cell Chem Biol 24*, 339-345.

11. Feldman, J. L., Dittenhafer-Reed, K. E., Kudo, N., Thelen, J. N., Ito, A., Yoshida, M., and Denu, J. M. (2015) Kinetic and Structural Basis for Acyl-Group Selectivity and NAD <sup>+</sup> Dependence in Sirtuin-Catalyzed Deacylation, *Biochemistry 54*, 3037-3050.

12. Jin, J., He, B., Zhang, X., Lin, H., and Wang, Y. (2016) SIRT2 Reverses 4-Oxononanoyl Lysine Modification on Histones, *J. Am. Chem. Soc. 138*, 12304-12307.

13. Seo, K. S., Park, J. H., Heo, J. Y., Jing, K., Han, J., Min, K. N., Kim, C., Koh, G. Y., Lim, K., Kang, G. Y., Uee Lee, J., Yim, Y. H., Shong, M., Kwak, T. H., and Kweon, G. R. (2015) SIRT2 regulates tumour hypoxia response by promoting HIF-1α hydroxylation, *Oncogene 34*, 1354-1362.

14. North, B. J., Marshall, B. L., Borra, M. T., Denu, J. M., and Verdin, E. (2003) The Human Sir2 Ortholog, SIRT2, Is an NAD+-Dependent Tubulin Deacetylase, *Mol. Cell 11*, 437-444.

15. Zhou, W., Ni, T. K., Wronski, A., Glass, B., Skibinski, A., Beck, A., and Kuperwasser, C. (2016) The SIRT2 Deacetylase Stabilizes Slug to Control Malignancy of Basal-like Breast Cancer, *Cell Rep. 17*, 1302-1317.

16. Zhao, D., Zou, S. W., Liu, Y., Zhou, X., Mo, Y., Wang, P., Xu, Y. H., Dong, B., Xiong, Y., Lei, Q. Y., and Guan, K. L. (2013) Lysine-5 acetylation negatively regulates lactate dehydrogenase A and is decreased in pancreatic cancer, *Cancer Cell 23*, 464-476.

17. Jing, H., Hu, J., He, B., Negrón Abril, Y. L., Stupinski, J., Weiser, K., Carbonaro,

M., Chiang, Y.-L., Southard, T., Giannakakou, P., Weiss, R. S., and Lin, H. (2016) A SIRT2-Selective Inhibitor Promotes c-Myc Oncoprotein Degradation and Exhibits Broad Anticancer Activity, *Cancer Cell 29*, 297-310.

18. Teng, Y.-B., Jing, H., Aramsangtienchai, P., He, B., Khan, S., Hu, J., Lin, H., and Hao, Q. (2015) Efficient Demyristoylase Activity of SIRT2 Revealed by Kinetic and Structural Studies, *Sci. Rep. 5*, 8529.

19. Jing, H., Zhang, X., Wisner, S. A., Chen, X., Spiegelman, N. A., Linder, M. E., and Lin, H. (2017) SIRT2 and lysine fatty acylation regulate the transforming activity of K-Ras4a, *Elife 6*.

20. Spiegelman, N. A., Zhang, X., Jing, H., Cao, J., Kotliar, I. B., Aramsangtienchai, P., Wang, M., Tong, Z., Rosch, K. M., and Lin, H. (2019) SIRT2 and Lysine Fatty Acylation Regulate the Activity of RalB and Cell Migration, *ACS Chem. Biol. 14*, 2014-2023.

21. Outeiro, T. F., Kontopoulos, E., Altmann, S. M., Kufareva, I., Strathearn, K. E., Amore, A. M., Volk, C. B., Maxwell, M. M., Rochet, J.-C., McLean, P. J., Young, A. B., Abagyan, R., Feany, M. B., Hyman, B. T., and Kazantsev, A. G. (2007) Sirtuin 2 inhibitors rescue alpha-synuclein-mediated toxicity in models of Parkinson's disease, *Science 317*, 516-519.

22. Rumpf, T., Schiedel, M., Karaman, B., Roessler, C., North, B. J., Lehotzky, A., Olah, J., Ladwein, K. I., Schmidtkunz, K., Gajer, M., Pannek, M., Steegborn, C., Sinclair, D. A., Gerhardt, S., Ovadi, J., Schutkowski, M., Sippl, W., Einsle, O., and Jung, M. (2015) Selective Sirt2 inhibition by ligand-induced rearrangement of the active site, *Nat. Commun. 6*, 6263.

23. Li, Y., Zhang, M., Dorfman, R. G., Pan, Y., Tang, D., Xu, L., Zhao, Z., Zhou, Q., Zhou, L., Wang, Y., Yin, Y., Shen, S., Kong, B., Friess, H., Zhao, S., Wang, L., and Zou, X. (2018) SIRT2 Promotes the Migration and Invasion of Gastric Cancer through RAS/ERK/JNK/MMP-9 Pathway by Increasing PEPCK1-Related Metabolism, *Neoplasia 20*, 745-756.

24. Kozako, T., Mellini, P., Ohsugi, T., Aikawa, A., Uchida, Y. I., Honda, S. I., and Suzuki, T. (2018) Novel small molecule SIRT2 inhibitors induce cell death in leukemic cell lines, *BMC Cancer 18*, 791.

25. Mellini, P., Itoh, Y., Elboray, E. E., Tsumoto, H., Li, Y., Suzuki, M., Takahashi, Y., Tojo, T., Kurohara, T., Miyake, Y., Miura, Y., Kitao, Y., Kotoku, M., Iida, T., and Suzuki, T. (2019) Identification of Diketopiperazine-Containing 2-Anilinobenzamides as Potent Sirtuin 2 (SIRT2)-Selective Inhibitors Targeting the "Selectivity Pocket", Substrate-Binding Site, and NAD(+)-Binding Site, *J Med Chem 62*, 5844-5862.

26. Kudo, N., Ito, A., Arata, M., Nakata, A., and Yoshida, M. (2018) Identification of a

novel small molecule that inhibits deacetylase but not defatty-acylase reaction catalysed by SIRT2, *Philos Trans R Soc Lond B Biol Sci 373*.

27. Spiegelman, N. A., Price, I. R., Jing, H., Wang, M., Yang, M., Cao, J., Hong, J. Y., Zhang, X., Aramsangtienchai, P., Sadhukhan, S., and Lin, H. (2018) Direct Comparison of SIRT2 Inhibitors: Potency, Specificity, Activity-Dependent Inhibition, and On-Target Anticancer Activities, *ChemMedChem 13*, 1890-1894.

28. Kawaguchi, M., Ieda, N., and Nakagawa, H. (2019) Development of Peptide-Based Sirtuin Defatty-Acylase Inhibitors Identified by the Fluorescence Probe, SFP3, That Can Efficiently Measure Defatty-Acylase Activity of Sirtuin, *J. Med. Chem. 62*, 5434-5452.

29. Spiegelman, N. A., Hong, J. Y., Hu, J., Jing, H., Wang, M., Price, I. R., Cao, J., Yang, M., Zhang, X., and Lin, H. (2019) A Small-Molecule SIRT2 Inhibitor That Promotes K-Ras4a Lysine Fatty-Acylation, *ChemMedChem 14*, 744-748.

30. Sun, B., Fiskus, W., Qian, Y., Rajapakshe, K., Raina, K., Coleman, K. G., Crew, A. P., Shen, A., Saenz, D. T., Mill, C. P., Nowak, A. J., Jain, N., Zhang, L., Wang, M., Khoury, J. D., Coarfa, C., Crews, C. M., and Bhalla, K. N. (2018) BET protein proteolysis targeting chimera (PROTAC) exerts potent lethal activity against mantle cell lymphoma cells, *Leukemia 32*, 343-352.

31. Raina, K., Lu, J., Qian, Y., Altieri, M., Gordon, D., Rossi, A. M. K., Wang, J., Chen, X., Dong, H., Siu, K., Winkler, J. D., Crew, A. P., Crews, C. M., and Coleman, K. G. (2016) PROTAC-induced BET protein degradation as a therapy for castration-resistant prostate cancer, *Proc. Natl. Acad. Sci. USA 113*, 7124-7129.

32. Ottis, P., and Crews, C. M. (2017) Proteolysis-Targeting Chimeras: Induced Protein Degradation as a Therapeutic Strategy, *ACS Chem. Biol. 12*, 892-898.

33. Schiedel, M., Herp, D., Hammelmann, S., Swyter, S., Lehotzky, A., Robaa, D., Olah, J., Ovadi, J., Sippl, W., and Jung, M. (2018) Chemically Induced Degradation of Sirtuin 2 (Sirt2) by a Proteolysis Targeting Chimera (PROTAC) Based on Sirtuin Rearranging Ligands (SirReals), *J Med Chem 61*, 482-491.

34. Hong, J. Y., Price, I. R., Bai, J. J., and Lin, H. (2019) A Glycoconjugated SIRT2 Inhibitor with Aqueous Solubility Allows Structure-Based Design of SIRT2 Inhibitors, *ACS Chem. Biol. 14*, 1802-1810.

35. Wurz, R. P., Dellamaggiore, K., Dou, H., Javier, N., Lo, M. C., McCarter, J. D., Mohl, D., Sastri, C., Lipford, J. R., and Cee, V. J. (2018) A "Click Chemistry Platform" for the Rapid Synthesis of Bispecific Molecules for Inducing Protein Degradation, *J Med Chem 61*, 453-461.

36. Lu, J., Qian, Y., Altieri, M., Dong, H., Wang, J., Raina, K., Hines, J., Winkler,

James D., Crew, Andrew P., Coleman, K., and Crews, Craig M. (2015) Hijacking the E3 Ubiquitin Ligase Cereblon to Efficiently Target BRD4, *Chem. Biol. 22*, 755-763.

37. Zeng, M., Xiong, Y., Safaee, N., Nowak, R. P., Donovan, K. A., Yuan, C. J., Nabet, B., Gero, T. W., Feru, F., Li, L., Gondi, S., Ombelets, L. J., Quan, C., Janne, P. A., Kostic, M., Scott, D. A., Westover, K. D., Fischer, E. S., and Gray, N. S. (2020) Exploring Targeted Degradation Strategy for Oncogenic KRAS(G12C), *Cell Chem. Biol. 27*, 19-31 e16.

## 3.6 Methods

**General experimental methods**

All reagents and organic solvents used were purchased as analytical or higher grade from commercial vendors. Unless noted, all reactions occurred under nitrogen gas. Reported molecular weights were determined using a Shimadzu HPLC LC20-AD and Thermo Scientific LCQ Fleet Mass spectrometer at positive ion modes, unless specified otherwise. The column for LC-MS was Kinetex 5u EVO C18 100 Å Column (30 x 2.1 mm, 5 µm), and solvents for LC-MS were HPLC-grade water with 0.1 % HPLC-grade acetic acid and HPLC-grade acetonitrile with 0.1% HPLC-grade acetic acid. The LC-MS monitored the UV peaks of the compounds using both 215 and 260 nm. All reported NMR spectra were collected on a Bruker 500 spectrometer. The silica used for simple column purification for the synthesis was SiliaFlash Irregular Silica Gel, P60, 40 – 63 µm, 60 Å. The analytical HPLC used for the sirtuins *in vitro* enzymatic reaction was Shimadzu HPLC LC20-AD connected to Kinetex 5u EVO C18 100 Å column (100 mm x 4.60 mm, 5 µm). To monitor the UV peaks of the modified H3K9 and unmodified H3K9 peptides, 215 and 280 nm absorbance was used. Solvents for such analytical HPLC set-up was HPLC-grade water with 0.1%

HPLC-grade trifluoroacetic acid and HPLC-grade acetonitrile with 0.1 % HPLC-grade trifluoroacetic acid. The compounds were eluted at 0.5 mL/min flow rate. The purities of the compounds were confirmed to be at least 95% using a Shimadzu HPLC LC20-AD connected to Kinetex 5u EVO C18 100 Å column (100 mm x 4.60 mm, 5 μm). High Resolution Mass Spectrometry data was collected at Cornell Chemistry Mass Spectrometry Facility, using Thermo Exactive Orbitrap ESI Mass Spectrometer.

**Antibodies and plasmids**

The anti-human SIRT1 antibody (D739, #2494), anti-human SIRT2 antibody (D4050, #12650), anti-human SIRT3 antibody (D22A3, #5490), and anti-rabbit IgG-horseradish peroxidase (#7074) were purchased from Cell Signaling Technology. The anti-acetyl-α tubulin (6-11B-1) (MABT868), anti-Flag-M2 conjugated to horseradish peroxidase (A8592) and anti-Flag M2 affinity agarose gel (A2220) were purchased from Sigma-Aldrich. The goat anti-Mouse IgG (H+L) cross-adsorbed secondary antibody, Cyanine3 (A10521), and anti-Ras antibody (1862335) was purchased from ThermoFisher. The anti-β-Actin (C4) conjugated to horseradish peroxidase (sc-4777) mouse anti-rabbit IgG-horseradish peroxidase (sc-2357) were purchased from Santa Cruz Biotechnology. Human SIRT2 with C-terminal Flag-tagged expression vector was generated following previously reported procedure.[1]

**Western Blots**

Western blots were performed as reported previously.[2-4] All samples for this paper was lysed using 1% NP-40 lysis buffer (25 mM Tris-HCl pH 8.0, 150 mM NaCl, 10% glycerol, 1% Igepal CA-630 (Substitute for NP-40)) with protease inhibitor cocktail (Sigma).

**Cell culture and transfection**

MCF-7, MDA-MB-231, MDA-MB-468, and K-Ras4a-expressing HEK 293T cells were cultured in Dulbecco's Modified Eagle Medium (DMEM) with 10 % Fetal Bovine Serum (Invitrogen). BT-549 was cultured in Roswell Park Memorial Institute medium (RPMI) with 10 % Fetal Bovine Serum (Invitrogen). All cells were incubated at 37 °C with 5% $CO_2$. To overexpress SIRT2 in cells, the pCMV-tag-4a vector with SIRT2 was transfected into the cells with FuGene6 (Promega) according to the manufacturers' protocol. Empty vector was used as a negative control.

**Cloning, expression and purification of SIRT1, 2, 3, 5 and 6**

Human SIRT1, 2, 3, 5 and 6 used in this paper were cloned, expressed and purified as previously reported.[1-3, 5, 6]

**Analytical HPLC *In vitro* sirtuin deacylation $IC_{50}$ assay**

*In vitro* $IC_{50}$ values of TM, TM-P4-Thal and TM-P2-Thal for SIRT1, 2, 3, 5 and 6 deacylation were measured with pre-incubation, using analytic HPLC, as previously reported.[1, 3]

**Development of HEK 293T stably overexpressing Flag-tagged K-Ras4a cells**

The human *K-RAS4A* lentiviral vector was obtained by inserting FLAG-*K-RAS4A* into pCDH-CMV-MCS-EF1-Puro vector between the EcoRI and NotI sites. Lentiviral infection for overexpressing K-Ras4a was performed as previously described[2]. Puromycin (1.5 μg/mL) was added to the cell culture media to select and maintain cells with stable K-Ras4a expression.

**Detection of sirtuins degradation in cells after treatment with inhibitors**

About 300,000 MCF7 or Flag-K-Ras4a expressing HEK 293T cells were seeded to Corning 60 mm x 15 mm Tissue Culture Treated Polystyrene plates. After overnight incubation, the cells were treated with indicated concentrations of TM, TM-P2-Thal, TM-P4-Thal, Compound 8 or TM-P4-Thal-CH3 for the indicated time periods before collection. The cells were lysed in 1% NP40 lysis buffer with protease inhibitor cocktail and SIRT1, 2 and 3 levels were detected by the western blot using anti-human SIRT1, SIRT2 and SIRT3 antibodies. β-Actin was used as a loading control.

**Rescue of sirtuins degradation in cells after treatment with inhibitors**

About 400,000 MCF7 cells were seeded to Corning 60 mm x 15 mm Tissue Culture Treated Polystyrene plates. After overnight incubation, the cells were treated with 5 μM MG132 for 2 hours. Then, the cells were co-treated with 5 μM MG132 and 5 μM TM-P4-Thal for additional 16 hours. The cells were collected and lysed in 1% NP40 lysis buffer with protease inhibitor cocktail and SIRT2 level was detected by the western blot using anti-human SIRT2 antibodies. β-Actin was used as a loading control.

**Inhibition of SIRT2 deacetylation activity in cells.**

To 35 mm-glass bottom dishes from MatTek, 200,000 MCF7 cells were seeded. After overnight incubation, the cells were treated with the TM (1 and 10 μM) and TM-P4-Thal (1 and 10 μM) for 12 hours. After washing the cells with cold PBS three times, the cells were fixed with ice-cold methanol. Then, 0.5% Triton-X in PBS was added to cells for 10 minutes. After washing the cells with cold PBS three times, the cells were blocked by 1% BSA in TBST buffer (10 mM Tris-HCl pH 7.4, 150 mM

NaCl and 0.1% Tween-20) for 30 minutes. Then, the cells were incubated with Ac-α-tubulin antibody (1:100) for 18 hours overnight at 4 °C. The cells were washed with TBST three times. After adding Cy3 conjugated antibody (1:100) in 1% BSA in TBST, the cells were incubated in the dark at room temperature for 1 hour. After washing the cells with TBST three times, the cells were stained by DAPI fluoromount, and imaged by Cytation 5 Cell Imaging Reader. The quantifications were done through ImageJ.

**Detection of K-Ras4a levels in HEK 293T cells stably overexpressing Flag-tagged K-Ras4a**

HEK 293T cells that stably overexpress Flag-tagged K-Ras4a and control HEK 293T cells were collected and lysed with 1% NP40 lysis buffer with protease inhibitor cocktail. The levels of Flag-tagged K-Ras4a in these two cell lines were detected by western blot using anti-Ras antibody (1862335).

**Inhibition of K-Ras4a de-fatty acylation in cells**

HEK 293T cells stably overexpressing Flag-tagged K-Ras4a were treated with 10 μM of TM or 1 μM of TM-P4-Thal. Control cells were treated with the same amount of DMSO (vehicle control). After 42 hours of incubation, media was replaced with fresh media containing 10 μM of TM or 1 μM TM-P4-Thal with 50 μM of Alk-14 for additional 6 hours. Immunoprecipitation and click chemistry were performed as previously reported.[7, 8] The quantifications were measured by ImageJ.

**Protein Digestion and TMT10-plex Labeling**

After checking the protein quantification using Bradford Assay, protein processing was performed following Thermo Scientific's TMT Mass Tagging Kits and

Reagents Protocol (90113) with few modifications as reported.[9-11] A total of 60 μg protein of each sample in the buffer (50 mM TEAB pH 8.5, 6 M urea, 2 M thiourea, 1% SDS) was reduced with 10 mM tris(2-carboxyethyl)phosphine for 1 hour at 34 °C, alkylated with 20 mM iodoacetamide for 1 hour in the dark, and then quenched with a final concentration of 32 mM DTT. Each sample was digested individually using S-Trap Micro Spin column (Protifi).[12] Then, 12% phosphoric acid was added to a final concentration of 1.2%, followed by 1:7 dilution (v/v) with 90% methanol, 0.1 M TEAB pH 8.5. The samples were placed into the spin column and centrifuged for 30 seconds at 4000 g. Then, they were washed three times with 150 μL of 90% methanol and 0.1 M TEAB pH 8.5. Digestion was performed by adding 25 μL trypsin at 80 ng/μL (1:10 w/w) in 50 mM TEAB pH 8.5 to the top of the spin column. Digest solution was absorbed into the hydrophilic matrix. After incubating the spin columns overnight at 37 °C, the digested peptides were eluted off the S-trap column sequentially with 40 μL of 50 mM TEAB pH 8.5, 0.2% formic acid, 50% acetonitrile and 0.2% formic acid. Three eluted peptide washes were pooled together and further dried in speed vac. Before labeling, each sample was reconstituted in 30 μL of 0.1 M TEAB pH 8.5. The TMT 10-plex labels were reconstituted with 15 μL of anhydrous acetonitrile before labeling and was added to each of 30 μL tryptic digest samples with 1:2 ratio. The samples were labeled for 1 hour at room temperature. Using Orbitrap Fusion (ThermoFisher), the label incorporation was confirmed by taking 1 μL aliquots from each sample and desalting with SCX Ziptip (Millipore). Then, the labeled peptides from the 10 samples were pool together. The pooled peptides of each set were then evaporated to dryness and further cleaned up with solid phase extraction of MCX

Catridges (Waters). The eluted tryptic peptides were evaporated to dryness for high pH reverse phase chromatography.

**High pH Reverse Phase (hpRP) Fractionation**

The high pH Reverse Phase (hpRP) chromatography was carried out sing a Dionex UltiMate 3000 HPLC system with the built-in micro fraction collection option in the autosampler and UV detection (ThermoFisher), as reported previously.[9, 10] Specifically, the TMT 10-plex tagged tryptic peptides were reconstituted in buffer A (20 mM ammonium formate pH 9.5 in water) and loaded onto the Xterra MS C18 column (3.5 μm, 2.1 x 150 mm, Waters), with 20 mM ammonium formate pH 9.5 as buffer A, and 80% acetonitrile/20% ammonium formate as buffer B. The liquid chromatography was performed using a gradient from 10-45% of buffer B in 30 minutes at a flow rate of 200 μL/min. 48 fractions were collected at 1 minute intervals, and pooled into 10 total fractions based on the UV absorbance at 214 nm and with multiple fraction concatenation strategy.[13] Each of the 10 fractions was dried and reconstituted in 125 μL of 2% acetonitrile/0.5% ammonium formate for nanoLC-MS/MS system.

**Nano-scale Reverse Phase Chromatography and Tandem MS (nanoLC-MS/MS)**

The nanoLC-MS/MS analysis was carried out using Orbitrap Eclipse (ThermoFisher) equipped with a nanospray Flex Ion Source using real-time search SPS MS3 method coupled with the UltiMate3000 RSLCnano (Dionex).[9, 14] Each reconstituted fraction (5 μL for global proteomics fractions) was injected onto a PepMap C-18 RP nano trap column (5 μM, 100 μM x 20 mm, Dionex) at 20 μL/min flow rate for on-line desalting, and further separated on a PepMap C-18 RP nano

column (2 μm, 75 μm x 25 cm). The column was equilibrated with 2% acetonitrile in 0.1% aqueous formic acid (eluant A) prior to each run. The labeled peptides were eluted in a 120 min gradient of 5% to 33% eluant B containing 95% acetonitrile in 0.1% formic acid at 300 nL/min, followed by an 8-min ramping to 90% B, a 9-min hold and 25 min re-equilibration with 2% acetonitrile-0.1% formic acid prior to the next run. The Orbitrap Eclipse is operated in a positive ion mode with nano spray voltage set at 1.8 kV and source temperature at 300 °C. External calibration for FT, IT and quadrupole mass analyzers were performed. For global proteomics fractions, the instrument was operating using the RTS SPS MS3 workflow based on the manufacturer's provided template. Specifically, the RTS MS3 template contained 2.5 second "Top Speed" data-dependent CID-MS/MS scans followed by SPS of 10 $MS^2$ product ions for subsequent $MS^3$ in FT. In RTS mode, the *Homo sapiens* Uniprot database containing 20,304 entries was imported as the FASTA database with trypsin as the enzyme for the real-time spectral database search. The search parameters included: TMT 6-plex modifications on lysine and N-terminal amines (Δ mass 57.0215), and maximum 2 variable methionine oxidation per peptide, and 1 missed cleavage. A maximum search time for 35 ms allowed for RTS $MS^3$ searching. The $MS^3$ scan was carried out using a mass range of 100-500 m/z, an MS isolation window of 1.1 m/z and $MS^2$ isolation window of 3.0 m/z were used. A resolving power of 50,000 with a normalized collision energy of 55% was used for peptide quantitation. Other parameters included 500% normalized AGT target and 118 ms for maximum injection time. Dynamic exclusion parameters were set at 1 within 50s exclusion

duration with ±10 ppm exclusion mass window. All data were acquired under Xcalibur 4.3 operation software in Orbitrap Eclipse (ThermoFisher).

**Data Processing, Protein Identification and Data Analysis**

All raw MS spectra were processed and searched using the Sequest HT search engine within the Proteome Discoverer 2.3 (PD2.3, ThermoFisher). The *Homo sapiens* Uniprot database containing 20,304 entries was downloaded from Uniprot and used for database searches. The default search settings used for 10-plex TMT quantitative processing and protein identification in PD2.3 searching software were: two mis-cleavage for full trypsin with fixed carbamidomethyl modification of cysteine, fixed 10-plex TMT modifications on lysine and N-terminal amines and variable modification of methionine oxidation, deamidation on asparagine/glutamine residues and protein N-terminal acetylation. The peptide mass tolerance and fragment mass tolerance values were 10 ppm, 0.6 Da for $MS^2$ and 20 ppm for $MS^3$, respectively. Identified peptides were further filtered for maximum 1% FDR using the Percolator algorithm in PD 2.3 along with additional peptide confidence set to high and peptide mass accuracy $\leq$ 5 ppm. The TMT10-plex quantification method within Proteome Discoverer 2.3 software was used to calculate the reporter ion abundances in $MS^3$ spectra that were corrected for the isotopic impurities. Both unique and razor peptides were used to quantitation. Signal-to-noise (S/N) values were used to represent the reporter ion abundance with a co-isolation threshold of 50% and an average reporter S/N threshold of 10 and above required for quantitation spectra. The S/N values of peptides from such values of the PSMs, were summed to represent the abundance of the proteins. For the relative ratio between the two groups, normalization on total

peptide amount for each sample was applied. The search result including ratio, p-value, peptide abundance for each sample was output to Microsoft Excel for further data analysis.

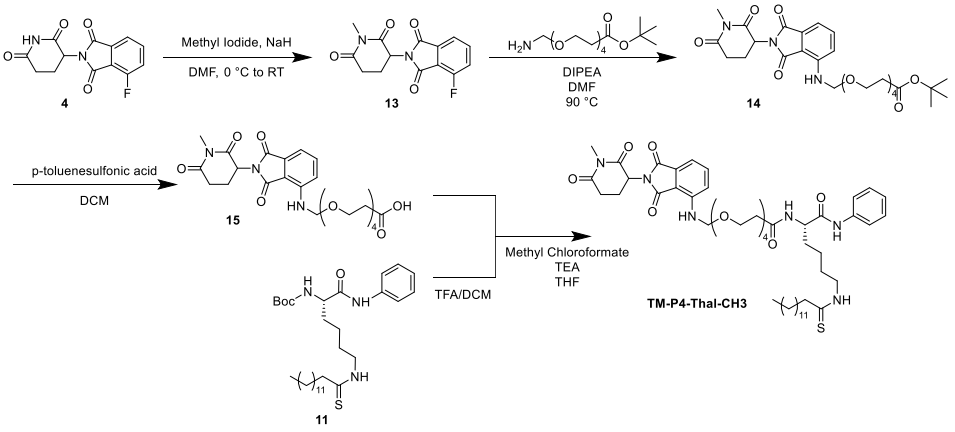


**Scheme 3.2 Synthesis of TM-P4-Thal-CH3**

**Synthesis of Acetyl-H3K9, Succinyl-H3K9 and Myristoyl-H3K9**

Acetyl-H3K9, Succinyl-H3K9 and Myristoyl-H3K9 were prepared as previously reported. The sequence was KQTAR-(Acetyl/Succinyl/Myristoyl-K)-STGGWW.[1, 5]

**Synthesis of Alk-14 probe**

Alk-14 was synthesized as previously reported.[15]

**Synthesis of Compound 2-15, TM, TM-P2-Thal and TM-P4-Thal**

Compound 2-4, 13 and TM were synthesized as previously reported[16].

***tert*-butyl 3-(2-(2-((2-(2,6-dioxopiperidin-3-yl)-1,3-dioxoisoindolin-4-yl)amino)ethoxy)ethoxy)propanoate (5).**

To *tert*-butyl 3-(2-(2-aminoethoxy)ethoxy)propanoate (0.211 g, 0.766 mmol) dissolved in dimethyl formamide (DMF, 7.6 mL), diisopropylethylamine (DIPEA, 0.267 mL, 1.53 mmol) and Compound 4 (0.178 g, 0.766 mmol) were added slowly. The reaction mixture was stirred overnight at 90 °C. DMF was removed by rotary evaporation at 80 °C. Ethyl acetate (50 mL) was added to dissolve the residue, which was further washed with water (40 mL) and brine (40 mL). The collected ethyl acetate layer was dried over $Na_2SO_4$ and concentrated by rotary evaporation. The crude residue was purified by silica gel column chromatography using hexane and ethyl acetate to afford the final product 5 (0.112 g, 30% yield). $^1$H NMR (500 MHz, $CD_3OD$) δ 7.57 (dd, J = 8.6, 7.1 Hz, 1H), 7.09 (dd, J = 19.7, 7.8 Hz, 2H), 5.07 (dd, J = 12.6, 5.5 Hz, 1H), 3.75 – 3.68 (m, 4H), 3.68 – 3.59 (m, 4H), 3.51 (t, J = 5.3 Hz, 2H), 2.96 – 2.66 (m, 3H), 2.47 (t, J = 6.2 Hz, 2H), 2.12 (dtd, J = 13.0, 5.1, 2.3 Hz, 1H), 1.44 (s, 9H). $^{13}$C NMR (126 MHz, $CD_3OD$) δ 173.24, 171.47, 170.16, 169.23, 167.89, 146.83, 135.76, 132.50, 116.82, 110.57, 109.94, 80.32, 70.18, 70.09, 69.24, 66.61, 48.78, 41.85, 35.87, 30.81, 26.94, 22.41. LCMS (ESI) calcd. for $[M+H\text{-}tbu]^+$ $C_{20}H_{24}N_3O_8$ 434.15, obsd. 434.10. Calcd. for [M] $C_{24}H_{31}N_3O_8$ 489.21, obsd. 489.77. Calcd. for $[M+Na^-]$ $C_{24}H_{31}N_3O_8Na$ 512.21, obsd. 512.05.

**_tert_-butyl 1-((2-(2,6-dioxopiperidin-3-yl)-1,3-dioxoisoindolin-4-yl)amino)-3,6,9,12-tetraoxapentadecan-15-oate (6).**

To *tert*-butyl 1-amino-3,6,9,12-tetraoxapentadecan-15-oate (0.367 g, 1.33 mmol) dissolved in DMF (13 mL), DIPEA (0.463 mL, 2.66 mmol) and Compound 4 (0.427 g, 1.33 mmol) were added slowly. After stirring overnight at 90 °C, DMF was removed by rotary evaporation at 80 °C. The residue was dissolved with ethyl acetate

(40 mL) and washed with water (30 mL) and brine (30 mL). The ethyl acetate layer was dried over $Na_2SO_4$ and concentrated by rotary evaporation. The crude residue was purified by silica gel column purification using hexane and ethyl acetate to afford the final product 6 (0.333 g, 44%). $^1$H NMR (500 MHz, $CD_3OD$) δ 7.57 (dd, J = 8.5, 7.1 Hz, 1H), 7.09 (dd, J = 20.7, 7.8 Hz, 2H), 5.07 (dd, J = 12.5, 5.5 Hz, 1H), 3.77 – 3.50 (m, 18H), 2.95 – 2.66 (m, 3H), 2.47 (t, J = 6.2 Hz, 2H), 2.19 – 2.07 (m, 1H), 1.45 (s, 9H). $^{13}$C NMR (126 MHz, $CD_3OD$) δ 173.25, 171.39, 170.13, 169.24, 167.88, 146.82, 135.78, 132.49, 116.85, 110.59, 109.90, 80.32, 70.27, 70.25, 70.23, 70.20, 70.08, 69.98, 69.25, 66.48, 48.79, 41.86, 35.83, 30.82, 26.96, 22.42. LCMS (ESI) calcd. for [M+H-*tbu*]$^+$ $C_{24}H_{32}N_3O_{10}$ 522.20, obsd. 522.12. Calcd. for [M] $C_{28}H_{39}N_3O_{10}$ 577.26, obsd. 577.95.

**3-(2-(2-((2-(2,6-dioxopiperidin-3-yl)-1,3-dioxoisoindolin-4-yl)amino)ethoxy)ethoxy)propanoic acid (7).**

To Compound 5 (0.109 g, 0.222 mmol) dissolved in dichoromethane (DCM, 2.2 mL), *p*-toluenesulfonic acid (0.0843 g, 0.444 mmol) was added. After stirring overnight at room temperature, the reaction mixture was diluted with DCM (50 mL) and further washed with water (40 mL) and brine (40 mL). The collected DCM layer was dried over $Na_2SO_4$ and concentrated by rotary evaporation. The crude residue was purified by silica gel column chromatography using DCM and methanol to afford the final product 7 (0.0557 g, 58%). $^1$H NMR (500 MHz, $CD_3OD$) δ 7.57 (dd, J = 8.5, 7.1 Hz, 1H), 7.09 (dd, J = 20.2, 7.8 Hz, 2H), 5.07 (dd, J = 12.6, 5.4 Hz, 1H), 3.74 (dt, J = 7.9, 5.8 Hz, 4H), 3.71 – 3.61 (m, 4H), 3.52 (t, J = 5.3 Hz, 2H), 2.92 – 2.68 (m, 3H), 2.56 (t, J = 6.3 Hz, 2H), 2.13 (dtd, J = 13.1, 5.0, 2.2 Hz, 1H). $^{13}$C NMR (126 MHz,

$CD_3OD$) δ 174.18, 173.28, 170.21, 169.24, 167.91, 146.82, 135.76, 132.49, 116.84, 110.57, 109.91, 70.12, 70.04, 69.22, 66.58, 48.78, 41.83, 34.56, 30.81, 22.40. LCMS (ESI) calcd. for $[M+H]^+$ $C_{20}H_{24}N_3O_8$ 434.15, obsd. 434.12.

**1-((2-(2,6-dioxopiperidin-3-yl)-1,3-dioxoisoindolin-4-yl)amino)-3,6,9,12-tetraoxapentadecan-15-oic acid (8).**

To Compound 6 (0.329 g, 0.570 mmol) dissolved in DCM (5.7 mL), *p*-toluenesulfonic acid (0.217 g, 1.14 mmol) was added. After stirring overnight at room temperature, the reaction mixture was diluted with DCM (50 mL) and washed with water (40 mL) and brine (40 mL). The collected DCM layer was dried over $Na_2SO_4$ and concentrated by rotary evaporator. The crude residue was purified by silica gel column chromatography using DCM and methanol to afford the final product 8 (0.136 g, 46%). $^1$H NMR (500 MHz, $CD_3OD$) δ 7.55 (dd, J = 8.6, 7.1 Hz, 1H), 7.08 (dd, J = 20.2, 7.8 Hz, 2H), 5.06 (dd, J = 12.4, 5.5 Hz, 1H), 3.76 – 3.48 (m, 18H), 2.92 – 2.63 (m, 3H), 2.53 (t, J = 6.3 Hz, 2H), 2.19 – 2.02 (m, 1H). $^{13}$C NMR (126 MHz, $CD_3OD$) δ 178.14, 177.22, 174.10, 173.18, 171.83, 150.75, 139.73, 136.42, 120.80, 114.53, 113.83, 74.17, 74.16, 74.15, 74.11, 73.97, 73.88, 73.17, 70.44, 52.73, 45.78, 38.54, 34.75, 26.35. LCMS (ESI) $C_{24}H_{32}N_3O_{10}$ calcd. for $[M+H]^+$ 522.20, obsd. 522.15.

**$N^2$-(*tert*-butoxycarbonyl)-$N^6$-tetradecanoyl-*L*-lysine (9).**

*Boc-L*-lysine (10 g, 40.6 mmol) was dissolved in water (100 mL) and dioxane (100 mL). To the mixture, $NaHCO_3$ (10.2 g, 122 mmol) was added slowly. The mixture was then stirred at room temperature until no precipitation is observed. After 2 – 4 hours, myristoyl chloride (12.1 mL, 44.6 mmol) was added to the mixture. After stirring overnight at room temperature, the reaction mixture was diluted with DCM

(150 mL) and washed with 15% citric acid (125 mL) and brine (100 mL). The collected DCM layer was dried over $Na_2SO_4$ and concentrated using rotary evaporation. The crude residue was purified by silica gel column chromatography using DCM and methanol to afford the final compound 9 (11.7 g, 63%). $^1$H NMR (500 MHz, $CD_3OD$) δ 4.06 (dd, J = 9.2, 4.7 Hz, 1H), 3.17 (t, J = 6.9 Hz, 2H), 2.16 (t, J = 7.5 Hz, 2H), 1.88 – 1.75 (m, 1H), 1.71 – 1.49 (m, 5H), 1.44 (s, 11H), 1.31 – 1.21 (m, 20H), 0.90 (t, J = 6.9 Hz, 3H). $^{13}$C NMR (126 MHz, $CD_3OD$) δ 174.89, 174.83, 156.76, 79.03, 53.42, 38.63, 35.77, 31.68, 31.06, 29.40, 29.36, 29.32, 29.23, 29.07, 29.03, 28.91, 28.58, 27.34, 25.69, 22.91, 22.33, 13.03. LCMS (ESI) calcd. for [M+H-*Boc*]$^+$ $C_{20}H_{41}N_2O_3$ 357.30, obsd. 357.90.

**$N^2$-(*tert*-butoxycarbonyl)-$N^6$-tetradecanethioyl-*L*-lysine (10).**

To $P_2S_5$ (0.779 g, 3.50 mmol) dissolved in tetrahydrofuran (THF, 60 mL), $NaHCO_3$ (0.184 g, 2.19mmol) was added. Then, the mixture was stirred for 1 – 2 hours at room temperature. To the reaction mixture, Compound 9 (2.00 g, 4.38 mmol) was added slowly at 0 °C. After 1 hour of stirring at 0 °C, the reaction mixture was stirred overnight at room temperature. After removing THF by rotary evaporation, the residue was dissolved in DCM (70 mL) and washed with 15% citric acid (65 mL), water (65 mL) and brine (70 mL). The collected DCM layer was dried over $Na_2SO_4$ and concentrated using a rotary evaporator. The crude residue was purified by column chromatography using hexane and ethyl acetate, affording the final compound 10 (0.931 g, 45%). $^1$H NMR (500 MHz, $CD_3OD$) δ 4.08 (dd, J = 9.1, 4.7 Hz, 1H), 3.19 (t, J = 6.9 Hz, 2H), 2.18 (t, J = 7.5 Hz, 2H), 1.92 – 1.77 (m, 1H), 1.73 – 1.50 (m, 5H), 1.46 (s, 11H), 1.31 – 1.21 (m, 20H), 0.92 (t, J = 6.9 Hz, 3H). $^{13}$C NMR (126 MHz,

$CD_3OD$) δ 205.06, 174.78, 156.77, 79.08, 53.35, 45.66, 45.16, 31.68, 31.11, 29.41, 29.40, 29.35, 29.31, 29.22, 29.08, 29.06, 28.53, 27.34, 26.87, 23.03, 22.34, 13.04. LCMS (ESI) calcd. for $[M+H]^+$ $C_{25}H_{49}N_2O_4S$ 473.33, obsd. 473.06.

***tert*-butyl (*S*)-(1-oxo-1-(phenylamino)-6-tetradecanethioamidohexan-2-yl)carbamate (11).**

To Compound 10 (0.714 g, 1.51 mmol) dissolved in THF (18 mL), isobutyl chloroformate (0.254 mL, 1.96 mmol) and DIPEA (0.790 mL, 4.53 mmol) was added at room temperature. After 1 hour of stirring at room temperature, aniline (0.206 mL, 2.26 mmol) was added to the reaction mixture. After stirring overnight at room temperature, THF was removed by rotary evaporation. The residue was dissolved in ethyl acetate (70 mL) and further washed with 15% citric acid (65 mL), water (65 mL) and brine (65 mL). The collected ethyl acetate layer was dried over $Na_2SO_4$ and concentrated by rotary evaporation. The crude residue was purified by column purification using DCM and methanol to afford the final product 11 (0.438 g, 53%). $^1H$ NMR (500 MHz, $CD_3OD$) δ 7.57 (d, J = 7.9 Hz, 2H), 7.31 (t, J = 7.8 Hz, 2H), 7.11 (t, J = 7.4 Hz, 1H), 4.19 (dd, J = 8.7, 5.4 Hz, 1H), 3.62 (t, J = 7.2 Hz, 2H), 2.69 – 2.49 (m, 2H), 1.85 (m, J = 19.0, 7.5, 6.6 Hz, 1H), 1.72 (m, J = 8.8, 2.7 Hz, 5H), 1.47 (s, 11H), 1.31 – 1.21 (m, 20H), 0.95 – 0.88 (t, J = 6.9 Hz, 3H). $^{13}C$ NMR (126 MHz, $CD_3OD$) δ 205.04, 172.10, 156.52, 138.09, 128.42, 124.00, 120.06, 79.29, 55.21, 45.72, 45.15, 31.92, 31.71, 29.45, 29.44, 29.39, 29.35, 29.26, 29.11, 29.08, 28.59, 27.39, 27.04, 23.04, 22.37, 13.13. LCMS (ESI) calcd. for $[M+H]^+$ $C_{31}H_{54}N_3O_3S$ 548.38, obsd. 548.14.

**(2*S*)-2-(3-(2-(2-((2-(2,6-dioxopiperidin-3-yl)-1,3-dioxoisoindolin-4-yl)amino)ethoxy)ethoxy)propanamido)-*N*-phenyl-6-tetradecanethioamidohexanamide (TM-P2-Thal).**

To Compound 11 (0.0505 g, 0.0921 mmol) dissolved in DCM (0.6 mL), trifluoroacetic acid (0.4 mL) was added at room temperature. After stirring 2 hours at room temperature, the reaction mixture was diluted with toluene, which was then removed by rotary evaporation. Addition and evaporation of toluene was repeated three more times. The reaction crude was taken to the next step without further purification.

To Compound 7 (0.0399 g, 0.0921 mmol) dissolved in DMF (0.8 mL), *N*-methylmorpholine (15.3 µL, 0.138 mmol) was added at room temperature. After 10 minutes of stirring at room temperature, isobutyl chloroformate (14.3 µL, 0.111 mmol) was added to the mixture. The reaction mixture was stirred for additional 2 hours at room temperature. To this reaction mixture, the reaction crude from above was added. After stirring overnight at room temperature, DMF was removed by rotary evaporation at 60 – 80 °C. The reaction mixture was diluted with ethyl acetate (40 mL) and washed with water (35 mL) and brine (35 mL). The collected ethyl acetate layer was dried over $Na_2SO_4$ and concentrated by rotary evaporation. The crude residue was purified by silica gel column chromatography using hexane and ethyl acetate to afford the final product TM-P2-Thal (0.0302 g, 38%). $^1$H NMR (500 MHz, $CD_3OD$) δ 7.58 – 7.51 (m, 3H), 7.30 (t, J = 7.8 Hz, 2H), 7.13 – 6.96 (m, 3H), 5.15 – 5.03 (m, 1H), 4.48 (td, J = 9.0, 5.5 Hz, 1H), 3.78 (tt, J = 5.8, 2.3 Hz, 2H), 3.70 (t, J = 5.0 Hz, 2H), 3.65 (d, J = 2.8 Hz, 4H), 3.57 (t, J = 7.2 Hz, 1H), 3.47 (td, J = 5.3, 2.2 Hz,

2H), 3.15 (t, J = 6.9 Hz, 1H), 2.95 – 2.80 (m, 1H), 2.73 (tt, J = 17.3, 6.5 Hz, 2H), 2.55 (dt, J = 8.7, 6.6 Hz, 3H), 2.12 (q, J = 9.1, 8.4 Hz, 2H), 1.93 – 1.80 (m, 1H), 1.79 – 1.61 (m, 3H), 1.50 (ddq, J = 39.0, 23.8, 7.3 Hz, 4H), 1.32 – 1.26 (m, 20H), 0.90 (t, J = 6.9 Hz, 3H). $^{13}$C NMR (126 MHz, $CD_3OD$) δ 205.04, 174.86, 173.23, 172.78, 171.11, 170.34, 169.35, 167.86, 146.77, 138.08, 135.82, 132.47, 128.40, 123.99, 120.01, 116.84, 110.61, 109.89, 69.97, 69.07, 66.96, 53.89, 48.80, 45.67, 45.16, 41.77, 38.62, 36.21, 35.77, 31.68, 30.81, 29.40, 29.36, 29.33, 29.22, 29.08, 29.04, 28.92, 28.67, 28.55, 26.99, 25.68, 22.76, 22.34, 13.04. LCMS (ESI) calcd. for $[M+H]^+$ $C_{46}H_{67}N_6O_8S$ 863.47, obsd. 863.32. HRMS (ESI) calcd. for $[M+H]^+$ $C_{46}H_{67}N_6O_8S$ 863.4741, obsd. 863.4729.

**1-((2-(2,6-dioxopiperidin-3-yl)-1,3-dioxoisoindolin-4-yl)amino)-*N*-((*S*)-1-oxo-1-(phenylamino)-6-tetradecanethioamidohexan-2-yl)-3,6,9,12-tetraoxapentadecan-15-amide (TM-P4-Thal)**

To Compound 11 (0.428 g, 0.781 mmol) dissolved in DCM (2.4 mL), trifluoroacetic acid (1.6 mL) was added at room temperature. After stirring 2 hours at room temperature, the reaction mixture was diluted with toluene, which was then removed by rotary evaporator. Addition and evaporation of toluene was repeated three more times. The reaction crude was taken to next step without further purification. To Compound 8 (0.408 g, 0.781 mmol) dissolved in DMF (7.8 mL), DIPEA (0.272 mL, 1.56 mmol) was added at room temperature. After 10 minutes of stirring at room temperature, isobutyl chloroformate (0.152 mL, 1.17 mmol) was added. The reaction mixture was stirred for additional 2 hours at room temperature. To this reaction mixture, the reaction crude from above was added slowly. After stirring overnight at

room temperature, DMF was removed by rotary evaporation at 60 – 80 °C. The reaction mixture was diluted with ethyl acetate (70 mL) and washed with water (65 mL) and brine (65 mL). The collected ethyl acetate layer was dried over $Na_2SO_4$ and concentrated by rotary evaporation. The crude residue was purified by silica gel column chromatography using DCM and methanol to afford the final product TM-P4-Thal (0.198 g, 27%). $^1$H NMR (500 MHz, $CD_3OD$) δ 7.65 – 7.49 (m, 3H), 7.30 (t, J = 7.8 Hz, 2H), 7.18 – 7.02 (m, 3H), 5.06 (dd, J = 12.5, 5.5 Hz, 1H), 4.46 (dd, J = 8.6, 5.5 Hz, 1H), 3.77 – 3.49 (m, 18H), 3.22 – 3.13 (m, 2H), 2.95 – 2.65 (m, 3H), 2.53 (td, J = 6.0, 2.8 Hz, 2H), 2.26 – 2.01 (m, 3H), 1.99 – 1.83 (m, 1H), 1.81 – 1.69 (m, 1H), 1.64 – 1.39 (m, 6H), 1.32 – 1.25 (m, 20H), 0.90 (t, J = 6.9 Hz, 3H). $^{13}$C NMR (126 MHz, $CD_3OD$) δ 205.01, 174.87, 173.25, 172.71, 171.16, 170.19, 169.21, 167.87, 146.82, 138.08, 135.79, 132.49, 128.41, 124.01, 120.09, 116.86, 110.60, 70.24, 70.23, 70.19, 70.16, 70.02, 69.94, 69.23, 66.89, 53.96, 48.79, 41.85, 38.63, 36.06, 35.78, 31.68, 31.52, 30.81, 29.40, 29.36, 29.33, 29.23, 29.08, 29.02, 28.93, 28.69, 25.69, 22.82, 22.43, 22.33, 13.04. LCMS (ESI) calcd. for $[M+H]^+$ $C_{50}H_{75}N_6O_{10}S$ 951.52, obsd. 951.20. HRMS (ESI) calcd. for $C_{50}H_{75}N_6O_{10}S$ $[M+H]^+$ 951.5265, obsd. 951.5231.

***tert*-butyl 1-((2-(1-methyl-2,6-dioxopiperidin-3-yl)-1,3-dioxoisoindolin-4-yl)amino)-3,6,9,12-tetraoxapentadecan-15-oate (14).**

To *tert*-butyl 1-amino-3,6,9,12-tetraoxapentadecan-15-oate (0.0722 g, 0.225 mmol) and DIPEA (98 μL, 0.562 mmol) dissolved in DMF (1.5 ml), Compound 13 (0.0544 g, 0.187 mmol) was added slowly. After stirring overnight at 90 °C, DMF was removed by rotary evaporator at 80 °C. Ethyl acetate (20 mL) was added to dissolve the residue. Then, the crude mixture was washed with water (15 ml) and brine (15 ml).

The organic layer was dried over $Na_2SO_4$ and concentrated by rotary evaporator. The crude residue was further purified by silica gel column chromatography using hexane and ethyl acetate to afford the final product 14 (0.0309 g, 28% yield). $^1$H NMR (500 MHz, $CD_3OD$) δ 7.49 (dd, J = 8.5, 7.1 Hz, 1H), 7.14 – 7.05 (m, 1H), 6.93 (d, J = 8.5 Hz, 1H), 5.05 – 4.80 (m, 1H), 3.74 – 3.60 (m, 18H), 3.21 (s, 3H), 3.03 – 2.90 (m, 1H), 2.85 – 2.66 (m, 2H), 2.49 (t, J = 6.6 Hz, 2H), 2.13 – 2.04 (m, 1H), 1.44 (s, 9H). $^{13}$C NMR (126 MHz, $CD_3OD$) δ 171.41, 171.05, 170.29, 169.59, 169.14, 146.99, 136.14, 132.71, 116.88, 111.76, 110.53, 80.68, 70.85, 70.82, 70.78, 70.76, 70.65, 70.51, 69.73, 67.05, 49.77, 42.58, 36.41, 32.10, 28.25, 27.40, 22.28. LfCMS (ESI) calcd. for $[M+H]^+$ C29H42N3O10 592.28, obsd. 592.58

**1-((2-(1-methyl-2,6-dioxopiperidin-3-yl)-1,3-dioxoisoindolin-4-yl)amino)-3,6,9,12-tetraoxapentadecan-15-oic acid (15).**

To compound 14 (0.0309 g, 0.0522 mmol) dissolved in DCM (0.7 mL), *p*-toluenesulfonic acid (0.0298 g, 0.157 mmol) was added. The reaction mixture was stirred overnight at room temperature. Then, the reaction mixture was diluted with DCM (20 mL) and washed with water (15 mL) and brine (15 mL). The collected organic layer was dried over $Na_2SO_4$ and concentrated by rotary evaporator. The crude residue was purified by silica gel column chromatography using DCM and methanol to afford the final product 15 (0.0231 g, 83%). $^1$H NMR (500 MHz, $CD_3OD$) δ 7.49 (dd, J = 8.5, 7.1 Hz, 1H), 7.10 (d, J = 7.0 Hz, 1H), 6.93 (d, J = 8.5 Hz, 1H), 4.96 – 4.86 (m, 1H), 3.81 – 3.60 (m, 18H), 3.21 (s, 3H), 3.05 – 2.87 (m, 1H), 2.79 – 2.73 (m, 2H), 2.59 (t, J = 6.0 Hz, 2H), 2.09 – 2.04 (m, 1H). $^{13}$C NMR (126 MHz, $CD_3OD$) δ 171.49, 169.66, 169.23, 167.96, 167.91, 146.96, 136.20, 132.68, 116.94, 111.80, 110.49,

70.85, 70.72, 70.71, 70.56, 70.52, 70.21, 69.68, 66.86, 49.77, 42.46, 32.07, 27.40, 22.26, 14.27. LCMS (ESI) calcd. for $[M+H]^+$ C25H34N3O10 536.22, obsd. 536.82

**1-((2-(1-methyl-2,6-dioxopiperidin-3-yl)-1,3-dioxoisoindolin-4-yl)amino)-*N*-(1-oxo-1-(phenylamino)-6-tetradecanethioamidohexan-2-yl)-3,6,9,12-tetraoxapentadecan-15-amide (TM-P4-Thal-CH3).**

To Compound 11 (0.0314 g, 0.0573 mmol) dissolved in DCM (0.4 mL), trifluoroacetic acid (0.3 mL) was added at room temperature. After stirring 2 hours, the reaction mixture was diluted with toluene, which was removed by rotary evaporator. Addition and evaporation of toluene was repeated three times. The reaction crude was taken to next step without further purification.

To Compound 15 (0.0231 g, 0.0431 mmol) dissolved in THF (0.6 mL), TEA (24 μL, 0.173 mmol) was added at room temperature. After 15 minutes of stirring at room temperature, methyl chloroformate (5 μL, 0.0647 mmol) was added. The reaction mixture was stirred for additional 2 hours at room temperature. To this reaction mixture, the reaction crude from above was added slowly. After stirring overnight at room temperature, THF was removed by rotary evaporator. Then, the reaction mixture was diluted with ethyl acetate (20 mL) and washed with water (15 mL) and bring (15 mL). The collected organic layer was dried over $Na_2SO_4$ and concentrated by rotary evaporator. The crude residue was purified by silica gel chromatography using DCM and methanol to afford the final product TM-P4-Thal-CH3 (0.0124 g, 30%). $^1$H NMR (500 MHz, $CH_3OD$) δ 7.56 (dd, J = 8.6, 7.1 Hz, 3H), 7.35 – 7.22 (m, 2H), 7.15 – 6.99 (m, 3H), 5.09 (dd, J = 12.9, 5.4 Hz, 1H), 4.46 (dd, J = 8.6, 5.6 Hz, 1H), 3.78 – 3.49 (m, 18H), 3.16 (m, 5H), 2.95 – 2.62 (m, 3H), 2.62 – 2.48 (m, 2H), 2.19 – 2.05 (m, 3H),

1.96 – 1.83 (m, 1H), 1.74 (dtd, J = 13.6, 9.4, 5.0 Hz, 1H), 1.59 – 1.42 (m, 6H), 1.31 – 1.28 (m, 20H), 0.90 (t, 3H). $^{13}$C NMR (126 MHz, $CH_3OD$) δ 176.28, 174.10, 173.68, 172.56, 171.41, 169.31, 148.27, 139.50, 137.23, 133.90, 129.82, 125.43, 121.51, 118.30, 112.03, 71.64, 71.61, 71.57, 71.44, 71.36, 70.67, 68.30, 55.37, 50.85, 49.51, 49.34, 49.17, 49.00, 48.83, 48.66, 48.49, 43.27, 40.04, 37.48, 37.19, 33.08, 32.93, 32.50, 30.80, 30.76, 30.73, 30.63, 30.48, 30.43, 30.33, 30.11, 27.36, 27.09, 24.23, 23.74, 23.08, 14.44. LCMS (ESI) cald. For $[M+H]^+$ $C_{51}H_{77}N_6O_{10}S$ 965.53, obsd. 965.91 HRMS (ESI) calcd. for $[M+H+Na]^+$ $C_{51}H_{77}N_6O_{10}SNa$ 988.531961 obsd. 988.5339.

### 3.6.1 References for methods


1. Jing, H., Hu, J., He, B., Negron Abril, Y. L., Stupinski, J., Weiser, K., Carbonaro, M., Chiang, Y. L., Southard, T., Giannakakou, P., Weiss, R. S., and Lin, H. (2016) A SIRT2-Selective Inhibitor Promotes c-Myc Oncoprotein Degradation and Exhibits Broad Anticancer Activity, *Cancer Cell 29*, 767-768.

2. Jiang, H., Khan, S., Wang, Y., Charron, G., He, B., Sebastian, C., Du, J., Kim, R., Ge, E., Mostoslavsky, R., Hang, H. C., Hao, Q., and Lin, H. (2013) SIRT6 regulates TNF-α secretion through hydrolysis of long-chain fatty acyl lysine, *Nature 496*, 110-113.

3. Spiegelman, N. A., Price, I. R., Jing, H., Wang, M., Yang, M., Cao, J., Hong, J. Y., Zhang, X., Aramsangtienchai, P., Sadhukhan, S., and Lin, H. (2018) Direct Comparison of SIRT2 Inhibitors: Potency, Specificity, Activity-Dependent Inhibition, and On-Target Anticancer Activities, *ChemMedChem 13*, 1890-1894.

4. Schindelin, J., Arganda-Carreras, I., Frise, E., Kaynig, V., Longair, M., Pietzsch, T., Preibisch, S., Rueden, C., Saalfeld, S., Schmid, B., Tinevez, J. Y., White, D. J., Hartenstein, V., Eliceiri, K., Tomancak, P., and Cardona, A. (2012) Fiji: an open-source platform for biological-image analysis, *Nat Methods 9*, 676-682.

5. Hong, J. Y., Zhang, X., and Lin, H. (2018) HPLC-Based Enzyme Assays for Sirtuins, *Methods Mol Biol 1813*, 225-234.

6. Du, J., Zhou, Y., Su, X., Yu, J. J., Khan, S., Jiang, H., Kim, J., Woo, J., Kim, J. H., Choi, B. H., He, B., Chen, W., Zhang, S., Cerione, R. A., Auwerx, J., Hao, Q.,

and Lin, H. (2011) Sirt5 Is a NAD-Dependent Protein Lysine Demalonylase and Desuccinylase, *Science 334*, 806-809.

7. Jing, H., Zhang, X., Wisner, S. A., Chen, X., Spiegelman, N. A., Linder, M. E., and Lin, H. (2017) SIRT2 and lysine fatty acylation regulate the transforming activity of K-Ras4a, *Elife 6*.

8. Spiegelman, N. A., Hong, J. Y., Hu, J., Jing, H., Wang, M., Price, I. R., Cao, J., Yang, M., Zhang, X., and Lin, H. (2019) A Small-Molecule SIRT2 Inhibitor That Promotes K-Ras4a Lysine Fatty-Acylation, *ChemMedChem 14*, 744-748.

9. Zhang, Z., Ahmed-Braimah, Y. H., Goldberg, M. L., and Wolfner, M. F. (2019) Calcineurin-dependent Protein Phosphorylation Changes During Egg Activation in Drosophila melanogaster, *Mol. Cell. Proteomics 18*, S145-S158.

10. Qin, L., Walk, T. C., Han, P., Chen, L., Zhang, S., Li, Y., Hu, X., Xie, L., Yang, Y., Liu, J., Lu, X., Yu, C., Tian, J., Shaff, J. E., Kochian, L. V., Liao, X., and Liao, H. (2019) Adaption of Roots to Nitrogen Deficiency Revealed by 3D Quantification and Proteomic Analysis, *Plant Physiol. 179*, 329-347.

11. Yang, S., Li, X., Liu, X., Ding, X., Xin, X., Jin, C., Zhang, S., Li, G., and Guo, H. (2018) Parallel comparative proteomics and phosphoproteomics reveal that cattle myostatin regulates phosphorylation of key enzymes in glycogen metabolism and glycolysis pathway, *Oncotarget 9*, 11352-11370.

12. Yang, Y., Anderson, E., and Zhang, S. (2018) Evaluation of six sample preparation procedures for qualitative and quantitative proteomics analysis of milk fat globule membrane, *Electrophoresis 39*, 2332-2339.

13. Yang, Y., Qiang, X., Owsiany, K., Zhang, S., Thannhauser, T. W., and Li, L. (2011) Evaluation of different multidimensional LC-MS/MS pipelines for isobaric tags for relative and absolute quantitation (iTRAQ)-based proteomic analysis of potato tubers in response to cold storage, *J. Proteome Res. 10*, 4647-4660.

14. Erickson, B. K., Mintseris, J., Schweppe, D. K., Navarrete-Perea, J., Erickson, A. R., Nusinow, D. P., Paulo, J. A., and Gygi, S. P. (2019) Active Instrument Engagement Combined with a Real-Time Database Search for Improved Performance of Sample Multiplexing Workflows, *J. Proteome Res. 18*, 1299-1306.

15. Zhang, X., Spiegelman, N. A., Nelson, O. D., Jing, H., and Lin, H. (2017) SIRT6 regulates Ras-related protein R-Ras2 by lysine defatty-acylation, *eLife 6*, e25158.

16. Lu, J., Qian, Y., Altieri, M., Dong, H., Wang, J., Raina, K., Hines, J., Winkler, James D., Crew, Andrew P., Coleman, K., and Crews, Craig M. (2015) Hijacking the E3 Ubiquitin Ligase Cereblon to Efficiently Target BRD4, *Chem.*

*Biol. 22*, 755-763.

# CHAPTER 4

# PHARMACOLOGICAL ADVANTAGE OF SIRT2-SELECTIVE VERSUS PAN-SIRT1-3 INHIBITORS

This is a revised version of the published paper: Hong JY, Fernandez I, Anmangandla A, Lu X, Bai JJ, Lin H. Pharmacological Advantage of SIRT2-Selective versus pan-SIRT1-3 Inhibitors. *ACS Chem Biol.* 2021 Jun 17;16(7):1266-1275.

J.Y.H., I.F. and H.L. conceived the concept. J.Y.H. designed, synthesized the inhibitors. J.Y.H. tested these inhibitors in solubility tests, in vitro enzymatic assays, cell proliferation assays, cell permeability tests, and in-cell sirtuin inhibition tests. I.F. evaluated the inhibitors in mice serum detection and tumor xenograft mice studies. A. A. purified enzymes. X.L. helped mice experiments, and J. J. B. assisted cellular assays. J. Y. H., I. F., and H.L. wrote the manuscript. All the authors have given approval to the final version of the manuscript.

## 4.1 Abstract

Due to wide involvement in various biological pathways, the sirtuin enzyme family members SIRT1, SIRT2, and SIRT3 play both tumor promoting and suppressing roles based on the context and experimental conditions. Thus, an interesting question is whether inhibiting one of them or inhibiting all of them would be better for treating cancers. Pharmacologically, this is difficult to address, due in part to potential off-target effects of different compounds. Compounds with almost identical properties but differing in SIRT1-3 selectivity will be useful for addressing this question. In this paper, we have developed a pan SIRT1-3 inhibitor (NH4-6) and a SIRT2-selective inhibitor (NH4-13) with very similar chemical structures, the only difference being the substitution of an ester bond to an amide bond. Such minimal difference allows us to accurately compare the anticancer effect of pan SIRT1-3 inhibition and SIRT2-

selective inhibition in cellular and mouse models. NH4-6 showed stronger cytotoxicity than NH4-13 in cancer cell lines. In mice, both inhibitors showed similar anticancer efficacy. However, NH4-6 is toxic to mice, which hinders the use of higher dosages. These results highlight the advantage of SIRT2-selective inhibitors as potential anticancer therapeutics.

## 4.2 Introduction

The class III histone deacetylase, sirtuins, require nicotinamide adenine dinucleotide ($NAD^+$) as a co-substrate. They transfer the acyl group on protein lysine residues to $NAD^+$, forming O-acyl ADP-ribose, nicotinamide, and deacylated proteins.[1-3] Sirtuins have various biological functions and have been implicated in various diseases, such as cancer, inflammation, and neurodegenerative disorders.[4-15] There are seven sirtuins in humans, SIRT1-7, each with unique enzymatic activities, functions, and subcellular localizations.[16-19] Among them, SIRT1, 2, and 3 have been studied extensively due to their robust deacetylase activity and biological importance in stress response, genome stability, cell physiology, metabolism, inflammation, and tumorigenesis.[8, 9, 12, 20-23] In terms of tumorigenesis, SIRT1, 2, and 3 have been reported to have contradictory roles, acting as both tumor suppressors and promoters.[12, 24-26]

SIRT1, predominantly located in the nucleus, is the most well-studied sirtuin.[23] As a tumor suppressor, SIRT1 inactivates various tumor-promoting transcription factors, such as NF-κB and HIF1-α.[27-30] Transgenic mice with SIRT1 overexpression had less tumor formation than wild-type mice.[31, 32] In normal cells, SIRT1 promotes genome stability through activation of high-fidelity DNA repair, which would

suppress tumorigenesis.[12] Meanwhile, as a tumor activator, SIRT1 inhibits FOXO1-induced apoptosis and stabilizes c-Myc, which is responsible for increased expression levels of genes associated with cell proliferation.[33, 34] However, in cancer cells, SIRT1 activated low-fidelity DNA repair, which causes increased mutation occurrences.[12]

SIRT2, which is mainly cytosolic, has been reported to be a tumor suppressor because SIRT2 knockout mice develop more tumors as they age. The reported model is that SIRT2 regulates cell cycle by deacetylating APC/C, and the loss of SIRT2 leads to abnormal cell division and promotes tumor formation.[35] Nevertheless, more recent reports highlighted SIRT2's tumor-promoting role. SIRT2 deacetylates many metabolic enzymes, transcription factors and signaling proteins to promote tumorigenesis. For instance, similar to SIRT1, SIRT2 deactivates FOXO-1 to inhibit apopotsis.[36] Also, SIRT2 stabilizes c-Myc and Slug, thereby promoting breast cancer

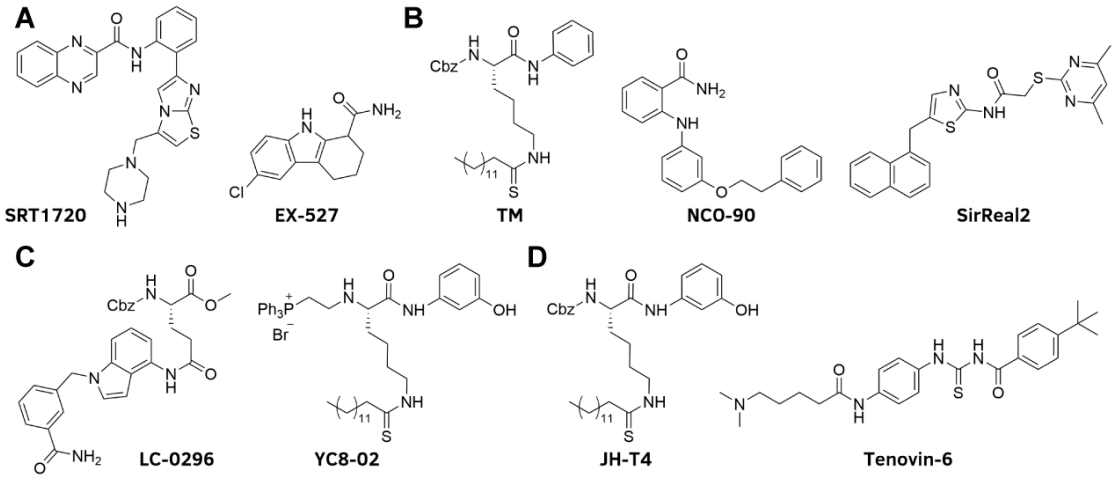


**Figure 4.1 Structures of previously reported sirtuin inhibitors. (**A) SIRT1 activator and inhibitor. (B) SIRT2 inhibitors. (C) SIRT3 inhibitors (D) Pan-sirtuin inhibitors.

cell proliferation.[37, 38] Through deacetylating LDH-A, which is responsible for lactate production, SIRT2 promotes pancreatic cell proliferation.[39] Through its defatty-acylase activity on K-Ras4a, SIRT2 also regulates the transforming ability of K-Ras4a.[40]

SIRT3 was initially viewed as a tumor suppressor. Mainly localized in mitochondria, SIRT3 promotes mitochondrial metabolism, promotes ROS removal, and suppresses the Warburg effect.[23, 41] Furthermore, SIRT3 KO mice develop mammary tumors, while SIRT3 WT mice do not.[42] On the other hand, a recent report suggested that SIRT3 is required for proliferation, survival, and metabolism of diffusive large B cell lymphomas (DLBCL), suggesting a tumor promoting role of SIRT3.[43]

Thus, due to their involvements in various biological pathways, SIRT1, 2, and 3 can have either tumor promoting or suppressing roles depending on the contexts and conditions. Accordingly, the anticancer effect of pharmacological inhibition of sirtuins may also be complicated and need detailed investigation in different type of cancers.

Because of the important roles of sirtuins in physiology and diseases, numerous sirtuin modulators have been developed. Because SIRT1 was initially reported as a tumor suppressor, several SIRT1-activating compounds (STACs) have been synthesized and tested as anticancer agents. SRT1720 (Figure 4.1A) activated SIRT1 *in vitro* and effectively reduced breast and pancreatic tumors in xenograft mouse studies.[44, 45] Yet, the compound promoted lung cancer cell migration and lung metastasis.[46] Later, the SIRT1 activation effect of SRT1720 was questioned, as the activation effect *in vitro* required specific peptides.[47] Furthermore, a SIRT1-specific

inhibitor, EX-527 (Figure 4.1A), impaired PANC-1 cell proliferation *in vitro*, but promoted its growth *in vivo*.[48] As such, activation and inhibition of SIRT1 portrayed conflicting results in cancer studies.

Many SIRT2 inhibitors have been developed and tested as potential anticancer agents. SirReal2 decreased the migration and invasion of gastric cancer cells.[49, 50] NCO-90/140 induced apoptosis and autophagy cell deaths against leukemia cells.[51] An NCO-90-derived Compound 53 slowed down breast cancer cell proliferation.[52] A mechanism-based SIRT2 selective inhibitor, TM, showed broad anti-cancer effects in both cellular and animal studies partially through the degradation of c-Myc (Figure 4.1B).[38] AF-8, a compound similar to TM, showed promising anti-cancer effect in cellular and mouse models of colorectal cancer.[53]

As for SIRT3, only a few SIRT3 small molecule modulators have been reported. Initially designed to be a SIRT1 activator, SRT1720 was discovered to inhibit SIRT3.[54] LC-0296 with selective SIRT3 inhibition portrayed anti-proliferative effects against head and neck squamous cell carcinoma (HNSCC).[55] Recently, YC8-02, a mitochondrial-targeting SIRT3 inhibitor, further confirmed SIRT3's importance in DLBCLs (Figure 4.1A, C).[43] YC8-02 also inhibits SIRT1 and SIRT2, but the mitochondrial targeting moiety enhances its SIRT3 inhibition ability in cells.

Along with sirtuin isoform-selective inhibitors, several non-selective sirtuin inhibitors have been synthesized as well. Given that SIRT1, SIRT2, and SIRT3 are all connected to cancer, one interesting question is whether small molecules that inhibit all three sirtuins will be better or worse as anticancer agents. Tenovin-6 inhibits both SIRT1 and 2 and can significantly impair ARN8 melanoma cell proliferation in

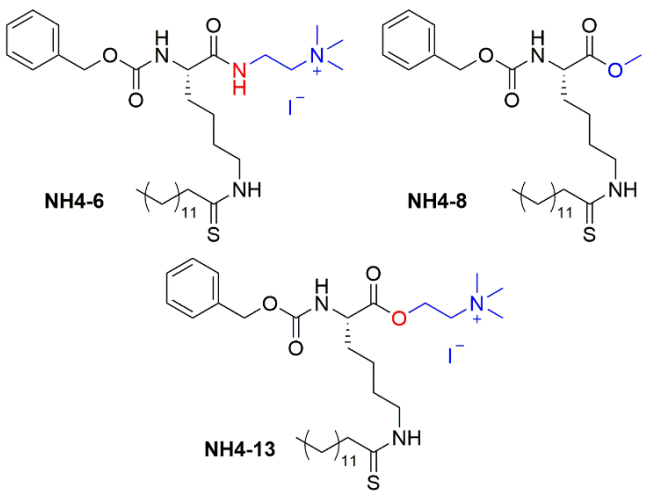


**Figure 4.2 Chemical structures of synthesized TM analogs.**

xenograft studies.[56] The mechanism-based sirtuin inhibitor, JH-T4, inhibits SIRT1, 2, and 3 and can further inhibit the defatty-acylase activity of SIRT2.[57] Interestingly, JH-T4 differs from the SIRT2-selective inhibitor TM by only one oxygen atom. The non-selective sirtuin inhibitors Tenovin-6 and JH-T4 (Figure 4.1D) displayed much stronger cellular cytotoxicity compared to the SIRT2-specific inhibitor TM. However, Tenovin-6 and JH-T4 are cytotoxic to both normal epithelial cells and cancer cells, while TM's cytotoxicity is selective toward cancer cells.[57, 58] These data suggest that inhibiting multiple sirtuins (SIRT1, 2, and 3) may cause more general cytotoxicity. However, Tenovin-6 is known to have significant off-target effect and JH-T4 may also have off-target effect. Thus, it is not clear whether the increased general cytotoxicity comes from off-target effects or from inhibiting multiple sirtuins. Whether inhibiting all three sirtuins with a non-selective inhibitor will be better than an isoform-selective inhibitor as an anticancer strategy requires further investigation.

Towards addressing this question, here we made two structurally similar sirtuin inhibitors, NH4-6 and NH4-13. The only difference between these two compounds is that NH4-6 contains an amide bond while the corresponding part in NH4-13 is an ester bond. This minimal structural change, however, enables NH4-13 to be SIRT2-selective while NH4-6 inhibits SIRT1, 2, and 3. Thus, NH4-6 and NH4-13 provide a unique opportunity for us to investigate and compare the anticancer activity of inhibiting just SIRT2 versus inhibiting SIRT1, 2, and 3.

## 4.3 Results and Discussion

### 4.3.1 Design of NH4-6 and NH4-13

TM exerted wide anti-cancer effects by selectively inhibiting SIRT2.[38] However, because of its long hydrophobic thiomyristoyl chain, TM possesses poor aqueous solubility, thereby hindering its bioavailability. Thus, we have attempted to improve TM's aqueous solubility in the past few years. Shortening the chain length resulted in loss of SIRT2 selective inhibition.[38] Based on the crystal structure of the SIRT2 in complex with a glucose-conjugated TM (Glucose-TM), we found that the main interactions of SIRT2 and TM originate from a series of hydrogen bonds with the TM peptide backbone and the hydrophobic interaction with the thiomyristoyl chain.[59] From this, we designed two new derivatives with improved aqueous solubility, NH4-6 and NH4-8. At the C-terminal, NH4-8 contains a methyl ester group and inhibited SIRT2 selectively. In contrast, NH4-6, with a trimethylamine functional group connected to the thiomyristoyl lysine via an amide bond, inhibited all three sirtuins, SIRT1-3 (Figure 4.2). Comparing the structures of NH4-6 and NH4-8, we hypothesized that the amide bond of NH4-6 could be crucial for the simultaneous

inhibition of the three sirtuins. To test this hypothesis, we synthesized NH4-13, substituting the amide bond of NH4-6 with an ester bond (Figure 4.2). The synthesis of NH4-13 is shown in Scheme 4.1.

**Table 12. *In vitro* enzymatic $IC_{50}$ values (μM) of NH4-6 and NH4-13.**

| | NH4-6* | NH4-13 |
|---|---|---|
| **SIRT1** | 3 ± 2 | > 50 |
| **SIRT2** | 0.032 ± 0.04 | 0.087 ± 0.01 |
| **SIRT3** | 2.3 ± 0.5 | > 50 |
| **SIRT5** | > 83 | > 83 |
| **SIRT6** | > 83 | > 83 |

*Previously reported values[59]

### 4.3.2 NH4-6 inhibits SIRT1, SIRT2, and SIRT3, while NH4-13 selectively inhibits SIRT2 *in vitro.*

We evaluated NH4-6 and NH4-13 against the deacetylation activities of SIRT1, 2, and 3 *in vitro* using reported methods.[58] NH4-6 inhibited SIRT1, 2 and 3 deacetylases at $IC_{50}$ values of 3, 0.032 and 2.3 μM, respectively.[59] In contrast, NH4-13 only inhibited SIRT2 deacetylase with an $IC_{50}$ value of 0.087 μM, comparable to that of TM and NH4-6. Even at 50 μM, NH4-13 did not inhibit SIRT1 or SIRT3. Also, both NH4-6 and NH4-13 could not inhibit SIRT5 and 6, even at 83 μM. Thus, a simple substitution of NH to O transformed the non-selective inhibitor (NH4-6) into a SIRT2-selective inhibitor (NH4-13) (Table 12).

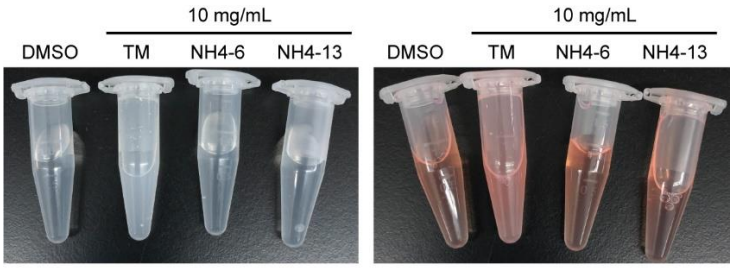


**Figure 4.3 Solubility tests of NH4-6 and NH4-13 in PBS and DMEM.** 50 mM DMSO stock of TM, NH4-6 and NH4-13 were diluted to 10 mg/mL final concentration in 1 x PBS and DMEM media.

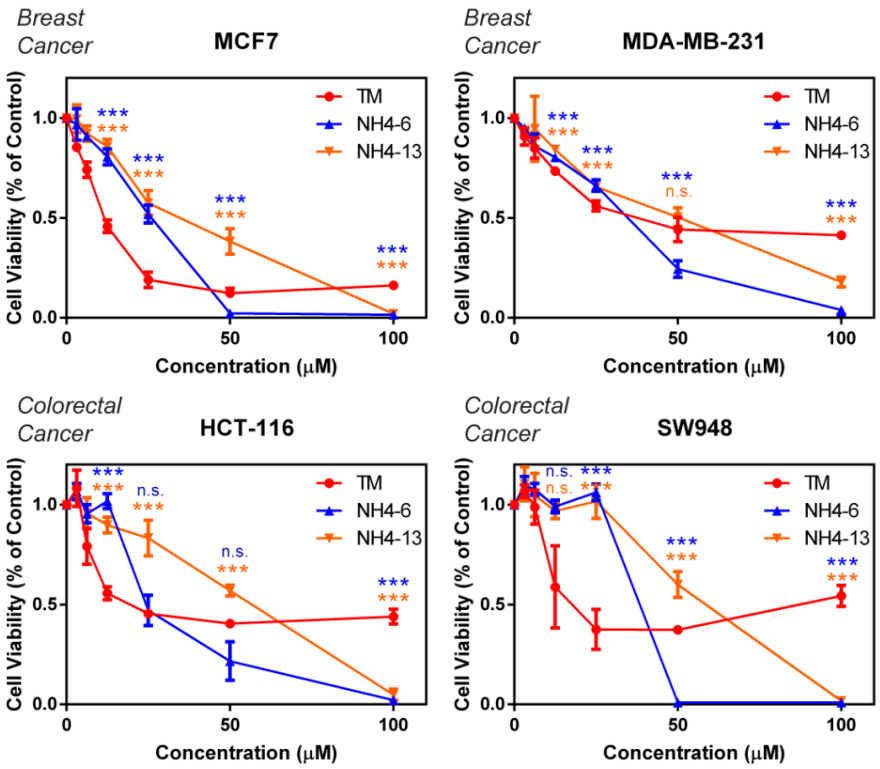


**Figure 4.4 NH4-13 is less toxic than NH4-6 in several cancer cell lines.** Cell viability of MCF7, MDA-MB-231, HCT-116, and SW948 cells were measured after treatment with TM, NH4-6, or NH4-13 for 72 hours.*

* Blue stars indicate the p-value from grouped multiple t-tests between NH4-6 and TM at the indicated concentration (n=3, triplicate at each concentration). Orange stars indicate the p-value from grouped multiple t-tests between NH4-13 and TM at the indicated concentration (n=3, triplicate at each concentration). For these multiple t-tests, the four highest concentrations in the graph were used.

Because of this simple modification, we assumed NH4-13 to possess similar aqueous solubility as NH4-6. To test their aqueous solubilities, both compounds were initially dissolved at 50 mM in DMSO. Then, the dissolved DMSO stock was diluted to 10 mg $mL^{-1}$ in phosphate buffered saline (PBS) and Dulbecco's Modified Eagle Media (DMEM). As expected, both dissolved solutions of NH4-6 and NH4-13 remained transparent, whereas white precipitation formed immediately in the solutions of TM (Figure 4.3). These experiments not only confirmed the enhanced aqueous solubilities of NH4-6 and NH4-13, but also their chemical similarities. With this confirmation, we were able to use NH4-6 and NH4-13 to compare the functional effects of pan-SIRT1-3 inhibition and SIRT2-selective inhibition.

### 4.3.3 NH4-6 shows stronger cytotoxicity than NH4-13.

We compared the effects of TM, NH4-6, and NH4-13 on cellular growth in MCF7, MDA-MB-231, HCT-116, and SW948 cancer cells. The cells were treated with various concentrations of the inhibitors for 72 hours, and the proliferations were quantified using Cell-Titer Blue. In all four cell lines, at lower concentrations, TM treatment showed stronger cytotoxicity than NH4-6 and NH4-13. However, as the concentration increased, TM's effect plateaued out and 50 μM of TM had similar effects with 100 μM of TM. At 50 μM, NH4-6 exceeded TM's effectiveness and killed essentially all the cells at 100 μM. At 50 μM, NH4-13 exerted a weaker effect than TM, but eventually killed all the cells at 100 μM (Figure 4.4). In addition to the breast and colorectal cancer cell lines tested above, we have tested the cytotoxicity of TM, NH4-6, and NH4-13 against various cancer and normal cell lines, including

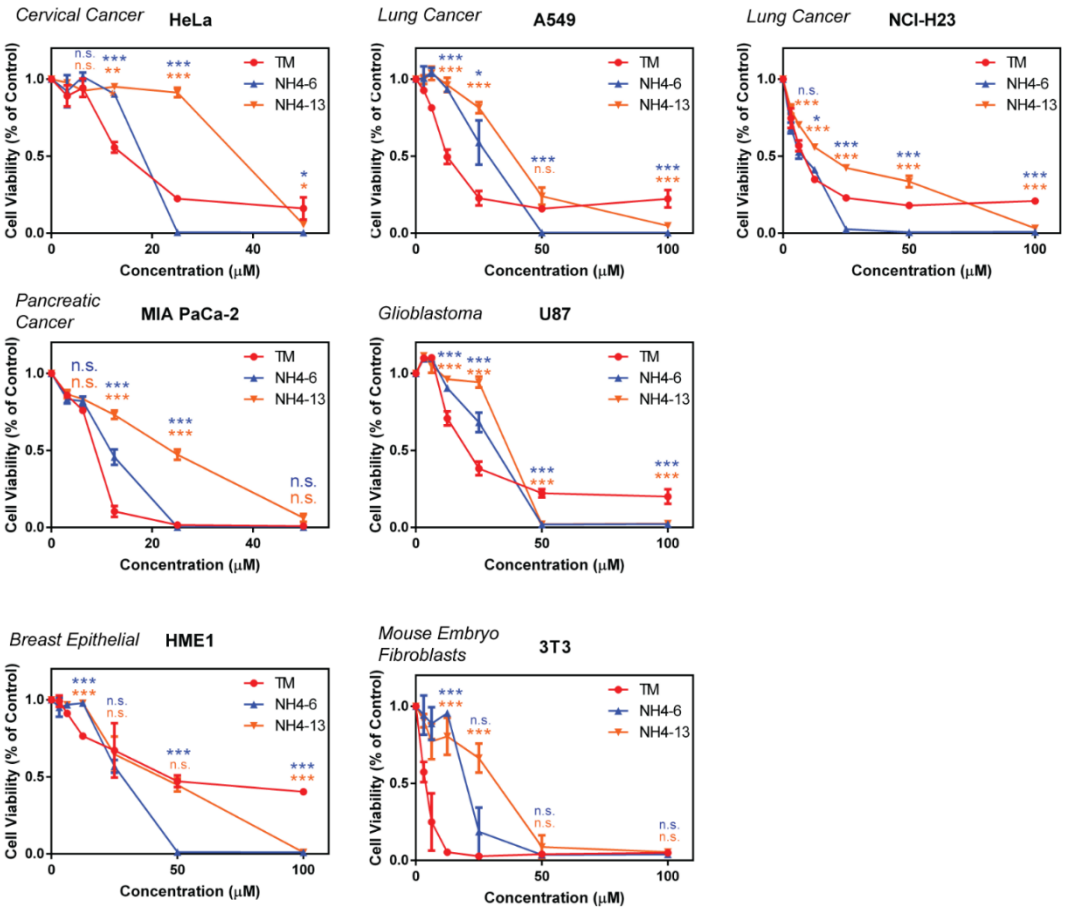


**Figure 4.5 NH4-13 is less toxic than NH4-6 in cervical, lung, pancreatic cancer cells, breast epithelial cells, and mouse embryo fibroblasts.** Cell viability of HeLa, A549, NCI-H23, MIA PaCa-2, U87, HME1, and 3T3 cells were measured after treatment with TM, NH4-6, or NH4-13 for 72 hours.**

**Blue stars indicate the p-values from grouped multiple t-tests between NH4-6 and TM at the indicated concentration (n=3, triplicate at each concentration). Orange stars indicate the p-value from grouped multiple t-tests between NH4-13 and TM at the indicated concentration (n=3, triplicate at each concentration). * $p < 0.05$, ** $p < 0.01$, *** $p < 0.001$, n.s., not significant. For these multiple t-tests, the four highest concentrations in the graph were used.

cervical, lung, pancreatic, breast epithelial, and mouse embryo fibroblasts (Figure 4.5). Similar trends were observed in these cell lines.

The observation that NH4-6 and NH4-13 showing weaker effects in lower concentrations, but stronger effects in higher concentrations compared to TM can be explained by their increased solubility but decreased permeability. Charged groups often portray weaker cellular permeability. Thus, at lower concentrations, because of the charged trimethylamine, NH4-6 and NH4-13 may not efficiently pass-through membranes. However, at higher concentrations, with higher aqueous solubility, more NH4-6 and NH4-13 could remain dissolved, resulting in increased cytotoxicity.

**Table 13. Calculated concentrations (µg/million cells) of TM, NH4-6, and NH4-13 detected from MCF7 cells.**

| | Calculated Concentrations (µg/million cells) | |
|---|---|---|
| | 20 µM treatment | 40 µM treatment |
| **TM** | 0.20 | 0.28 |
| **NH4-6** | 0.092 | 0.23 |
| **NH4-13** | 0.12 | 0.19 |

To confirm this, after treating MCF7 cells with 20 and 40 µM of inhibitors for 6 hours, we carefully washed the cells and extracted small molecules from cells with ice-cold methanol. Then, the extraction was analyzed by liquid chromatography-mass spectrometry (LC-MS) to detect the amounts of the compounds that had entered the cells. The amounts of TM were 0.20 and 0.28 µg/million cells after 20 and 40 µM treatments, respectively. As the difference was quite minimal, this explained why

TM's cytotoxicity flattened out with increasing concentrations. After 20 and 40 μM treatments, 0.092 and 0.23 μg/million cells of NH4-6 and 0.12 and 0.19 μg/million cells of NH4-13 were detected, respectively (Table 13). At 40 μM, similar concentrations of NH4-6 and TM were detected. The cellular concentration trend of NH4-6 and TM can explain the observed cytotoxicity trends of NH4-6 and TM. At lower concentrations, less NH4-6 was able to pass through membranes, due to its positively charged triethylamine, lowering its cytotoxicity. In contrast, at higher concentrations, more NH4-6 could be dissolved and enter the cells, increasing its cytotoxicity.

Next, we compared the cytotoxicity of NH4-6 and NH4-13 to see the differences between the pan-SIRT1-3 and SIRT2-selective inhibitors. Generally, NH4-13 showed weaker cytotoxicity than NH4-6. For instance, in all four cell lines (MCF7, MDA-MB-231, HCT-116, and SW948), 50 μM of NH4-13 showed effects about twice weaker than that of NH4-6. At 100 μM, NH4-13 could kill most of the cells, reaching a similar efficacy level as NH4-6 (Figure 4.4). This trend was also observed in other cell lines, as well (Figure 4.5). Interestingly, even though the cellular concentrations of NH4-6 and NH4-13 were similar when applied at 40 μM (Table 7), the cytotoxicity of NH4-6 was stronger than NH4-13. Given that their structures and chemical properties are similar, we hypothesized that such cytotoxicity disparity comes from the different sirtuin inhibitory actions. In other words, NH4-6 exerted stronger cytotoxicity because it could concurrently inhibit all three sirtuins, SIRT1, 2, and 3. Meanwhile, NH4-13 exerted milder cytotoxicity, as it could only inhibit SIRT2. Another possibility was that NH4-13 may be less effective at inhibiting SIRT2. However, as will be

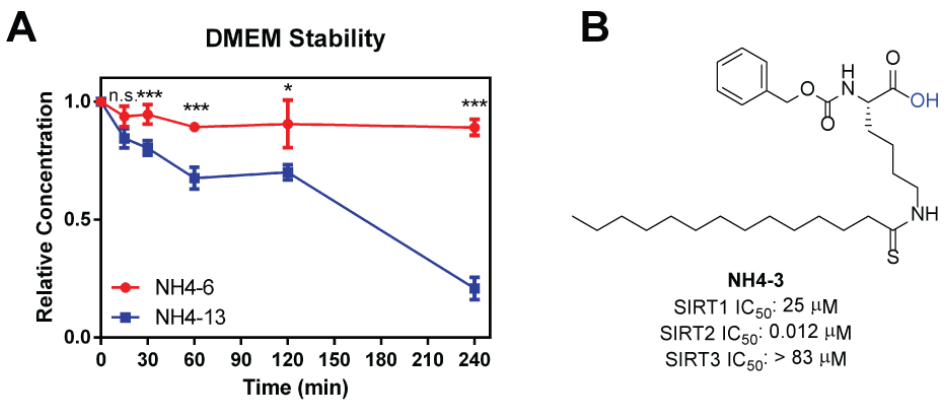


**Figure 4.6 The stability of NH4-6 and NH4-13 in Dulbecco's Modified Eagle Medium (DMEM).** (A) 150 μM of NH4-6 and NH4-13 in DMEM was kept shaking at 37 °C and collected at the indicated incubation time. The detection of the compound peaks was done by high-performance liquid chromatography (HPLC).***

***Black stars indicate the p-values from grouped multiple t-tests between NH4-6 and NH4-13 at the indicated concentration (n = 3, triplicate at each concentration). * $p < 0.05$, *** $p < 0.001$, n.s., not significant. (B) Structure of NH4-3 and its *in vitro* enzymatic $IC_{50}$ values.

demonstrated below, NH4-6 and NH4-13 seemed to inhibit SIRT2 similarly based on tubulin acetylation.

Since an ester bond is less stable and prone to hydrolysis in cells, we tested whether the amide bond of NH4-6 and ester bond of NH4-13 affect the stability of the compounds in Dulbecco's Modified Eagle Medium (DMEM) media with 10% fetal bovine serum (FBS) (Figure 4.6). NH4-6 with the amide bond maintained its structure, even after a 4-hour incubation. However, NH4-13 with the ester bond at the 4-hour ester bond at the 4-hour incubation was significantly hydrolyzed into NH4-3 without the trimethylamine moiety (Figure 4.6B). This stability difference may contribute to the lower cytotoxicity of NH4-13 compared to NH4-6 in the cell proliferation assays. However, we believe this contribution may be minimal as we identified that the

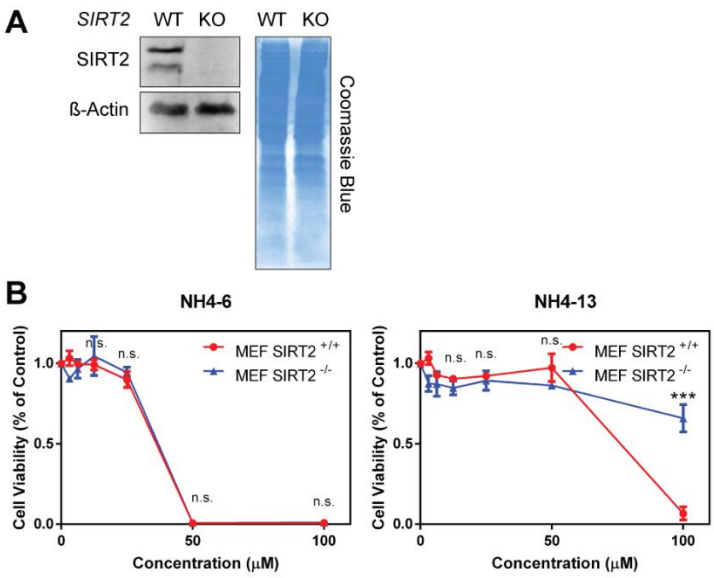


**Figure 4.7 NH4-6 show no difference in cytotoxicity between *SIRT2* WT and KO MEF cells while NH4-13 is less cytotoxic in *SIRT2* KO than WT MEF cells.** (A) Immunoblots of SIRT2, showing the Sirt2 levels in MEF *SIRT2* WT and KO cells. (B) Cell viability of *SIRT2* WT and KO MEF cells were measured after treatment with NH4-6 or NH4-13 for 72 hours.****

****Black stars indicate the p-values from grouped multiple t-tests between $SIRT2^{+/+}$ and $SIRT2^{-/-}$ MEF at the indicated concentration (n=3, triplicate at each concentration). *** $p < 0.001$, n.s., not significant. For these multiple t-tests, the four highest concentrations in the graph were used.

hydrolysis product NH4-3 is also a selective SIRT2 inhibitor with $IC_{50}$ of 25 μM and 0.012 μM for SIRT1 and SIRT2, respectively. Thus, even if NH4-13 gets hydrolyzed into NH4-3, SIRT2 selective inhibition will be maintained.

To further confirm whether the cytotoxicity of NH4-13 originates from single inhibition of SIRT2, and the cytotoxicity of NH4-6 was due to pan SIRT1-3 inhibition, we treated SIRT2 wild-type and knockout mouse embryo fibroblast (MEF) cell lines with NH4-6 and NH4-13 for 72 hours and checked the cell proliferation using Cell-Titer Blue (Figure 4.7). For NH4-6, the pan-SIRT1-3 inhibitor, there was

no difference in the cytotoxicity curve between the SIRT2 WT and KO MEF cell lines, suggesting that the cytotoxicity of NH4-6 may mainly come from the simultaneous inhibition of SIRT1 and SIRT3. In contrast, for NH4-13, there was only a significant cytotoxicity effect in SIRT2 WT MEF cells at 100 μM. At the same concentration, no severe cytotoxicity was observed in SIRT2 KO MEF cells. This difference indicates that the cytotoxicity of NH4-13 mainly comes from the selective inhibition of SIRT2 (Figure 4.7B).

We also co-incubated NH4-6 and NH4-13 with 50 μM of EX-527, a SIRT1-selective inhibitor, and monitored the cell viability of MDA-MB-231 cells (Figure 4.8). EX-527 at 50 μM had only minor inhibition on cell viability. The co-treatment of NH4-6 and EX-527 affected the cell viability similarly to the treatment of NH4-6 alone. As NH4-6 already inhibits SIRT1, the addition of EX-527 was expected not to produce further effects. In contrast, the co-incubation of NH4-13 and EX-527 resulted in stronger cytotoxicity than the incubation with only NH4-13. This increase verified that NH4-13 only inhibits SIRT2 and the combination with EX-527 increases the cytotoxicity. This also provided additional support that the mild cytotoxicity of NH4-13 may come from its selective SIRT2 inhibition in cells.

### 4.3.4 NH4-6 inhibits SIRT1, SIRT2, and SIRT3, while NH4-13 selectively inhibits SIRT2 in cells.

To examine sirtuin inhibition effects of these compounds in cells, we examined acetylation levels of known substrates of SIRT1, 2, and 3. First, we looked at the acetylation level of p53 (K382), a SIRT1 substrate.[60] Because p53 can also be

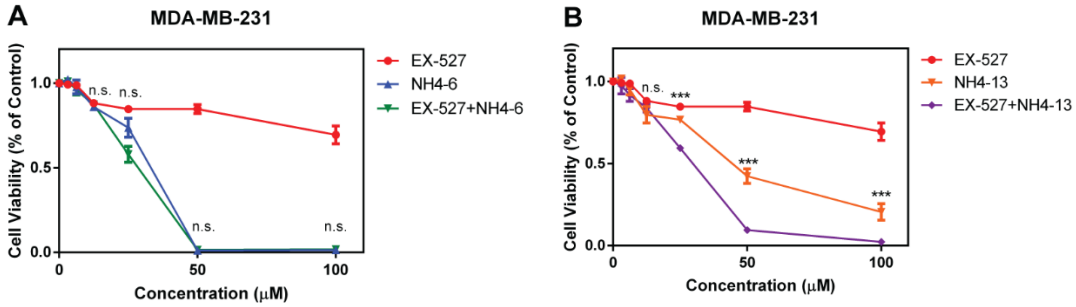


**Figure 4.8 The combination of EX5-27 with NH4-13 does not increase cytotoxicity, while combination of EX-527 with NH4-13 increases the cytotoxicity.** (A) Cell viability of MDA-MB-231 cells after treatment with different concentrations of NH4-6 and with or without 50 μM of EX-527 for 72 hours. The cell viability after treatment with different concentrations of EX-527 was also shown as a reference. Black stars indicate the p-value from grouped multiple t-tests between NH4-6 and EX-527+NH4-6 (n=3, triplicate at each concentration). (B) Cell viability of MDA-MB-231 cells were measured after treatment with different concentrations of NH4-13 and with or without 50 μM of EX-527 for 72 hours. The cell viability after treatment with different concentrations of EX-527 was also shown as a reference.[+]

[+]Black stars indicate the p-value from grouped multiple t-tests between NH4-13 and EX-527+NH4-13 (n=3, triplicate at each concentration). *** $p < 0.001$, n.s., not significant. For these multiple t-tests, the four highest concentrations in the graph were used.

deacetylated by zinc-dependent HDACs, we treated MCF7 cells with Trichostatin A, a class I and II HDAC inhibitor, and the indicated sirtuin inhibitors to detect the effect of SIRT1 inhibition.[61, 62] Using EX-527 as a positive control, we observed a clear increase in acetylated p53, in accordance with previous reports.[63] With an in vitro $IC_{50}$ value of 3 μM against SIRT1, 100 μM of NH4-6 increased the acetylation level of p53 in MCF7 cells. This confirmed that NH4-6 could inhibit SIRT1 in living cells. Consistent with *in vitro* $IC_{50}$ values of TM (> 83 μM) and NH4-13 (50 μM) for

SIRT1, either compound did not increase the acetylation level of p53 at 100 μM (Figure 4.9A).

Next, we examined changes in acetylation levels of α-tubulin, a previously reported SIRT2 target, through immunofluorescence after treating cells with TM, NH4-6, and NH4-13 for 6 hours.[64] We had chosen immunofluorescence imaging, instead of immunoblots, because several reports failed to observe a significant increase in acetyl-α tubulin with the treatment of SIRT2 inhibitors in cells via western blots, but were able to detect acetylation increases via immunofluorescence.[49, 65] At 10, 25, and 50 μM, TM treatment increased the acetylation level of α-tubulin significantly, compared to the DMSO control treatment. For these TM-treated samples, we also had detected a dose-dependent increase of acetyl-α-tubulin. For both NH4-6 and NH4-13 at 10 and 25 μM, there was no increase in the acetylation level. However, at 50 μM, NH4-6 and NH4-13 increased tubulin acetylation levels, equivalent to that of TM treatment (Figure 4.9B, 4.10). This is consistent with the cell proliferation and permeability assays, in which these two compounds showed weaker SIRT2 inhibition at lower concentrations, due to their low permeability, but their effects increased at higher concentration due to better solubility. Based on the increased acetylation levels of α-tubulin, NH4-6 and NH4-13 inhibited SIRT2 similarly in cells at a high concentration.

To assess the in-cell inhibition of SIRT3, we monitored acetylation levels of IDH2, a previously reported SIRT3 target.[66, 67] We treated MDA-MB-231 cells that express a flag-tagged IDH2 in a doxycycline-inducible manner with the inhibitors for 6 hours. Then, the flag-tagged IDH2 was pulled down by immunoprecipitation, and

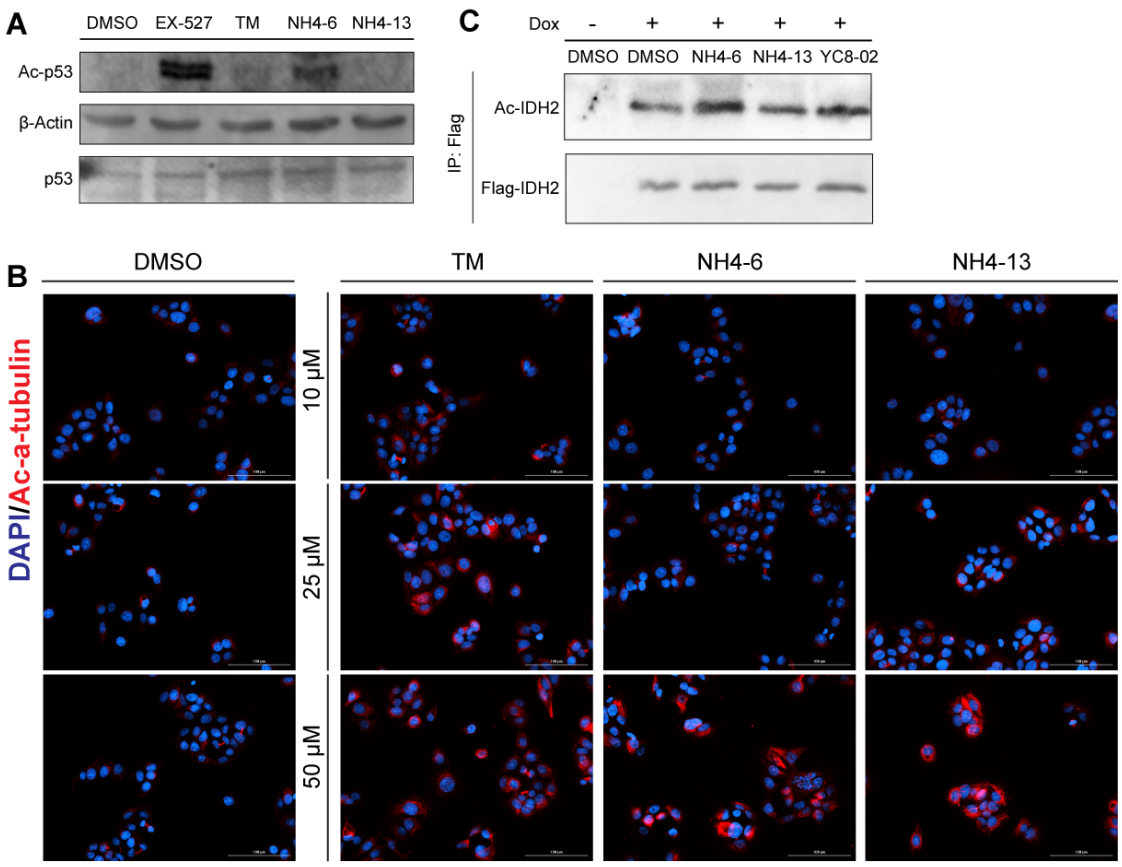


**Figure 4.9 NH4-6 simultaneously inhibited SIRT1, 2 and 3 while NH4-13 selectively inhibits SIRT2 in cells.** (A) Immunoblots for the acetylation of p53 (K382) in MCF7 cells treated with control (DMSO) or indicated concentrations of EX-527, TM, NH4-6, or NH4-13 for 6 hours. (B) Immunofluorescence detection of acetylated α-tubulin (K40) in MCF7 cells treated with control or indicated concentrations of TM, NH4-6, or NH4-13 for 6 hours. (C) Immunoblots for acetylated IDH2 after immunoprecipitation of Flag-tagged IDH2 in MDA-MB-231 cells treated with indicated concentrations of YC8-02, TM, NH4-6, or NH4-13 for 6 hours.

the acetylation level was detected using an Ac-IDH2 antibody. NH4-13 did not increase the acetylation level of IDH2, which is consistent with its SIRT3 deacetylase $IC_{50}$ values greater than 50 μM. Meanwhile, as expected, 50 μM of YC8-02, a previously reported mitochondria-targeting SIRT3 inhibitor, increased the acetylation level of IDH2 in cells (Figure 4.9C). Consistent with its SIRT3 deacetylase $IC_{50}$ of 2.3 μM, NH4-6 at 100 μM inhibited SIRT3 in cells. Based on the immunoblot, 100 μM of NH4-6 produced higher IDH2 acetylation level than 40 μM of YC8-02 (due to severe cytotoxicity, the cells were only treated with 40 μM of YC8-02, while a higher concentration, 100 μM, of NH4-6 was used in the experiment). Overall, the IDH2 acetylation result suggests that NH4-6 could effectively inhibit SIRT3, while NH4-13 could not.

By monitoring the acetylation levels of p53 (SIRT1), α-tubulin (SIRT2) and IDH2 (SIRT3), we confirmed that in cells, NH4-13 inhibits SIRT2 selectively, while NH4-6 simultaneously inhibits SIRT1, 2, and 3. Thus, the stronger toxicity of NH4-6 likely comes from its pan-sirtuin inhibition, and the milder toxicity of NH4-13 likely comes from its SIRT2-selective inhibition.

### 4.3.5 NH4-6 and NH4-13 show similar anticancer effect, but NH4-6 causes over-toxicity in mice.

Then, we assessed the bioavailability of these two compounds through pharmacokinetics studies. After treating the mice with NH4-6 or NH4-13 (in 10% DMSO and 90% PBS) for 30 minutes, we collected blood and extracted the compounds for detection by LC-MS. As expected, clear traces of both NH4-6 and NH4-13 were observed in the serum samples collected after 30 minutes (Figure

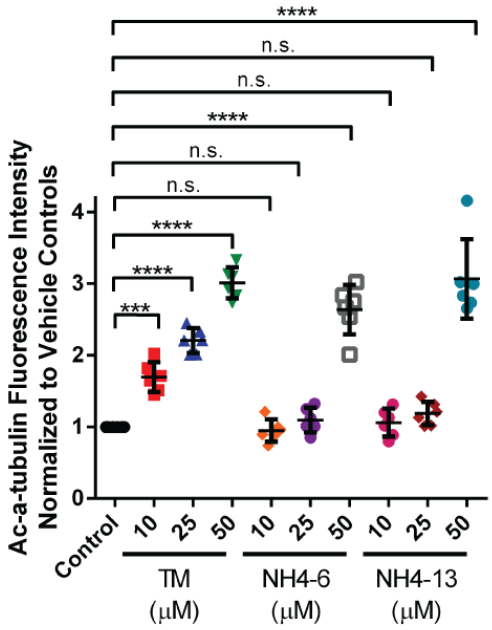


**Figure 4.10 Quantification of acetyl α-tubulin immunofluorescence intensity from Figure 4.9.** Acetyl α-tubulin fluorescence intensity was normalized by DAPI signal, and the relative acetyl α-tubulin level of the vehicle control was set to 1.0.[++]

[++]Black stars indicate p-value from the two-tailed Student's t-test (n=6). *** $p < 0.001$, **** $p < 0.0005$, n.s., not significant.

4.11A). The serum concentrations of NH4-6 and NH4-13 decreased in later time points. The clearance rate of NH4-13 was faster than that of NH4-6 (Figure 4.11B).

After confirming that NH4-6 and NH4-13 can be detected in the serum, we tested their toxicities by daily injection of different dosages to the NSG mice for five days and monitoring their body weights, behaviors, and physical appearances. At 30 and 50 mg/kg, NH4-6 showed severe toxicities after the first day of injection. At 50 mg/kg, all mice lost about 20% of their body weight in 24 hours. At both dosages, most of the treated mice showed very little physical activity or grooming. After the second and third days, most of the mice had to be sacrificed due to the severe toxicity.

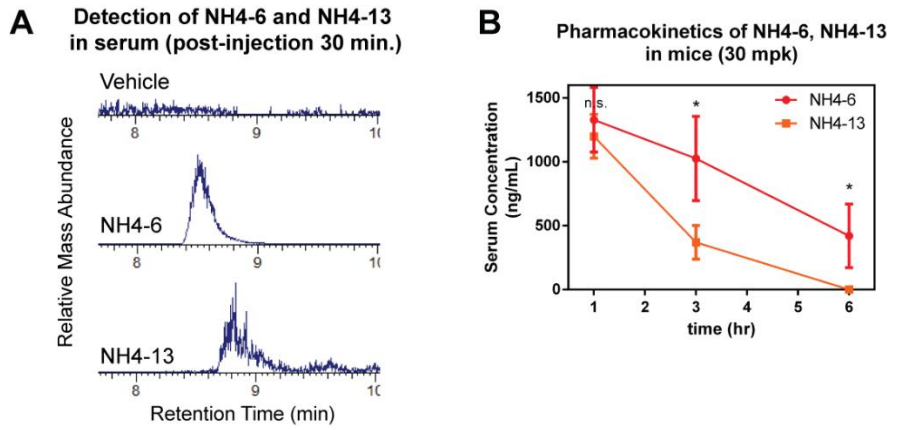


**Figure 4.11 The stability of NH4-6 and NH4-13 in mice.** (A) Detection of NH4-6 and NH4-13 in mice serum collected after 30 minutes of intraperitoneal injection at 50 mg/kg injection. (B) Pharmacokinetics of NH4-6 and NH4-13 in mice. NH4-6 and NH4-13 (dissolved in 10% DMSO, 90% PBS) was injected at 30 mg/kg. At the indicated time, blood was taken. After isolating serum and extracting the small molecule with methanol, the samples were injected into high-performance liquid chromatography for detection.[+++]

[+++]Black stars indicate the p-value from grouped multiple t-tests between NH4-6 and NH4-13 at the indicated concentration (n = 3 for each concentration). * $p < 0.05$, n.s., not significant.

In contrast, at 30 and 50 mg/kg dosages, NH4-13 did not cause severe weight loss or decrease in physical activity. The toxicity discrepancy between the two compounds could be due to the different sirtuin inhibition profile and clearance rate.

After the initial acute toxicity studies, we tested the two inhibitors' antitumor effects in a tumor xenograft mouse model. A colon cancer cell line, HCT-116, was subcutaneously injected into immunocompromised male NSG mice. Once the tumors had formed and grown to 100-200 $mm^3$, the mice were randomly divided into two groups and treated by IP injection of inhibitors or the control vehicle (10% DMSO,

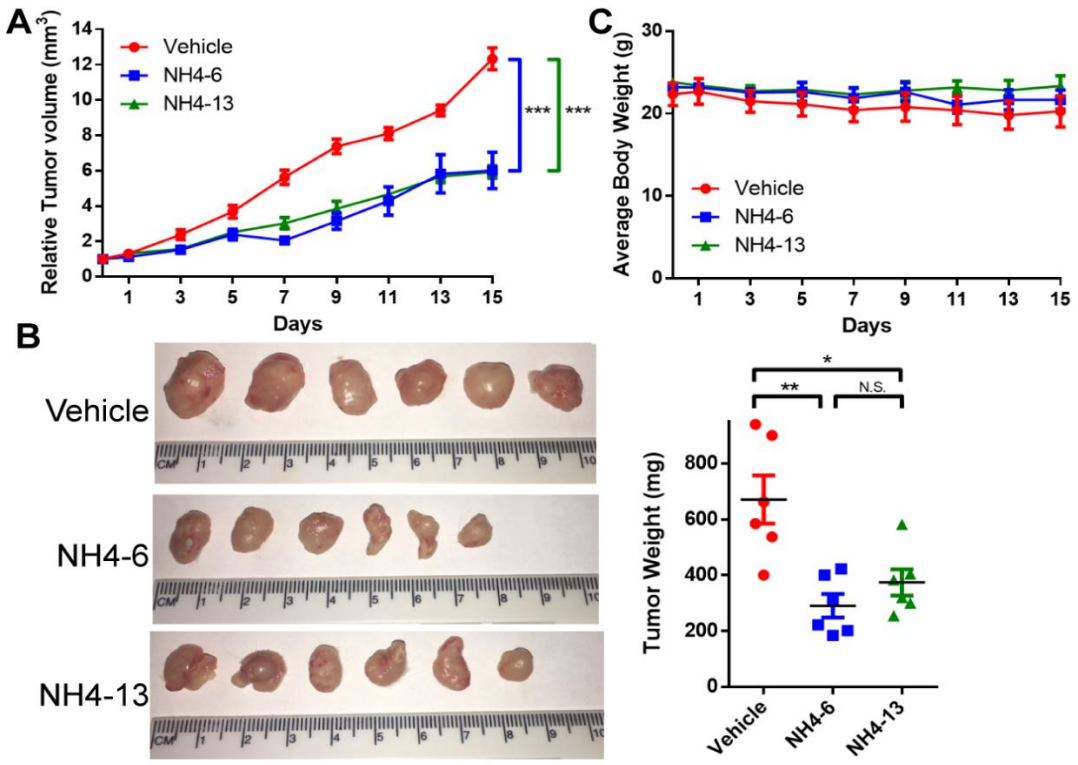


**Figure 4.12 NH4-6 and NH4-13 significantly impaired tumor growth in HCT-116 tumor xenograft.** (A) Tumor volume over time for NH4-6 and NH4-13 (30 mg/kg) treated mice relative to vehicle treated mice. NSG mice injected with HCT-116 human colorectal cancer cells were treated every other day for 15 days. (*** P value = 0.00074 (NH4-6), 0.000017 (NH4-13), Two-tailed Student's t-test, n = 3 mice per group, n = 6 tumors per group). (B) Tumor images and quantification of tumor weight of HCT-116 xenograft mice treated with 30 mg/kg NH4-6, NH4-13, or vehicle control for 15 days. (** P value = 0.0051 (NH4-6), * P value = 0.018 (NH4-13), Two-tailed Student's t-test, n = 3 mice per group, n = 6 tumors per group). (C) Average body weight of mice treated with 30 mg/kg of NH4-6, NH4-13, or vehicle control for 15 days. No significant changes in body weight over time were observed. N = 3 mice per group. ‡

‡ Data shown in Figures A, B, C, are the mean values ± standard deviation.

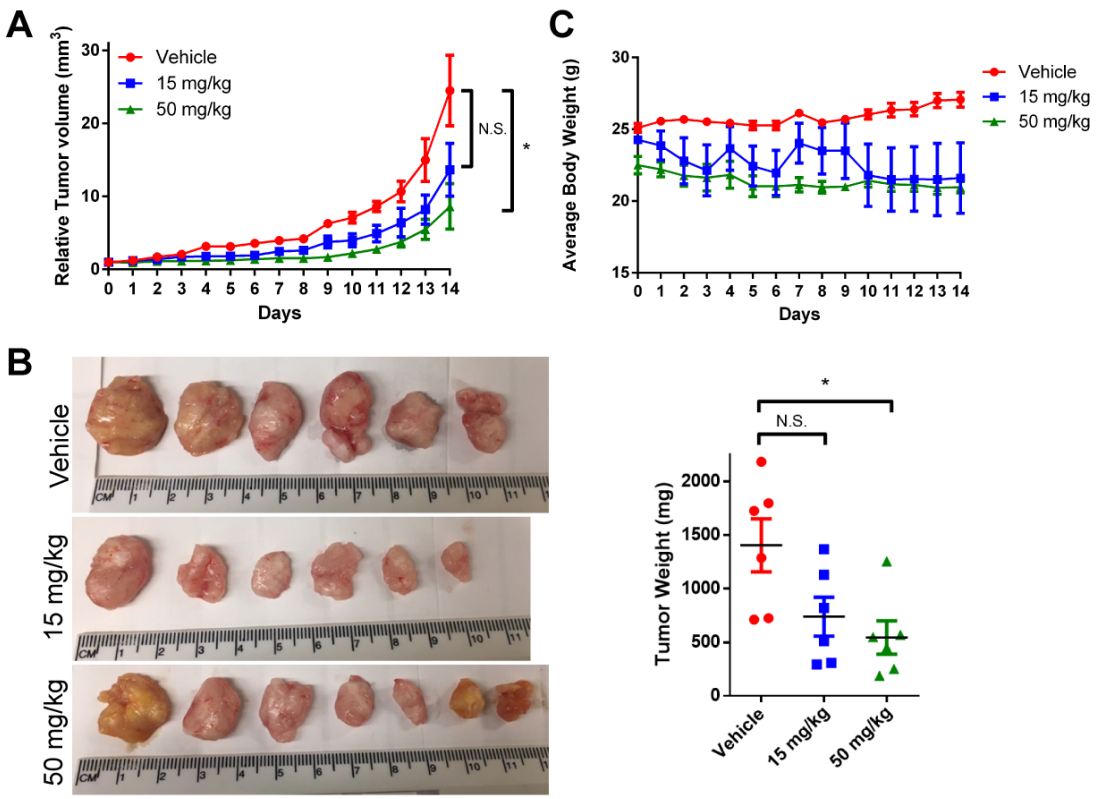


**Figure 4.13 Effects of NH4-13 in HCT-116 tumor xenograft mice models at 0, 15, and 50 mg/kg dosages.** (A) Tumor volume over time for NH4-13 (0, 15, and 50 mg/kg) treated mice. NSG mice injected with HCT-116 human colorectal cancer cells were treated five times per week for 15 days. (* P value = 0.032, Two-tailed Student's t-test, n=3 mice per group, n=6 tumors per group). (B) Representative tumor images and quantification of tumor weight of HCT-116 xenograft mice treated with NH4-13. (* P value = 0.0018, Two-tailed Student's t-test, n=3 mice per group, n=6 tumors per group). (C) Average body weight of mice treated with different dosages of NH4-13 for 15 days. No significant changes in body weight over time were observed. n=3 mice per group.

‡ ‡Data shown in Figures A, B, C are the mean values ± standard deviation.

90% 1X PBS). Male mice were specifically chosen, as the recent report demonstrates higher incidence in male.[68]

Due to the toxicity from NH4-6, we injected 30 mg/kg of NH4-6 or NH4-13 every other day. Mice were able to tolerate the decreased NH4-6 injection frequency at 30 mg/kg. NH4-6 or NH4-13 treatment significantly impeded tumor progression, as seen through tumor volumes and weights. At the end of the study, compared to that of the vehicle-treated mice, the tumor volumes of mice treated with NH4-6 or NH4-13 were significantly reduced by ~50% (Figure 4.12A). The average tumor weights of NH4-6 and NH4-13 treated mice were 311 and 383 mg, respectively, while the average tumor weight for vehicle control was 662 mg (Figure 4.12B). Hence, overall tumor size and weight were reduced in mice by NH4-6 and NH4-13. Furthermore, between NH4-6 and NH4-13 samples, there was no clear difference in tumor volumes or weights (Figure 4.12A, B). At this dose, we did not see any major weight loss in either treatment group (Figure 4.12C). Based on this experiment, despite their differences in sirtuin inhibitory characteristics and clearance rate, NH4-6 and NH4-13 portrayed similar efficacies in tumor xenograft studies at the same dosage.

Because there was no observed toxicity from the previous experiment, we wanted to assess the efficacy of NH4-13 by injecting a higher dosage in NSG mice. We conducted the same experimental procedure described above but used 15 and 50 mg/kg of NH4-13. We chose one lower and one higher dosage to see if the effect of NH4-13 was dose-dependent in mice. In both dosages, we observed differences in tumor volumes and weights. Tumor volumes and tumor weights from mice treated with 15 mg/kg of NH4-13 were significantly reduced compared to the vehicle control

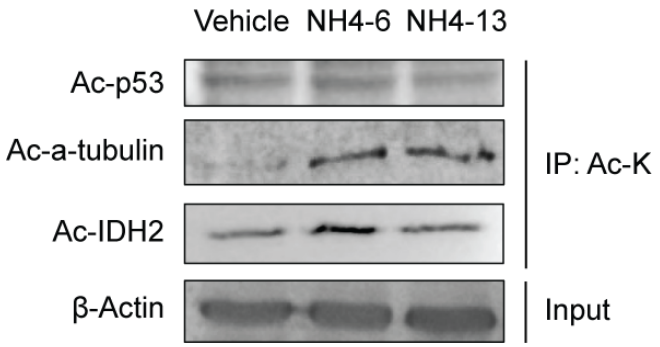


**Figure 4.14 SIRT1/2/3 inhibition assessment in tumors.** Immunoblots for acetylated p53, a-tubulin, and IDH2 after immunoprecipitation (with a pan-acetyllysine antibody) of proteins in HCT-116 tumors treated with NH4-6 and NH4-13.

(Figure 4.13). The higher dosage of 50 mg/kg of NH4-13 showed even stronger effects in tumor growth than the lower dosage of 15 mg/kg. Compared to that of the vehicle control, tumor volumes of the 50 mg/kg treatment were about three times smaller (Figure 4.13A). The average tumor weight from the 50 mg/kg treatment was about 544 mg, while those from the vehicle control and the 15 mg/kg treatment were 1418 and 731 mg respectively (Figure 4.13B). Furthermore, the 15 mg/kg treatment failed to achieve statistical significance, but the 50 mg/kg treatment did. Throughout the xenograft experiment, the mice in both dosages looked normal (their body weights were stable, Figure 4.13C, and there were no behavioral changes). The individual tumor xenograft study of NH4-13 showed that pharmacological inhibition of SIRT2 specifically has strong anticancer properties in mice without much toxicity issues.

To confirm whether NH4-6 and NH4-13 inhibited SIRT1-3 in the tumors, we homogenized the collected tumors and assessed the acetylation levels of p53 (SIRT1 substrate), α-tubulin (SIRT2 substrate), and IDH2 (SIRT3 substrate) by immunoblots

after immunoprecipitation using pan-acetyllysine antibody beads (Figure 4.14). For acetyl-p53, we have not observed any significant increase from tumors treated with NH4-6 and NH4-13. This was expected as p53 is a substrate for HDACs and in cellular studies we had to co-treat the cells with Trichostatin A, an HDAC inhibitor, to detect the increase in acetylation level of p53 by SIRT1 inhibitors. For the tumor xenograft, since we only treated the mice with NH4-6 and NH4-13, we expected to see no changes in acetyl-p53. Both NH4-6 and NH4-13 had increased the acetylated levels of α-tubulin, thereby suggesting effective SIRT2 inhibition in tumors by NH4-6 and NH4-13. Lastly, only NH4-6 had increased the acetylation level of IDH2, while NH4-13 did not induce any change. This indicates that only NH4-6 could inhibit SIRT3 in tumors. Overall, these results were in accordance with the cellular data and show that NH4-6 simultaneously inhibited SIRT2 and 3, and NH4-13 selectively inhibited SIRT2 in the tumor xenograft mice study.

## 4.4 Conclusion

Overall, our comparison studies showed that NH4-6, a pan-SIRT1-3 inhibitor, showed stronger cytotoxicity than NH4-13, a SIRT2-selective inhibitor in cancer cells. However, in vivo, even though NH4-6 showed slightly better pharmacokinetics, both NH4-6 and NH4-13 equivalently impaired tumor growth. Furthermore, high dosage of NH4-6 treatments caused severe toxicity issues, which is likely due to the simultaneous inhibition of SIRT1, 2, and 3. Thus, it would be beneficial to develop SIRT2-selective inhibitors. Furthermore, as pan-SIRT1-3 inhibitors and SIRT2-selective inhibitors show similar effects in vivo, the study suggests that the anticancer effect is mainly from SIRT2 inhibition in mice. Of course, this may be cancer cell

specific and in other cancer cell lines, such as DLBCL cells, inhibiting SIRT3 produces the beneficial anticancer effect.[43] Based on our study presented here, it would also be interesting to investigate the effects of SIRT3-selective inhibition versus pan-SIRT1-3 inhibition in DLBCL. Our study further bolsters the need for additional research focus on sirtuin isoform-selective inhibitors for future biological studies and anticancer applications.

## 4.5 References


1. Sauve, A. A., Wolberger, C., Schramm, V. L., and Boeke, J. D. (2006) The biochemistry of sirtuins, *Annu. Rev. Biochem. 75*, 435-465.

2. Sauve, A. A., Celic, I., Avalos, J., Deng, H., Boeke, J. D., and Schramm, V. L. (2001) Chemistry of gene silencing: the mechanism of NAD+-dependent deacetylation reactions, *Biochemistry 40*, 15456-15463.

3. Feldman, J. L., Dittenhafer-Reed, K. E., Kudo, N., Thelen, J. N., Ito, A., Yoshida, M., and Denu, J. M. (2015) Kinetic and Structural Basis for Acyl-Group Selectivity and NAD <sup>+</sup> Dependence in Sirtuin-Catalyzed Deacylation, *Biochemistry 54*, 3037-3050.

4. Blank, M. F., Chen, S., Poetz, F., Schnolzer, M., Voit, R., and Grummt, I. (2017) SIRT7-dependent deacetylation of CDK9 activates RNA polymerase II transcription, *Nucleic Acids Res. 45*, 2675-2686.

5. Tao, R., Xiong, X., DePinho, R. A., Deng, C. X., and Dong, X. C. (2013) FoxO3 transcription factor and Sirt6 deacetylase regulate low density lipoprotein (LDL)-cholesterol homeostasis via control of the proprotein convertase subtilisin/kexin type 9 (Pcsk9) gene expression, *J Biol Chem 288*, 29252-29259.

6. Wang, F., Nguyen, M., Qin, F. X., and Tong, Q. (2007) SIRT2 deacetylates FOXO3a in response to oxidative stress and caloric restriction, *Aging Cell 6*, 505-514.

7. Du, C., Lin, X., Xu, W., Zheng, F., Cai, J., Yang, J., Cui, Q., Tang, C., Cai, J., Xu, G., and Geng, B. (2019) Sulfhydrated Sirtuin-1 Increasing Its Deacetylation Activity Is an Essential Epigenetics Mechanism of Anti-Atherogenesis by Hydrogen Sulfide, *Antioxid Redox Signal 30*, 184-197.

8. Jing, H., and Lin, H. (2015) Sirtuins in Epigenetic Regulation, *Chem. Rev. 115*, 2350-2375.

9. Kosciuk, T., Wang, M., Hong, J. Y., and Lin, H. (2019) Updates on the epigenetic roles of sirtuins, *Curr. Opin. Chem. Biol. 51*, 18-29.

10. Jang, J., Huh, Y. J., Cho, H. J., Lee, B., Park, J., Hwang, D. Y., and Kim, D. W. (2017) SIRT1 Enhances the Survival of Human Embryonic Stem Cells by Promoting DNA Repair, *Stem Cell Reports 9*, 629-641.

11. Zhang, M., Zhang, Q., Hu, Y., Xu, L., Jiang, Y., Zhang, C., Ding, L., Jiang, R., Sun, J., Sun, H., and Yan, G. (2017) miR-181a increases FoxO1 acetylation and promotes granulosa cell apoptosis via SIRT1 downregulation, *Cell Death Dis. 8*, e3088.

12. Hu, J., Jing, H., and Lin, H. (2014) Sirtuin inhibitors as anticancer agents, *Future Med. Chem. 6*, 945-966.

13. Herskovits, A. Z., and Guarente, L. (2013) Sirtuin deacetylases in neurodegenerative diseases of aging, *Cell Res. 23*, 746-758.

14. Barber, M. F., Michishita-Kioi, E., Xi, Y., Tasselli, L., Kioi, M., Moqtaderi, Z., Tennen, R. I., Paredes, S., Young, N. L., Chen, K., Struhl, K., Garcia, B. A., Gozani, O., Li, W., and Chua, K. F. (2012) SIRT7 links H3K18 deacetylation to maintenance of oncogenic transformation, *Nature 487*, 114-118.

15. Seo, K. S., Park, J. H., Heo, J. Y., Jing, K., Han, J., Min, K. N., Kim, C., Koh, G. Y., Lim, K., Kang, G. Y., Uee Lee, J., Yim, Y. H., Shong, M., Kwak, T. H., and Kweon, G. R. (2015) SIRT2 regulates tumour hypoxia response by promoting HIF-1alpha hydroxylation, *Oncogene 34*, 1354-1362.

16. Avalos, J. L., Bever, K. M., and Wolberger, C. (2005) Mechanism of sirtuin inhibition by nicotinamide: altering the NAD(+) cosubstrate specificity of a Sir2 enzyme, *Mol. Cell 17*, 855-868.

17. Bheda, P., Jing, H., Wolberger, C., and Lin, H. (2016) The Substrate Specificity of Sirtuins, *Annu. Rev. Biochem 85*, 405-429.

18. Chiang, Y. L., and Lin, H. (2016) An improved fluorogenic assay for SIRT1, SIRT2, and SIRT3, *Org. Biomol. Chem. 14*, 2186-2190.

19. Feldman, J. L., Baeza, J., and Denu, J. M. (2013) Activation of the protein deacetylase SIRT6 by long-chain fatty acids and widespread deacylation by mammalian sirtuins, *J Biol Chem 288*, 31350-31356.

20. Guarente, L. (2011) Sirtuins, Aging, and Medicine, *New England Journal of Medicine 364*, 2235-2244.

21. Houtkooper, R. H., Pirinen, E., and Auwerx, J. (2012) Sirtuins as regulators of metabolism and healthspan, *Nat. Rev. Mol. Cell Biol. 13*, 225-238.

22. Machado de Oliveira, R., Sarkander, J., Kazantsev, A. G., and Outeiro, T. F. (2012) SIRT2 as a Therapeutic Target for Age-Related Disorders, *Front. Pharmacol. 3*.

23. Carafa, V., Rotili, D., Forgione, M., Cuomo, F., Serretiello, E., Hailu, G. S., Jarho, E., Lahtela-Kakkonen, M., Mai, A., and Altucci, L. (2016) Sirtuin functions and modulation: from chemistry to the clinic, *Clin. Epigenet. 8*, 61.

24. Alhazzazi, T. Y., Kamarajan, P., Verdin, E., and Kapila, Y. L. (2011) SIRT3 and cancer: Tumor promoter or suppressor?, *Biochim. Biophys. Acta 1816*, 80-88.

25. Chen, Y., Fu, L. L., Wen, X., Wang, X. Y., Liu, J., Cheng, Y., and Huang, J. (2014) Sirtuin-3 (SIRT3), a therapeutic target with oncogenic and tumor-suppressive function in cancer, *Cell Death Dis. 5*, e1047.

26. Bosch-Presegue, L., and Vaquero, A. (2011) The dual role of sirtuins in cancer, *Genes Cancer 2*, 648-662.

27. Kauppinen, A., Suuronen, T., Ojala, J., Kaarniranta, K., and Salminen, A. (2013) Antagonistic crosstalk between NF-kappaB and SIRT1 in the regulation of inflammation and metabolic disorders, *Cell. Signal. 25*, 1939-1948.

28. Yeung, F., Hoberg, J. E., Ramsey, C. S., Keller, M. D., Jones, D. R., Frye, R. A., and Mayo, M. W. (2004) Modulation of NF-kappaB-dependent transcription and cell survival by the SIRT1 deacetylase, *EMBO J. 23*, 2369-2380.

29. Joo, H. Y., Yun, M., Jeong, J., Park, E. R., Shin, H. J., Woo, S. R., Jung, J. K., Kim, Y. M., Park, J. J., Kim, J., and Lee, K. H. (2015) SIRT1 deacetylates and stabilizes hypoxia-inducible factor-1alpha (HIF-1alpha) via direct interactions during hypoxia, *Biochem Biophys Res Commun 462*, 294-300.

30. Lim, J. H., Lee, Y. M., Chun, Y. S., Chen, J., Kim, J. E., and Park, J. W. (2010) Sirtuin 1 modulates cellular responses to hypoxia by deacetylating hypoxia-inducible factor 1alpha, *Mol. Cell 38*, 864-878.

31. Herranz, D., Munoz-Martin, M., Canamero, M., Mulero, F., Martinez-Pastor, B., Fernandez-Capetillo, O., and Serrano, M. (2010) Sirt1 improves healthy ageing and protects from metabolic syndrome-associated cancer, *Nat. Commun. 1*, 3.

32. Firestein, R., Blander, G., Michan, S., Oberdoerffer, P., Ogino, S., Campbell, J., Bhimavarapu, A., Luikenhuis, S., de Cabo, R., Fuchs, C., Hahn, W. C., Guarente, L. P., and Sinclair, D. A. (2008) The SIRT1 deacetylase suppresses intestinal tumorigenesis and colon cancer growth, *PLoS One 3*, e2020.

33. Yang, Y., Hou, H., Haller, E. M., Nicosia, S. V., and Bai, W. (2005) Suppression of FOXO1 activity by FHL2 through SIRT1-mediated deacetylation, *EMBO J. 24*, 1021-1032.

34. Menssen, A., Hydbring, P., Kapelle, K., Vervoorts, J., Diebold, J., Luscher, B., Larsson, L. G., and Hermeking, H. (2012) The c-MYC oncoprotein, the NAMPT enzyme, the SIRT1-inhibitor DBC1, and the SIRT1 deacetylase form a positive feedback loop, *Proc. Natl. Acad. Sci. USA 109*, E187-196.

35. Kim, H. S., Vassilopoulos, A., Wang, R. H., Lahusen, T., Xiao, Z., Xu, X., Li, C., Veenstra, T. D., Li, B., Yu, H., Ji, J., Wang, X. W., Park, S. H., Cha, Y. I., Gius, D., and Deng, C. X. (2011) SIRT2 maintains genome integrity and suppresses tumorigenesis through regulating APC/C activity, *Cancer Cell 20*, 487-499.

36. Jing, E., Gesta, S., and Kahn, C. R. (2007) SIRT2 Regulates Adipocyte Differentiation through FoxO1 Acetylation/Deacetylation, *Cell Metab. 6*, 105-114.

37. Zhou, W., Ni, T. K., Wronski, A., Glass, B., Skibinski, A., Beck, A., and Kuperwasser, C. (2016) The SIRT2 Deacetylase Stabilizes Slug to Control Malignancy of Basal-like Breast Cancer, *Cell Rep. 17*, 1302-1317.

38. Jing, H., Hu, J., He, B., Negrón Abril, Y. L., Stupinski, J., Weiser, K., Carbonaro, M., Chiang, Y.-L., Southard, T., Giannakakou, P., Weiss, R. S., and Lin, H. (2016) A SIRT2-Selective Inhibitor Promotes c-Myc Oncoprotein Degradation and Exhibits Broad Anticancer Activity, *Cancer Cell 29*, 297-310.

39. Zhao, D., Zou, S. W., Liu, Y., Zhou, X., Mo, Y., Wang, P., Xu, Y. H., Dong, B., Xiong, Y., Lei, Q. Y., and Guan, K. L. (2013) Lysine-5 acetylation negatively regulates lactate dehydrogenase A and is decreased in pancreatic cancer, *Cancer Cell 23*, 464-476.

40. Jing, H., Zhang, X., Wisner, S. A., Chen, X., Spiegelman, N. A., Linder, M. E., and Lin, H. (2017) SIRT2 and lysine fatty acylation regulate the transforming activity of K-Ras4a, *eLife 6*, e32436.

41. Morris, B. J. (2013) Seven sirtuins for seven deadly diseases of aging, *Free Radical Biol. Med. 56*, 133-171.

42. Finley, L. W., Carracedo, A., Lee, J., Souza, A., Egia, A., Zhang, J., Teruya-Feldstein, J., Moreira, P. I., Cardoso, S. M., Clish, C. B., Pandolfi, P. P., and Haigis, M. C. (2011) SIRT3 opposes reprogramming of cancer cell metabolism through HIF1alpha destabilization, *Cancer Cell 19*, 416-428.

43. Li, M., Chiang, Y. L., Lyssiotis, C. A., Teater, M. R., Hong, J. Y., Shen, H., Wang, L., Hu, J., Jing, H., Chen, Z., Jain, N., Duy, C., Mistry, S. J., Cerchietti, L., Cross, J. R., Cantley, L. C., Green, M. R., Lin, H., and Melnick, A. M. (2019) Non-oncogene Addiction to SIRT3 Plays a Critical Role in Lymphomagenesis, *Cancer Cell 35*, 916-931 e919.

44. Chini, C. C., Espindola-Netto, J. M., Mondal, G., Guerrico, A. M., Nin, V., Escande,

C., Sola-Penna, M., Zhang, J. S., Billadeau, D. D., and Chini, E. N. (2016) SIRT1-Activating Compounds (STAC) Negatively Regulate Pancreatic Cancer Cell Growth and Viability Through a SIRT1 Lysosomal-Dependent Pathway, *Clin Cancer Res 22*, 2496-2507.

45. Lahusen, T. J., and Deng, C. X. (2015) SRT1720 induces lysosomal-dependent cell death of breast cancer cells, *Mol Cancer Ther 14*, 183-192.

46. Suzuki, K., Hayashi, R., Ichikawa, T., Imanishi, S., Yamada, T., Inomata, M., Miwa, T., Matsui, S., Usui, I., Urakaze, M., Matsuya, Y., Ogawa, H., Sakurai, H., Saiki, I., and Tobe, K. (2012) SRT1720, a SIRT1 activator, promotes tumor cell migration, and lung metastasis of breast cancer in mice, *Oncol. Rep. 27*, 1726-1732.

47. Pacholec, M., Bleasdale, J. E., Chrunyk, B., Cunningham, D., Flynn, D., Garofalo, R. S., Griffith, D., Griffor, M., Loulakis, P., Pabst, B., Qiu, X., Stockman, B., Thanabal, V., Varghese, A., Ward, J., Withka, J., and Ahn, K. (2010) SRT1720, SRT2183, SRT1460, and resveratrol are not direct activators of SIRT1, *J. Biol. Chem. 285*, 8340-8351.

48. Oon, C. E., Strell, C., Yeong, K. Y., Ostman, A., and Prakash, J. (2015) SIRT1 inhibition in pancreatic cancer models: contrasting effects in vitro and in vivo, *Eur. J. Pharmacol. 757*, 59-67.

49. Rumpf, T., Schiedel, M., Karaman, B., Roessler, C., North, B. J., Lehotzky, A., Olah, J., Ladwein, K. I., Schmidtkunz, K., Gajer, M., Pannek, M., Steegborn, C., Sinclair, D. A., Gerhardt, S., Ovadi, J., Schutkowski, M., Sippl, W., Einsle, O., and Jung, M. (2015) Selective Sirt2 inhibition by ligand-induced rearrangement of the active site, *Nat. Commun. 6*, 6263.

50. Li, Y., Zhang, M., Dorfman, R. G., Pan, Y., Tang, D., Xu, L., Zhao, Z., Zhou, Q., Zhou, L., Wang, Y., Yin, Y., Shen, S., Kong, B., Friess, H., Zhao, S., Wang, L., and Zou, X. (2018) SIRT2 Promotes the Migration and Invasion of Gastric Cancer through RAS/ERK/JNK/MMP-9 Pathway by Increasing PEPCK1-Related Metabolism, *Neoplasia 20*, 745-756.

51. Kozako, T., Mellini, P., Ohsugi, T., Aikawa, A., Uchida, Y. I., Honda, S. I., and Suzuki, T. (2018) Novel small molecule SIRT2 inhibitors induce cell death in leukemic cell lines, *BMC Cancer 18*, 791.

52. Mellini, P., Itoh, Y., Elboray, E. E., Tsumoto, H., Li, Y., Suzuki, M., Takahashi, Y., Tojo, T., Kurohara, T., Miyake, Y., Miura, Y., Kitao, Y., Kotoku, M., Iida, T., and Suzuki, T. (2019) Identification of Diketopiperazine-Containing 2-Anilinobenzamides as Potent Sirtuin 2 (SIRT2)-Selective Inhibitors Targeting the "Selectivity Pocket", Substrate-Binding Site, and NAD(+)-Binding Site, *J Med Chem 62*, 5844-5862.

53. Farooqi, A. S., Hong, J. Y., Cao, J., Lu, X., Price, I. R., Zhao, Q., Kosciuk, T., Yang, M., Bai, J. J., and Lin, H. (2019) Novel Lysine-Based Thioureas as Mechanism-Based Inhibitors of Sirtuin 2 (SIRT2) with Anticancer Activity in a Colorectal Cancer Murine Model, *J Med Chem 62*, 4131-4141.

54. Nguyen, G. T., Schaefer, S., Gertz, M., Weyand, M., and Steegborn, C. (2013) Structures of human sirtuin 3 complexes with ADP-ribose and with carba-NAD+ and SRT1720: binding details and inhibition mechanism, *Acta Crystallogr., Sect. D: Biol. Crystallogr. 69*, 1423-1432.

55. Alhazzazi, T. Y., Kamarajan, P., Xu, Y., Ai, T., Chen, L., Verdin, E., and Kapila, Y. L. (2016) A Novel Sirtuin-3 Inhibitor, LC-0296, Inhibits Cell Survival and Proliferation, and Promotes Apoptosis of Head and Neck Cancer Cells, *Anticancer Res. 36*, 49-60.

56. Lain, S., Hollick, J. J., Campbell, J., Staples, O. D., Higgins, M., Aoubala, M., McCarthy, A., Appleyard, V., Murray, K. E., Baker, L., Thompson, A., Mathers, J., Holland, S. J., Stark, M. J., Pass, G., Woods, J., Lane, D. P., and Westwood, N. J. (2008) Discovery, in vivo activity, and mechanism of action of a small-molecule p53 activator, *Cancer Cell 13*, 454-463.

57. Spiegelman, N. A., Hong, J. Y., Hu, J., Jing, H., Wang, M., Price, I. R., Cao, J., Yang, M., Zhang, X., and Lin, H. (2019) A Small-Molecule SIRT2 Inhibitor That Promotes K-Ras4a Lysine Fatty-Acylation, *ChemMedChem 14*, 744-748.

58. Spiegelman, N. A., Price, I. R., Jing, H., Wang, M., Yang, M., Cao, J., Hong, J. Y., Zhang, X., Aramsangtienchai, P., Sadhukhan, S., and Lin, H. (2018) Direct Comparison of SIRT2 Inhibitors: Potency, Specificity, Activity-Dependent Inhibition, and On-Target Anticancer Activities, *ChemMedChem 13*, 1890-1894.

59. Hong, J. Y., Price, I. R., Bai, J. J., and Lin, H. (2019) A Glycoconjugated SIRT2 Inhibitor with Aqueous Solubility Allows Structure-Based Design of SIRT2 Inhibitors, *ACS Chem. Biol. 14*, 1802-1810.

60. Vaziri, H., Dessain, S. K., Ng Eaton, E., Imai, S. I., Frye, R. A., Pandita, T. K., Guarente, L., and Weinberg, R. A. (2001) hSIR2(SIRT1) functions as an NAD-dependent p53 deacetylase, *Cell 107*, 149-159.

61. Juan, L. J., Shia, W. J., Chen, M. H., Yang, W. M., Seto, E., Lin, Y. S., and Wu, C. W. (2000) Histone deacetylases specifically down-regulate p53-dependent gene activation, *J Biol Chem 275*, 20436-20443.

62. Vanhaecke, T., Papeleu, P., Elaut, G., and Rogiers, V. (2004) Trichostatin A-like hydroxamate histone deacetylase inhibitors as therapeutic agents: toxicological point of view, *Curr. Med. Chem. 11*, 1629-1643.

63. Solomon, J. M., Pasupuleti, R., Xu, L., McDonagh, T., Curtis, R., DiStefano, P. S., and Huber, L. J. (2006) Inhibition of SIRT1 catalytic activity increases p53 acetylation but does not alter cell survival following DNA damage, *Mol. Cell. Biol. 26*, 28-38.

64. North, B. J., Marshall, B. L., Borra, M. T., Denu, J. M., and Verdin, E. (2003) The Human Sir2 Ortholog, SIRT2, Is an NAD+-Dependent Tubulin Deacetylase, *Mol. Cell 11*, 437-444.

65. Nielsen, A. L., Rajabi, N., Kudo, N., Lundø, K., Moreno-Yruela, C., Bæk, M., Fontenas, M., Lucidi, A., Madsen, A. S., Yoshida, M., and Olsen, C. A. (2021) Mechanism-based inhibitors of SIRT2: structure–activity relationship, X-ray structures, target engagement, regulation of α-tubulin acetylation and inhibition of breast cancer cell migration, *RSC Chemical Biology*.

66. Yu, W., Dittenhafer-Reed, K. E., and Denu, J. M. (2012) SIRT3 protein deacetylates isocitrate dehydrogenase 2 (IDH2) and regulates mitochondrial redox status, *J. Biol. Chem. 287*, 14078-14086.

67. Zou, X., Zhu, Y., Park, S. H., Liu, G., O'Brien, J., Jiang, H., and Gius, D. (2017) SIRT3-Mediated Dimerization of IDH2 Directs Cancer Cell Metabolism and Tumor Growth, *Cancer Res. 77*, 3990-3999.

68. Siegel, R. L., Miller, K. D., Goding Sauer, A., Fedewa, S. A., Butterly, L. F., Anderson, J. C., Cercek, A., Smith, R. A., and Jemal, A. (2020) Colorectal cancer statistics, 2020, *Ca-Cancer J. Clin. 70*, 145-164.

## 4.6 Methods

**General Experiment methods**

All chemical reagents and organic solvents used for the synthesis and biological studies were purchased as analytical or higher grades from commercial vendors. Chemical reactions were under nitrogen gas. For mass spectrometry characterization of compounds, Shimadzu HPLC LC20-AD and Thermo Scientific LCQ Fleet Mass Spectrometer under positive mode was used. HPLC grade water with 0.1% HPLC-grade acetic acid (Buffer A) and HPLC-grade acetonitrile with 0.1% acetic acid (Buffer B) were used for the LC-MS solvents. The column for LC-MS was Kinetex 5u EVO C18 100 Å Column (30 x 2.1 mm, 5 µm). The UV traces of the

compounds were detected at 215 and 260 nm. The NMR spectra were collected by Bruker 500 spectrometer. For the silica column purification, SiliaFlash Irregular Silica Gel P60, 40 – 63 μm, 60 Å was used. For the sirtuin in vitro enzymatic assays, Shimadzu HPLC LC20—AD with Kinetex 5u EVO C18 100 Å column (100 mm x 4.60 mm, 5 μm) system was used, and the UV peaks of the peptides were monitored at 215 and 280 nm. Solvents for this HPLC enzymatic assay were HPLC-grade water with 0.1% trifluoroacetic acid (Buffer A) and HPLC-grade acetonitrile with 0.1% trifluoroacetic acid. The purities of the compounds were confirmed to be at least 95% using Shimadzu HPLC 20-AD system.

**Antibodies**

Anti-acetyl-α-tubulin (6-11B-1) (MABT868), anti-Flag-M2 conjugated to horseradish peroxidase (A8592) and anti-Flag M2 affinity agarose gel (A2220) were purchased from Sigma-Aldrich. Anti-rabbit IgG-horseradish peroxidase (#7074), anti-SIRT2 antibody (#12650), anti-acetyl-p53 antibody (K382) (#2525), and anti-p53 antibody (#2527) were purchased from Cell Signaling Technology. The goat anti-Mouse IgG (H+L) cross-adsorbed secondary antibody, Cyanine3 (A10521) was purchased from ThermoFisher. The anti-β-Actin (C4) conjugated to horseradish peroxidase (sc-4777) mouse anti-rabbit IgG-horseradish peroxidase (sc-2357) were purchased from Santa Cruz Biotechnology. Anti-mouse-GDH (14299-1-AP) was purchased from ProteinTech. Anti-rabbit acetyl K413 IDH2 (AC0004) was purchased from GeneTel Lab. Acetyl lysine antibody conjugated to agarose beads (ICP0388) was purchased from ImmuneChem.

**Immunoblots**

Immunoblots were done as previously reported.[1, 2] Collected cells were lysed using 1% NP-40 lysis buffer (25 mM Tris-HCl pH 8.0, 10% glycerol, 150 mM NaCl, 1% Igepal CA-630) with protease inhibitor cocktail purchased from Sigma.

**Cell culture and transfection**

MCF7, MDA-MB-231, HEK293T, U87, MIA PaCa-2, and HeLa cells were cultured in Dulbecco's Modified Eagle Medium (DMEM) supplemented with 10% Fetal Bovine Serum (FBS) purchased from Invitrogen. HCT-116 cells were cultured in McCoy's 5A Medium supplemented with 10% FBS. SW948, NCI-H23, and A549 cells were cultured in Roswell Park Memorial Institute Medium (RPMI) supplemented with 10% FBS. 3T3, MEF *SIRT2* KO, and MEF *SIRT2* WT cells were cultured in DMEM supplemented with 15% FBS and 1x non-essential amino acids (11140050, Gibco). Cells were incubated at 37 °C with 5% $CO_2$.

**Mice**

The animal protocol was approved by the Cornell University Institutional Animal Care and Use Committee. Mice were caged under pathogen-free condition at the Association for the Assessment and Accreditation of Laboratory Animal Care International accredited facility and cared for in compliance with the Guide for the Care and Use of Laboratory Animals. All the mice for this study were a 12:12 light:dark cycle and received irradiated food and reverse osmosis, hyper-acidified water.

**Cloning, expression, and purification of SIRT1, 2, 3, 5, and 6**

Human SIRT1, 2, 3, 5 and 6 were cloned, expressed, and purified as previously reported.[1-5]

**Analytical HPLC *in vitro* sirtuin deacylation $IC_{50}$ assay**

The *in vitro* enzymatic assays of SIRT1, 2, 3, 5, and 6 deacylase were carried out following previously reported methods.[2, 3]

**Detecting inhibition of SIRT1 deacetylation activity in cells (Immunoblots of Ac-p53)**

Initially, MCF7 cells in 10-cm dishes (70% confluency) were co-incubated with 400 nM of Trichostatin A and indicated concentrations of EX-527, TM, NH4-6, or NH4-13 for 6 hours. The cells were then collected and lysed. Using anti-Ac-p53 (K382) antibody, the acetylation levels of p53 was detected by immunoblotting. As the loading control, β-Actin was blotted.

**Detecting inhibition of SIRT2 deacetylation activity in cells (Immunofluorescence of Ac-α-tubulin)**

To 35 mm-glass bottom dishes from MatTek, 200,000 MCF7 cells were seeded. After overnight incubation, the cells were treated with either DMSO control or indicated concentrations of TM, NH4-6, or NH4-13 for 6 hours. The cells were then carefully washed with ice-cold PBS three times, and fixed with ice-cold methanol for 10 minutes. To the fixed cells, 0.1% Triton-X in PBS was added and incubated for 10 minutes. Then, the cells were washed with PBS three times and then incubated in 1% BSA in TBST buffer (10 mM Tris-HCl pH 7.4, 150 mM NaCl and 0.1% Tween-20) for 30 minutes. After that, the cells were incubated with Ac-α-tubulin antibody (1:100 dilution in 1% BSA in TBST buffer) overnight on the rocker at 4 °C. After washing the cells with TBST buffer three times, the cells were treated with Cy3 conjugated secondary antibody (1:1000) in 1% BSA in TBST and kept in dark at room

temperature for an hour. Again, the cells were washed with TBST three times and stained with DAPI fluoromount. The immunofluorescence was detected using Cytation 5 Cell Imaging Reader.

**Detecting inhibition of SIRT3 deacetylation activity in cells (Immunoblots of Ac-IDH)**

pSLIK-IDH2-FLAG was a gift from Christian Metallo (Addgene plasmid # 66806; http://n2t.net/addgene:66806 ; RRID:Addgene_66806) was used to generate tet-inducible expression of IDH2 in cells.[6] From HEK293T cells, the lentiviral particles were extracted. Then, MDA-MB-231 cells were treated with viral supernatant with 6 µg/mL of polybrene overnight, followed with hygromycin (250 µg/mL) selection. To induce the IDH2-flag overexpression, the cells were treated with doxycycline (1 µg/mL) for 48 hours. The cells were then treated with the indicated concentrations of YC8-02, NH4-6, or NH4-13 for 6 hours. After collection, the cells are lysed with RIPA lysis buffer (150 mM NaCl, 1% NP-40, 0.5% sodium deoxycholate, 0.1% SDS, 25 mM Tris HCl (pH 7.4)). With the lysates, flag immunoprecipitation was performed, and the acetylation levels of IDH2 was detected by immunoblotting.

**Cellular proliferation assay**

1000 (HCT-116), 2000 (MDA-MB-231), 3000 (MCF7) 3000 (HME1), 2000 (HeLa), 2000 (SW948), 1000 (A549), 2000 (NCI-H23), 3000 (3T3), 4000 (MEF *Sirt2* WT, KO) or 3000 (MIA PaCa-2) cells suspended in 100 µL of corresponding media were seeded to wells of a Corning Costar Flat Bottom 96-well plate. After overnight incubation, 100 µL of inhibitors dissolved in the corresponding media at various

concentrations was added to each well. The final concentrations of the inhibitors ranged from 1.56 μM to 100 μM. Experiments were done in triplicated. After 72 hours of additional incubation, CellTiter Blue purchased from Promega was added, and the viability was measured following the manufacturer's protocol.

**NH4-6 and NH4-13 cellular permeability assay**

To the MCF7 cells with 70 – 80% confluency in 10-cm plates, DMEM containing DMSO control or 20 or 40 μM of TM, NH4-6 or NH4-13 was added. After 6 hours of incubation, the cells were washed carefully with ice-cold PBS three times and collected. After centrifuging the cells at 4 °C, 110 μL of ice-cold methanol was added to extract small molecules. The tubes with methanol were vortexed thoroughly and centrifuged at 15,000*g* for 15 minutes. The supernatant was transferred into a 96-well plate and 100 μL of the supernatant was injected into LC-MS for detection. The standard curves with concentrations ranging from 2 μM to 200 μM were prepared similarly, which was used as the reference for the calculations.

**Compound solubility tests**

TM, NH4-6, and NH4-13 were initially dissolved with 100 μL of DMSO to reach 50 mM concentration. Then, the DMSO stock was diluted into the indicated final concentrations in PBS or DMEM. The final volume of the dilution was made to 1 mL. The mixtures were vortexed before taking the images with a digital camera.

**Compound stability tests in DMEM and human male serum**

NH4-6 and NH4-13 were dissolved with 1 mL DMEM or human male serum (Sigma, #H4522) to reach 150 μM. Using the 3D rocker, the tubes were shaken at 37 °C. At the indicated time, 45 μL of the sample was taken out. Then, 50 μL of 6 M

urea and 100 μL of ice-cold acetonitrile was added. After spinning at 15,000 *g* for 30 minutes, 95 μL of supernatant was injected into the HPLC or LC-MS for detection. Until the injection, all samples were kept at 0 ° for storage.

**Detection of NH4-6 and NH4-13 in mouse serum after 30 minutes of injection**

To the male NSG mice from the Jackson Laboratory, indicated dosage of NH4-6 and NH4-13 dissolved in 10% DMSO and 90% PBS were injected. After 30 minutes, 100 μL of blood were taken from the mice. The blood samples were centrifuged at 15,000 *g* for 15 minutes at 4 °C, and the supernatant was transferred to new tubes. The supernatant was centrifuged again 15,000 *g* for 15 minutes at 4 °C. The supernatant was transferred to new tubes, and equal volume of methanol was added to extract the small molecules. The tubes were vortexed thoroughly and centrifuged at 15,000 *g* for 15 minutes at 4 °C. The collected supernatant was again centrifuged at 15,000 *g* for 15 minutes at 4 °C. The final supernatant was loaded to the LC-MS to detect the compounds.

**Pharmacokinetics of NH4-6 and NH4-13 in mice**

To the male NSG mice from the Jackson Laboratory, indicated dosage of NH4-6 and NH4-13 dissolved in 10% DMSO and 90% PBS were injected. At the indicated time point, 20-40 μL of blood were taken from the mice. The blood samples were centrifuged at 15,000 *g* for 15 minutes at 4 °C, and 20 μL of supernatant was transferred to new tubes. The supernatant was centrifuged again 15,000 *g* for 15 minutes at 4 °C. The supernatant was transferred to new tubes, and 100 μL of methanol was added to extract the small molecules. The tubes were vortexed thoroughly and centrifuged at 15,000 *g* for 15 minutes at 4 °C. The collected

supernatant was again centrifuged at 15,000 *g* for 15 minutes at 4 °C. 95 μL of the final supernatant was loaded to the HPLC to detect the compounds.

**Mouse tumor xenograft experiments with HCT-116 cells**

Xenotransplantation studies were performed as previously described.[7] Briefly, one million HCT-116 colon cancer cells suspended in 100 μL of PBS were subcutaneously injected into the flanks of male NSG mice from the Jackson Laboratory. Once the tumor size grew to 100 – 200 $mm^3$, mice were treated by intraperitoneal injection for 15 days with vehicle control or indicated dosages of NH4-6 or NH4-13 dissolved in 10% DMSO and 90% PBS. The overall health, behaviors and body weights were monitored daily. The tumor volumes were measured using a caliper. Once the tumors reached the endpoint, mice were sacrificed by $CO_2$ asphyxiation. The tumors were collected and weighed for the data collection.

**Detecting inhibition of SIRT1/2/3 deacetylation activity in tumors**

30 mg of collected tumors in 750 mL of RIPA lysis buffer (150 mM NaCl, 1% NP-40, 0.5% sodium deoxycholate, 0.1% SDS, 25 mM Tris HCl (pH 7.4)) were homogenized by the Qiagen Tissuelyser LT for 1 minute under 30 $s^{-1}$ three times. After the BCA assay to normalize the loadings, proteins were immunoprecipitated using the acetyl-lysine agarose beads (ICP0388) for overnight at 4 °C. After running the western blot, the nitrocellulose membranes were blocked with peptone blocking buffer (0.1 M Tris-HCl (pH 7.5), 100 mM NaCl, 1% Peptone, and 10% Tween-20) for overnight at 4 °C. Then, the membranes were washed with TBST buffer (10 mM Tris-HCl pH 7.4, 150 mM NaCl and 0.1% Tween-20), and incubated with primary antibody (1:1000) in peptone antibody buffer (0.1 M Tris-HCl (pH 7.5), 100 mM

NaCl, 0.1% Peptone, and 0.5% Tween-20). After overnight incubation in 4 °C, the membranes were washed with TBST buffer three times, and were incubated with the secondary antibody (1:3000) in TBST buffer. After the three washes with TBST buffer, the membranes were imaged using Typhoon Imager.

**Synthesis of Acetyl-H3K9 Peptide**

Acetyl-H3K9 with the sequence of KQTAR-(Acetyl-K)-STGGWW was prepared and synthesized as previously reported.[3, 4]

**Synthesis of Compound 1, 2, 3, NH4-6 and TM**

Compound 1, 2 3, NH4-6 and TM were prepared and synthesized as previously reported.[3, 8]

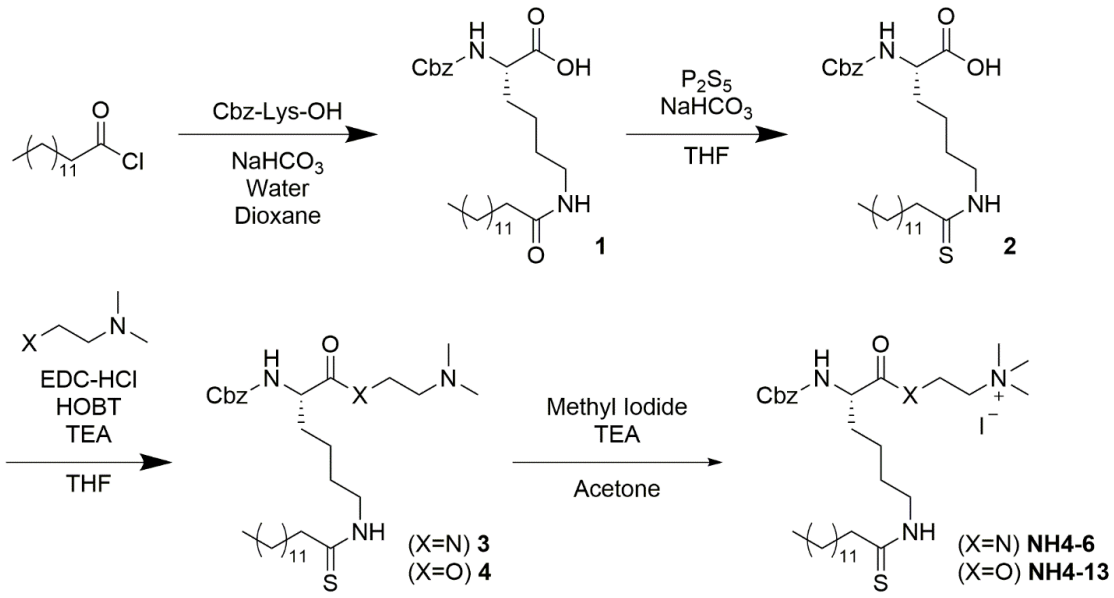


**Scheme 4.1 Synthesis for NH4-6 and NH4-13.**

**Synthesis of 3, 2-(dimethylamino)ethyl $N^2$-((benzyloxy)carbonyl)-$N^6$-tetradecanethioyl-*L*-lysinate (Compound 4)**

To Compound 2 (0.750 g, 1.48 mmol) dissolved in THF (15 mL), N-(3-dimethylaminopropyl)-N′-ethylcarbodiimide hydrochloride (0.369 g, 1.92 mmol), 1-hydroxybenzotriazole hydrate (0.291 g, 1.92 mmol), 2-(dimethylamino)ethan-1-ol (200 µL, 1.92 mmol), and N,N-diisopropylethylamine (0.733 mL, 4.44 mmol) were added at room temperature. After stirring overnight at room temperature, THF was removed by rotary evaporation. The residue was re-dissolved in ethyl acetate (100 mL) and further washed with 1N HCl (80 mL), saturated $NaHCO_3$ (80 mL) and brine (80 mL). The collected organic layer was dried over $Na_2SO_4$ and concentrated by rotary evaporation. The crude residue was purified by column purification using dichloromethane (DCM) and methanol to afford the final product compound 4 (0.660 g, 77%). $^1$H NMR (500 MHz, $CD_3OD$) δ 7.51 – 7.12 (m, 5H), 5.10 (d, J = 2.0 Hz, 2H), 4.24 (ddd, J = 13.4, 9.6, 5.2 Hz, 3H), 3.59 (td, J = 7.1, 3.2 Hz, 2H), 2.74 – 2.48 (m, 4H), 2.30 (s, 6H), 1.96 – 1.79 (m, 1H), 1.79 – 1.59 (m, 5H), 1.45 (h, J = 7.7, 7.0 Hz, 2H), 1.31 (m, 20H), 0.91 (t, J = 6.8 Hz, 3H). $^{13}$C NMR (126 MHz, $CD_3OD$) δ 205.10, 173.23, 157.28, 136.79, 128.07, 127.59, 127.34, 66.24, 62.13, 60.70, 58.75, 56.98, 53.94, 45.67, 45.07, 44.30, 31.68, 30.90, 29.41, 29.36, 29.32, 29.23, 29.09, 28.52, 26.80, 22.93, 22.34, 13.05. LCMS (ESI) calcd. for $[M+H]^+$ $C_{32}H_{56}N_3O_4S$ 578.39, obsd. 578.18.

**Synthesis of 2-(($N^2$-((benzyloxy)carbonyl)-*N6*-tetradecanethioyl-L-lysyl)oxy)-*N,N,N*-trimethylethan-1-aminium iodide (NH4-13)**

To compound 4 (0.660 g, 1.14 mmol) dissolved in acetone (12 mL), iodomethane (0.142 mL, 2.28 mmol) and triethylamine (0.320 mL, 2.28 mmol) were added at 0 °C. After overnight stirring at 0 °C, the reaction mixture was warmed up to room temperature and the solvent was removed using a rotary evaporator. The residue was re-dissolved in DCM (85 mL). To the flask with the residue in DCM, 40 mL of water was added slowly. The mixture was stirred slowly for 15 minutes, and then transferred to a separatory funnel. Without shaking, the organic layer was separated by draining and dried over $Na_2SO_4$. The solution was concentrated by rotary evaporation and purified by column purification using DCM and methanol to afford the final compound NH4-13 (0.355 g, 43%). $^1$H NMR (500 MHz, $CD_3OD$) δ 7.48 – 7.19 (m, 5H), 5.12 (d, J = 4.4 Hz, 2H), 4.75 – 4.42 (m, 2H), 4.21 (dd, J = 9.6, 5.0 Hz, 1H), 3.88 – 3.43 (m, 4H), 3.22 (d, J = 15.9 Hz, 9H), 2.60 (t, J = 7.5 Hz, 2H), 1.91 (d, J = 10.0 Hz, 1H), 1.71 (dq, J = 21.9, 7.2, 6.5 Hz, 5H), 1.48 (dp, J = 22.2, 7.3 Hz, 2H), 1.41 – 1.25 (m, 20H), 0.92 (t, J = 6.9 Hz, 3H). $^{13}$C NMR (126 MHz, $CD_3OD$) δ 205.15, 171.86, 157.34, 136.76, 128.15, 127.73, 127.45, 66.33, 64.63, 58.20, 55.59, 54.05, 53.14, 45.70, 44.80, 31.68, 30.19, 29.40, 29.36, 29.32, 29.23, 29.07, 28.54, 26.75, 22.77, 22.33, 13.04. LCMS calcd. for $[M\text{-}I]^+$ $C_{33}H_{58}N_3O4_S^+$ 592.41 obsd. 592.80.

### 4.6.1 References for methods


1. Jiang, H., Khan, S., Wang, Y., Charron, G., He, B., Sebastian, C., Du, J., Kim, R., Ge, E., Mostoslavsky, R., Hang, H. C., Hao, Q., and Lin, H. (2013) SIRT6 regulates TNF-a secretion through hydrolysis of long-chain fatty acyl lysine, *Nature 496*, 110-113.

2. Spiegelman, N. A., Price, I. R., Jing, H., Wang, M., Yang, M., Cao, J., Hong, J. Y., Zhang, X., Aramsangtienchai, P., Sadhukhan, S., and Lin, H. (2018) Direct Comparison of SIRT2 Inhibitors: Potency, Specificity, Activity-Dependent Inhibition, and On-Target Anticancer Activities, *ChemMedChem 13*, 1890-

1894.

3. Jing, H., Hu, J., He, B., Negrón Abril, Y. L., Stupinski, J., Weiser, K., Carbonaro, M., Chiang, Y.-L., Southard, T., Giannakakou, P., Weiss, R. S., and Lin, H. (2016) A SIRT2-Selective Inhibitor Promotes c-Myc Oncoprotein Degradation and Exhibits Broad Anticancer Activity, *Cancer Cell 29*, 297-310.

4. Hong, J. Y., Zhang, X., and Lin, H. (2018) HPLC-Based Enzyme Assays for Sirtuins, *Methods Mol Biol 1813*, 225-234.

5. Du, J., Zhou, Y., Su, X., Yu, J. J., Khan, S., Jiang, H., Kim, J., Woo, J., Kim, J. H., Choi, B. H., He, B., Chen, W., Zhang, S., Cerione, R. A., Auwerx, J., Hao, Q., and Lin, H. (2011) Sirt5 Is a NAD-Dependent Protein Lysine Demalonylase and Desuccinylase, *Science 334*, 806-809.

6. Lewis, C. A., Parker, S. J., Fiske, B. P., McCloskey, D., Gui, D. Y., Green, C. R., Vokes, N. I., Feist, A. M., Vander Heiden, M. G., and Metallo, C. M. (2014) Tracing compartmentalized NADPH metabolism in the cytosol and mitochondria of mammalian cells, *Mol Cell 55*, 253-263.

7. Farooqi, A. S., Hong, J. Y., Cao, J., Lu, X., Price, I. R., Zhao, Q., Kosciuk, T., Yang, M., Bai, J. J., and Lin, H. (2019) Novel Lysine-Based Thioureas as Mechanism-Based Inhibitors of Sirtuin 2 (SIRT2) with Anticancer Activity in a Colorectal Cancer Murine Model, *J Med Chem 62*, 4131-4141.

8. Hong, J. Y., Price, I. R., Bai, J. J., and Lin, H. (2019) A Glycoconjugated SIRT2 Inhibitor with Aqueous Solubility Allows Structure-Based Design of SIRT2 Inhibitors, *ACS Chem. Biol. 14*, 1802-1810.

# CHAPTER 5

BENZODIAZAPIENEDIONE-CORE SIRT2 SELECTIVE MECHANISM-BASED INHIBITOR WITH IMPROVED AQUEOUS SOLUBILITY AND CELLULAR PERMEABILITY DEMONSTRATES A POTENT ANTI-CANCER EFFECT.

## 5.1 Abstract

SIRT2 has been an attractive target for cancer treatment, because of its tumor growth contribution. Thus, a plethora of SIRT2 selective inhibitors has been developed. Among them, TM had shown the most promising anti-cancer effect, but its main drawback was low aqueous solubility. To improve this, NH4-13 with a trimethylammonium moiety was synthesized, but it portrayed poor cellular permeability. To overcome these issues, NH-C1-10 with a benzodiazapienedione core and 10-carbon thiourea acyl chain was designed, and showed improved aqueous solubility and cell permeability. Even though NH-C1-10 inhibited SIRT2 slightly weaker than TM *in vitro*, NH-C1-10 had shown stronger SIRT2 inhibition and cytotoxicity than TM in cellular studies. Moreover, NH-C1-10 had demonstrated a broad anti-cancer effect and impaired pancreatic tumor growth in the xenograft mice study. Overall, this study further confirms the demand for SIRT2 selective inhibitor with improved bioavailability for treating cancers.

## 5.2 Introduction

As class III histone deacetylase, sirtuins remove various acyl groups from protein lysine residues. Mechanistically, sirtuins use $NAD^+$ as a co-substrate and form O-acyl-ADP-ribose, the de-acylated protein, and nicotinamide.[1-4] In humans, there is a

total of seven sirtuins, SIRT1-7, with different subcellular localizations, preferred acyl groups, and tissue expression levels.[4-7] Through deacylation, sirtuins regulate various cellular functions, including metabolism, DNA repair, cell proliferation, transcription, and inflammation. As sirtuins are involved in a plethora of biological activities, they are viewed as the key targets for treating many diseases, such as cancer, neurodegenerative diseases, and cardiac hypertrophy.[4, 8-15]

Mainly localized in the cytoplasm, SIRT2 removes both short acetyl and long-chain fatty acyl groups from proteins.[4, 6, 16] Among the seven sirtuins, SIRT2 has been closely connected to cancer, due to its active involvement in many tumorigenic activities. By deacetylating lysine 116 of Slug, SIRT2 stimulates the growth of basal-like breast cancer.[17] SIRT2 increases the stability of c-Myc and accelerates pancreatic cancer cell proliferation.[18] SIRT2 regulates cell metabolism through deacetylating and inhibiting LDH-A, which is overexpressed and important in tumorigenesis.[19] In addition to deacetylation, SIRT2 removes long-chain fatty acyl groups to promote cancer growth.[16] For instance, through de-fatty acylation, SIRT2 promotes endomembrane localization of K-Ras4a and consequently enhances cellular transformation activity.[20] Moreover, SIRT2 removes the fatty acyl group on lysine 3 of ARF6 to promote ARF6 membrane localization and ERK activation.[21] Through its deacetylation and defatty-acylation, SIRT2 plays a key role in promoting cancer.

Along with the emergence of SIRT2 as a tumor activator, many SIRT2 inhibitors were developed as potential anticancer drugs. In leukemia cells, NCO-90/140 treatment stimulated apoptosis and autophagy-led cell deaths.[22] Targeting substrate-binding, $NAD^+$ and selectivity pockets, Compound 53 based on the NCO-90

structure impaired proliferation of MCF7 breast cancer cells.[23] SirReal2 occupied the selectivity pocket of SIRT2 and suppressed the invasion of gastric cancer cells.[24, 25] Mechanism-based SIRT2 inhibitors, Compound 26 and 26-D effectively decreased breast cancer cell motility.[26]

Previously, we have also reported a mechanism-based SIRT2 selective inhibitor, named TM. The sulfur atom of its acyl chain forms a covalent 1'-S-alkylimididate to stall the SIRT2 enzymatic activity. In cells, treatment of TM induced degradation of C-Myc, thereby leading to effective broad anti-cancer effect. Furthermore, in mice, TM effectively delayed breast cancer growth.[27] A similar compound to TM, AF-8 also impeded cell proliferation and tumor growth of colorectal cancer.[28] Although TM and AF-8 showed potent anti-cancer effects, both inhibitors possess poor aqueous solubility, due to their hydrophobicity. Such poor aqueous solubility makes cellular and animal studies practically difficult and could potentially decrease bioavailability of the compounds. Hence, increased aqueous solubility could potentially improve their anti-cancer potency.

The mechanism-based SIRT2 inhibitor TM has a very modular structure, which allowed us to easily modify it to improve the aqueous solubility. We previously synthesized NH4-6 and NH4-13 with a trimethyl quaternary ammonium group on the C-terminus, instead of TM's phenyl group. The trimethyl quaternary ammonium had improved aqueous solubility. However, due to its charged state, NH4-6 and NH4-13 showed poor cell permeability. Thus, at lower concentrations, both inhibitors have low intracellular concentrations are less efficient at inhibiting SIRT2 compared to TM.[29]

Thus, balancing the aqueous solubility and permeability are important for improving the potency of SIRT2 inhibitors as anti-cancer drugs.

Here, we report a new benzodiazapienedione-based SIRT2 selective inhibitor, named NH-C1-10. The simpler design of NH-C1-10 had improved the aqueous solubility and cellular permeability. Even though NH-C1-10 inhibited SIRT2 slightly weaker in the in vitro enzymatic assay, NH-C1-10 with its enhanced bioavailability inhibited SIRT2 stronger in cellular experiments. Moreover, NH-C1-10 effectively impaired cell proliferation of numerous cancer cell lines, including breast, pancreatic, colorectal, lung, glioblastoma, and melanoma cancers. We had focused on testing pancreatic cancer in mice, as it is the third-most common cause of death from cancer in the United States and has a poor prognosis.[30] In the xenograft mice studies, NH-C1-10 potently impeded pancreatic tumor growth, which further proved that SIRT2 is a desirable therapeutic target.

## 5.3 Results and Discussion

### 5.3.1 Design of a SIRT2 inhibitor with benzodiazapienedione core.

To improve the anticancer effect, we aimed to design a new SIRT2 selective inhibitor with enhanced aqueous solubility and cellular permeability. Because lower molecular weight is correlated to higher aqueous solubility and is recommended by the "Lipinski's Rule of 5," we aimed to simplify the structure of TM, even at a cost of lowering the SIRT2 inhibition potency. In other words, even though the new simpler inhibitor may inhibit SIRT2 slightly weaker than TM, we hypothesized that the

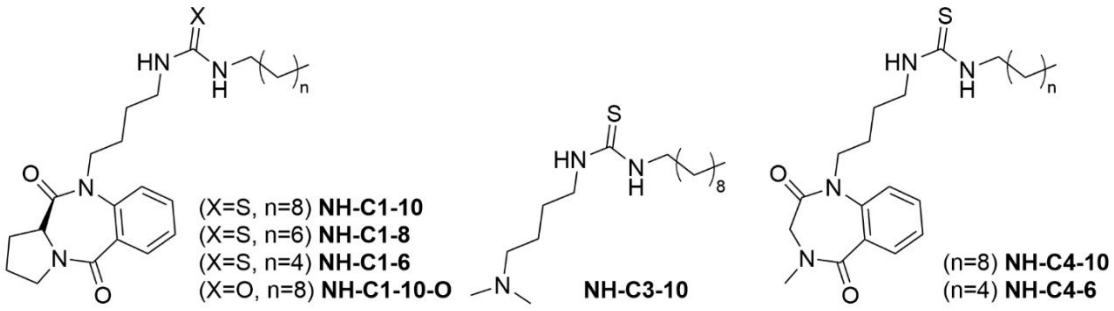


**Figure 5.1 Structures of synthesized SIRT2 inhibitors.**

enhanced bioavailability would increase the overall anti-cancer potency in cells and mice.

All our previous mechanism-based SIRT2 inhibitor design focused on using the lysine core and optimizing the thioacyl group as well as the N- and C-terminal attachments. Here we asked whether we could replace the lysine core to obtain SIRT2 inhibitors with improved solubility and cell permeability. Based on a SIRT2 co-crystal structure with a glycoconjuated TM, named Glucose-TM. From this structure, we discovered that the main interactions between SIRT2 and Glucose-TM originate from the thio-myristoyl chain occupying the hydrophobic tunnel and several hydrogen bonds forming a β-sheet-like interaction between the inhibitor's peptide chain and SIRT2's surface.[31] Between the two main interaction points, we would like to keep the thiomyristoyl group for the new inhibitor design, as it is the key for both the potency and the SIRT2 selectivity (compounds with shorter thioacyl chains have much weaker SIRT2 inhibitors and also inhibited SIRT1 and SIRT3).[27, 28] To improve the solubility and cell permeability, we decided to use a benzodiazapienedione to replace the lysine core in TM. The benzodiazapienedione ring was previously used as a

peptidomimetic moiety for Acyl Protein Thioesterase 1 (APT1). We thought the two carbonyl oxygens of benzodiazapienedione may still provide the needed hydrogen bonds to compete against natural SIRT2 substrates.[32] In addition, the benzodiazapienedione core contains rigid conformity and bridge that would increase the stability of the inhibitor from potential hydrolysis and degradation.

Using the benzodiazapienedione core, we synthesized the NH-C1 series (NH-C1-10, 8, and 6) with varying alkyl chain lengths (Figure 5.1). Because our objective was to improve the aqueous solubility, we did not want to attach alkyl chains longer than 10-carbon. Using the DataWarrior program, the simulated cLogP of NH-C1-10 is 5.64, significantly decreased from cLogP of TM (7.88). To test the importance of the sulfur atom in the inhibition mechanism, we also synthesized NH-C1-10-O, replacing the sulfur of NH-C1-10 with an oxygen atom. Also, to validate the importance of the benzodiazapienedione core, we synthesized NH-C3-10 without the core and NH-C4 series without the five-member ring of the core (Figure 5.1).

### 5.3.2 NH-C1-10 selectively inhibits SIRT2 *in vitro*.

Using the *in vitro* SIRT1-3 deacetylation enzymatic assays, we measured the $IC_{50}$ of the newly designed inhibitors (Table 14). All NH-C1 series inhibitors could not inhibit SIRT1 and 3 even at 83 μM. Among the three NH-C1 inhibitors, NH-C1-10 showed the strongest SIRT2 inhibition with $IC_{50}$ of 0.28 μM. NH-C1-8 inhibited SIRT2 with $IC_{50}$ of 7.2 μM, 25-fold weaker inhibition than NH-C1-10. NH-C1-6 showed the weakest SIRT2 inhibition with $IC_{50}$ of 39 μM, 140-fold weaker than NH-C1-10. TM showed selective SIRT2 inhibition with $IC_{50}$ of 0.042 μM, which was about 6.6-fold stronger than NH-C1-10. This is likely because SIRT2 forms fewer

**Table 14. *In Vitro* Enzymatic $IC_{50}$ values (n=3)**

| $IC_{50}$ (μM) | SIRT1 | SIRT2 | SIRT3 |
|---|---|---|---|
| **TM** | ~50 | 0.042 ± 0.015 | >83 |
| **NH-C1-10** | >83 | 0.28 ± 0.053 | >83 |
| **NH-C1-8** | >83 | 7.2 ± 2.12 | >83 |
| **NH-C1-6** | >83 | 39 ± 8.09 | >83 |
| **NH-C1-10-O** | > 83 | 7.7 ± 3.01 | > 83 |
| **NH-C3-10** | ~50 | 5.0 ± 0.42 | >83 |
| **NH-C4-10** | >83 | 1.1 ± 0.62 | >83 |
| **NH-C4-6** | >83 | >83 | >83 |

hydrogen bonds with the benzodiazapienedione core of NH-C1-10 than the lysine core in TM.

We also checked the $IC_{50}$ of NH-C1-10-O, NH-C3-10, and NH-C4 series (Table 14). All the tested inhibitors could not inhibit SIRT1 and 3 even at 50 μM. Since the sulfur atom is important for the mechanism-based inhibition, NH-C1-10-O was predicted to inhibit SIRT2 weaker than NH-C1-10. As expected, the SIRT2 $IC_{50}$ of NH-C1-10-O was 7.7 μM, about 28-fold weaker inhibition than NH-C1-10. Although NH-C1-10-O moderately inhibited SIRT2, most likely because it can bind the substrate pocket and compete with the acetyl lysine substrate, higher SIRT2 $IC_{50}$ of NH-C1-10-O verified the significance of NH-C1-10's sulfur atom for strengthening the SIRT2 inhibition.

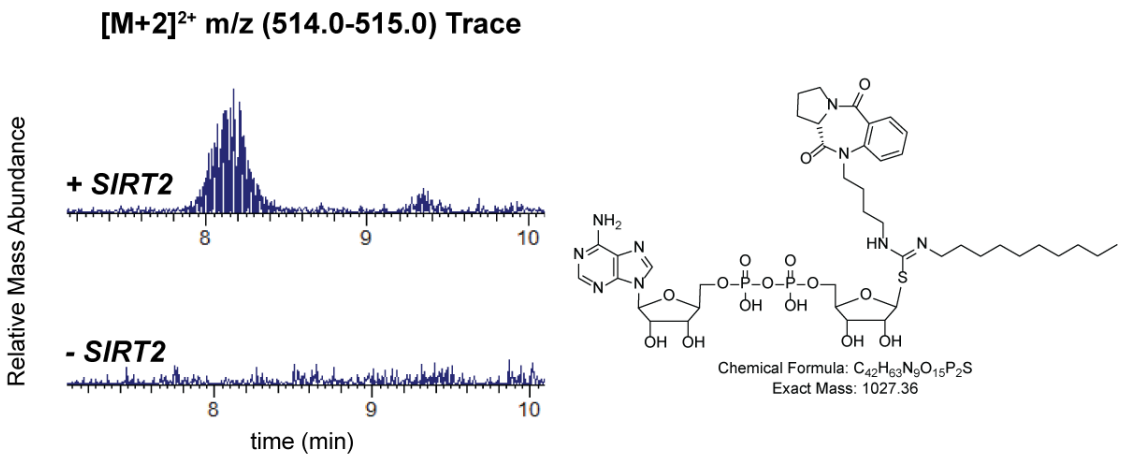


**Figure 5.2 Detection of the stalled covalent intermediate of NH-C1-10.** 100 μM of NH-C1-10 was incubated with 200 μM SIRT2, 120 μM NAD+, and 20 mM Ammonium Bicarbonate for 5 minutes at 37 °C. After quenching with acetonitrile, the supernatant was injected into LC-MS for detection.

NH-C3-10, without the benzodiazapienedione core, inhibits SIRT2 with an IC50 value of 5.0 μM, about 18-fold higher than NH-C1-10 (Table 14), suggesting that the core is needed for the SIRT2 inhibition. The SIRT2 $IC_{50}$ of NH-C4-10 without the five-member ring was 1.1 μM, 4-fold higher than that of NH-C1-10. The difference between $IC_{50}$ of NH-C1-10 and NH-C4-10 was small, but suggests that the five-member ring also contributes to the SIRT2 inhibition of NH-C1-10. In addition, NH-C4-10 showed stronger SIRT2 inhibition than NH-C3-10, which was likely because the carbonyl oxygens of the benzodiazapienedione core could form hydrogen bonds with SIRT2. Lastly, NH-C4-6 with a six-carbon alkyl chain could not inhibit SIRT2, even at 83 μM. This result confirmed that the shorter alkyl chain leads to loss of SIRT2 inhibition. Also, as NH-C4-6 (without the five-member ring) inhibited SIRT2 weaker than NH-C1-6 with the five-member ring, validating the importance of

this ring in SIRT2 inhibition. Overall, NH-C1-10-O, NH-C3-10, and NH-C4 series inhibitors confirmed the structural features of NH-C1-10 important for SIRT2 inhibition.

Previously, we had shown that the thiourea acyl group formed the covalent 1'-S-alkylimidate intermediate to inhibit SIRT2.[28] To confirm whether NH-C1-10 also inhibits SIRT2 by the formation of the stalled covalent intermediate, we have incubated NH-C1-10 and $NAD^+$ with SIRT2 for five minutes and injected the mixture into a liquid chromatography-mass spectrometer (LC-MS). As a result, NH-C1-10—ADP-ribose intermediate was detected. Without SIRT2, the corresponding intermediate was not observed (Figure 5.2).

### 5.3.3 NH-C1-10 selectively inhibits SIRT2 in cells.

To examine whether the benzodiazapienedione inhibitors also selectively inhibit SIRT2 in cells, we performed immunofluorescence imaging of acetylated α-tubulin, a previously reported SIRT2 substrate (Figure 5.3A).[33] MCF7 cells were treated with 50 μM of the inhibitors for 6 hours, and immunofluorescence images were taken using Cytation 5. The fluorescence level of NH-C1-10 treated samples had increased about 4-fold compared to the vehicle DMSO control. Meanwhile, that of NH-C1-8 and 6 had increased only about 2-fold and 1.2-fold, respectively (Figure 2A). This trend is consistent with the in vitro SIRT2 inhibition trend, in which NH-C1-10 had the lowest SIRT2 $IC_{50}$, and NH-C1-6 had the highest SIRT2 $IC_{50}$.

We then treated MCF7 cells with different concentrations of NH-C1-10 and measured the fluorescence level of acetyl α-tubulin (Figure 5.3B). For 10, 25, and 50

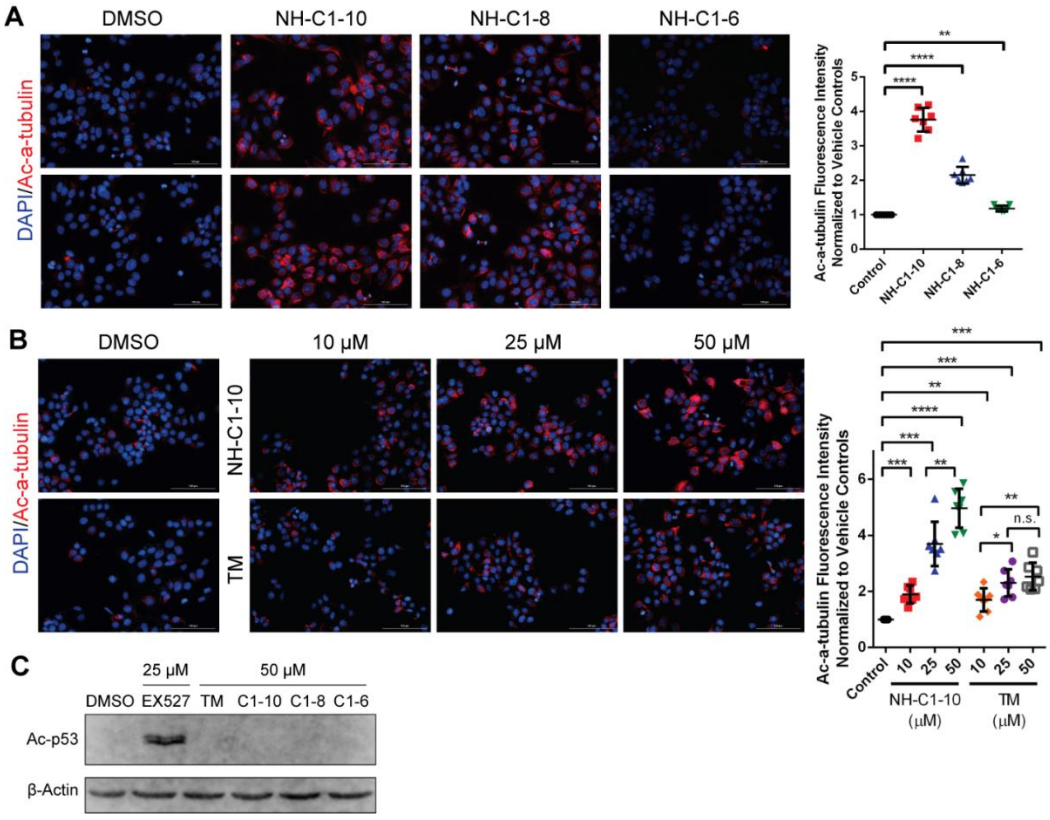


**Figure 5.3 NH-C1-10 selective inhibits SIRT2 in cells.** (A) Immunofluorescence detection of acetylated α-tubulin (K40) in MCF7 cells treated with DMSO control or 50 μM of NH-C1-10, NH-C1-8, and NH-C1-6 for 6 hours. (n=8) (B) Immunofluorescence detection of acetylated α-tubulin (K40) in MCF7 cells with DMSO or indicated concentrations of NH-C1-10 and TM for 6 hours. (n=6) (C) Immunoblots for the acetylation of p53 (K382) in MCF7 cells co-treated with 200 nM of Trichostatin A and DMSO or indicated concentration of EX-527, TM, NH-C1-10, NH-C1-8, and NH-C1-6.

μM of NH-C1-10, there was about 2, 4, and 5-fold increase in the fluorescence level, respectively. As such, a dose-dependent increase in the fluorescence level was observed. Furthermore, we compared NH-C1-10 to TM (Figure 5.3B). At 25 and 50 μM, TM treatment had only increased about 2.3 and 2.4-fold, respectively. In both concentrations, the fluorescence increase from TM was much lower than NH-C1-10. As such, although NH-C1-10 had higher *in vitro* SIRT2 $IC_{50}$ than TM, NH-C1-10 showed stronger SIRT2 inhibition in cells. At 10 μM, there was no significant difference between NH-C1-10 and TM. Interestingly, for TM, the difference in the increase between 25 and 50 μM was not significant. Because of its poor aqueous solubility, the concentration of TM in the media could have probably reached its maximum limit at 25 μM. These results suggested that compared to TM, the improved bioavailability of NH-C1-10 led to increased cellular SIRT2 inhibition.

After confirming that NH-C1-10 inhibits SIRT2 in cells, we wanted to demonstrate that it does not inhibit SIRT1. Thus, we examined the acetylation level of p53, a reported SIRT1 substrate (Figure 5.3C).[34] As HDACs also deacetylate p53, we co-treated MCF7 cells with Trichostatin A, a class I and II HDAC inhibitor, and indicated a concentration of sirtuin inhibitors. The SIRT1 selective inhibitor, EX-527 had increased the acetylation level of p53, verifying the accuracy of the immunoblot results. In contrast, TM, NH-C1-10, NH-C1-8, and NH-C1-6 did not alter the levels of acetyl p53. This indicated that NH-C1-series inhibitors cannot inhibit SIRT1 in cells, which is consistent with the *in vitro* enzymatic assay results.

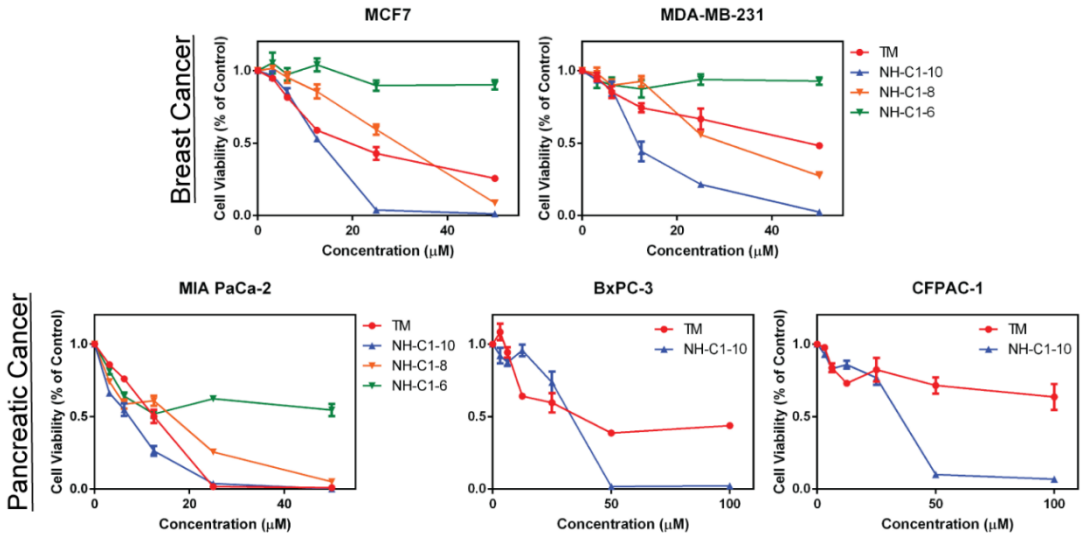


**Figure 5.4 NH-C1-10 shows stronger anti-proliferative effect than TM in breast and pancreatic cancer cells.** Cell viability of MCF7, MDA-MB-231, MIA PaCa-2, BxPC-3, and CFPAC-1 cells were measured with Cell Titer Blue after treatment of TM, NH-C1-10, NH-C1-8, and NH-C1-6 for 72 hours. (n=3 at each concentration)

### 5.3.4 NH-C1-10 shows stronger anti-proliferative effect than TM.

We next tested whether the improved SIRT2 inhibition by NH-C1-10 increased the anti-cancer potency. Thus, we treated various cancer cells with the indicated inhibitors for 72 hours and checked the cellular proliferation using Cell Titer Blue. We first treated MCF7 and MDA-MB-231 breast cancer cells with the inhibitors (Figure 5.4). Even though both NH-C1-10 and TM showed similar cytotoxicity at lower concentrations, NH-C1-10 treatment had reached 0% cell viability at higher concentrations, which TM could not. This suggests that the enhanced bioavailability of NH-C1-10 have increased the cytotoxicity. Like the immunofluorescence of acetyl α-tubulin, there was no significant cytotoxicity difference for TM at 25 and 50 μM. This

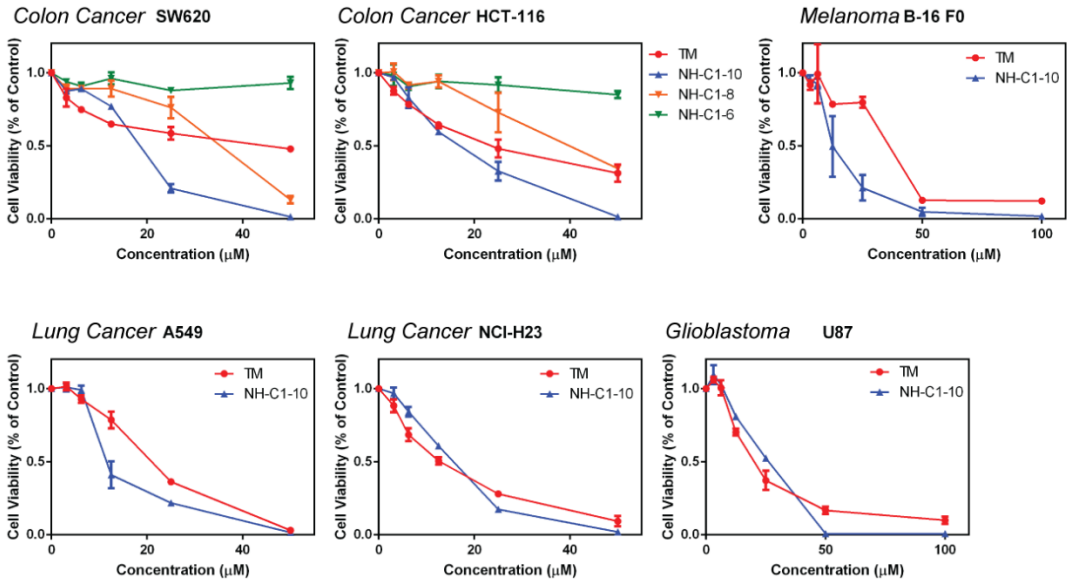


**Figure 5.5 NH-C1-10 shows stronger anti-proliferative effect than TM in colon, melanoma, lung, and glioblastoma cancer cells.** Cell viability of SW620, HCT-116, B-16 F0, A549, NCI-H23, and U87 cells were measured with Cell Titer Blue after treatment of TM, NH-C1-10, NH-C1-8, and NH-C1-6 for 72 hours. (n=3 at each concentration)

further confirmed that the limited bioavailability of TM could have restricted its anti-cancer potency. In these breast cancer cells, we have compared NH-C1-10 to NH-C1-8 and NH-C1-6. NH-C1-8 showed slightly weaker cytotoxicity than NH-C1-10, while NH-C1-6 did not have any effect. This trend also corresponds to their SIRT2 $IC_{50}$ values, which hints that the cytotoxicity of NH-C1-10 originates from its SIRT2 inhibition. Moreover, NH-C1-8 showed weaker cytotoxicity than TM at lower concentrations but stronger at higher concentrations. This could also be accounted for by the improved aqueous solubility of NH-C1-8.

**Table 15. Cellular $GI_{50}$ values (n=3 at each concentration)**

| | $GI_{50}$ (μM) | NH-C1-10 |
|---|---|---|
| **Breast Cancer** | MCF7 | 12.8 ± 1.03 |
| | MDA-MB-231 | 12.0 ± 1.05 |
| **Breast Epithelial** | HME-1 | 24.5 ± 1.04 |
| **Pancreatic Cancer** | BxPC-3 | 26.8 ± 3.04 |
| | CFPAC-1 | 31.8 ± 1.08 |
| | MIA PaCa-2 | 5.86 ± 1.56 |
| **Colon Cancer** | SW620 | 16.3 ± 1.04 |
| | HCT116 | 15.6 ± 1.08 |
| **Lung Cancer** | A549 | 11.3 ± 1.06 |
| | NCI-H23 | 14.5 ± 1.03 |
| **Glioblastoma** | U87 | 24.1 ± 1.07 |
| **Melanoma** | B-16 F0 | 12.9 ± 1.10 |

In addition to the breast cancer cell lines, we have also checked the inhibitors against several pancreatic cancer cells (Figure 5.4). In MIA PaCa-2, NH-C1-10 showed slightly stronger cytotoxicity than TM. Also, like the breast cancer cell lines, NH-C1-8 displayed slightly weaker cytotoxicity than NH-C1-10, and NH-C1-6 again had minimal effect. This trend further verified the cytotoxicity of NH-C1-10 in pancreatic cancer cells may originate from its SIRT2 inhibition. In BxPC-3 and CFPAC-1, NH-C1-10 showed stronger cytotoxicity than TM. At 100 μM, TM could only reach about 50% viability. In contrast, NH-C1-10 led to 0% viability at 50 μM.

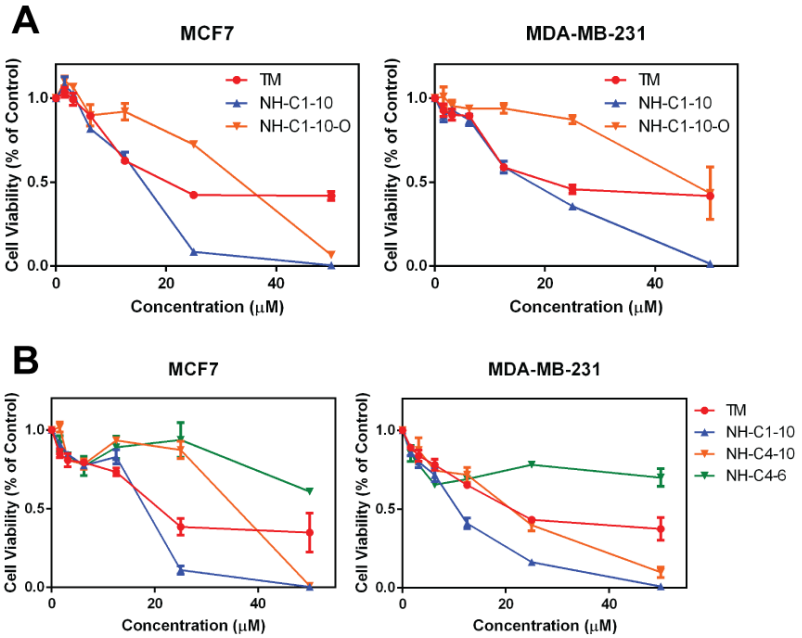


**Figure 5.6 NH-C1-10-O, NH-C4-10, and NHC4-6 show weaker anti-proliferative effect than NH-C1-10.** Cell viability of MCF7 and MDA-MB-231 cells were measured with Cell Titer Blue after treatment of TM, NH-C1-10, NH-C1-10-O, NH-C4-10, and NH-C4-6 for 72 hours. (n=3 at each concentration)

We also had compared the cytotoxicity of TM and NH-C1-10 in colorectal (SW620, HCT-116), melanoma (B-16 F0), lung (A549, NCI-H23), and glioblastoma (U87) cancer cell lines (Figure 5.5). In these cancer cell lines, we had observed stronger cytotoxicity of NH-C1-10, compared to TM. Consistent with the breast and pancreatic cancer cells, weaker cytotoxicity of NH-C1-8 and NH-C1-6 were observed in SW620 and HCT-116 colorectal cancer cells. We calculated the $GI_{50}$ values of the NH-C1-10 against these tested cell lines (Table 15). In most of the cancer cell types, the $GI_{50}$ values of NH-C1-10 were lower than 25 μM.

To confirm whether the cytotoxicity of NH-C1-10 is from its SIRT2 inhibition, we compared NH-C1-10-O and NH-C4 series inhibitors in MCF7 and MDA-MB-231 breast cancer cells (Figure 5.6A, B). Consistent with their worse SIRT2 $IC_{50}$, NH-C1-10-O, NH-C4 series of compounds showed significantly weaker cytotoxicity than NH-C1-10. This supported that the cytotoxicity of NH-C1-10 is due to its ability to inhibit SIRT2 and verified the importance of the benzodiazapienedione core and the thio-acyl group of NH-C1-10 for the SIRT2 inhibition.

**Table 16. Calculated concentrations (μg per million cells) of TM and NH-C1-10 detected from MDA-MB-231 cells.**

| μg per million cells | 25 μM | 50 μM |
|---|---|---|
| **TM** | 0.0701 | 0.0827 |
| **NH-C1-10** | 0.152 | 0.228 |

To directly test that NH-C1-10's better cellular activity and cytotoxicity was due to improved cellular permeabilities, we measured the amount of NH-C1-10 and TM in cells after treatment (Table 16). MDA-MB-231 breast cancer cells were treated with 25 and 50 μM of NH-C1-10 and TM for 6 hours. Then, the cells were carefully washed with phosphate-buffered saline (PBS) three times, and small molecules were extracted with ice-cold methanol. After centrifuging, the supernatant was loaded to LC-MS for analysis. For TM, 0.070 and 0.083 μg per million cells were detected at 25 and 50 μM treatment, respectively. For NH-C1-10, 0.15 and 0.23 μg per million cells were detected at 25 and 50 μM treatment, respectively. As shown, at both

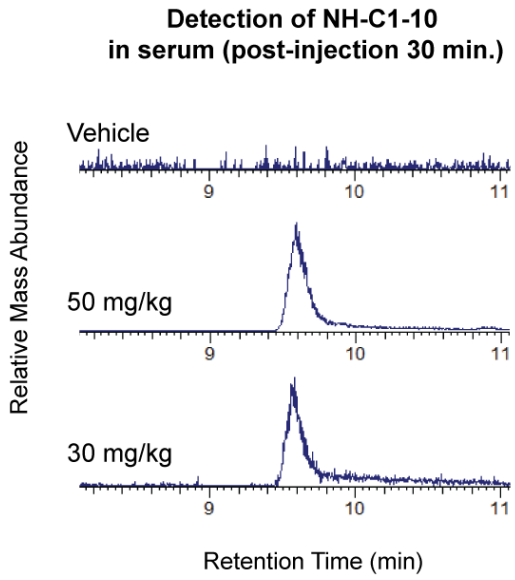


**Figure 5.7 Detection of NH-C1-10 in serum after 30 minutes of injection**. Detection of NH-C1-10 in mice serum collected after 30 minutes of intraperitoneal injection at 30 and 50 mg/kg injection.

concentrations, more NH-C1-10 was detected in the cells than TM. For TM, the difference between 25 and 50 μM was minimal, while there was an about 1.5-fold increase from 25 to 50 μM of NH-C1-10. This may explain why the cellular SIRT2 inhibition and cytotoxicity of TM have plateaued at high concentrations. Meanwhile, cellular SIRT2 inhibition and cytotoxicity of NH-C1-10 continued to increase in a dose-dependent manner. Overall, the decreased cLogP and increased permeability of NH-C1-10 could have led to stronger cellular SIRT2 inhibition and cytotoxicity.

### 5.3.5 NH-C1-10 impairs tumor growth in mice.

As NH-C1-10 showed effective cytotoxicity, we further tested its anticancer effect in tumor xenograft mice models. Among all the tested cell types, we have specifically chosen pancreatic cancer, because it is one of the most difficult cancers to

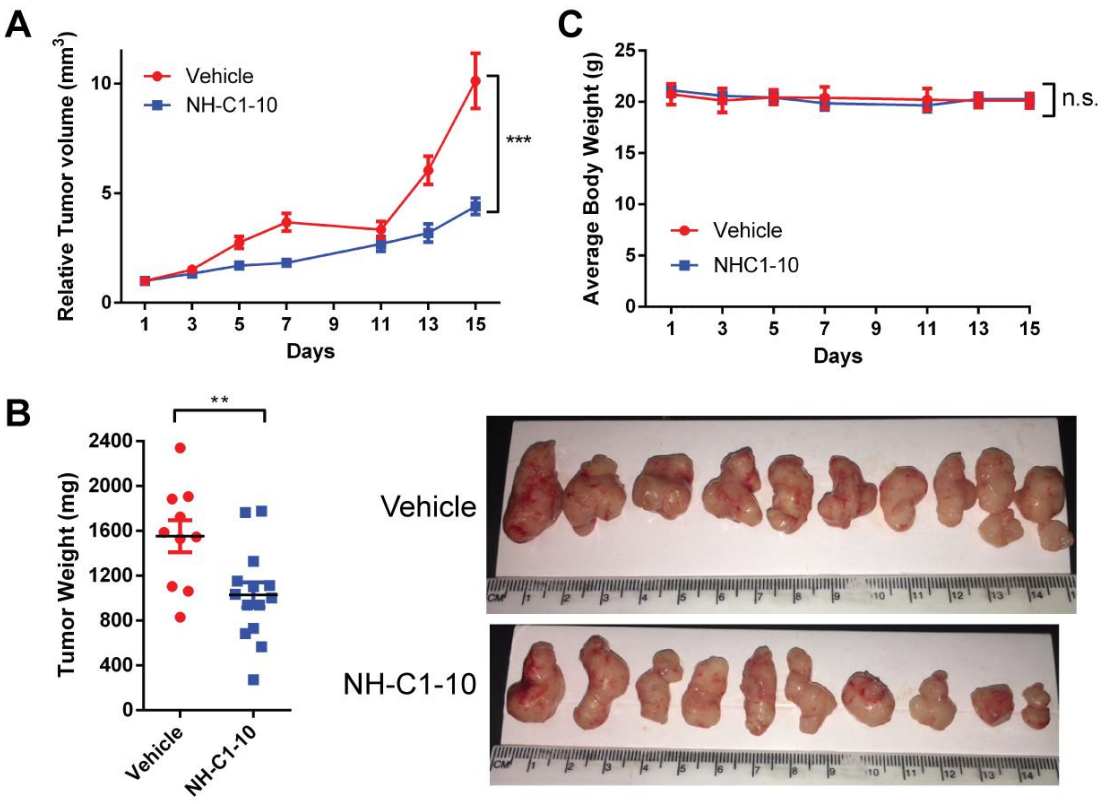


**Figure 5.8 NH-C1-10 significantly decreased tumor growth in BxPC-3 tumor xenograft.** (A) Tumor volume over time for NH-C1-10 (50 mg/kg) or vehicle (10% DMSO, 90% PBS) treated mice. NSG mice injected with BxPC-3 human pancreatic cancer cells were treated every day for 15 days. (*** P value = 0.0005, Two-tailed Student's t-test, n=10 tumors for vehicle, n=14 tumors for NH-C1-10). (B) Tumor weights and representative tumor images of BxPC-3 xenograft mice treated with NH-C1-10 (50 mg/kg) or vehicle for 15 days (** P value = 0.0096, Two-tailed Student's t-test, n=10 tumors for vehicle, n=14 tumors for NH-C1-10). (C) Average body weight of mice treated with NH-C1-10 (50 mg/kg) or vehicle for 15 days. No difference in body weight was observed between the groups. n=5 mice for vehicle and n=7 mice for NH-C1-10. ‡‡‡

‡‡‡ Data shown in Figures A, B, and C are the mean values ± standard deviation.

treat and the third-most common cause of cancer death in the United States with a poor prognosis. There is no readily used pancreatic cancer-specific chemotherapy. Common chemotherapy agents often cause severe side effects, including nausea, hair loss, and low white blood cells.

Before testing NH-C1-10 in tumor xenograft mice study, we assessed whether NH-C1-10 can be detected in the mice serum after interpretational administration (Figure 5.7). After treating the mice with NH-C1-10 (in 10% DMSO and 90% PBS) for 30 minutes, we collected blood and isolated the serum by centrifugation. Then, we extracted the small molecules with ice-cold methanol for detection by LC-MS. In both 30 mg/kg and 50 mg/kg dosages, clear mass traces of NH-C1-10 were detected.

After validating that NH-C1-10 can be detected in the serum, we assessed the toxicity of NH-C1-10 by daily injection of 50 mg/kg for five days. We have monitored their body weights, hair grooming behaviors, and physical appearances. Throughout the experiment period, NH-C1-10 did not induce any significant weight drop, hair loss, or lethargic behaviors.

Then, we tested NH-C1-10 in a pancreatic tumor xenograft mouse model. The pancreatic cancer cell line, BxPC-3, was subcutaneously injected into immunocompromised male NSG mice. Once the tumors had grown, the tumors were cut into pieces and transplanted to other immunocompromised NSG mice for the study. When the transplanted tumors have grown to 100-200 $mm^3$, the mice were divided into two s for the daily injection of NH-C1-10 and control injection of the vehicle (10% DMSO and 90% PBS). We used male mice as pancreatic cancer is more common in male than female.[30] As seen through the tumor volume, NH-C1-10

treatment had significantly impaired tumor growth. At the end of the study, the tumor volume of the vehicle group was twice bigger than that of the NH-C1-10 group (Figure 5.8A). Also, the average tumor weights of NH-C1-10 and vehicle group were 1030 and 1550 mg, respectively (Figure 5.8B). Thus, NH-C1-10 treatment decreased both volume and weight of BxPC-3 pancreatic tumors. Throughout the study, no significant weight loss or severe toxicity in both groups was not observed (Figure 5.8C).

## 5.4 Conclusion

To improve the aqueous solubility and permeability, we have designed NH-C1-10, a simpler SIRT2 inhibitor with a benzodiazapienedione core. Although NH-C1-10 showed slightly weaker SIRT2 inhibition than TM *in vitro*, NH-C1-10 had displayed stronger SIRT2 inhibition and cytotoxicity than TM in cellular studies. This improvement could be due to the enhanced aqueous solubility and permeability of NH-C1-10. Furthermore, NH-C1-10 had shown anti-cancer effects in breast, pancreatic, colorectal, melanoma, lung, and glioblastoma cancer cell lines. We anticipate that NH-C1-10 can also be used to treat other cancer cell lines. In the pancreatic tumor xenograft mouse study, NH-C1-10 impaired the tumor growth without any severe toxicity. Overall, this study confirms that SIRT2 inhibition serves as a promising target for cancer therapy and developed a SIRT2 inhibitor with enhanced aqueous solubility, cell permeability, and cellular potency.

## 5.5 References

1. Sauve, A. A., Wolberger, C., Schramm, V. L., and Boeke, J. D. (2006) The

biochemistry of sirtuins, *Annu. Rev. Biochem. 75*, 435-465.

2. Sauve, A. A., Celic, I., Avalos, J., Deng, H., Boeke, J. D., and Schramm, V. L. (2001) Chemistry of gene silencing: the mechanism of NAD+-dependent deacetylation reactions, *Biochemistry 40*, 15456-15463.

3. Feldman, J. L., Dittenhafer-Reed, K. E., Kudo, N., Thelen, J. N., Ito, A., Yoshida, M., and Denu, J. M. (2015) Kinetic and Structural Basis for Acyl-Group Selectivity and NAD <sup>+</sup> Dependence in Sirtuin-Catalyzed Deacylation, *Biochemistry 54*, 3037-3050.

4. Wang, M., and Lin, H. (2021) Understanding the Function of Mammalian Sirtuins and Protein Lysine Acylation, *Annu. Rev. Biochem.*

5. Avalos, J. L., Bever, K. M., and Wolberger, C. (2005) Mechanism of sirtuin inhibition by nicotinamide: altering the NAD(+) cosubstrate specificity of a Sir2 enzyme, *Mol. Cell 17*, 855-868.

6. Bheda, P., Jing, H., Wolberger, C., and Lin, H. (2016) The Substrate Specificity of Sirtuins, *Annu. Rev. Biochem. 85*, 405-429.

7. Feldman, J. L., Baeza, J., and Denu, J. M. (2013) Activation of the protein deacetylase SIRT6 by long-chain fatty acids and widespread deacylation by mammalian sirtuins, *J Biol Chem 288*, 31350-31356.

8. Jing, H., and Lin, H. (2015) Sirtuins in Epigenetic Regulation, *Chem. Rev. 115*, 2350-2375.

9. Kosciuk, T., Wang, M., Hong, J. Y., and Lin, H. (2019) Updates on the epigenetic roles of sirtuins, *Curr. Opin. Chem. Biol. 51*, 18-29.

10. Jang, J., Huh, Y. J., Cho, H. J., Lee, B., Park, J., Hwang, D. Y., and Kim, D. W. (2017) SIRT1 Enhances the Survival of Human Embryonic Stem Cells by Promoting DNA Repair, *Stem Cell Reports 9*, 629-641.

11. Hu, J., Jing, H., and Lin, H. (2014) Sirtuin inhibitors as anticancer agents, *Future Med. Chem. 6*, 945-966.

12. Herskovits, A. Z., and Guarente, L. (2013) Sirtuin deacetylases in neurodegenerative diseases of aging, *Cell Res. 23*, 746-758.

13. Barber, M. F., Michishita-Kioi, E., Xi, Y., Tasselli, L., Kioi, M., Moqtaderi, Z., Tennen, R. I., Paredes, S., Young, N. L., Chen, K., Struhl, K., Garcia, B. A., Gozani, O., Li, W., and Chua, K. F. (2012) SIRT7 links H3K18 deacetylation to maintenance of oncogenic transformation, *Nature 487*, 114-118.

14. Khan, D., Sarikhani, M., Dasgupta, S., Maniyadath, B., Pandit, A. S., Mishra, S.,

Ahamed, F., Dubey, A., Fathma, N., Atreya, H. S., Kolthur-Seetharam, U., and Sundaresan, N. R. (2018) SIRT6 deacetylase transcriptionally regulates glucose metabolism in heart, *J. Cell. Physiol. 233*, 5478-5489.

15. Jeong, S. G., and Cho, G. W. (2017) The tubulin deacetylase sirtuin-2 regulates neuronal differentiation through the ERK/CREB signaling pathway, *Biochem Biophys Res Commun 482*, 182-187.

16. Teng, Y.-B., Jing, H., Aramsangtienchai, P., He, B., Khan, S., Hu, J., Lin, H., and Hao, Q. (2015) Efficient Demyristoylase Activity of SIRT2 Revealed by Kinetic and Structural Studies, *Sci. Rep. 5*, 8529.

17. Zhou, W., Ni, T. K., Wronski, A., Glass, B., Skibinski, A., Beck, A., and Kuperwasser, C. (2016) The SIRT2 Deacetylase Stabilizes Slug to Control Malignancy of Basal-like Breast Cancer, *Cell Rep. 17*, 1302-1317.

18. Liu, P. Y., Xu, N., Malyukova, A., Scarlett, C. J., Sun, Y. T., Zhang, X. D., Ling, D., Su, S. P., Nelson, C., Chang, D. K., Koach, J., Tee, A. E., Haber, M., Norris, M. D., Toon, C., Rooman, I., Xue, C., Cheung, B. B., Kumar, S., Marshall, G. M., Biankin, A. V., and Liu, T. (2013) The histone deacetylase SIRT2 stabilizes Myc oncoproteins, *Cell Death Differ. 20*, 503-514.

19. Zhao, D., Zou, S. W., Liu, Y., Zhou, X., Mo, Y., Wang, P., Xu, Y. H., Dong, B., Xiong, Y., Lei, Q. Y., and Guan, K. L. (2013) Lysine-5 acetylation negatively regulates lactate dehydrogenase A and is decreased in pancreatic cancer, *Cancer Cell 23*, 464-476.

20. Jing, H., Zhang, X., Wisner, S. A., Chen, X., Spiegelman, N. A., Linder, M. E., and Lin, H. (2017) SIRT2 and lysine fatty acylation regulate the transforming activity of K-Ras4a, *eLife 6*, e32436.

21. Kosciuk, T., Price, I. R., Zhang, X., Zhu, C., Johnson, K. N., Zhang, S., Halaby, S. L., Komaniecki, G. P., Yang, M., DeHart, C. J., Thomas, P. M., Kelleher, N. L., Fromme, J. C., and Lin, H. (2020) NMT1 and NMT2 are lysine myristoyltransferases regulating the ARF6 GTPase cycle, *Nat. Commun. 11*, 1067.

22. Kozako, T., Mellini, P., Ohsugi, T., Aikawa, A., Uchida, Y. I., Honda, S. I., and Suzuki, T. (2018) Novel small molecule SIRT2 inhibitors induce cell death in leukemic cell lines, *BMC Cancer 18*, 791.

23. Mellini, P., Itoh, Y., Elboray, E. E., Tsumoto, H., Li, Y., Suzuki, M., Takahashi, Y., Tojo, T., Kurohara, T., Miyake, Y., Miura, Y., Kitao, Y., Kotoku, M., Iida, T., and Suzuki, T. (2019) Identification of Diketopiperazine-Containing 2-Anilinobenzamides as Potent Sirtuin 2 (SIRT2)-Selective Inhibitors Targeting the "Selectivity Pocket", Substrate-Binding Site, and NAD(+)-Binding Site, *J. Med. Chem. 62*, 5844-5862.

24. Rumpf, T., Schiedel, M., Karaman, B., Roessler, C., North, B. J., Lehotzky, A., Olah, J., Ladwein, K. I., Schmidtkunz, K., Gajer, M., Pannek, M., Steegborn, C., Sinclair, D. A., Gerhardt, S., Ovadi, J., Schutkowski, M., Sippl, W., Einsle, O., and Jung, M. (2015) Selective Sirt2 inhibition by ligand-induced rearrangement of the active site, *Nat. Commun. 6*, 6263.

25. Li, Y., Zhang, M., Dorfman, R. G., Pan, Y., Tang, D., Xu, L., Zhao, Z., Zhou, Q., Zhou, L., Wang, Y., Yin, Y., Shen, S., Kong, B., Friess, H., Zhao, S., Wang, L., and Zou, X. (2018) SIRT2 Promotes the Migration and Invasion of Gastric Cancer through RAS/ERK/JNK/MMP-9 Pathway by Increasing PEPCK1-Related Metabolism, *Neoplasia 20*, 745-756.

26. Nielsen, A. L., Rajabi, N., Kudo, N., Lundø, K., Moreno-Yruela, C., Bæk, M., Fontenas, M., Lucidi, A., Madsen, A. S., Yoshida, M., and Olsen, C. A. (2021) Mechanism-based inhibitors of SIRT2: structure–activity relationship, X-ray structures, target engagement, regulation of α-tubulin acetylation and inhibition of breast cancer cell migration, *RSC Chemical Biology*.

27. Jing, H., Hu, J., He, B., Negron Abril, Y. L., Stupinski, J., Weiser, K., Carbonaro, M., Chiang, Y. L., Southard, T., Giannakakou, P., Weiss, R. S., and Lin, H. (2016) A SIRT2-Selective Inhibitor Promotes c-Myc Oncoprotein Degradation and Exhibits Broad Anticancer Activity, *Cancer Cell 29*, 297-310.

28. Farooqi, A. S., Hong, J. Y., Cao, J., Lu, X., Price, I. R., Zhao, Q., Kosciuk, T., Yang, M., Bai, J. J., and Lin, H. (2019) Novel Lysine-Based Thioureas as Mechanism-Based Inhibitors of Sirtuin 2 (SIRT2) with Anticancer Activity in a Colorectal Cancer Murine Model, *J. Med. Chem. 62*, 4131-4141.

29. Hong, J. Y., Fernandez, I., Anmangandla, A., Lu, X., Bai, J. J., and Lin, H. (2021) Pharmacological Advantage of SIRT2-Selective versus pan-SIRT1-3 Inhibitors, *ACS Chem. Biol. 16*, 1266-1275.

30. Rawla, P., Sunkara, T., and Gaduputi, V. (2019) Epidemiology of Pancreatic Cancer: Global Trends, Etiology and Risk Factors, *World J. Oncol. 10*, 10-27.

31. Hong, J. Y., Price, I. R., Bai, J. J., and Lin, H. (2019) A Glycoconjugated SIRT2 Inhibitor with Aqueous Solubility Allows Structure-Based Design of SIRT2 Inhibitors, *ACS Chem. Biol. 14*, 1802-1810.

32. Biel, M., Deck, P., Giannis, A., and Waldmann, H. (2006) Synthesis and evaluation of acyl protein thioesterase 1 (APT1) inhibitors, *Chemistry (Easton) 12*, 4121-4143.

33. North, B. J., Marshall, B. L., Borra, M. T., Denu, J. M., and Verdin, E. (2003) The Human Sir2 Ortholog, SIRT2, Is an NAD+-Dependent Tubulin Deacetylase, *Mol. Cell 11*, 437-444.

34. Vaziri, H., Dessain, S. K., Ng Eaton, E., Imai, S. I., Frye, R. A., Pandita, T. K., Guarente, L., and Weinberg, R. A. (2001) hSIR2(SIRT1) functions as an NAD-dependent p53 deacetylase, *Cell 107*, 149-159.

Methods

**General Experimental Methods**

All chemical and biological reagents used for this study was purchased as analytical or higher grades from commercial vendors. Unless specifically notified, all chemical reactions took place under nitrogen gas balloon. SiliaFlash Irregular Silica Gel P60, 40 – 63 μm, 60 Å was used. Shimadzu HPLC LC20-AD and Thermo Scientific LCQ Fleet Mass spectrometer with Kinetex 5u EVO C18 100 Å Column (30 x 2.1 mm, 5 μm) was used for the mass spectrometry detection of compounds. Positive-ion mode was used for the detection. For this setup, HPLC-grade water with 0.1% HPLC-grade acetic acid and HPLC-grade acetonitrile with 0.1% HPLC-grade acetic acid were used as Buffer A and B, respectively. The UV traces of the compounds were detected at 260 nm. The measured NMR spectra was collected by Bruker 500 spectrometer. For sirtuin in vitro enzymatic assays, Shimadzu HPLC LC20-AD with Kinetex 5u EVO C18 100 Å (100 mm x 4.60, 5 μm) was used, and the UV peaks were detected at 215 and 280 nm. For this instrument, HPLC-grade water with 0.1% trifluoroacetic acid and HPLC-grade acetonitrile with 0.1% trifluoroacetic acid were used as Buffer A and B, respectively. The synthesized compounds were verified to be at least 95% pure using Shimadzu HPLC 20-AD system.

**Antibodies**

Anti-acetyl-α-tubulin (6-11B-1) (MABT868) was purchased from Sigma-Aldrich. Anti-rabbit IgG-horseradish peroxidase (#7074), and anti-acetyl-p53 antibody (K382) (#2525) were purchased from Cell Signaling Technology. The goat anti-Mouse IgG (H+L) secondary antibody, Cyanine3 (A10521) were purchased from ThermoFisher. The anti-β-Actin (C4) conjugated horseradish peroxidase (sc-4777) mouse anti-rabbit IgG-horseradish peroxidase ("sc-2357) were purchased from Santa Cruz Biotechnology.

**Immunoblots**

Immunoblots were performed as previously reported. Collected cells were lysed by 1% NP-40 lysis buffer (25 mM Tris-HCl, pH 8.0, 10% glycerol, 150 mM NacL, 1%  Igepal CA-630) with 1 x protease inhibitor cocktail (Sigma).

**Cell culture and transfection**

All cells were incubated at 37 °C with 5% $CO_2$. MCF7, MDA-MB-231, B-16 F0, U87, and MIA PaCa-2 cells were cultured in Dulbecco's Modified Eagle Medium (DMEM) with 10% Heat Inactivated Fetal Bovine Serum (FBS) from Invitrogen. HCT-116 cells were cultured in McCoy's 5A Medium with 10% FBS. SW620, A549, NCI-H23, and BxPC-3 cells were cultured in Roswell Park Memorial Institute Medium (RPMI) with 10% FBS. CFPAC-1 cells were cultured in Iscove's Modified Dulbecco's Medium (IMEM) with 10% FBS.

**Mice**

The mice protocol for this study was approved by the Cornell University Institutional Animal Care and Use Committee. The studied mice were caged under pathogen-free condition at the Association for the Assessment and Accreditation of

Laboratory Animal Care International accredited facility and cared for in compliance with the Guide for the Care and Use of Laboratory Animals. All the mice for this study were kept at 12:12 light:dark cycle and had received irradiated food and reverse osmosis, hyper-acidified water.

**Preparation of SIRT1, 2, and 3**

Human SIRT1, 2, and 3 were prepared as previously reported.[1-5]

**Analytical HPLC in vitro sirtuin deacetylation IC50 assay**

Analytical HPLC in vitro SIRT1, 2, and 3 deacetylation IC50 assays were done by following previously reported procedures.[2, 3]

**Intermediate trapping of NH-C1-10**

To the mixture of 200 μM SIRT2, 120 μM NAD+, and 20 mM Ammonium Bicarbonate, 100 μM of NH-C1-10 was added. After 5 minutes of incubation at 37 °C, the reaction was quenched with acetonitrile. Then, the mixture was centrifuged at 17.0 x g for 5 minutes to remove the precipitated protein, and the supernatant was injected into LC-MS using water and acetonitrile as solvents. The intermediate was detected by alternating detection method of positive and negative ion mode.

**Assessing inhibition of SIRT1 deacetylation in cells**

MCF7 cells at 70% confluency in 10-cm plates were incubated with 400 nM of Trichostatin A, and indicated concentrations of EX-527, TM, NH-C1-10, 8, or 6 for 6 h ours. The cells were collected and lysed with 1% NP-40 lysis buffer (50 mM Tris-HCl pH 8.0, 150 mM NaCl, 1% NP-40, and 1 x Protease Inhibitor Cocktail). The membrane was blotted with anti-Ac-p53 (K382) antibody to detect the acetylation levels of p53. As the loading control, β-Actin was used.

**Assessing inhibition of SIRT2 deacetylation in cells**

200,000 MCF7 cells were seeded to 35-mm glass bottom dishes (MatTek). After overnight incubation at 37 °C and 5% $CO_2$, the cells were treated with DMSO control or indicated concentrations of the inhibitors (TM, NH-C1-10, 8, and 6) for 6 hours. The cells were washed with ice-cold phosphate buffered saline (PBS) three times, and fixed with ice-cold methanol for 10 minutes. After one wash with PBS, 0.1% Triton-X in PBS was added. After 10 minutes of incubation, the cells were washed with PBS three times, and further incubated with 1% BSA in TBST (10 mM Tris-HCl pH 7.4, 150 mM NaCl, and 0.1% Tween-20) for 30 minutes. The cells were then incubated with Ac-α-tubulin antibody (1:100 dilution in 1% BSA in TBST buffer) overnight at 4 °C. Then, the cells are washed with TBST buffer three times, and were treated with Cy3 conjugated secondary antibody (1:1000) in 1% BSA in TBST. The cells were kept in dark at room temperature for 1 hour. The cells were washed with TBST three times and mounted with DAPI fluoromount. The immunofluorescence imaging was done by Cytation 5 Cell Imaging Reader.

**Cellular proliferation assay**

1000 (HCT-116), 2000 (MDA-MB-231, A549, SW620), 3000 (MCF7, B-16 F0, NCI-H23, U87, MIA PaCa-2), or 4000 (BxPC-3, CFPAC-1) cells in 100 μL of media were seeded to the wells of a Corning Costar Flat Bottom 96-well plate. After overnight incubation at 37 °C and 5% $CO_2$, 100 μL of inhibitors dissolved in media at various concentrations was added to each well. The final inhibitor concentrations ranged from 1.56 μM to 100 μM. At each concentration, triplicate wells were done.

After 72 hours of incubation, CellTiter Blue from Promega was added and the cell proliferation was detected according to the manufacturer's protocol.

**NH4-6 and NH4-13 cellular permeability assay**

10 mL DMEM with DMSO or the indicated concentration of the inhibitors was added to the MDA-MB-231 cells at 70% confluency in 10-cm plates. After 6 hours, the cells were washed carefully with ice-cold PBS three times and collected. After centrifuging the cells at 4 °C, 100 μL of ice-cold methanol was added to extract small molecules. The tubes were vortexed and centrifuged at 15,000g for 20 minutes. 100 μL of the supernatant was loaded to LC-MS for detection. The standard curves with concentrations ranging from 2 μM to 100 μM were prepared similarly.

**Detection of NH-C1-10 in mouse serum**

To the male NSG mice from Jackson Laboratory, 30 mg/kg or 50 mg/kg NH-C1-10 dissolved in 10% DMSO and 90% PBS was injected. After 30 minutes, 200 μL of blood were taken from the mice. The collected blood were centrifuged at 15,000 g for 20 minutes at 4 °C, and supernatant was transferred to new tubes. Then, the supernatant was centrifuged again for 15,000 g for 20 minutes at 4 °C. 80 μL of supernatant was transferred to new tubes, and 80 μL methanol was added. The tubes were vigorously vortexed and centrifuged at 15,000 g for 15 minutes at 4 °C. The collected supernatant was loaded to the LC-MS to detect NH-C1-10.

**Mouse tumor xenograft experiments with BxPC-3**

Xenotransplantation studies were performed as previously described.[6] Four million BxPC-3 pancreatic cancer cells suspended in 100 μL PBS were subcutaneously injected into flanks of male NSG mice from the Jackson Laboratory.

Once the tumor sizes grew to 100 – 200 $mm^3$, the transplanted tumor pieces were collected and cut into equal sizes. Then, each piece was transplanted into flanks of new mice. Again, once the tumor sizes grew to 100 – 200 $mm^3$, mice were treated by intraperitoneal injection for 15 days with vehicle (10% DMSO, 90% PBS) or 50 mg/kg NH-C1-10 (10% DMSO, 90% PBS). The overall health, behaviors, and body weights were monitored daily. The tumor volumes were measured every other day using a caliper. Once the tumors reached the endpoint, mice were sacrificed by $CO_2$ asphyxiation. The tumors were collected and weighed for the data collection.

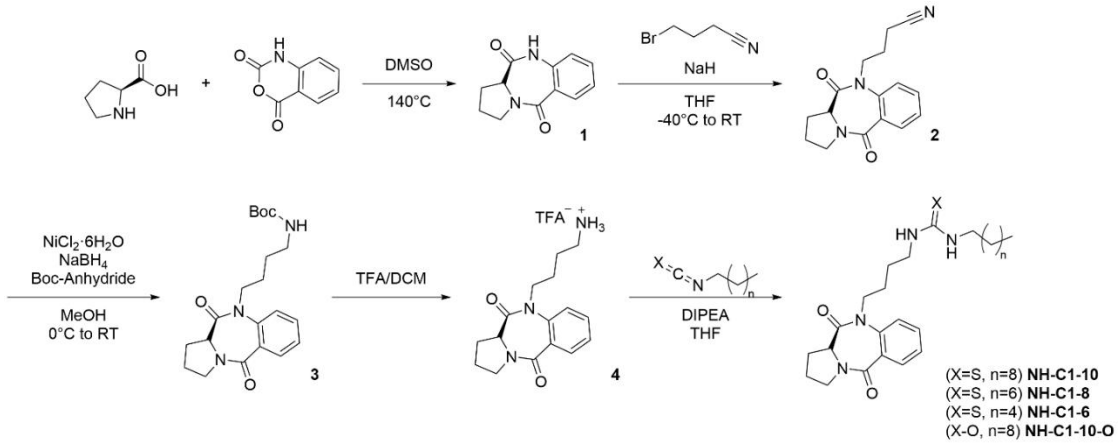


**Scheme 5.1 Synthesis of NH-C1-10, NH-C1-8, NH-C1-6, and NH-C1-10-O**

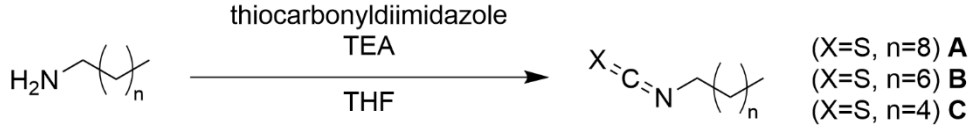


**Scheme 5.2 Synthesis of Compound A, B, and C**

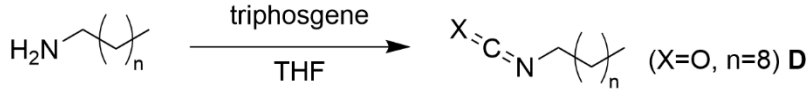


**Scheme 5.3 Synthesis of Compound D**

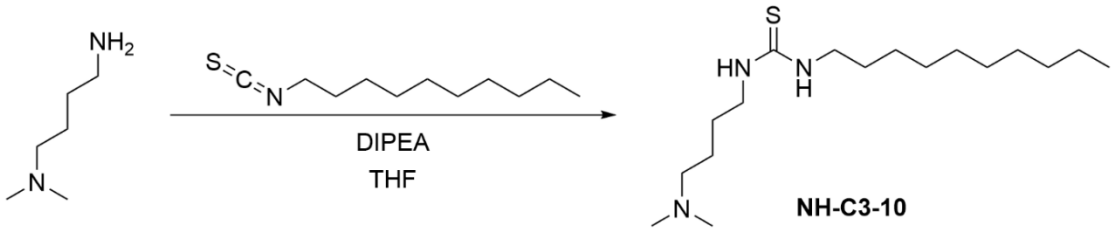


**Scheme 5.4 Synthesis of NH-C3-10**

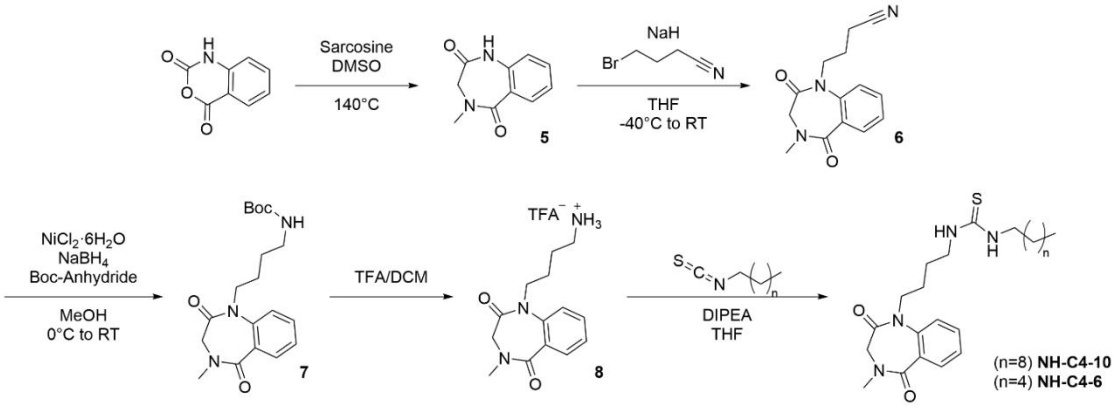


**Scheme 5.5 Synthesis of NH-C4-10, and NH-C4-6**

**Preparation of TM and Compound 1**

TM and Compound 1 were synthesized and prepared by following a previous report.[3, 7]

**Synthesis of (*R*)-4-(5,11-dioxo-2,3,11,11a-tetrahydro-1*H*-benzo[e]pyrrolo[1,2-a][1,4]diazepin-10(5*H*)-yl)butanenitrile (2)**

At -40 °C, to a solution of sodium hydride (60% in mineral oil, 0.087 g, 2.20 mmol) in THF (10 mL), Compound 1 (0.3963 g, 1.83 mmol) dissolved in THF (10 mL) was added dropwise. After stirring for 1 hour, 4-bromobutrylnitrile (0.220 mL, 2.20 mmol) was added to the mixture. The mixture was slowly warmed to room temperature and stirred overnight. Then, the solvent was removed by the rotary evaporator and the crude was re-dissolved in DCM (50 mL). The mixture was washed

with water (40 mL) and brine (40 mL). The collected organic layer was dried over $Na_2SO_4$ and concentrated by rotary evaporation. The crude residue was purified by silica gel column chromatography (DCM: MeOH = 97:3) to afford the final product 2 (0.480 g, 93%). $^1$H NMR (500 MHz, $CD_3OD$) δ 7.89 (dd, J = 7.9, 1.7 Hz, 1H), 7.69 (ddd, J = 8.7, 7.4, 1.7 Hz, 1H), 7.55 (d, J = 8.2 Hz, 1H), 7.50 – 7.37 (m, 1H), 4.44 (dt, J = 14.6, 7.5 Hz, 1H), 4.32 – 4.16 (m, 1H), 3.95 – 3.74 (m, 2H), 3.56 (dt, J = 11.9, 8.2 Hz, 1H), 2.67 (td, J = 10.6, 9.4, 6.4 Hz, 1H), 2.51 – 2.32 (m, 2H), 2.24 – 2.02 (m, 3H), 2.01 – 1.74 (m, 2H). $^{13}$C NMR (126 MHz, $CD_3OD$) δ 171.41, 167.23, 140.50, 133.93, 131.95, 130.86, 127.39, 124.29, 120.21, 58.93, 47.73, 47.61, 27.45, 24.96, 24.72, 14.88. LCMS (ESI) calcd. for $[M+H]^+$ C16H18N3O2 284.13, obsd. 284.37

**Synthesis of *tert*-butyl (*R*)-(4-(5,11-dioxo-2,3,11,11a-tetrahydro-1*H*-benzo[e]pyrrolo[1,2-a][1,4]diazepin-10(5*H*)-yl)butyl)carbamate (3)**

To a stirred solution of Compound 2 (0.480 g, 1.69 mmol) in methanol (15 mL), nickel (II) chloride (0.0805 g, 0.330 mmol) and di-tert-butyl dicarbonate (0.779 mL, 3.39 mmol) was added at 0 °C. Then, sodium borohydride (0.320 g, 8.50 mmol) was added slowly in small portions to the mixture. After stirring at 0 °C for 1 hour, the ice bath was removed. The mixture was stirred overnight at room temperature. To the mixture, diethylenetriamine (0.183 mL, 1.69 mmol) was added. After stirring 1 hour at room temperature, the solvents were removed by rotary evaporator, and the mixture was re-dissolved in ethyl acetate (50 mL). The ethyl acetate layer was washed with saturated sodium bicarbonate (40 mL) and brine (40 mL). The collected organic layer was dried over $Na_2SO_4$ and concentrated by rotary evaporation. The crude residue was further purified by silica gel column chromatography (Hexane: EtOAc = 1:4) to afford

the final product 3 (0.200 g, 31%). $^{1}$H NMR (500 MHz, DMSO-*d6*) δ 7.74 (dd, J = 7.8, 1.7 Hz, 1H), 7.60 (ddd, J = 8.7, 7.2, 1.7 Hz, 1H), 7.52 (dd, J = 8.3, 1.1 Hz, 1H), 7.35 (td, J = 7.5, 1.1 Hz, 1H), 6.74 (t, J = 5.7 Hz, 1H), 4.17 (ddd, J = 14.7, 8.7, 6.4 Hz, 1H), 4.09 (dd, J = 7.5, 2.2 Hz, 1H), 3.73 – 3.52 (m, 2H), 3.41 (dt, J = 11.6, 8.0 Hz, 1H), 2.82 (q, J = 6.4 Hz, 2H), 2.49 – 2.42 (m, 1H), 1.97 – 1.87 (m, 3H), 1.35 (s, 13H). $^{13}$C NMR (126 MHz, DMSO-*d6*) δ 169.08, 164.04, 155.53, 138.87, 132.02, 130.68, 129.51, 125.45, 123.13, 77.34, 56.70, 46.50, 46.06, 28.24, 26.52, 26.20, 24.68, 23.34. LCMS (ESI) calcd. for $[M+H]^+$ $C_{21}H_{30}N_3O_4$ 388.22, obsd. 388.07. LCMS (ESI) calcd. for $[M+H\text{-}Boc]^+$ $C_{16}H_{22}N_3O_2$ 288.16, obsd. 288.36.

**Synthesis of (*R*)-4-(5,11-dioxo-2,3,11,11a-tetrahydro-1*H*-benzo[e]pyrrolo[1,2-a][1,4]diazepin-10(5*H*)-yl)butan-1-aminium (4)**

To a stirred solution of Compound 3 (0.200 g, 0.516 mmol) in DCM (3 mL), trifluoroacetic acid (2 mL) was added dropwise. After stirring for 2 hours, the mixture was co-evaporated with toluene three times by rotary evaporation. The crude residue was taken to next step without any further purification.

**Synthesis of (*R*)-1-decyl-3-(4-(6,11-dioxo-6a,7,8,9-tetrahydro-6*H*-pyrido[4,3-e]pyrrolo[1,2-a][1,4]diazepin-5(11*H*)-yl)butyl)thiourea (NH-C1-10)**

To a stirred solution of Compound 4 (0.516 mmol) from the previous step in THF (5 mL), 1-isothiocyanatodecane (0.205 g, 1.03 mmol) and DIPEA (0.400 mL, 2.06 mmol) was added. After stirring overnight at room temperature, the solvents were removed by rotary evaporator. The crude was re-dissolved in ethyl acetate (60 mL) and washed with water (40 mL x 2) and brine (40 mL). The collected organic layer was dried over $Na_2SO_4$ and concentrated by rotary evaporation. The crude residue was

further purified by silica gel column chromatography (Hexane: EtOAc = 1:3) to afford the final product NH-C1-10 (0.201 g, 81%). $^{1}$H NMR (500 MHz, $CD_3OD$) δ 7.84 (dd, J = 7.8, 1.7 Hz, 1H), 7.65 (ddd, J = 8.8, 7.3, 1.7 Hz, 1H), 7.53 (dd, J = 8.4, 1.1 Hz, 1H), 7.40 (td, J = 7.5, 1.0 Hz, 1H), 4.38 (dt, J = 14.2, 7.2 Hz, 1H), 4.25 – 4.11 (m, 1H), 3.77 (dtt, J = 11.8, 8.4, 4.0 Hz, 2H), 3.59 – 3.50 (m, 1H), 3.39 (s, 4H), 2.69 – 2.56 (m, 1H), 2.16 – 1.99 (m, 3H), 1.64 – 1.39 (m, 6H), 1.33 (d, J = 11.2 Hz, 14H), 0.92 (t, J = 6.9 Hz, 3H). $^{13}$C NMR (126 MHz, $CD_3OD$) δ 182.10, 169.75, 165.96, 139.28, 132.40, 130.68, 129.27, 125.80, 123.22, 57.56, 46.27, 31.67, 29.31, 29.29, 29.06, 26.55, 26.05, 24.70, 23.38, 22.34, 13.04. LCMS (ESI) calcd. for $[M+H]^+C27H43N4O2S$ 487.30, obsd. 487.21.

**Synthesis of (*R*)-1-(4-(6,11-dioxo-6a,7,8,9-tetrahydro-6*H*-pyrido[4,3-e]pyrrolo[1,2-a][1,4]diazepin-5(11*H*)-yl)butyl)-3-octylthiourea (NH-C1-8)**

To a stirred solution of Compound 4 (0.168 mmol) in THF (1.6 mL), 1-isothiocyanatooctane (0.0575 g, 0.336 mmol) and DIPEA (0.118 mL, 0.672 mmol) was added. After stirring overnight at room temperature, the solvents were removed by rotary evaporator and the residue was re-dissolved in ethyl acetate (15 mL). The organic layer was washed with water (10 mL x 2) and brine (10 mL), and dried over $Na_2SO_4$. After concentrating in vacuo, the crude residue was further purified by column chromatography (Hexane: EtOAc = 1:3) to afford the final product NH-C1-8 (0.0535, 69%). $^{1}$H NMR (500 MHz, $CD_3OD$) δ 7.84 (dd, J = 7.8, 1.6 Hz, 1H), 7.65 (ddd, J = 8.7, 7.3, 1.7 Hz, 1H), 7.53 (dd, J = 8.3, 1.0 Hz, 1H), 7.39 (td, J = 7.6, 1.1 Hz, 1H), 4.37 (dt, J = 14.2, 7.2 Hz, 1H), 4.32 – 3.97 (m, 1H), 3.79 – 3.61 (m, 2H), 3.61 – 3.34 (m, 5H), 2.75 – 2.53 (m, 1H), 2.21 – 1.95 (m, 3H), 1.62 – 1.38 (m, 6H), 1.38 –

1.25 (m, 10H), 0.92 (t, 3H). $^{13}$C NMR (126 MHz, $CD_3OD$) δ 183.20, 171.11, 167.33, 140.67, 133.79, 132.05, 130.67, 127.18, 124.61, 58.94, 48.37, 47.67, 32.99, 30.44, 30.39, 30.22, 27.97, 27.46, 27.31, 26.11, 24.78, 23.72, 14.45. LCMS (ESI) calcd. for $[M+H]^+C_{25}H_{39}N_4O_2S$ 459.27, obsd. 459.31.

**Synthesis of (*R*)-1-(4-(6,11-dioxo-6a,7,8,9-tetrahydro-6*H*-pyrido[4,3-e]pyrrolo[1,2-a][1,4]diazepin-5(11H)-yl)butyl)-3-hexylthiourea (NH-C1-6)**

To a stirred solution of Compound 4 (0.0358 mmol) in THF (0.35 mL), 1-isothiocyanatohexane (0.0103 g, 0.0716 mmol) and triethylamine (0.0250 mL, 0.143 mmol) was added. After stirring overnight at room temperature, the solvents were removed by rotary evaporator and the residue was re-dissolved in ethyl acetate (10 mL). The organic layer was washed with water (8 mL x 2) and brine (8 mL), and dried over $Na_2SO_4$. After concentrating in vacuo, the crude residue was further purified by column chromatography (Hexane: EtOAc = 1:3) to afford the final product NH-C1-6 (0.103 g, 67%). $^1$H NMR (500 MHz, $CD_3OD$) δ 7.84 (dd, J = 7.8, 1.7 Hz, 1H), 7.64 (ddd, J = 8.8, 7.4, 1.7 Hz, 1H), 7.52 (dd, J = 8.3, 1.1 Hz, 1H), 7.39 (td, J = 7.6, 1.1 Hz, 1H), 4.37 (dt, J = 14.2, 7.2 Hz, 1H), 4.26 – 4.06 (m, 1H), 3.86 – 3.68 (m, 2H), 3.65 – 3.34 (m, 5H), 2.63 (tdd, J = 9.4, 7.1, 3.1 Hz, 1H), 2.24 – 1.95 (m, 3H), 1.65 – 1.40 (m, 6H), 1.34 (dq, J = 7.0, 2.8, 2.3 Hz, 6H), 0.92 (t, 3H). 13C NMR (126 MHz, $CD_3OD$) δ 181.32, 171.17, 167.37, 140.69, 133.81, 132.08, 130.67, 127.20, 124.63, 58.96, 48.36, 47.68, 32.72, 27.65, 27.45, 26.11, 24.79, 23.67, 14.38. LCMS (ESI) calcd. for $[M+H]^+$ $C_{23}H_{35}N_4O_2S$ 431.24, obsd. 431.11.

**Synthesis of (*R*)-1-decyl-3-(4-(6,11-dioxo-6a,7,8,9-tetrahydro-6*H*-pyrido[4,3-e]pyrrolo[1,2-a][1,4]diazepin-5(11*H*)-yl)butyl)urea (NH-C1-10-O)**

To a stirred solution of Compound 4 (0.0994 mmol) in THF (2.5 mL), 1-isocyanatodecane (0.094 g, 0.513 mmol) and DIPEA (0.180 mL, 1.03 mmol) was added. After stirring overnight at room temperature, the solvents were removed by rotary evaporator and the residue was re-dissolved in ethyl acetate (20 mL). The organic layer was washed with water (15 mL x2) and brine (15 mL), and dried over $Na_2SO_4$. After concentrating in vacuo, the crude residue was further purified by column chromatography (DCM: MeOH = 95:5) to afford the final product NH-C1-10-O (0.0342 g, 28%). $^1$H NMR (500 MHz, $CD_3OD$) δ 7.83 (dd, J = 7.8, 1.7 Hz, 1H), 7.64 (ddd, J = 8.8, 7.3, 1.7 Hz, 1H), 7.51 (dd, J = 8.3, 1.0 Hz, 1H), 7.39 (td, J = 7.6, 1.0 Hz, 1H), 4.36 (dt, J = 13.9, 7.6 Hz, 1H), 4.28 – 4.02 (m, 1H), 3.86 – 3.66 (m, 2H), 3.66 – 3.45 (m, 1H), 3.04 (dt, J = 18.3, 6.8 Hz, 4H), 2.75 – 2.45 (m, 1H), 2.32 – 1.85 (m, 3H), 1.61 – 1.37 (m, 4H), 1.37 – 1.27 (m, 16H), 0.91 (t, J = 6.9 Hz, 3H). $^{13}$C NMR (126 MHz, $CD_3OD$) δ 171.10, 167.35, 161.18, 140.70, 133.77, 132.09, 130.67, 127.18, 124.59, 58.94, 48.37, 47.65, 41.01, 40.30, 33.07, 31.34, 30.75, 30.71, 30.50, 30.47, 28.36, 27.96, 27.45, 26.12, 24.78, 23.74, 14.44. LCMS (ESI) calcd. for $[M+H]^+$ $C_{27}H_{43}N_4O_3$ 471.33, obsd. 471.52.

**Synthesis of 1-isothiocyanatodecane (A)**

To a solution of decylamine (0.382 mL, 1.91 mmol) in THF (20 mL), thiocarbonyldiimidazole (0.408 g, 2.29 mmol) and TEA (0.798 mL, 5.72 mmol) was added. After stirring overnight at room temperature, the solvent was removed by rotary evaporation and the residue was re-dissolved in ethyl acetate (50 mL). The organic layer was washed with water (40 mL) and brine (40 mL), and dried over $Na_2SO_4$. After concentrating in vacuo, the crude residue was further purified by

column chromatography (Hexane: EtOAc = 4:1) to afford the final product A (0.316 g, 83%). $^{1}$H NMR (500 MHz, $CD_3OD$) δ 3.56 (t, J = 6.5 Hz, 2H), 1.79 – 1.63 (m, 2H), 1.50 – 1.23 (m, 14H), 0.92 (t, J = 6.9 Hz, 3H). $^{13}$C NMR (126 MHz, $CD_3OD$) δ 131.24, 45.94, 33.06, 31.12, 30.60, 30.58, 30.42, 29.90, 27.65, 23.74, 14.45.

**Synthesis of 1-isothiocyanatooctane (B)**

To a solution of octylamine (0.767 mL, 4.64 mmol) in THF (40 mL), thiocarbonyldiimidazole (0.992 g, 5.56 mmol) and TEA (1.94 mL, 13.9 mmol) was added. After stirring overnight at room temperature, the solvent was removed by rotary evaporation and the residue was re-dissolved in ethyl acetate (70 mL). The organic layer was washed with water (60 mL) and brine (60 mL), and dried over $Na_2SO_4$. After concentrating in vacuo, the crude residue was further purified by column chromatography (Hexane: EtOAc = 4:1) to afford the final product B (0.739 g, 93%). $^{1}$H NMR (500 MHz, $CD_3OD$) δ 3.56 (t, J = 6.5 Hz, 2H), 1.78 – 1.60 (m, 2H), 1.53 – 1.20 (m, 10H), 0.99 – 0.83 (m, 3H). $^{13}$C NMR (126 MHz, $CD_3OD$) δ 131.24, 45.94, 32.90, 31.12, 30.26, 29.87, 27.66, 23.68, 14.42.

**Synthesis of 1-isothiocyanatohexane (C)**

To a solution of hexylamine (0.500 mL, 3.80 mmol) in THF (30 mL), thiocarbonyldiimidazole (0.814 g, 4.56 mmol) and TEA (1.60 mL, 11.4 mmol) was added. After stirring overnight at room temperature, the solvent was removed by rotary evaporation and the residue was re-dissolved in ethyl acetate (40 mL). The organic layer was washed with water (30 mL) and brine (30 mL), and dried over $Na_2SO_4$. After concentrating in vacuo, the crude residue was further purified by column chromatography (Hexane: EtOAc = 4:1) to afford the final product C (0.474 g,

87%). 1H NMR (500 MHz, $CD_3OD$) δ 3.56 (t, J = 6.5 Hz, 2H), 1.78 – 1.62 (m, 2H), 1.56 – 1.25 (m, 6H), 1.03 – 0.76 (m, 3H). 13C NMR (126 MHz, $CD_3OD$) δ 131.38, 45.94, 32.13, 31.09, 27.35, 23.56, 14.29.

**Synthesis of 1-isocyanatodecane (D)**

To a stirred solution of decylamine (1 mL, 5.00 mmol) and TEA (2.1 mL, 15.0 mmol) in THF (40 mL), triphosgene (1.78 g, 6.00 mmol) was slowly added at room temperature. After stirring overnight, the solvents were removed by rotary evaporation. The residue was re-dissolved in ethyl acetate (100 mL), and washed with water (90 mL) and brine (90 mL). The collected organic layer was dried over $Na_2SO_4$ and concentrated by rotary evaporation. The crude residue was further purified by silica gel column chromatography (Hexane: EtOAc = 4:1) to afford the final product D (0.797 g, 87%). 1H NMR (500 MHz, $CD_3OD$) δ 3.07 (t, J = 7.1 Hz, 2H), 1.47 (t, J = 7.0 Hz, 2H), 1.32 – 1.28 (m, 14H), 0.90 (t, J = 6.9 Hz, 3H). 13C NMR (126 MHz, $CD_3OD$) δ 119.63, 41.87, 33.07, 30.98, 30.71, 30.69, 30.45, 27.84, 23.74, 14.44.

**Synthesis of 1-decyl-3-(4-(dimethylamino)butyl)thiourea (NH-C3-10)**

To a stirred solution of 4-dimethylaminobutylamine (0.150 mL, 1.08 mmol) in THF (10 mL), 1-isothiocyanatodecane (0.259 g, 1.30 mmol) and DIPEA (0.377 mL, 2.17 mmol) was added at room temperature. After stirring overnight, the solvents were removed by rotary evaporation. The crude residue was re-dissolved in ethyl acetate (30 mL), and washed with water (25 mL) and brine (25 mL). The collected organic layer was dried over $Na_2SO_4$ and concentrated by rotary evaporation. The crude residue was further purified by silica gel column chromatography (DCM: MeOH = 8:2 → 75:25) to afford the final product NH-C3-10 (0.176 g, 77%). 1H NMR (500 MHz,

$CD_3OD$) δ 3.66 – 3.36 (m, 4H), 2.40 (t, J = 7.4 Hz, 2H), 2.30 (s, 6H), 1.70 – 1.49 (m, 6H), 1.48 – 1.22 (m, 14H), 0.94 (t, J = 6.7 Hz, 3H). 13C NMR (126 MHz, $CD_3OD$) δ 179.22, 60.29, 45.35, 33.06, 30.71, 30.68, 30.47, 30.45, 30.26, 28.19, 27.96, 25.50, 23.73, 14.43. LCMS (ESI) calcd. for $[M+H]^+$ $C_{17}H_{38}H_3S$ 316.27, obsd. 316.26.

**Synthesis of 4-methyl-3,4-dihydro-1H-benzo[*e*][1,4]diazepine-2,5-dione (5)**

To a mixture of sarcosine (2.00 g, 22.5 mmol) in DMSO (22 mL), isatoic anhydride (2.82 g, 17.3 mmol). After stirring overnight at 130 °C, cold water (50 mL) was added to the mixture. Then, the aqueous layer was washed with ethyl acetate twice (50 mL x 2). The collected organic layer was further washed with brine (80 mL) and dried over $Na_2SO_4$. After concentrating by rotary evaporation, the crude residue was further purified by silica gel column chromatography (DCM: MeOH 95:5) to afford the final product 5 (1.05 g, 32%). $^1$H NMR (500 MHz, DMSO-*d6*) δ 10.44 (s, 1H), 7.73 (dd, J = 7.8, 1.6 Hz, 1H), 7.49 (ddd, J = 8.0, 7.2, 1.6 Hz, 1H), 7.20 (ddd, J = 8.1, 7.3, 1.2 Hz, 1H), 7.08 (dd, J = 8.2, 1.1 Hz, 1H), 3.83 (s, 2H), 3.10 (s, 3H). $^{13}$C NMR (126 MHz, DMSO-*d6*) δ 169.81, 166.57, 136.98, 132.00, 130.88, 126.19, 123.92, 120.72, 52.18, 35.88. LCMS (ESI) calcd. for $[M+H]^+$ $C_{10}H_{11}N_2O_2$ 191.07, obsd. 191.32.

**Synthesis of 4-(4-methyl-2,5-dioxo-2,3,4,5-tetrahydro-1H-benzo[*e*][1,4]diazepin-1-yl)butanenitrile (6)**

To a solution of sodium hydride (60% in mineral oil, 0.0644 g, 1.61 mmol) in THF (6 mL), Compound 5 (0.255 g, 1.34 mmol) in THF (6 mL) was added dropwise at -40 °C. After stirring for 1 hour, 4-bromobutrylnitrile (0.160 mL, 1.61 mmol) was added to the mixture. The reaction mixture was stirred overnight at room temperature.

Then, the solvent was removed by the rotary evaporator and the crude was re-dissolved in DCM (50 mL). The mixture was washed with water (40 mL) and brine (40 mL). The collected organic layer was dried over $Na_2SO_4$ and concentrated by rotary evaporation. The crude residue was purified by silica gel column chromatography (DCM: MeOH = 97:3) to afford the final product 6 (0.188 g, 54%). 1H NMR (500 MHz, $CD_3OD$) δ 7.81 (dd, J = 7.8, 1.7 Hz, 1H), 7.66 (ddd, J = 8.8, 7.3, 1.7 Hz, 1H), 7.51 (dd, J = 8.2, 1.1 Hz, 1H), 7.41 (td, J = 7.5, 1.1 Hz, 1H), 4.44 – 4.25 (m, 1H), 4.14 (d, J = 14.8 Hz, 1H), 3.87 (ddd, J = 13.9, 8.0, 5.4 Hz, 1H), 3.74 (d, J = 14.8 Hz, 1H), 3.25 (s, 3H), 2.42 – 2.32 (m, 2H), 2.00 – 1.74 (m, 2H). 13C NMR (126 MHz, $CD_3OD$) δ 170.21, 169.33, 140.72, 133.80, 131.32, 130.96, 127.50, 123.40, 120.17, 54.03, 46.44, 36.02, 24.89, 14.83.

**Synthesis of tert-butyl (4-(4-methyl-2,5-dioxo-2,3,4,5-tetrahydro-1*H*-benzo[*e*][1,4]diazepin-1-yl)butyl)carbamate (7)**

To a stirred solution of Compound 6 (0.188 g, 0.729 mmol) in methanol (7 mL), nickel (II) chloride (0.0346 g, 0.146 mmol) and di-tert-butyl dicarbonate (0.335 mL, 1.46 mmol) was added at 0 °C. Then, sodium borohydride (0.138 g, 3.64 mmol) was added slowly in small portions to the mixture. After stirring at 0 °C for 1 hour, the ice bath was removed. The mixture was stirred overnight at room temperature. To the mixture, diethylenetriamine (0.0790 mL, 0.729 mmol) was added. After stirring 1 hour at room temperature, the solvents were removed by rotary evaporator, and the mixture was re-dissolved in ethyl acetate (40 mL). The ethyl acetate layer was washed with saturated sodium bicarbonate (30 mL) and brine (30 mL). The collected organic layer was dried over $Na_2SO_4$ and concentrated by rotary evaporation. The crude residue was

further purified by silica gel column chromatography (Hexane: EtOAc = 1:4) to afford the final product 3 (0.161 g, 61%). 1H NMR (500 MHz, $CD_3OD$) δ 7.79 (dd, J = 7.8, 1.7 Hz, 1H), 7.63 (ddd, J = 8.7, 7.4, 1.7 Hz, 1H), 7.50 (d, J = 8.3 Hz, 1H), 7.45 – 7.33 (m, 1H), 4.33 (dt, J = 14.7, 7.7 Hz, 1H), 4.12 (d, J = 14.6 Hz, 1H), 3.86 – 3.58 (m, 2H), 3.25 (s, 3H), 2.96 (t, J = 6.8 Hz, 2H), 1.59 – 1.31 (m, 13H). $^{13}C$ NMR (126 MHz, $CD_3OD$) δ 170.03, 169.46, 140.94, 133.65, 131.16, 131.08, 127.32, 123.68, 79.82, 54.12, 47.19, 40.62, 35.97, 28.76, 27.89, 25.96. LCMS (ESI) calcd. for $[M+H]^+$ $C_{19}H_{28}N_3O_4$ 362.20, obsd. 362.17.

**Synthesis of 4-(4-methyl-2,5-dioxo-2,3,4,5-tetrahydro-1*H*-benzo[*e*][1,4]diazepin-1-yl)butan-1-aminium (8)**

To a stirred solution of Compound 7 (0.0520 g, 0.144 mmol) in DCM (1 mL), trifluoroacetic acid (0.6 mL) was added dropwise. After stirring for 2 hours, the mixture was co-evaporated with toluene three times by rotary evaporation. The crude residue was taken to next step without any further purification.

Synthesis of 1-decyl-3-(4-(4-methyl-2,5-dioxo-2,3,4,5-tetrahydro-1*H*-pyrido[4,3-*e*][1,4]diazepin-1-yl)butyl)urea (NH-C4-10)

To a stirred solution of Compound 8 (0.144 mmol) from the previous step in THF (1.2 mL), 1-isothiocyanatodecane (65 μL, 0.288 mmol) and DIPEA (0.101 mL, 0.575 mmol) was added. After stirring overnight at room temperature, the solvents were removed by rotary evaporator. The crude was re-dissolved in ethyl acetate (20 mL) and washed with water (15 mL x 2) and brine (15 mL). The collected organic layer was dried over $Na_2SO_4$ and concentrated by rotary evaporation. The crude residue was further purified by silica gel column chromatography (Hexane: EtOAc = 1:3) to afford

the final product NH-C4-10 (0.0331 g, 50%). $^{1}$H NMR (500 MHz, $CD_3OD$) δ 7.79 (dd, J = 7.9, 1.7 Hz, 1H), 7.64 (ddd, J = 8.7, 7.3, 1.7 Hz, 1H), 7.51 (dd, J = 8.4, 1.1 Hz, 1H), 7.39 (td, J = 7.6, 1.1 Hz, 1H), 4.35 (dt, J = 14.3, 7.3 Hz, 1H), 4.12 (d, J = 14.7 Hz, 1H), 3.88 – 3.57 (m, 2H), 3.56 – 3.34 (m, 4H), 3.25 (s, 3H), 1.62 – 1.42 (m, 6H), 1.36 – 1.29 (m, 14H), 0.91 (t, J = 6.8 Hz, 3H). $^{13}$C NMR (126 MHz, $CD_3OD$) δ 181.03, 170.05, 169.49, 140.90, 133.69, 131.14, 131.10, 127.33, 123.74, 54.13, 47.18, 36.01, 33.07, 30.72, 30.70, 30.47, 27.96, 26.03, 23.74, 17.44, 14.44. LCMS (ESI) calcd. for $[M+H]^+$ $C_{25}H_{41}N_4O_2S$ 461.29, obsd. 461.41.

### 5.5.1 References for methods


1. Jiang, H., Khan, S., Wang, Y., Charron, G., He, B., Sebastian, C., Du, J., Kim, R., Ge, E., Mostoslavsky, R., Hang, H. C., Hao, Q., and Lin, H. (2013) SIRT6 regulates TNF-alpha secretion through hydrolysis of long-chain fatty acyl lysine, *Nature 496*, 110-113.

2. Spiegelman, N. A., Price, I. R., Jing, H., Wang, M., Yang, M., Cao, J., Hong, J. Y., Zhang, X., Aramsangtienchai, P., Sadhukhan, S., and Lin, H. (2018) Direct Comparison of SIRT2 Inhibitors: Potency, Specificity, Activity-Dependent Inhibition, and On-Target Anticancer Activities, *ChemMedChem 13*, 1890-1894.

3. Jing, H., Hu, J., He, B., Negron Abril, Y. L., Stupinski, J., Weiser, K., Carbonaro, M., Chiang, Y. L., Southard, T., Giannakakou, P., Weiss, R. S., and Lin, H. (2016) A SIRT2-Selective Inhibitor Promotes c-Myc Oncoprotein Degradation and Exhibits Broad Anticancer Activity, *Cancer Cell 29*, 767-768.

4. Hong, J. Y., Zhang, X., and Lin, H. (2018) HPLC-Based Enzyme Assays for Sirtuins, *Methods Mol. Biol. 1813*, 225-234.

5. Du, J., Zhou, Y., Su, X., Yu, J. J., Khan, S., Jiang, H., Kim, J., Woo, J., Kim, J. H., Choi, B. H., He, B., Chen, W., Zhang, S., Cerione, R. A., Auwerx, J., Hao, Q., and Lin, H. (2011) Sirt5 Is a NAD-Dependent Protein Lysine Demalonylase and Desuccinylase, *Science 334*, 806-809.

6. Farooqi, A. S., Hong, J. Y., Cao, J., Lu, X., Price, I. R., Zhao, Q., Kosciuk, T., Yang, M., Bai, J. J., and Lin, H. (2019) Novel Lysine-Based Thioureas as Mechanism-

Based Inhibitors of Sirtuin 2 (SIRT2) with Anticancer Activity in a Colorectal Cancer Murine Model, *J. Med. Chem. 62*, 4131-4141.

7. Clark, R. L., Carter, K. C., Mullen, A. B., Coxon, G. D., Owusu-Dapaah, G., McFarlane, E., Duong Thi, M. D., Grant, M. H., Tettey, J. N., and Mackay, S. P. (2007) Identification of the benzodiazepines as a new class of antileishmanial agent, *Bioorg. Med. Chem. Lett. 17*, 624-627.

# CHAPTER 6

## CONCLUSION AND FUTURE DIRECTIONS

### 6.1 Conclusion and Future Directions

With the emergence of SIRT2 as a therapeutic target for cancer, we have designed many SIRT2 inhibitors to improve anticancer potency. The current lead SIRT2 selective inhibitor from the H. Lin group is TM.[1] It contains a long chain thiomyristoyl group, which not only is the key part for SIRT2 selective inhibition but also significantly impairs aqueous solubility. Consequently, the poor aqueous solubility of TM may hamper the delivery of the compound in the cells and animal studies. Furthermore, due to this characteristic of TM, obtaining a co-crystal structure with SIRT2 was challenging. Hence, we have hypothesized that improved aqueous solubility and bioavailability could enhance the anticancer potency of SIRT2 selective inhibitors. Another drawback of TM is that it can only inhibit SIRT2 deacetylase, not de-fatty acylase.[2] Obtaining an inhibitor that can inhibit SIRT2 de-fatty acylase can be useful to further understand the importance of SIRT2 de-fatty acylase activity in cells.

The first strategy we tried was glycoconjugation. With glucose attached to TM, glucose-TM had shown improved aqueous solubility, as it got dissolved in PBS at 10 mg/mL without precipitation. However, glucose-TM did not show any antiproliferative effect.[3] The polar glucose moiety had ameliorated the aqueous solubility but significantly decreased the cellular permeability. Nevertheless, we were able to collect the co-crystal structure with glucose-TM and SIRT2, which revealed that the N-terminal carboxybenzoyl and C-terminal aniline groups of TM do not

contribute much to the interaction. Based on this finding, we had synthesized several analogs of TM, which showed a promising anticancer effect.[3]

To inhibit both SIRT2 deacetylase and de-fatty acylase, we have applied the Proteolysis Targeting Chimera (PROTAC) strategy to completely degrade SIRT2.[4] TM-P4-Thal with thalidomide attached to TM selectively degraded SIRT2 without any alteration of SIRT1 and SIRT3 expression levels. In addition, TM-P4-Thal had successfully inhibited both SIRT2 deacetylase and de-fatty acylase in cells. TM-P4-Thal had stronger cytotoxicity than TM only at low concentrations. At higher concentrations, we found that TM-P4-Thal had much weaker cytotoxicity. One potential reason is that TM inhibits SIRT2 by forming a stalled covalent intermediate with $NAD^+$. Because TM moiety of TM-P4-Thal will eventually lose its structure, the reusability of TM-P4-Thal will be limited. Once it degrades the target, a PROTAC probe gets released and fetches another target nearby. The reusability of a PROTAC probe is essential as it can lower the effective concentration to a nanomolar scale from a micromolar scale. [5] Because TM-P4-Thal has limited reusability, its cytotoxicity had slightly improved. Thus, a design with another handle that interacts with SIRT2 could solve this issue. A potential candidate could be NCO-90 or NCO-141 as the site where the thalidomide and the linker can be attached has been reported.[6] Moreover, we have not yet utilized TM-P4-Thal to further scrutinize the importance of SIRT2 de-fatty acylase in cancer cells. Comparison of TM-P4-Thal and TM in cancer cells will be intriguing to see if there is any difference from inhibiting SIRT2 de-fatty acylase.

Given that the N-terminal and C-terminal of TM can be freely changed, we had synthesized many TM analogs to specifically improve the aqueous solubility. Among

them, NH4-6 and NH4-13 had gained special attention from us. Both NH4-6 and NH4-13 contain a trimethylammonium moiety on the C-terminal. [REF] However, NH4-6 has an amide bond (NH) and NH4-13 has an ester bond (O) to connect the trimethylammonium moiety to the lysine. This one atom difference led to a significantly different sirtuin inhibition profile. NH4-6 with an amide bond inhibited SIRT1, SIRT2, and SIRT3. Meanwhile, NH4-13 with an ester bond selectively inhibited SIRT2. Comparing these two very similar inhibitors in cellular and animal models would allow us to accurately assess the importance of SIRT2 inhibition. When using two completely distinct inhibitors, such evaluation could be challenging, as the inhibitors possess different bioavailability. As a result, NH4-6 showed stronger cytotoxicity than NH4-13 in cellular proliferation assays. In HCT-116 tumor xenograft study, interestingly NH4-6 and NH4-13 had a similar anticancer effect. However, a higher dosage of NH4-6 caused severe weight loss and lethargic behaviors. NH4-13 at higher dosages did not have any over-toxicity issue and induced an even stronger anticancer effect in mice. Overall, administrating a SIRT2 selective inhibitor can be beneficial when treating cancer, as there is no advert over-toxicity issue [REF].

To further validate this, a comprehensive toxicity measurement of NH4-6 and NH4-13 will be desired. Measuring the maximum tolerated dosage or long-term dosage can depict the toxicity of the two inhibitors. Additionally, investigating the mechanism of the cytotoxicity can help us understand why there is a discrepancy in the cellular and animal studies with NH4-6 and NH4-13. These future studies can decipher the complex roles of SIRT1, SIRT2, and SIRT3 in tumorigenesis.

Even though NH4-6 and NH4-13 had improved aqueous solubility, they showed weaker cytotoxicity than TM at lower concentrations, due to the poor cell permeability from their charged moiety. Thus, we ultimately wanted to design a SIRT2 selective inhibitor that possesses superior aqueous solubility and permeability. One way was to simplify the structure of TM. This strategy could lower the molecular weight and improve bioavailability. A potential disadvantage was that a simplified inhibitor structure can exert weaker SIRT2 inhibition. From the previous reports, the benzodiazapienedione core structure had been used as a biomimetic for an amino acid.[7] Hence, we have synthesized NH-C1-10 with a benzodiazapienedione core and a 10-carbon thiourea acyl chain. As expected, NH-C1-10 portrayed improved aqueous solubility and inhibited SIRT2 slightly weaker than TM. In cellular proliferation assay, NH-C1-10 showed stronger cytotoxicity than TM. This had confirmed that the increased bioavailability of NH-C1-10 had consequently led to an enhanced anticancer effect in cellular studies. Moreover, NH-C1-10 had shown a broad anti-cancer effect and effectively inhibited BxPC-3 pancreatic tumor growth in the xenograft mice study.

Additional studies with NH-C1-10 are still needed. Medicinal chemistry modification on NH-C1-10 could potentially improve the anticancer potency. With the improved aqueous solubility, we can obtain the crystal structure of NH-C1-10 with SIRT2, which will deepen the understanding of the inhibitory interaction. Also, smaller modifications on the benzodiazapienedione core could additionally enhance the bioavailability and potency of NH-C1-10. For example, adding a nitrogen atom to the aromatic ring of the core could improve the aqueous solubility. A previous report had shown that the thiourea acyl group is relatively unstable compared with the

thioamide.[8] Hence, replacing the thiourea to a thioamide could also enhance the structural stability in media and serum, and thereby increase the anticancer effect.

Mechanistically, examining why NH-C1-10 shows strong cytotoxicity in pancreatic cancer cells can be interesting. NH-C1-10 showed stronger cytotoxicity in MIA-PaCa-2 than BxPC-3 cells. Finding the reason for this sensitivity difference can further narrow down the cancer patient types for the treatment. Hypothetically, this difference could be related to the c-Myc degradation. Previously, a SIRT2 knockdown in MIA-PaCa-2 cells had degraded c-Myc, an oncoprotein essential for tumor proliferation.[9] As such, inhibition of NH-C1-10 could potentially degrade c-Myc in MIA-PaCa-2 cells at a faster rate than in BxPC-3 cells. Consequently, this could have induced the sensitivity difference. Another factor could be the mutated level of K-Ras4a. We had demonstrated that SIRT2 removes the fatty acyl group from K-Ras4a to promote transformation activity.[10] NH-C1-10 could have impaired cell proliferation by regulating the K-Ras4a pathway. Overall, studying the mechanism of NH-C1-10 will be crucial to understand the importance of SIRT2 in cancer. If NH-C1-10 will be used in additional animal or preclinical studies, detailed toxicity information and pharmacokinetics of NH-C1-10 will be needed.

Overall, my research on the SIRT2 inhibitors design had not only proposed new structures but also confirmed the importance of SIRT2 in tumorigenesis. I strongly anticipate that my research had contributed to the understanding and treating cancer.

## 6.2 References


1. Jing, H., Hu, J., He, B., Negron Abril, Y. L., Stupinski, J., Weiser, K., Carbonaro, M., Chiang, Y. L., Southard, T., Giannakakou, P., Weiss, R. S., and Lin, H. (2016) A SIRT2-Selective Inhibitor Promotes c-Myc Oncoprotein Degradation and Exhibits Broad Anticancer Activity, *Cancer Cell 29*, 297-310.

2. Spiegelman, N. A., Hong, J. Y., Hu, J., Jing, H., Wang, M., Price, I. R., Cao, J., Yang, M., Zhang, X., and Lin, H. (2019) A Small-Molecule SIRT2 Inhibitor That Promotes K-Ras4a Lysine Fatty-Acylation, *ChemMedChem 14*, 744-748.

3. Hong, J. Y., Price, I. R., Bai, J. J., and Lin, H. (2019) A Glycoconjugated SIRT2 Inhibitor with Aqueous Solubility Allows Structure-Based Design of SIRT2 Inhibitors, *ACS Chem. Biol. 14*, 1802-1810.

4. Hong, J. Y., Jing, H., Price, I. R., Cao, J., Bai, J. J., and Lin, H. (2020) Simultaneous Inhibition of SIRT2 Deacetylase and Defatty-Acylase Activities via a PROTAC Strategy, *ACS Med. Chem. Lett. 11*, 2305-2311.

5. Lu, J., Qian, Y., Altieri, M., Dong, H., Wang, J., Raina, K., Hines, J., Winkler, James D., Crew, Andrew P., Coleman, K., and Crews, Craig M. (2015) Hijacking the E3 Ubiquitin Ligase Cereblon to Efficiently Target BRD4, *Chem. Biol. 22*, 755-763.

6. Kozako, T., Mellini, P., Ohsugi, T., Aikawa, A., Uchida, Y. I., Honda, S. I., and Suzuki, T. (2018) Novel small molecule SIRT2 inhibitors induce cell death in leukemic cell lines, *BMC Cancer 18*, 791.

7. Biel, M., Deck, P., Giannis, A., and Waldmann, H. (2006) Synthesis and evaluation of acyl protein thioesterase 1 (APT1) inhibitors, *Chemistry (Easton) 12*, 4121-4143.

8. Nielsen, A. L., Rajabi, N., Kudo, N., Lundø, K., Moreno-Yruela, C., Bæk, M., Fontenas, M., Lucidi, A., Madsen, A. S., Yoshida, M., and Olsen, C. A. (2021) Mechanism-based inhibitors of SIRT2: structure–activity relationship, X-ray structures, target engagement, regulation of α-tubulin acetylation and inhibition of breast cancer cell migration, *RSC Chemical Biology*.

9. Liu, P. Y., Xu, N., Malyukova, A., Scarlett, C. J., Sun, Y. T., Zhang, X. D., Ling, D., Su, S. P., Nelson, C., Chang, D. K., Koach, J., Tee, A. E., Haber, M., Norris, M. D., Toon, C., Rooman, I., Xue, C., Cheung, B. B., Kumar, S., Marshall, G. M., Biankin, A. V., and Liu, T. (2013) The histone deacetylase SIRT2 stabilizes Myc oncoproteins, *Cell Death Differ. 20*, 503-514.

10. Jing, H., Zhang, X., Wisner, S. A., Chen, X., Spiegelman, N. A., Linder, M. E., and Lin, H. (2017) SIRT2 and lysine fatty acylation regulate the transforming activity of K-Ras4a, *eLife 6*, e32436.